

DISS. ETH NO. ....

# **Computational analysis of multi-omics data to understand the molecular mechanisms of germline-dependent epigenetic inheritance**

A thesis submitted to attain the degree of  
DOCTOR OF SCIENCES of ETH ZURICH

(Dr. sc. ETH Zurich)

presented by  
Deepak Kumar Tanwar  
M.Sc., McGill University, Canada

born on 30.10.1991

citizen of India

accepted on the recommendation of

Prof. Isabelle Mansuy, examiner  
Prof. Tuncay Baubec, co-examiner  
Prof. Mark Robinson, co-examiner

2022



# Acknowledgements

This doctoral thesis has been an accomplishment that would not have been possible, or anywhere near as enjoyable, without the help and support of a number of incredible individuals. Thank you for all that you have contributed to this thesis.

I am eternally grateful to Prof. Dr. Isabelle Mansuy for allowing me to do Doctoral research in her lab. It is a pleasure to be a member of the Neuroepigenetics lab. Thank you to all the members of the Neuroepigenetics lab, past and present. The Neuroepigenetics group was always fun to work with and I learned a lot about experiments. Thank you so much! A special thanks to the present and past members of Y38 for motivating, and various scientific and non-scientific discussions.

My sincere thanks to Prof. Dr. Mark Robinson and Prof. Dr. Tuncay Baubec for accepting to be my co-examiners and supporting me throughout my doctoral research. Thank you so much Mark for always being available and providing all the help in writing proposals, helping in supervising students, and discussing and providing solutions to the problems I was facing.

I am indebted to Dr. Pierre-Luc Germain for his expert supervision and all the support he has provided. I am grateful for all discussions and suggestions on both scientific and non-scientific issues. Thank you for being so nice and for all the support which was extremely helpful to reach this point. I have learnt a lot from you.

I would also like to thank the Directors and members of the Brain Research Institute for creating such a stimulating environment for research.

I am extremely grateful for my doctoral funding, the Swiss Government Excellence Scholarship. Thank you so much Sandra Zweifel for always being there.

Looking back into the past, this thesis would not have happened without my bache-

lor's thesis supervisors Rainer König and Sandro Lindig, who got me interested in the field of bioinformatics data science.

Finally, I am very grateful to my family for their continuous support and belief in me. Visiting you always helped me to relax and to not worry about work so much. Last of all, I want to thank my wife, Palni Kundra, for always cheering me up when I was down and for helping me with stupid issues.

# Table of Contents

<b>List of Abbreviations</b> . . . . .	<b>2</b>
<b>Summary</b> . . . . .	<b>5</b>
<b>Zusammenfassung</b> . . . . .	<b>9</b>
<b>Thesis overview</b> . . . . .	<b>13</b>
<b>Introduction</b> . . . . .	<b>15</b>
Epigenetics . . . . .	15
Germline epigenetics . . . . .	17
Spermatogonial Stem Cells . . . . .	17
Reprogramming . . . . .	18
Epigenetic Inheritance . . . . .	21
Transgenerational Epigenetic Inheritance . . . . .	22
Reprogramming in epigenetic inheritance . . . . .	22
Models of Epigenetic Inheritance . . . . .	23
MSUS mouse model . . . . .	23
Vectors of epigenetic inheritance . . . . .	25
DNA methylation . . . . .	26
Histone modifications . . . . .	26
RNA . . . . .	27
Non-coding RNA . . . . .	28
Transcription factors . . . . .	29
Extracellular vesicles . . . . .	29
Challenges in data analysis . . . . .	30
Multi-omics data integration . . . . .	30
Ad-hoc approaches . . . . .	30
Systematic approaches . . . . .	31

Short RNA data analysis . . . . .	32
Goals of thesis . . . . .	33
<b>Bioinformatics methods . . . . .</b>	<b>35</b>
Version controlled data analysis using git . . . . .	35
Data analysis directory organization . . . . .	37
Pipelines for data analysis . . . . .	37
Quality check and trimming of sequencing datasets . . . . .	38
RNA sequencing . . . . .	39
Pseudo-alignment and alignment . . . . .	40
Duplicated reads analysis . . . . .	41
Differential expression analysis . . . . .	41
Exploratory data analysis . . . . .	42
Differential transcript usage and differential isoform switching . . . . .	42
Differential exon usage and differential 3' untranslated regions usage .	43
Functional analysis . . . . .	43
Assay of Transposase Accessible Chromatin sequencing . . . . .	43
Alignment, post-alignment quality control, and peak calling . . . . .	44
Peaks annotation and differential accessibility analysis . . . . .	46
Functional analysis . . . . .	46
Differential accessibility analysis at transposable elements . . . . .	46
Chromatin immunoprecipitation followed by sequencing . . . . .	47
Alignment and peak calling . . . . .	47
Peaks annotation, differential analysis, and functional analysis . . . . .	47
Bisulfite sequencing . . . . .	49
Alignment and methylation calling . . . . .	49
Differential methylation analysis . . . . .	50
Copy number variation analysis . . . . .	50
DML and DMR annotation, and functional analysis . . . . .	50
Short RNA-seq . . . . .	51
Multi-omics analysis . . . . .	51
<b>Chapter 1: Dynamic chromatin accessibility in spermatogonial cells for transcriptional programmings from early postnatal to adult stages . . . . .</b>	<b>55</b>
1.1 Update on the new data analysis . . . . .	56
1.1.1 Code availability . . . . .	56
1.1.2 Inclusion of RNA-seq data from the literature . . . . .	56

1.1.3	New RNA-seq data from lab . . . . .	57
1.1.3.1	Identification of clusters of genes with distinct expression profiles . . . . .	59
1.1.3.2	Multi-omics data integration . . . . .	59
1.2	Graphical Abstract . . . . .	65
1.3	Abstract . . . . .	66
1.4	Introduction . . . . .	67
1.5	Results . . . . .	68
1.5.1	Enrichment of spermatogonial cells from postnatal and adult mouse testis . . . . .	68
1.5.2	Chromatin is remodelled in spermatogonial cells during the development . . . . .	68
1.5.3	Differentially accessible chromatin regions associated with distinct gene expression dynamics . . . . .	69
1.5.4	Differentially accessible chromatin regions associated with distinct epigenetic profiles . . . . .	70
1.5.5	Accessibility changes at open chromatin regions carry binding sites for distinct families of transcription factors . . . . .	72
1.5.6	Chromatin accessibility at transposable elements undergoes significant remodelling in the transition from postnatal to adult spermatogonia . . . . .	73
1.6	Discussion . . . . .	76
1.7	Methods . . . . .	80
1.7.1	Mouse husbandry . . . . .	80
1.7.2	Germ cells isolation . . . . .	80
1.7.3	Spermatogonial cells enrichment by FACS . . . . .	81
1.7.4	Immunocytochemistry . . . . .	81
1.7.5	RNA extraction and library preparation for RNA-seq . . . . .	82
1.7.6	Library preparation for Omni-ATAC . . . . .	82
1.7.7	RNA sequencing . . . . .	82
1.7.8	Omni-ATAC . . . . .	83
1.7.9	Chromatin immunoprecipitation sequencing . . . . .	85
1.7.10	Bisulfite sequencing (BS) . . . . .	85
1.7.11	High-throughput sequencing data analysis . . . . .	86
1.7.12	Figures . . . . .	86
1.8	Authors contribution . . . . .	86
1.9	Acknowledgements . . . . .	87
1.10	Competing interest . . . . .	87

1.11 Funding . . . . .	87
1.12 Data and materials availability . . . . .	87
1.13 Figures . . . . .	88
1.14 Supplementary Figures . . . . .	99
1.15 Supplementary tables . . . . .	107
<b>Chapter 2: Early life stress affects the miRNA cargo of epididymal extracellular vesicles in mouse . . . . .</b>	<b>109</b>
2.1 Graphical Abstract . . . . .	110
2.2 Abstract . . . . .	111
2.3 Summary sentence . . . . .	111
2.4 Key words . . . . .	111
2.5 Introduction . . . . .	112
2.6 Results . . . . .	113
2.6.1 Isolation of cauda epididymosomes confirmed by several methods . .	113
2.6.2 The number and size of epididymosomes in adult males are not altered by postnatal stress . . . . .	113
2.6.3 miRNAs are persistently altered by postnatal stress in cauda epididymosomes . . . . .	114
2.6.4 mRNA targets of miRNAs from cauda epididymosomes are altered by postnatal stress in sperm and in zygotes . . . . .	115
2.7 Discussion . . . . .	116
2.8 Materials and methods . . . . .	117
2.8.1 Animals . . . . .	117
2.8.2 MSUS . . . . .	118
2.8.3 Tissue collection . . . . .	118
2.8.4 Electron microscopy images . . . . .	118
2.8.5 Epididymosomes isolation by ultracentrifugation . . . . .	119
2.8.6 Immunoblotting . . . . .	119
2.8.7 Nanoparticle tracking analysis . . . . .	119
2.8.8 RNA isolation and epididymosomes profiling . . . . .	119
2.8.9 Preparation and sequencing of sRNA-seq libraries from epididymosomes	120
2.8.10 RT-qPCR . . . . .	120
2.8.11 Cholesterol measurements . . . . .	120
2.8.12 Bioinformatics data analysis . . . . .	120
2.9 Data availability . . . . .	121

2.10 Authors' contributions . . . . .	121
2.11 Grant Support . . . . .	122
2.12 Acknowledgements . . . . .	122
2.13 Figures . . . . .	123
2.14 Supplementary figures . . . . .	127
2.15 Supplementary Tables . . . . .	131
<b>Chapter 3: shortRNA . . . . .</b>	<b>135</b>
3.1 Abstract . . . . .	135
3.2 Introduction and background . . . . .	136
3.3 Methods . . . . .	138
3.3.1 Development and testing environment . . . . .	138
3.3.2 Backbone data structures of <b>shortRNA</b> . . . . .	138
3.3.2.1 <b>phylo</b> . . . . .	138
3.3.2.2 <b>FactorList</b> . . . . .	138
3.3.2.3 <b>DataFrame</b> . . . . .	139
3.3.2.4 <b>TreeSummarizedExperiment</b> . . . . .	139
3.3.3 Pipeline . . . . .	141
3.3.3.1 Quality control and trimming . . . . .	142
3.3.3.2 Sequence count matrix . . . . .	145
3.3.3.3 Annotation preparation . . . . .	145
3.3.3.4 Alignment . . . . .	147
3.3.3.5 Reads annotation and assignment . . . . .	148
3.3.3.6 Assignment rules . . . . .	149
3.3.3.7 Features tree . . . . .	152
3.3.3.8 Reads assignment ambiguity . . . . .	154
3.3.3.9 Construction of <b>TreeSummarizedExperiment</b> object . . . . .	154
3.3.3.10 Differential analysis . . . . .	154
3.3.3.11 Table of important functions . . . . .	157
3.4 Results . . . . .	157
3.4.1 Datasets used for testing the pipeline . . . . .	157
3.4.2 Comparison of quantification and identification of miRNAs . . . . .	158
3.4.2.1 <b>shortRNA</b> quantification is positively correlated with <b>Oasis2</b> and <b>Sports1</b> . . . . .	158
3.4.2.2 <b>shortRNA</b> accurately identify miRNAs . . . . .	159
3.4.3 Data simulation to check the alignment and reads assignment by <b>shortRNA</b>	159

3.4.4	Differential expression analysis . . . . .	161
3.4.5	Validation using human data and quantitative real-time PCR . . . . .	161
3.4.6	Qualitative comparison with other tools . . . . .	163
3.5	Discussion & Outlook . . . . .	167
3.6	Limitations . . . . .	169
3.7	Conclusion . . . . .	170
3.8	Data and code availability . . . . .	170
<b>Conclusion and outlook</b>	. . . . .	<b>171</b>
Overall conclusion . . . . .	171	
MSUS-associated differences . . . . .	171	
RNA sequencing data analysis pipeline . . . . .	172	
ATAC sequencing data analysis pipeline . . . . .	172	
Updating manuscript from Chapter 1 in light of latest RNA-seq data . . . . .	173	
Low correlations of quantification between <b>shortRNA</b> and qPCR . . . . .	174	
<b>Appendix A</b>	. . . . .	<b>175</b>
Datasets analyzed from lab's MSUS model . . . . .	175	
Human dataset from the Schratt lab . . . . .	175	
Mouse datasets analyzed from literature . . . . .	176	
<b>Appendix B</b>	. . . . .	<b>177</b>
Other publications and manuscripts during doctoral thesis work . . . . .	177	
Involvement of circulating factors in the transmission of paternal experiences through the germline . . . . .	177	
Symposium summary: Epigenetic inheritance-impact for biology and society 26–28 August 2019, Zurich, Switzerland . . . . .	177	
OmniSperm: Multiomic analyses of sperm and offspring production from a single male . . . . .	178	
Early life stress alters chromatin accessibility landscape and transcript usage in spermatogonial cells during postnatal testis maturation . . . . .	178	
<b>Appendix C</b>	. . . . .	<b>179</b>
shortRNA analysis steps in R (a short vignette) . . . . .	179	
Package installation . . . . .	179	
Quality check and trimming . . . . .	179	
FastQ files to sequence by counts matrix . . . . .	179	

Unique sequences for alignment . . . . .	179
Obtaining databases for analysis . . . . .	179
Annotation preparation and genome index generation for alignment . . . . .	180
Alignment . . . . .	180
Overlapping aligned data with annotations . . . . .	180
Assignment of overlapping reads to features with assignment rules . . . . .	181
Converting features to FactorList . . . . .	181
Assignment of reads to the features tree . . . . .	181
Creation of TreeSummarizedExperiment object . . . . .	181
Differential analysis . . . . .	182
<b>Appendix D . . . . .</b>	<b>183</b>
Simulated reads for testing shortRNA . . . . .	183
Libraries . . . . .	183
miRNAs . . . . .	183
cluster chr17:17830188-17830879 . . . . .	183
Imputing differences for differential analysis . . . . .	184
Read counts . . . . .	184
miRNA precursor . . . . .	184
Data to be simulated . . . . .	185
<b>Appendix E . . . . .</b>	<b>187</b>
3.9 CV . . . . .	188
<b>References . . . . .</b>	<b>193</b>



# List of Tables

1.1	Datasets used in this manuscript . . . . .	86
2.1	Supplementary table 1 . . . . .	131
2.2	Supplementary table 2 . . . . .	131
2.3	Supplementary table 3 . . . . .	132
2.4	Supplementary table 4 . . . . .	133
3.1	Important functions from shortRNA . . . . .	157
3.2	Assignment of simulated reads by shortRNA . . . . .	161



# List of Figures

1	History of the term epigenetics . . . . .	16
2	Graphical summary of the biology of germline stem cell specification and transitions . . . . .	18
3	Graphical summary of the biology of germline stem cell specification and transitions . . . . .	20
4	MSUS paradigm . . . . .	24
5	Dataset collected from the MSUS model . . . . .	25
6	Overview of version control system . . . . .	36
7	Organization of data analysis projects . . . . .	37
8	Workflow for quality check and quality control for sequencing data . . . . .	39
9	Workflow for RNA sequencing data analysis . . . . .	40
10	Workflow for ATAC sequencing data analysis . . . . .	45
11	Workflow for ChIP sequencing data analysis . . . . .	48
12	Workflow for Bisulfite sequencing data analysis . . . . .	50
13	Workflow for multi-omics data integration . . . . .	52
1.1	Log <sub>2</sub> fold-change comparison of RNA-seq data from the literature and lab (old and new) . . . . .	57
1.2	Volcano plot of differentially expressed genes . . . . .	58
1.3	K-means clustering of differentially expressed genes . . . . .	59
1.4	Enriched heatmap of distal DARs . . . . .	61
1.5	Enriched heatmap of proximal DARs . . . . .	62
1.6	Enriched heatmap of distal DARs with ChIP-seq and BS-seq data . . . . .	63
1.7	Enriched heatmap of proximal DARs with ChIP-seq and BS-seq data . . . . .	64
1.8	Graphical abstract . . . . .	65
1.9a	Regions of differential chromatin accessibility in spermatogonial cells between postnatal and adult stages . . . . .	88

1.9b Regions of differential chromatin accessibility in spermatogonial cells between postnatal and adult stages . . . . .	89
1.10a Transcriptomic profile in postnatal and adult spermatogonial cells . . . . .	90
1.10b Transcriptomic profile in postnatal and adult spermatogonial cells . . . . .	91
1.11a Chromatin accessibility and histone modifications at proximal regions of genes dynamically expressed between PND15 and adult spermatogonial cells . . . . .	92
1.11b Chromatin accessibility and histone modifications at proximal regions of genes dynamically expressed between PND15 and adult spermatogonial cells . . . . .	93
1.12a Transcription factor dynamics at differentially accessible regions is predicted by motif enrichment in adult spermatogonial cells . . . . .	94
1.12b Transcription factor dynamics at differentially accessible regions is predicted by motif enrichment in adult spermatogonial cells . . . . .	95
1.13a Differential chromatin accessibility at transposable elements (TEs) in adult spermatogonial cells compared to PND15 . . . . .	96
1.13b Differential chromatin accessibility at transposable elements (TEs) in adult spermatogonial cells compared to PND15 . . . . .	97
1.14 Increased accessibility at LINE L1 subtypes located near Olfr gene clusters .	98
1.15a FACS leads to enrichment of PLZF+ cells in testicular preparations from mouse	99
1.15b FACS leads to enrichment of PLZF+ cells in testicular preparations from mouse	100
1.16a Omni-ATAC profiles of PND15 and adult spermatogonial cells and their genomic distribution . . . . .	101
1.16b Omni-ATAC profiles of PND15 and adult spermatogonial cells and their genomic distribution . . . . .	102
1.17 Representative examples from Categories 1-3 resulted from the overlap of chromatin accessibility, gene expression and histone profiling datasets . . . . .	103
1.18 DNAme profiles of spermatogonial cells do not show major changes over the period of testis postnatal maturation . . . . .	104
1.19 Distinct chromatin profiles between PND15 and adult spermatogonia are present at distal regions across the genome . . . . .	105
1.20 Differentially accessible TEs exhibit enriched TF motifs and correspond to regions nearby non-random gene families . . . . .	106
2.1 Graphical abstract . . . . .	110
2.2 Isolation and characterization of cauda epididymosomes . . . . .	123
2.3 Comparison of epididymosomal number, size, and release machinery in adult MSUS and control males . . . . .	124

2.4	Target pathways of up- and down-regulated miRNAs in adult MSUS cauda epididymosomes and alterations in steroidogenesis in postnatal and adult MSUS males . . . . .	125
2.5	<b>Targets of miRNAs from cauda epididymosomes are altered by MSUS in sperm and zygotes.</b>	
	Cumulative distribution plots of miR-31-5p targets from 5-months old MSUS and control caudal sperm RNA-seq <b>A</b> and from RNA-seq of zygotes originating from 3-months old MSUS and control males <b>B</b> .	
	<b>C:</b> miRNA abundance of sperm plotted against abundance in cauda epididymosomes. Coefficient of determination ( $R^2=0.74$ ).	
	<b>D:</b> Dot plot of the top target pathways (adjusted $P < 0.05$ ) of miRNAs differentially expressed (adjusted $P \leq 0.1$ ) in adult MSUS cauda epididymosomes. Color-scale of the dot represents $-\log_{10}$ adjusted $P$ of miRNA in a pathway and size of the dot represents $-\log_{10}$ adjusted $P$ of the pathway. . . . .	126
2.6	Electron microscopy image and electrophoresis . . . . .	127
2.7	Data overview . . . . .	128
2.8	Scatterplot of log fold-change of miRNAs in sperm and cauda epididymosomes	129
2.9	Profiles of cauda epididymosomal small RNAs by high-resolution automated electrophoresis . . . . .	129
2.10	Cumulative distribution plots of miRNA targets in differentially expressed genes	130
2.11	Immunoblot images of cauda epididymosomes and liver cell lysate, stained with cellular marker GAPDH (37kDa) and extracellular vesicle marker CD9 (25kDa) . . . . .	130
3.1	Schematic of A: <code>SummarizedExperiment</code> (Morgan et al., 2020), B: <code>TreeSummarizedExperiment</code> (R. Huang et al., 2020) . . . . .	140
3.2	Overview of <code>shortRNA</code> pipeline . . . . .	141
3.3	Benchmark of four different Bioconductor tools for reading and storing FASTQ file quality data. Performance of four tools is measured in <b>A:</b> the amount of time they take for reading the file, <b>B:</b> the amount of memory they take to store the data. . . . .	142
3.4	Exemplary QC report plots of a sperm sample from (Katharina Gapp et al., 2021). <b>A:</b> Quality control table, <b>B:</b> Quality score lines plot at each nucleotide in the sequencing reads, <b>C:</b> Barplot of reads duplication level with the mean GC ratio represented as lines, <b>D:</b> Histogram of reads distribution, before and after quality control . . . . .	143

3.5	Schematic of quality check and quality control of FASTQ files, UMIs collapsing (if present), and collapsing FASTQ files to obtain unique sequences for alignment and making a sequence by samples counts matrix . . . . .	144
3.6	Schematic of obtaining database, preparing annotations and custom genome indexes for alignment . . . . .	147
3.7	Schematic of alignment, overlapping features and aligned sequences, and assigning reads to features using assignment rules . . . . .	148
3.8	General framework of feature tree and assignment of sequences to the tree. <b>A:</b> Example of two sequences. <b>B:</b> Alignment of both the sequences to miRNA. <b>C:</b> General outline of the feature tree and assignment of both the sequences to the tree . . . . .	153
3.9	Hierarchical organization of <b>A:</b> tRNA features and <b>B:</b> mitochondrial tRNA features. . . . .	153
3.10	Hierarchical organization of miRNA features . . . . .	154
3.11	Multiple assignments of a sequence mapping to a tRNA. <b>A:</b> Exemplary sequence. <b>B:</b> Multiple sequence alignment plot of the sequence and the features to which it is mapping. <b>C:</b> Assignment of the reads to the tRNA feature tree	155
3.12	Schematic of assigning reads to the features tree of features, creation of <code>TreeSummarizedExperiment</code> object, and downstream analysis and plotting .	156
3.13	Comparison of Log2 TMM normalized quantification of miRNAs from <code>shortRNA</code> with <code>Oasis2</code> , <code>Sports1</code> , and <code>seqpac</code> . . . . .	158
3.14	Upset plot of overlaps of detected features between four methods: <code>shortRNA</code> , <code>Oasis2</code> , <code>Sports1</code> , and <code>seqpac</code> . . . . .	160
3.15	Genomic plots of simulated reads from miRNA precursor. . . . .	160
3.16	Hierarchical representation of features and assigned reads to them. Differential expression analysis of features from two miRNA clusters. Simulated read nodes are highlighted in orange colour . . . . .	162
3.17	Comparison of quantifications of five miRNAs from four different tools with - Delta Ct values from qPCR. <b>A:</b> Overall correlation. <b>B:</b> Correlation at individual miRNA . . . . .	164
3.18a	Genomic plots of validated miRNAs . . . . .	165
3.18b	Genomic plots of validated miRNAs . . . . .	166



# List of Abbreviations

---

Abbreviation	Term
5mc	5-Methylcytosine
ATAC-seq	Assay for Transposase-Accessible Chromatin using sequencing
BS-seq	Bisulfite sequencing
ChIP-seq	Chromatin immunoprecipitation with sequencing
DARs	Differentially accessible regions
DGEs	Differentially expressed genes
DNAm	DNA methylation
EV	Extracellular vesicles
GO	Gene ontology
GSEA	Gene set enrichment analysis
HTS	High-throughput sequencing
miRNA	micro RNA
ncRNA	non-coding RNA
piRNA	Piwi-interacting RNA
PND	Postnatal day
PNW	Postnatal week
PGCs	Primordial germ cells
qPCR	quantitative polymerase chain reaction
RRBS	Reduced representation bisulfite sequencing
RNA-seq	RNA sequencing
sRNA-seq	Short RNA sequencing
siRNA	Small interfering RNA
SSCs	Spermatogonial stem cells
TF	Transcription factor
TFBS	Transcription factor binding site
MSUS	Unpredictable maternal separation combined with unpredictable maternal stress
VCS	Version control system

---





# Summary

The environment has a strong influence on an organism's development, especially in the early stages. Environmental influences and life experiences can alter the phenotypic features of exposed individuals and their offspring in many animals. In mammals, traumatic stress is a type of environmental event that can change their behaviour, cognition, and physiological functions. Some of the impacts of severe stress can be passed down through generations, even if those generations have never been exposed to a traumatic stressor. Environmentally generated effects that involve non-genetic germline alterations can be an important route of trait transmission over generations. Even if the subsequent generations have never been exposed to similar stressful exposures, they may be impaired in similar functions. The host lab's unpredictable maternal separation combined with unpredictable maternal stress (MSUS) mouse model is perfect for learning more about the mechanisms behind epigenetic inheritance induced by environmental perturbations.

In this thesis, to study the mechanisms of epigenetic inheritance, multi-omics data analysis pipelines were built, Methods, and a number of high-throughput sequencing datasets generated using the MSUS model were analyzed using these pipelines, Appendix A and Appendix B. Also, the datasets generated from spermatogonial cells were used to study the developmental trajectory across postnatal and adult stages. Further, the effect of early life trauma on epididymal extracellular vesicles transcriptome was investigated using short RNA sequencing data. At last, a tool was built to analyze short RNA sequencing data to address issues in the current tools and pipelines.

Spermatogonial cells are the postnatal initiators of spermatogenesis, and they undertake critical proliferative and differentiation tasks throughout one's life. They are the only type of stem cell capable of transmitting genetic information to an embryo. Open chromatin in spermatogonial cells undergoes significant remodelling throughout testes development. Throughout postnatal testes development, they have significantly different transcriptional pathways. We investigated the dynamics of chromatin accessibility and gene expression during the developmental stages of postnatal day 8 (PND8), PND15, and postnatal week 21 (PNW21) using multi-omics data collected from spermatogonial cells. By comparing chromatin

accessibility changes between early postnatal and steady-state adult cells in the mouse testes, the age-dependent molecular phenotype of spermatogonial cells was identified. The differentially accessible regions were discovered to be relevant to developmental and metabolic processes and enriched for important transcription factors. Also, the accessibility of chromatin at transposable elements in spermatogonia has been examined. Specific transposable elements subtypes become less accessible as the adult testis matures, whereas specific LINE L1 subtypes become more accessible. The genome's olfactory receptor gene regions were discovered to be highly connected to several of the more accessible subtypes. In conclusion, these findings reveal that chromatin accessibility in spermatogonial cells changes from postnatal to adult stage, as well as interesting biological patterns when combined with expression and histone modifications data. Furthermore, we show how bioinformatics approaches may be used to integrate multi-omics datasets. These results are available in Chapter 1.

If environmentally-triggered marks are not inherited from SSCs, another possible way in which sperm may carry them is through the uptake of extracellular vesicles, in particular those produced by epididymal cells. By using the MSUS model, we studied the impact of early postnatal stress on the transcriptome of epididymal extracellular vesicles. The short RNA profile of epididymal EVs, particularly miRNAs, were found to be altered in adult males exposed to postnatal stress. In certain cases, these miRNA changes have been related to differences in the expression of their target genes in sperm and zygotes produced from those sperm. To summarize, chronic stress in early postnatal life changes miRNAs in mature extracellular vesicles of the male reproductive tract, with implications for mature sperm and zygotes. These results are summarized in Chapter 2.

While working on Chapter 1 and Chapter 2, we discovered a lot of issues with tools available for analyzing short RNA sequencing data. Short RNAs are significant molecules that play an important role in the control of the genome. Short RNAs have been classified into several categories, including miRNA, tRNA and tRNA fragments, and piRNAs, all of which have a complex biosynthesis. As a result, an analysis framework is necessary that is both sufficiently specialized to reflect the specificities of different classes of short RNA and their biogenesis, as well as sufficiently generic and thorough to conduct global analyses. We created a user-friendly, highly customizable, and comprehensive R package, **shortRNA** to do a full end-to-end analysis of short RNA sequencing data. Our package has been specifically designed to account for changes in short RNA types and their biogenesis, and it may readily be modified to include further annotations. We also use a customised genome annotation with pseudo chromosomes to account for post-transcriptional modifications, as well as a flexible rule-based approach to allocate reads along a tree of hierarchically ordered attributes. This enables systematic querying, exploration, and differential expression analysis of short

RNAs at several levels of granularity, ranging from single sequences to entire RNA classes. The shortRNA R package, which is platform-agnostic, was designed to carry out all of the analysis steps from within R. These results are available in Chapter 3.

In summary, the work presented in this thesis investigated various mechanisms of epigenetic inheritance and developed several pipelines for data analysis from the MSUS model, investigated changes in spermatogonial cells across development, studied the impact of early life stress on the transcriptome of epididymal extracellular vesicles, and developed an R package for short RNA sequencing data analysis.



# Zusammenfassung

Die Umwelt hat einen starken Einfluss auf die Entwicklung eines Organismus, insbesondere in den frühen Stadien. Umwelteinflüsse und Lebenserfahrungen können bei vielen Tieren die phänotypischen Merkmale exponierter Individuen und ihrer Nachkommen verändern. Bei Säugetieren ist traumatischer Stress eine Art Umweltereignis, das ihr Verhalten, ihre Wahrnehmung und ihre physiologischen Funktionen verändern kann. Einige der Auswirkungen von starkem Stress können über Generationen weitergegeben werden, auch wenn diese Generationen noch nie einem traumatischen Stressor ausgesetzt waren. Umweltbedingte Effekte, die nicht-genetische Veränderungen der Keimbahn beinhalten, können ein wichtiger Übertragungsweg von Merkmalen über Generationen hinweg sein. Auch wenn die nachfolgenden Generationen noch nie ähnlichen Belastungen ausgesetzt waren, können sie in ähnlichen Funktionen beeinträchtigt sein. Die unvorhersehbare mütterliche Trennung des Wirtslabors in Kombination mit dem Mausmodell für unvorhersehbaren mütterlichen Stress (MSUS) ist perfekt, um mehr über die Mechanismen hinter der epigenetischen Vererbung durch Umweltstörungen zu erfahren.

Um die Mechanismen der epigenetischen Vererbung zu untersuchen, wurden in dieser Dissertation Multi-Omics-Datenanalysepipelines erstellt, Methoden und eine Reihe von Hochdurchsatz-Sequenzierungsdatensätzen, die mit dem MSUS-Modell generiert wurden, unter Verwendung dieser Pipelines analysiert, Anhang A und Anhang B. Auch , wurden die aus Spermatogonien generierten Datensätze verwendet, um den Entwicklungsverlauf über postnatale und adulte Stadien hinweg zu untersuchen. Darüber hinaus wurde die Wirkung eines frühen Lebenstraumas auf das Transkriptom der extrazellulären Vesikel der Nebenhoden unter Verwendung von kurzen RNA-Sequenzierungsdaten untersucht. Schließlich wurde ein Tool entwickelt, um kurze RNA-Sequenzierungsdaten zu analysieren, um Probleme in den aktuellen Tools und Pipelines zu beheben.

Spermatogoniale Zellen sind die postnatalen Initiatoren der Spermatogenese und übernehmen lebenslang kritische Proliferations- und Differenzierungsaufgaben. Sie sind die einzige Art von Stammzellen, die genetische Informationen an einen Embryo übertragen können. Offenes Chromatin in Spermatogonialzellen wird während der Hodenentwicklung

signifikant umgebaut. Während der postnatalen Hodenentwicklung weisen sie signifikant unterschiedliche Transkriptionswege auf. Wir untersuchten die Dynamik der Zugänglichkeit von Chromatin und der Genexpression während der Entwicklungsstadien des 8. postnatalen Tages (PND8), PND15 und postnatalen Woche 21 (PNW21) unter Verwendung von Multi-Omics-Daten aus Spermatogonien. Durch den Vergleich Chromatins der Veränderungen der Zugänglichkeit deszwischen frühen postnatalen und stationären adulten Zellen in den Hoden von Mäusen wurde der altersabhängige molekulare Phänotyp von Spermatogonien identifiziert. Die unterschiedlich zugänglichen Regionen wurden als relevant für Entwicklungs- und Stoffwechselprozesse entdeckt und um wichtige Transkriptionsfaktoren angereichert. Auch die Zugänglichkeit von Chromatin an transponierbaren Elementen in Spermatogonien wurde untersucht. Spezifische Subtypen der transponierbaren Elemente werden mit zunehmender Reife des adulten Hodens weniger zugänglich, während spezifische LINE L1-Subtypen leichter zugänglich werden. Es wurde entdeckt, dass die Genregionen des olfaktorischen Rezeptors des Genoms stark mit mehreren der leichter zugänglichen Subtypen verbunden sind. Zusammenfassend zeigen diese Ergebnisse, dass sich die Zugänglichkeit von Chromatin in Spermatogonien vom postnatalen bis zum adulten Stadium ändert, sowie interessante biologische Muster, wenn sie mit Expressions- und Histonmodifikationsdaten kombiniert werden. Darüber hinaus zeigen wir, wie bioinformatische Ansätze verwendet werden können, um Multi-Omics-Datensätze zu integrieren. Diese Ergebnisse sind in Kapitel 1 verfügbar.

Wenn umweltbedingte Markierungen nicht von SSCs vererbt werden, können Spermien sie auch durch die Aufnahme extrazellulärer Vesikel, insbesondere solcher, die von Nebenhodenzellen produziert werden, übertragen. Mit dem MSUS-Modell untersuchten wir den Einfluss von frühem postnatalem Stress auf das Transkriptom extrazellulärer Nebenhodenvesikel. Es wurde festgestellt, dass das kurze RNA-Profil von Nebenhoden-EVs, insbesondere miRNAs, bei erwachsenen Männern, die postnatalem Stress ausgesetzt waren, verändert war. In bestimmten Fällen wurden diese miRNA-Veränderungen mit Unterschieden in der Expression ihrer Zielgene in Spermien und Zygoten, die aus diesen Spermien produziert wurden, in Verbindung gebracht. Zusammenfassend lässt sich sagen, dass chronischer Stress im frühen postnatalen Leben miRNAs in reifen extrazellulären Vesikel des männlichen Fortpflanzungstrakts verändert, mit Auswirkungen auf reife Spermien und Zygoten. Diese Ergebnisse sind in Kapitel 2 zusammengefasst.

Während der Arbeit an Kapitel 1 und Kapitel 2 entdeckten wir viele Probleme mit verfügbaren Werkzeugen zur Analyse von kurzen RNA-Sequenzierungsdaten. Kurze RNAs sind bedeutende Moleküle, die eine wichtige Rolle bei der Kontrolle des Genoms spielen. Kurze RNAs wurden in mehrere Kategorien eingeteilt, darunter miRNA, tRNA und tRNA-Fragmente

sowie piRNAs, die alle eine komplexe Biosynthese aufweisen. Daher ist ein Analyserahmen erforderlich, der sowohl ausreichend spezialisiert ist, um die Spezifitäten verschiedener Klassen kurzer RNA und deren Biogenese widerzuspiegeln, als auch ausreichend generisch und gründlich ist, um globale Analysen durchzuführen. Wir haben ein benutzerfreundliches, hochgradig anpassbares und umfassendes R-Paket, **shortRNA**, erstellt, um eine vollständige End-to-End-Analyse von kurzen RNA-Sequenzierungsdaten durchzuführen. Unser Paket wurde speziell entwickelt, um Veränderungen in kurzen RNA-Typen und deren Biogenese zu berücksichtigen, und es kann leicht modifiziert werden, um weitere Anmerkungen aufzunehmen. Wir verwenden auch eine angepasste Genom-Annotation mit Pseudochromosomen, um posttranskriptionelle Modifikationen zu berücksichtigen, sowie einen flexiblen regelbasierten Ansatz, um Reads entlang eines Baums hierarchisch geordneter Attribute zuzuordnen. Dies ermöglicht die systematische Abfrage, Exploration und differentielle Expressionsanalyse kurzer RNAs auf mehreren Granularitätsebenen, die von einzelnen Sequenzen bis hin zu ganzen RNA-Klassen reichen. Das plattformunabhängige Paket **shortRNA R** wurde entwickelt, um alle Analyseschritte innerhalb von R durchzuführen. Diese Ergebnisse sind in Kapitel 3 verfügbar.

Zusammenfassend wurden in dieser Arbeit verschiedene Mechanismen der epigenetischen Vererbung untersucht und entwickelt mehrere Pipelines für die Datenanalyse aus dem MSUS-Modell, untersuchten Veränderungen in Spermatogonien während der Entwicklung, untersuchten die Auswirkungen von Stress im frühen Leben auf das Transkriptom extrazellulärer Vesikel der Nebenhoden und entwickelten ein R-Paket für die Analyse von kurzen RNA-Sequenzierungsdaten.



# Thesis overview

This thesis is divided into three parts: introduction and methods, scientific contributions, and concluding remarks. First, I introduce the biological context for my thesis, Introduction, followed by the method section with the flowcharts and description of various data analysis pipelines, Methods. Next, in scientific contributions, there are three chapters: Chapter 1 is the latest version of the manuscript submitted to BioRxiv (Lazar-Contes et al. 2020), Chapter 2 is published (Alshanbayeva et al. 2021), and Chapter 3 is included as a descriptive chapter on shortRNA and a manuscript is in preparation. My contribution to each paper is summarized at the beginning of each chapter. In the end, the thesis concludes with a summary and outlook, Conclusion and outlook.



# Introduction

## Epigenetics

Conrad Hal Waddington, a British developmental biologist, coined the term “epigenetics” in 1942. He was also a pioneer in the fields of epigenetics, systems biology, and evolutionary developmental biology. What came to be known as “Waddington’s landscape” describes how genes interact with the environment to produce, from the same genotype, the variety of cellular phenotypes of a multicellular organism (Waddington, 1942). While epigenetics has been given various meanings throughout history (Figure 1, taken from (Pisco, Fouquier d’Herouel, & Huang, 2016), it can be broadly understood as the study of how our genes, which we inherit from our forefathers and mothers, are controlled and interact with the environment: how our genes form who we are. Epigenetics is the study of how additional factors communicate with genes to guide the processes that make our cells and bodies function. “Epi” means “on top of” or “in addition to.”

Epigenetic mechanisms regulate the transcriptional programs in response to developmental and environmental cues and encompass a variety of pre-transcriptional to post-translational events, including DNA methylation (DNAme), post-translational histone modifications (e.g. acetylation and methylation), histone variations, non-coding RNA (ncRNA) and their modifications, and nucleosome remodelling (Susiarjo, 2016). Epigenetic mechanisms in the somatic cell regulate vital cellular function, including differentiation or adaptation of cellular function in response to environmental indications. However, epigenetic control in germ cells can trigger changes in phenotype over many successive generations, known as transgenerational epigenetic inheritance, section Transgenerational epigenetic inheritance, and contribute to changes in susceptibility to health and disease.

## ep•i•genet•ics: (n) ...

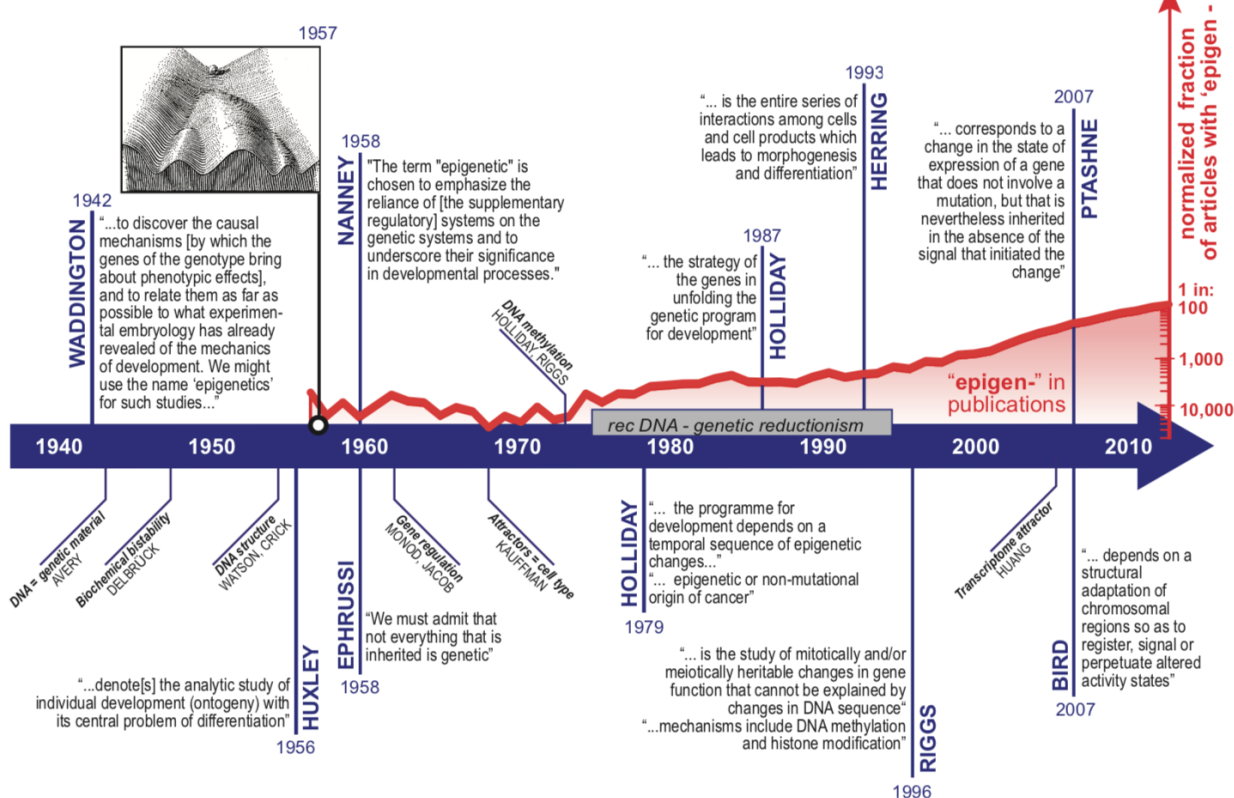


**Figure 1: History of the term ‘epigenetics’.** The discovery of DNA methylation launched the associated modern (molecular) notion of ‘epigenetics’ (1975) and is reflected in the surge of the number of publications after that. Note the stagnation in the two decades after that DNA recombinant technology and genetic determinism dominated mindset in biology (grey horizontal bar). We are now seeing an enormous increase in the use of the term, as the post-genome era findings challenge the textbook gene-centred mindset. Textboxes display quotes, of selected authors (vertical text). The red curve indicates the number of Medline entries containing the wildcarded search term ‘epigen\*’ per year, normalized for a number of publications that contain the generic keywords ‘cell’ and ‘function’. Diagonal text boxes highlight key discoveries or findings in biology influencing the history of epigenetics but not directly related to it. Taken from (Susiarjo, 2016).

## Germline epigenetics

### Spermatogonial Stem Cells

The germ stem cells of the seminiferous epithelium in the testis are known as spermatogonial stem cells (SSCs). They are the building blocks of spermatogenesis, the mechanism of producing mature male germ cells. The SSCs are responsible for the continuous creation of the massive number of sperm cells required for a male's reproductive lifespan. They are present in the testis from birth and for the rest of the male's life. SSCs have a dual biological function: they replicate themselves to maintain the stem cell pool while also generating progenitors that will differentiate into spermatozoa. They begin life in the testicular seminiferous tubules and continue to serve this dual purpose throughout adulthood. SSCs are the male adult stem cells of the seminiferous epithelium in the testis that are capable of transferring a species' genome from generation to generation while also possessing the ability to differentiate into pluripotent stem cells.

In mice, the primordial germ cells (PGCs), the precursors of prospermatogonia, appear at 5.5 days post-coitum. Prospermatogonia establishes SSCs shortly after birth (gonocytes). PGCs undergo global DNA demethylation (which involves the full erasure of parental imprints) through both active and passive mechanisms as they migrate toward the gonads. DNA methylation (DNAm) is gradually restored after that (between embryonic day 13.5 [E13.5] and E16.5), and both maternal and paternal-specific imprints are believed to be completely formed by birth in male prospermatogonia (Hammoud et al., 2015).

The prospermatogonia are mitotically arrested at birth, but they begin cycling on postnatal days 1–2 (PND1 – PND2). A population of spermatogonial cells continues to proliferate throughout the first week after birth, giving rise to the undifferentiated  $A_{\text{single}}$ ,  $A_{\text{paired}}$ , and  $A_{\text{aligned}}$  spermatogonial pools (Kolasa, Misiakiewicz, Marchlewicz, & Wiszniewska, 2012). Cycling spermatogonia proliferate and populate the seminiferous tubule over the next week (PND3–PND10); here, a subset gives rise to self-renewing SSCs, while the rest differentiates without self-renewal, resulting in the first wave of spermatogenesis or commits apoptosis. As a result, this stage of germ cell growth is critical for initiating and maintaining male fertility during adulthood. Following puberty, after 35–37 days, SSCs go through many phases of proliferation, eventually forming sister stem cells that will maintain a stable pool or more differentiated intermediates that will initiate meiosis I and II and form mature sperm cells. Please see Figure 2 for an overview. These transitions are timed to correlate with global epigenome shifts, which represent the spermatogonial cell's developmental path, current transcriptional program, and future commitment to differentiation. Since the transcriptome and epigenetic landscape of spermatogonial stem cells is so complex during proliferation and

differentiation, drastic changes in the environment may not go unnoticed.

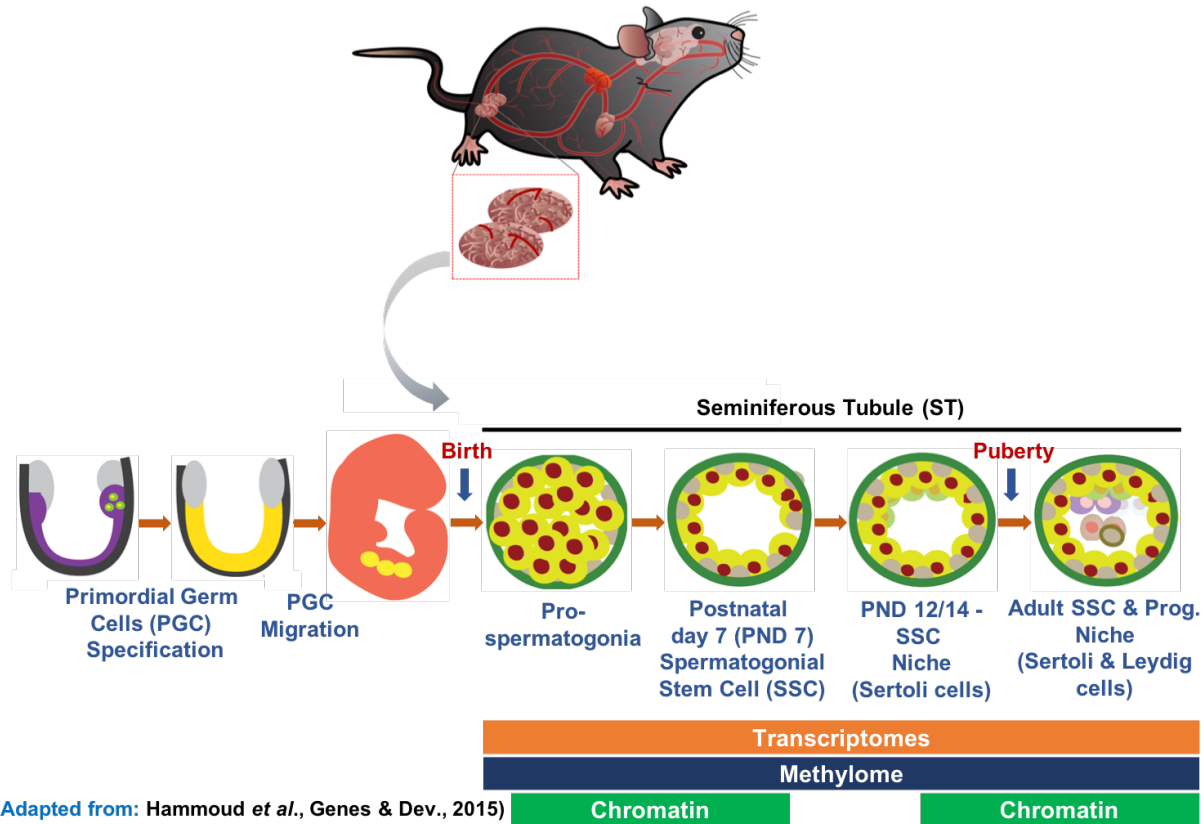


**Figure 2: Graphical summary of the biology of germline stem cell specification and transitions.** Adapted from (Hammoud et al., 2015)

It is difficult to distinguish SSCs from progenitor spermatogonia that don't have stem cell activity and are committed to differentiation. Specific cell surface markers like Thy1 and TSPAN8 can be used to enrich SSCs. Further, cells extracted from Id4-eGFP transgenic mice that express a high amount of GFP signal, and combinations of reporter gene and cell surface marker signal can be used to further enrich the population (F. Chan et al., 2014; Mutoji et al., 2016).

## Reprogramming

Reprogramming refers to the erasure and remodelling of epigenetic markers such as DNAmc throughout mammalian development (Reik, Dean, & Walter, 2001). Diverse cells and tissues acquire different gene expression patterns during the evolution of multicellular organisms. Some cells undergo extensive epigenetic reprogramming in normal developmental or pathological conditions, which involves the removal of epigenetic marks in the nucleus and the installation of a new set of marks. Genome-wide epigenetic reprogramming occurs at stages

when the developmental potency of cells changes. There is passive DNA demethylation and further reorganization of histone modifications. The epigenetic reprogramming is likely to be needed for totipotency, correct initiation of embryonic gene expression, and early lineage development in the embryo. Extensive epigenetic reprogramming of DNA and histone marks occur in mammalian development in totipotent early embryos and pluripotent germ cells (Canovas & Ross, 2016).

The germ cell lineage is unique in carrying genetic and epigenetic information from one generation to the next. In the germline, epigenetic reprogramming resets genomic potential and erases epigenetic memory. Epigenetic reprogramming involves genome-wide demethylation of 5mC, which is important for genome imprinting, X inactivation, transposon silencing, centromeric/telomeric structural stability, and gene expression (Surani, Hayashi, & Hajkova, 2007). After a sperm fertilizes an ovum, nearly all epigenetic marks are reprogrammed in two short intervals early in development. By eliminating random changes in epigenetic marks (i.e., epimutations) that have occurred in the germ cells, reprogramming restores the ability of the fertilized egg cell (i.e., zygote) to develop into all the different cell types and tissues (Reik et al., 2001). During embryo development, there are two waves of epigenetic reprogramming, Figure 3. After fertilization in the preimplantation embryo (i.e., the blastocyst), the first phase begins; preimplantation refers to the time between the embryo implanting and forming a placenta. The embryo in mice undergoes genome-wide demethylation after fertilization, which is finished by E5 (Reik et al., 2001; Smallwood & Kelsey, 2012). The paternal genome undergoes rapid, active demethylation, whereas the maternal genome experiences passive demethylation. The embryonic DNA begins to be re-methylated on day E5 and is finished before birth. The second wave of epigenetic reprogramming takes place in the germ cells of the developing embryo, which will eventually give rise to gametes with sex-specific epigenetic markers (gametogenesis). The methylation signatures of the parental genomes are found in the PGCs, which are progenitors to both male and female germ cells in the developing embryo. PGCs are epiblast cells that first appear in the posterior primitive streak at E7.5, after which they begin to migrate from E8.5 to the genital ridge, arriving by E11.5. PGCs undergo rapid demethylation beginning around E7–8, which is completed by E15–16. In PGCs, parental imprints are erased and totipotency is restored, followed by the restoration of sex-specific methylation. Reprogramming is complete in the male germline at birth, but not in the female germline until adolescence.

Embryonic development involves epigenetic reprogramming to replenish totipotency from a germline state in each generation. To begin with, because there is no hereditary germplasm and germ cell precursors are formed from a post-implantation epiblast that has acquired epigenetic markers throughout early development, a germline reprogramming phase may be

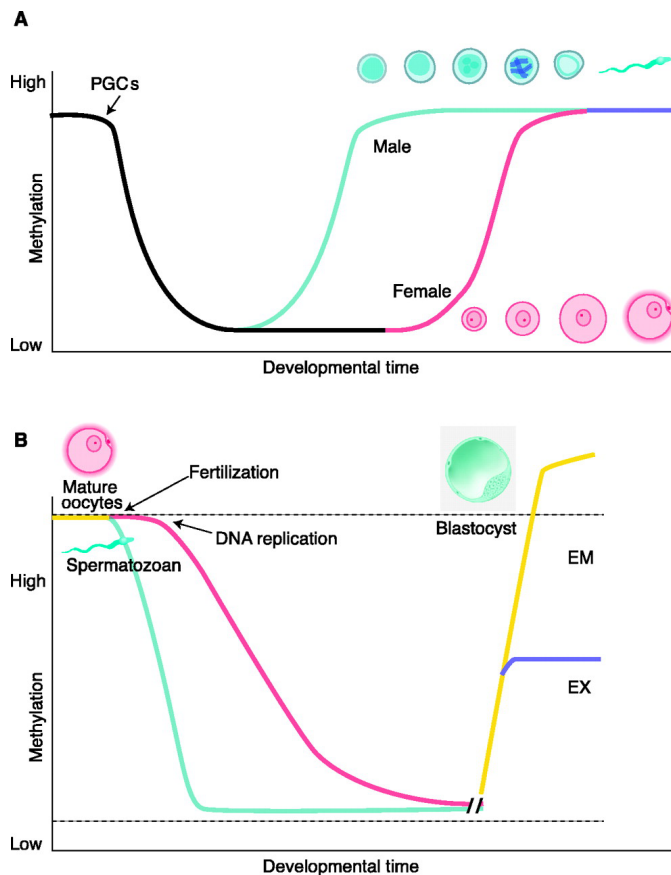


**Figure 3: Methylation reprogramming in the germline.**

**A:** Primordial germ cells (PGCs) in the mouse become demethylated early in development. Remethylation begins in prospermatogonia on E16 in male germ cells, and after birth in growing oocytes. Some stages of germ cell development are shown.

**B:** Methylation reprogramming in preimplantation embryos. The paternal genome (blue) is demethylated by an active mechanism immediately after fertilization. The maternal genome (red) is demethylated by a passive mechanism that depends on DNA replication. Both are remethylated around the time of implantation to different extents in embryonic (EM) and extraembryonic (EX) lineages. Methylated imprinted genes and some repeat sequences (dashed line) do not become demethylated. Unmethylated imprinted genes (dashed line) do not become methylated. Taken from (Reik et al., 2001).

---

required to ensure that this acquired information is erased. Then, in the post-implantation epiblast, the parent-of-origin markers of mature gametes fuse in the zygote and are passed down to nascent PGCs from their predecessors. Another goal could be to reverse the effects of accumulating epigenetic changes that are influenced by both genetic and environmental factors. However, epigenetic information can be inherited through the germline (or after fertilization) on occasion, which is most likely due to insufficient germline erasure. Finally, demethylation in the germline may have the added benefit of reducing the frequency of mutations caused by 5-methylcytosine (5mC) deamination.

## Epigenetic Inheritance

Inheritance is the process of passing traits or information from one generation of individuals or cells to the next. Charles Darwin proposed natural selection as the primary mechanism for species evolution in his 1859 book: “On the origin of species”. According to Darwin, natural selection is a key mechanism of evolution, characterized by changes in the heritable traits of a population over generations. Jean-Baptiste Lamarck was an early proponent of the idea that biological evolution occurred and proceeded in accordance with natural laws. He is well known for the principle of “inheritance of acquired characteristics”, an idea known as Lamarckism. According to Lamarckian theories of inheritance, physical traits inherited by a generation during its lifetime (e.g. strength and body size) are passed down to offspring. In 1868, Darwin proposed pangenesis theory as a supplement to his 1859 theory of evolution by natural selection in his book “The Variation of Animals and Plants Under Domestication.” The term pangenesis was coined by Darwin, with “pan-” referring to the whole and “genesis” referring to the origin. Using the term pangenesis, Darwin proposed that all parts of the parents could contribute to the evolution and development of the offspring. Darwin’s theory of pangenesis was based on the idea that somatic cells would release ‘gemmules’ or ‘pangenes’ in response to environmental stimulation (use and disuse), which travelled around the body but not necessarily in the bloodstream. These pangenes were microscopic particles that supposedly contained information about the characteristics of their parent cell, and Darwin believed that they eventually accumulated in germ cells, where they could pass on the newly acquired characteristics of the parents to the next generation (Darwin, 1871). As a result, Darwin advocated Lamarckian use and disuse inheritance, as well as Lamarckian soft inheritance. In the 1880s, August Weismann challenged this concept. Weismann proposed the germ plasm theory, which states that germ cells in the gonads contain information that is passed down from generation to generation unaffected by experience and independent of somatic cells (Weismann, 1893). Hereditary information is only transferred from germline

cells to somatic cells. This is referred to as the Weismann barrier.

However, recent epigenetic discoveries have revealed that acquired traits can be passed down to future generations. Our recent work showed that serum from adult male mice exposed to postnatal stress, injected chronically to naïve males, can induce metabolic symptoms associated with stress in the offspring of the injected males (van Steenwyk et al., 2020). Also, we identified circulating extracellular vesicles as vectors of communication with germ cells that can reproduce symptoms of exposure in the offspring when injected into fathers *in vivo* (Alshanbayeva, Tanwar, Roszkowski, Manuella, & Mansuy, 2021). These results highlight the importance of circulating factors in the mechanisms of epigenetic inheritance, Chapter 2.

## **Transgenerational Epigenetic Inheritance**

The transmission of epigenetic information from one generation to the next is referred to as intergenerational epigenetic inheritance, while that across multiple generations is referred to as transgenerational epigenetic inheritance. Both intergenerational and transgenerational imply the parents' exposure to the environmental factor in question, as well as the gametes they already have. Transgenerational exposure refers to people who have never been specifically exposed to the environmental factor during their lifetime (either as individuals or as future gametes). This may be the third generation after *in utero* exposure or the second generation after preconception exposure. It is assumed that fetal or *in utero* exposure to an environmental factor is not heritable because the offspring are specifically exposed. However, the mechanisms of adverse development following *in utero* exposure to drugs, alcohol, diet, and other factors also influence offspring through epigenetic mechanisms.

## **Reprogramming in epigenetic inheritance**

Epigenetic reprogramming refers to the process of removing and resetting relevant epigenetic information in germ cells, which is primarily accomplished through DNA demethylation. Epigenetic reprogramming prevents the transmission of epigenetic information from mature gametes, which is in line with the germ-plasm theory of Weissman (Weissmann, 1893). The extent of epigenetic reprogramming, however, is unknown, leaving the question of how much epigenetic information from adult gametes is preserved in the embryo unanswered. In mammals, DNAm and histone marks are effectively reset during reprogramming both in the germline, and in the zygote immediately after conception, leaving epigenetic changes with minimal possibility of passing down. Evidence for the survival of histone modifications across reprogramming has been identified in sperm, where histones are largely replaced by protamines. Surprisingly, H3K27me3 enrichment has been discovered in reprogramming

resistant sperm nucleosomes (Casas & Vavouri, 2020), suggesting that this mark may be a hereditary signal. Further, findings in (Kremsky & Corces, 2020) imply that transcription factors can operate as epigenetic information carriers during germ cell and pre-implantation development by maintaining the CpG methylation state.

## Models of Epigenetic Inheritance

Given limitations such as the inability to conduct controlled experiments in humans and the availability of data for successive generations, rodent models have become critical for correlating human findings (Jawaid, Jehle, & Mansuy, 2021) and to investigate the penetrance of effects across generations to provide mechanistic insight. There are several experimental paradigms for studying epigenetic inheritance. In mammals, dietary changes, stress, medications, and environmental toxins have all been linked to altered phenotypes in offspring (K. Gapp & Bohacek, 2018). Epigenetic inheritance appears to be initiated or modulated by mutations in the epigenetic machinery, such as DNA/RNA methylation enzymes or histone modification complexes, such as overexpression of *Kdm1a*, an H3K4me3 demethylase in mice (Siklenka et al., 2015).

Alternatively, environmental perturbations may initiate epigenetic inheritance, with various insults leading to offspring phenotypes in a variety of model systems (Jawaid & Mansuy, 2019). Environmental factors like vinclozolin (an antiandrogenic compound), methoxychlor (an estrogenic compound), stress responses, high-fat diet, high-sugar diet, low-protein diet, air pollutant exposure in pregnant mice, in utero Bisphenol-A (BPA), di(2- Ethylhexyl) phthalate (DEHP) and dibutyl phthalate (DBP) exposure in rats, in utero exposure to jet fuel (JP-8) in mice, in utero valproic acid exposure in mice, olfactory fear conditioning in Filial 0 (F0) mice, and Female mice fed a high-fat/ high-sugar diet have been linked to epigenetic inheritance (Bohacek & Mansuy, 2015; Hanson & Skinner, 2016; Heard & Martienssen, 2014; Mao, Li, Liu, & Chi, 2017; Nagy & Turecki, 2015; Rando, 2016; Schaefer & Nadeau, 2015). These models shed new light on the mechanisms of epigenetic inheritance. However, distinguishing evidence of epigenetic mark transmission from the evidence of exposure transmission is difficult.

## MSUS mouse model

**A unique transgenerational model to assess the effects of trauma:** unpredictable maternal separation combined with unpredictable maternal stress (MSUS) is a firmly established transgenerational model in the Mansuy lab, that does not involve any chemical or mutagenic agent but, depends only on psychological and emotional trauma, Figure 4. It is an

ideal model to study the possible transgenerational effects of life experiences on the genome and the epigenome.

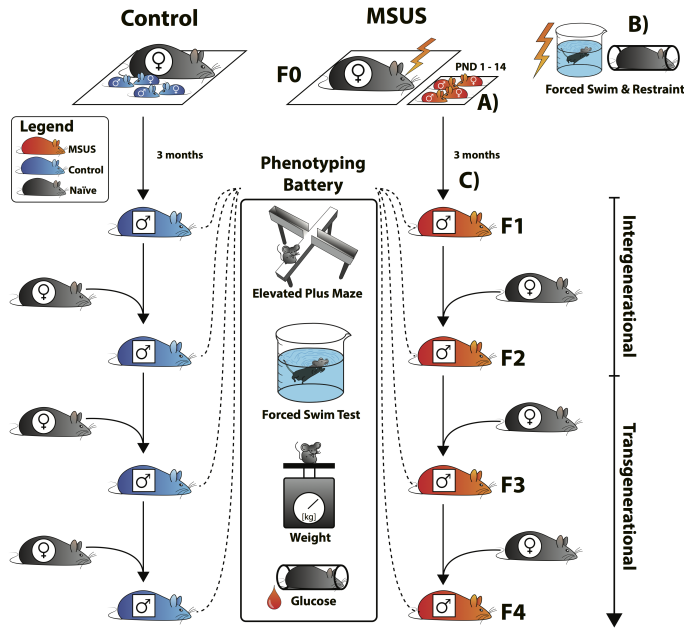


**Figure 4: MSUS paradigm.** MSUS consists of (A) separating mouse pups (F1) from their mother (F0, naïve primiparous control females mated with naïve males) daily for 3 hours per day at an unpredictable time during the 12 hours active cycle, starting 1 day after birth (postnatal day 1, PND1) until PND14. (B) During separation, dams are exposed to an additional unpredictable stressor by being subjected to either, a forced swim in 18°C water for 5 minutes or a 20-minute physical restraint in a tube, anytime (unpredictably) during the 3 hours. From PND15, mice are left undisturbed with their mother until PND21 (no further MSUS), are then weaned at PND21 and raised normally until adulthood (C). Control litters are raised normally (left). Males used to generate the pups are removed from the breeding cage shortly after mating thus, fathers never encounter their offspring and do not contribute to their rearing. When adult (3–8 months of age), F1 males are paired with naïve primiparous control females to sire the F2 generation, then F2 and F3 males are bred with naïve primiparous control females to generate an F3 and F4 offspring, respectively. Males from each generation are tested on the elevated plus-maze, forced swim test, weight measurements and glucose response after physical restraint. MSUS is applied only to F1 mice, mice from F2, F3 and F4 generations are not exposed to any manipulation. Phenotypes transmitted from father to offspring are intergenerational, phenotypes that persist from father to offspring then grand-offspring or great grand-offspring are transgenerational. Taken from (van Steenwyk, Roszkowski, Manuella, Franklin, & Mansuy, 2018).

MSUS consists in separating mouse pups from their mother unpredictably (any time during the day) each day for 3 hours from postnatal day 1 (PND1) to PND14 and exposing the mothers to stressful situations such as restraint stress or forced swim in cold water (18°C), unpredictably during separation. F1 generation males are mated with naïve control females, and F2 males are mated with control females to obtain F3. MSUS induces several

behavioural symptoms including depression, increased risk-taking, antisocial behaviours and memory deficits, and metabolic alterations across several generations (Franklin et al., 2010; van Steenwyk et al., 2018). Further, metabolic phenotypes like decreased bodyweight, insulin hypersensitivity and glucose intolerance are also observed. For studying the molecular mechanisms of epigenetic inheritance, a number of high-throughput sequencing (HTS) datasets have been collected and sequenced, Figure 5.

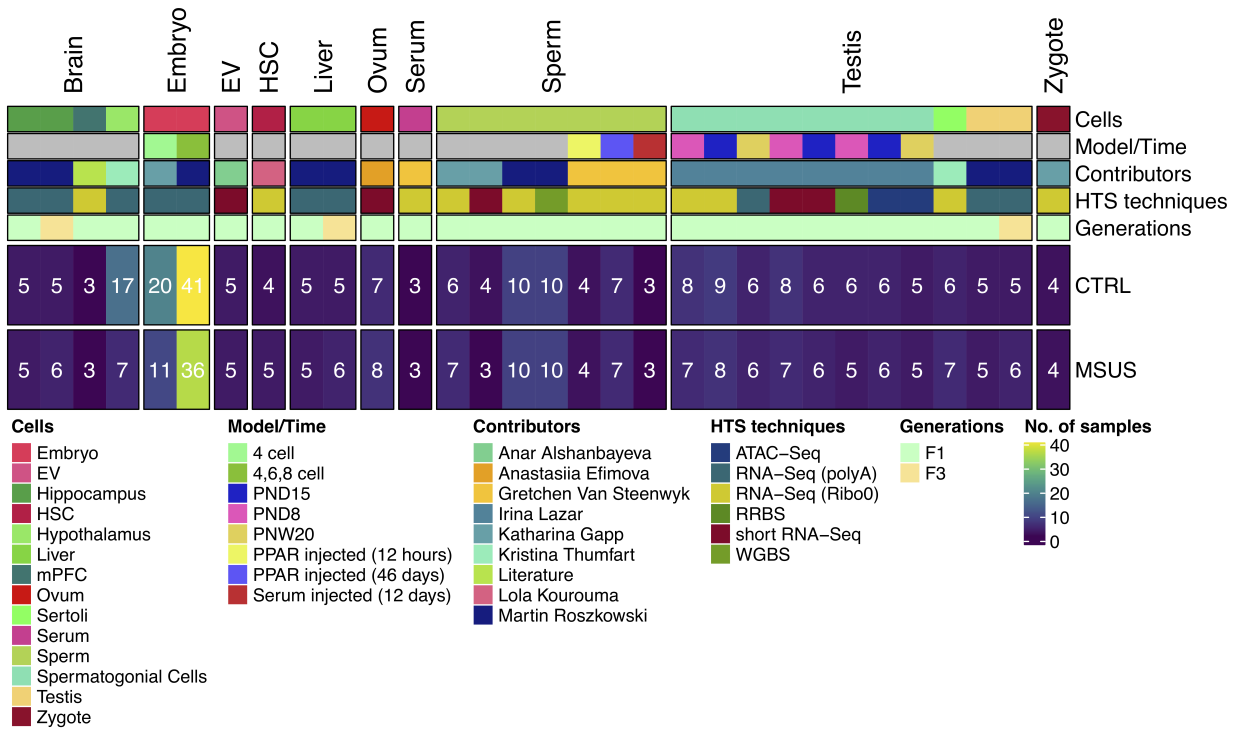


**Figure 5: Dataset collected from the MSUS model.**

## Vectors of epigenetic inheritance

Epigenetic marks, such as DNAm, histone modifications, and non-coding RNAs, have been proposed as information-carrying vectors passed down through generations. These three candidates have been investigated in a variety of epigenetic inheritance paradigms. It is hypothesized that stable changes in epigenetic marks caused by an environmental insult (epimutations) may affect gene expression or chromatin stability, increasing the risk of a phenotype or disease in offspring (Miska and Ferguson-Smith, 2016). DNAm, histone modifications, RNA, and ncRNAs are all interconnected and interdependent within individual cells. They are likely to act in a coordinated and collaborative manner to cause disease phenotypes in the context of epigenetic inheritance.

## DNA methylation

The most common type of DNA methylation in mammals is cytosine residue methylation. Cytosine residues are methylated on the 5' carbon and are referred to as 5-methylcytosines (5mC). Methylation of a cytosine residue is a binary process – either methylation or non-methylation. In mammals, DNA methylation is typically found in the context of CpG dinucleotides (Bird, 2002). Cytosine methylation can be copied from one DNA strand to the next in this manner during replication and meiosis. DNA methylation patterns, on the other hand, are dynamic. The patterns of DNA methylation vary over time and space, changing during development and differing between cell types (Luo, Hajkova, & Ecker, 2018). DNA methyltransferase (DNMT) enzymes methylate cytosine residues. DNMT1 is a methyltransferase that reads hemimethylated DNA after cell division and adds methylation to the newly synthesized strand (Z. Chen & Riggs, 2011). The de novo methyltransferases DNMT3a and 3b can add methylation to previously unmethylated residues (Smith & Meissner, 2013). Although DNA methylation in gene control regions is generally associated with gene repression, its precise role in gene regulation is likely locus dependent (Deaton & Bird, 2011). Methylated DNA is a true epigenetic mark because there are “readers” that preferentially recognize 5mC and can interpret the methylation mark’s meaning (H. Zhu, Wang, & Qian, 2016). Many properties of DNA methylation make it an appealing mechanistic candidate for epigenetic inheritance, including the following: it can be environmentally modulated; machinery exists to replicate methylation patterns onto newly synthesized DNA, making it mitotically heritable; and methylated loci resistant to epigenetic reprogramming have been identified in the zygote and germline. Disruption of the DNA methylation machinery may also play a role in the initiation of EI.

## Histone modifications

In somatic cells, DNA is wrapped around an octameric core of histone proteins (H2A, H2B, H3, and H4) to form a nucleosome (Marmorstein & Trievel, 2009). Histones’ N-terminal tails and globular domains undergo post-translational modifications (PTMs). Histone modifications are dynamic during development, vary across tissues, are regulated by specific enzymes, play a significant role in gene expression, and interact with other epigenetic control systems such as DNA methylation (Barth & Imhof, 2010). On the histone tails, there are over 60 different amino acid residues where modifications have been detected (Iwasaki et al., 2013). Histones can undergo various modifications, including acetylation, methylation, phosphorylation, ubiquitination and sumoylation among others (Kouzarides, 2007). Histone methyltransferase (HMT) enzymes methylate histones on Lysine (K) and Arginine (R) amino acids. Histone lysine residues can be mono-, di-, or tri-methylated, and these modifications

can function as either active or repressive marks. Methylation of H3K4, H3K36, and H3K79 is associated with transcriptional activation, whereas methylation of H3K9, H3K27, and H4K20 is associated with transcriptional repression (Sims, Houston, Magazinnik, & Rice, 2006; Vakoc, Sachdeva, Wang, & Blobel, 2006). These modifications can influence chromatin packaging and nucleosome positioning. Histone modifications, like DNAm, are spatially and temporally dynamic. Certain histone modifications, such as trimethylation of lysine 27 on histone 3 (H3K27me3), are generally associated with gene repression, whereas acetylation of the same residue (H3K27ac) is generally associated with gene activation (Lawrence, Daujat, & Schneider, 2016). Histone modifications regulate gene expression by recruiting protein complexes and controlling the accessibility of DNA to the transcription machinery (Lawrence et al., 2016). Histone modifications are a plausible mechanistic candidate in epigenetic inheritance because they can be modulated by the environment. During epigenetic reprogramming, some histone modifications in the germline and zygote are retained. Histones are spread onto newly assembled chromatin by sophisticated machinery (Marmorstein & Triivel, 2009). However, it is still unclear how histone codes are maintained during mitosis and meiosis (Erkek et al., 2013). Furthermore, during spermatogenesis, most histones are removed and replaced with protamines (Casas & Vavouri, 2014). Sperm contains protamine modifications that are similar to histone modifications (Brunner, Nanni, & Mansuy, 2014), despite this, their functional significance remains unknown, particularly during epigenetic inheritance. Disruption of the machinery that regulates histone modification could also be a key initiator of epigenetic inheritance (Siklenka et al., 2015). H3K9 and H3K27 methylation appear to be the most likely to be epigenetic among the various histone lysine methylation states, not only because they are key regulators of classic epigenetic phenomena (C. Huang, Xu, & Zhu, 2013). According to one model of epigenetic inheritance, marked parental histones inherited via DNA replication recruit histone modifiers to deposit similar marks on new adjacent nucleosomes, reestablishing the previous local landscape of histone modification (Saxton & Rine, 2019). These findings suggest that histone modifications can aid in epigenetic inheritance, though such a mechanism is normally obscured by H3K9 demethylation activity (Saxton & Rine, 2019).

## RNA

One haploid copy of the genome exists in the sperm nucleus, which is transcriptionally silent and not replicated due to the packaging of sperm chromatins during spermiogenesis. Also, the sources of sperm RNAs are unknown. Some RNAs are probably expressed endogenously within germ cells, but considering that short RNAs have been demonstrated to impact gene

expression outside of their tissue of origin, sperm RNA could come from elsewhere. Because RNAs are easily degraded, they are most likely transported with protein chaperones and, more likely, enclosed in extracellular vesicles. For example, in epididymosomes, which are extracellular vesicles that are released from the epididymal epithelium contain proteins, ncRNAs and a distinct set of lipids that are transferred to spermatozoa while they pass through the different epididymal regions (Sullivan, 2016). Aside from epididymosomes, RNAs have been found in exosomes and high-density lipoproteins (HDLs) in the bloodstream, as well as vesicles secreted by prostate cells (protostomes) and Sertoli cells, which come into direct contact with developing sperm. These interactions have not been studied in the context of transgenerational inheritance. Microinjections of RNA mixtures were used to recapitulate mutant phenotypes in functional tests of RNAs contribution to inheritance patterns. These findings imply that RNA plays a significant role in non-genetic inheritance. It is unclear how these transient RNA molecules can mediate epigenetic inheritance across cell divisions and generations on their own. Nonetheless, a growing body of evidence suggests that RNA may aid in the stable propagation of paternal effects from the soma to the germline, where they will be inherited by the next generation (Andersson et al., 2014; K. Gapp et al., 2020; van Steenwyk et al., 2020).

## Non-coding RNA

ncRNAs are broadly classified into two types: 1) long-ncRNA, greater than 200 nucleotides in length (lncRNAs) (Z. Li et al., 2012) and 2) small-ncRNA, less than 200 nucleotides (sncRNA) (Bouckenheimer et al., 2018). Small regulatory RNAs (siRNAs, miRNAs, tRNAs, and piRNAs) are non-coding RNAs that are expressed in the majority of eukaryotic cells. These small RNAs are bound by the Argonaute (AGO) or PIWI proteins and function as specificity factors (guide RNAs) to regulate other homologous RNAs at the transcription, stability, and translation levels. Small RNAs are found in the nuclei of most eukaryotes, where they regulate genome stability, heterochromatin formation, and transcription. ncRNAs are uniquely suited to transmit information across generations. A variety of ncRNA species can be found in both sperm and oocytes (Rando, 2016; Veselovska et al., 2015). There is evidence that sperm can acquire ncRNAs from surrounding somatic tissues (Robles, Valcarce, & Riesco, 2019). Thus, RNAs can circumvent and penetrate the theoretically impenetrable wall between somatic cells and the germline (the so-called Weismann barrier). This has significant implications for our understanding of epigenetic inheritance as a result of adult-life environmental insults. However, it is currently unknown how epigenetic messages transmitted by RNA are maintained across multiple cell divisions, let alone multiple generations.

## Transcription factors

Transcription factors (TFs) may also act as epigenetic information carriers. TFs are proteins that play a role in the process of transcribing DNA to RNA. TFs are found on the genomes of mature gametes, and there is evidence that TF binding can influence DNAm at the binding sites (Jones & Takai, 2001; Smith & Meissner, 2013). CpG sites bound by TFs during germ cell re-methylation are protected from methylation throughout development (Kremsky & Corces, 2020). During PGC and preimplantation development, DNAm can only occur at CpGs that are resistant to demethylation. This is due to the fact that TF binding during the re-methylation phase maintains the methylation status between generations (Kremsky & Corces, 2020). This suggests that transcription factors can act as carriers of epigenetic information during germ cell and pre-implantation development by maintaining CpG methylation status, and serve as the foundation for a mechanistic description of the transgenerational transmission of such information in mammals (Kremsky & Corces, 2020). Mammalian gametes contain complex patterns of 3D interactions that can also be transmitted to the zygote after fertilization (Jung et al., 2019). TFs may remain bound to chromatin after fertilization and influence gene expression in the developing embryo. According to a recent publication, BPA, either directly or indirectly, induces the binding of TFs at different regions of the genome in F1 generation sperm, altering the 3D organization of chromatin in mature F1 generation sperm, many of which are conserved in subsequent generations (Jung et al., 2020). Thus, TFs are a plausible candidate for transmitting epigenetic information.

## Extracellular vesicles

All cells can secrete various types of membrane vesicles known as extracellular vesicles (EVs). EVs vary greatly in size (30 nm to several micrometres in diameter), chemical composition, secretion mechanism and carrying molecules, all of the properties that lead to their different functions. EVs mediate cell-to-cell communication by activating receptors on the surface of acceptor cells (Bonsergent et al., 2021) and play roles in a variety of physiological and pathological processes, including blood coagulation, inflammation, stem cell expansion, neuronal communication, and tumorigenesis (Lo Cicero, Stahl, & Raposo, 2015). There are two major EV biogenesis pathways. The first biogenesis pathway buds EVs directly from the plasma membrane, resulting in what is known as microvesicles. The second biogenesis pathway involves intraluminal vesicle release caused by multivesicular endosome fusion with the plasma membrane, resulting in the formation of exosomes. Exosomes and microvesicles contain cargoes such as nucleic acids, proteins and lipids, RNAs (extracellular RNAs, exRNAs) and DNA (O'Brien, Breyne, Ughetto, Laurent, & Breakefield, 2020). The majority of known

ncRNA biotypes, including small nuclear RNAs, small nucleolar RNAs (snoRNAs), rRNAs, lncRNAs, piRNAs, tRNAs, mitochondrial RNAs, Y RNAs, and vault RNAs (vtRNAs), have been discovered in EVs in more comprehensive studies (Abels & Breakefield, 2016; O'Brien et al., 2020). ExRNA extraction, purification, and sequencing methods are much more susceptible to contamination and artefacts than cellular RNA preparations, due to the low amount of RNA available from EVs. As a result, analyzing exRNA samples can be difficult, and a specific tool for EV ncRNA data analysis has been developed (Rozowsky et al., 2019). A number of studies have shown the role of extracellular vesicles in epigenetic inheritance. Also, we found that extracellular vesicles are vectors of communication with the germline that play a role in epigenetic inheritance (Alshanbayeva et al., 2021), Chapter 2.

## Challenges in data analysis

### Multi-omics data integration

A single omics analysis may not provide enough information to provide a deep understanding of a biological system, but combining multiple omics experiments and data analyses can provide a more holistic view of a system. Performing different experiments on the same or different samples from the same biological conditions, such as RNA sequencing (RNA-seq), Assay for Transposase-Accessible Chromatin sequencing (ATAC-seq), chromatin immunoprecipitation with sequencing (ChIP-seq), and Bisulfite sequencing (BS-seq), results in multi-dimensional omics datasets, which enable the study of relationships between different biological processes, such as gene expression, chromatin accessibility, histone modifications, transcription factor binding, and DNAm, as well as the leveraging of multiple data types to draw inferences about these processes. Data integration is the process of combining disparate sources of information in order to gain a better understanding of complex systems. The researchers execute two forms of data integration: custom or ad-hoc integration and more systematic integration.

### Ad-hoc approaches

Integrating BS-seq data with RNA-seq is one example of an ad-hoc technique. The expressed genes are known to be demethylated. As a result, the methylation values of the promoters can be linked to the genes that are expressed. Integrating ATAC-seq data with RNA-seq data can be used to analyze TF activity. Regions with increased accessibility and expression would show a TF's role as an activator, while regions with increased accessibility and decreased expression would represent a TF's role as a repressor. For this, a tool exists, diffTF (Berest

et al., 2019), which estimates differential TF activity based on expression and chromatin data. The ad-hoc methods are scientifically motivated and produce biologically relevant outcomes. However, these ad-hoc approaches have several drawbacks, such as the need for extensive exploratory investigation and the inability to be applied consistently to all projects. Furthermore, these methods are frequently applied to a maximum of two omics datasets.

## Systematic approaches

Systematic methods developed for data integration in biological research can be classified into three types: supervised, unsupervised, and semi-supervised. Unsupervised data integration refers to methods that draw conclusions from input datasets without the use of labelled response variables (e.g., factorization, Bayesian, clustering, dimensionality reduction, coexpression and correlation). On the other hand, supervised data integration methods take into account phenotype labels (e.g., control or treatment) and use, for example, machine learning approaches to evaluate models (network-based and multi-kernel); semi-supervised data integration methods fall somewhere between supervised and unsupervised methods and use both labelled and unlabeled samples to develop a learning algorithm to infer information from unlabeled samples (S. Huang, Chaudhary, & Garmire, 2017). A few methods for integrating data from multivariate multi-omics experiments have been developed: Data Integration Analysis Using Latent Components for Biomarker Discovery (DIABLO) (Rohart, Gautier, Singh, & Lê Cao, 2017) - an extension to sparse generalized canonical correlation analysis (sGCCA) (Tenenhaus et al., 2014), a supervised approach which seeks for common information across different data types through the selection of a subset of molecular features; Multi-Omics Factor Analysis (MOFA) - an unsupervised method for decomposing the sources of heterogeneity in multi-omics data sets (Argelaguet et al., 2018, 2020) and; mixOmics (Rohart et al., 2017) - a package that hosts several supervised methods under its umbrella (DIABLO; sparse Partial Least Square—Discriminant Analysis, PLS-DA (Lê Cao, Boitard, & Besse, 2011) and Multivariate INTEGRative method, MINT (Rohart et al., 2017)).

Despite the fact that these tools have addressed critical challenges for multi-omics applications, they are not without limitations. One of the major limitations of most of these tools is that they can only incorporate data from the same omics experiments. This restricts users to utilize the same samples for all experiments, which is never the case in biological research due to the limited quantity of components of interest (DNA or RNA) and the high demand for these components for library preparation and sequencing. Another issue is that these methods assume that users have already normalized the data and corrected it for batches or confounding factors such as cage effect, sample composition, and time of day (Bruning et al., 2016). Based on the data types, methods should be able to optimally normalize the

data and correct it for confounding factors using supervised learning, which could improve uniformity, robustness, and precision. Another disadvantage is that some of the existing methods necessitate exploratory analysis prior to data integration. Exploratory data analysis is a critical process in many data science projects that requires advanced coding skills and takes a significant amount of time. The method should be able to perform automated data cleaning functions, such as outlier clipping, missing value imputation, and zero-variance variables, depending on the data types. It should also aid in exploratory analysis by providing summary statistics and plots for visual examination. Finally, most existing methods are designed to work with linear relationships and thus cannot be applied to more complex datasets that are related in a non-linear manner.

To summarize, integrating diverse and huge omics data is both a conceptual and practical problem in data analysis. Data integration has been used in omics research since the beginning of the era, and it is both a challenge and an opportunity. It is surely growing more popular. We devised and implemented a more straightforward and scientifically motivated approach to integrate multi-omics datasets, involving more than two omics datasets, please see Methods and Chapter 1.

## Short RNA data analysis

Short RNAs are a type of non-coding RNA that plays an important role in nearly all aspects of organismal development in both health and disease. Despite their importance in a wide range of biological processes, analyzing short RNA sequencing data remains a difficult task. Specifically, a number of computational challenges arise when analyzing short RNA sequencing:

- Even after size selection, we expect to sequence other RNA biotypes in addition to short RNAs.
- Short RNAs have a length of less than 200bp, often much shorter (e.g. miRNAs at 21-22bp), and can therefore often map to multiple positions. In this case, standard pipelines either map the reads randomly to one position, making it difficult to determine their true origin, or they are discarded, resulting in a large proportion of reads being lost.
- Many short RNAs are post-transcriptionally modified. For example, tRNAs receive a “CCA” sequence at the 3’ end (Hou, 2010), additionally, Histidine tRNAs receive a “G” sequence at the 5’ end (Cooley, Appel, & Soll, 1982), resulting in an unalignment problem.

- Because of their biogenesis, short RNAs often overlap multiple features. For example, mature miRNAs overlap with precursors, which can result in misassignment.
- rRNAs are typically masked in the genome, and the Ensembl (Howe et al., 2021) or GENCODE (Harrow et al., 2012) databases' annotations are unavailable, which make it difficult to quantify for rRNAs fragments.

All the aforementioned issues could lead to misalignment and low mappability of the sequenced data. Several tools have been developed to analyze short RNA-seq data, however, they typically fall prey to some of these issues. In Chapter 3, we, therefore, developed a novel approach to address them.

## Goals of thesis

We defined the following goals for my thesis:

1. Collaboration with all the members of the Mansuy lab to study epigenetic inheritance in the MSUS mouse model. Please see Chapter 2, Appendix A, and Appendix B for this part. I was responsible for:
  - Version controlled and reproducible data analysis for data generated from RNA-seq, short RNA-seq (sRNA-seq), ATAC-seq, whole-genome bisulfite sequencing (WGBS), and reduced representation bisulfite sequencing (RRBS)
  - Determine the qualitative and quantitative effects of early life experiences on the epigenome, particularly in germ cells. This includes identifying the epigenetic changes, including DNAm, RNA expression, ncRNAs, and chromatin accessibility, induced in germ cells due to early life experiences like traumatic stress in mice relating these changes to genome activity. This also includes determining whether and to what extent changes in the epigenome persist across life, and if they can be passed to the offspring and underlie epigenetic inheritance, and further, whether they can result in changes in DNA sequence across generations
  - Supervising and collaborating with colleagues who were performing data analyses themselves
  - Analyses of datasets using different tools
  - Multi-omics analysis of data from same cells/ tissues
  - Figure generation and interpretation for the manuscripts

2. Development of data analysis pipelines. Please see the Methods, for this part. I was responsible for:
  - Benchmarking methods for including in the pipeline
  - Testing different parameters of the tools for including in the pipeline
3. Collaboration with Dr. Irina Lazar for studying changes in spermatogonial stem cells across development. Please see Chapter 1 for this part. I was responsible for:
  - Computational design of the project
  - Version controlled and reproducible analysis of the datasets
  - Analyzing spermatogonial stem cells dataset generated from RNA-seq, sRNA-seq, RRBS, and ATAC-seq from the data generated in the lab
  - Analyzing spermatogonial stem cells dataset generated from RNA-seq, WGBS, and ChIP-seq from the publicly available datasets
  - Comparison of published datasets with the lab's
  - Analysis of ID4 ATAC-seq data from the literature and comparison with lab's dataset
  - Multi-omics data integration
  - Figures outline, figures generation, and interpretation for the manuscript
  - Writing methods, figure legends, and updating/ revising manuscript
4. Collaboration with Dr. Pierre-Luc Germain for the development of **shortRNA**, a tool for comprehensive analysis of sRNA-seq data in R. Please see Chapter 3 for this part. I was responsible for:
  - Development and testing of the tool
  - Data analysis using different methods for qualitative and quantitative comparison with shortRNA

# Bioinformatics methods

## Version controlled data analysis using git

Version control (also known as source control or revision control) is a software engineering process that involves managing changes to a computer program or document using a version control system (VCS). In graph theory, revisions form a directed acyclic graph that represents the growth line. The revisions to a computer program occur over time and can be tracked using revision numbers, timestamps, or descriptive text. While file copies have been used in the past to provide some form of version control, they are error-prone and time-consuming. The file is typically copied to another location, and unless the files are cleverly time-stamped, this simple approach may be error-prone.

Programmers developed a local VCS with a database that records all modifications to the files under revision control to keep track of the versions. A local VCS is an example of a revision control system (RCS). Since it is difficult to collaborate with a local VCS, a centralized VCS was developed, such as Apache Subversion (SVN). All changes to files are monitored under the centralized server using Centralized VCS. A centralized VCS, on the other hand, has significant drawbacks. No one can connect or save versioned changes to something they are working on if the server goes down for an hour. This leads to the development of the distributed VCS, such as git. In a distributed VCS, the repository can be completely mirrored, including the entire version history. A schematic of distributed VCS is shown in Figure 6, adapted from (Chacon & Straub, 2021).

GitHub ([github.com](https://github.com)) a distributed version control system, was used to manage data analysis projects and software development projects throughout this doctoral thesis work. One downside of using GitHub is that files greater than 50 megabytes cannot be hosted, which means that large files such as sequencing data, FASTQ files, and BAM files are not version managed. To solve this issue, git-fat was used, a version-controlled tool that offloads files to a local directory or another server (Brown, 2018).

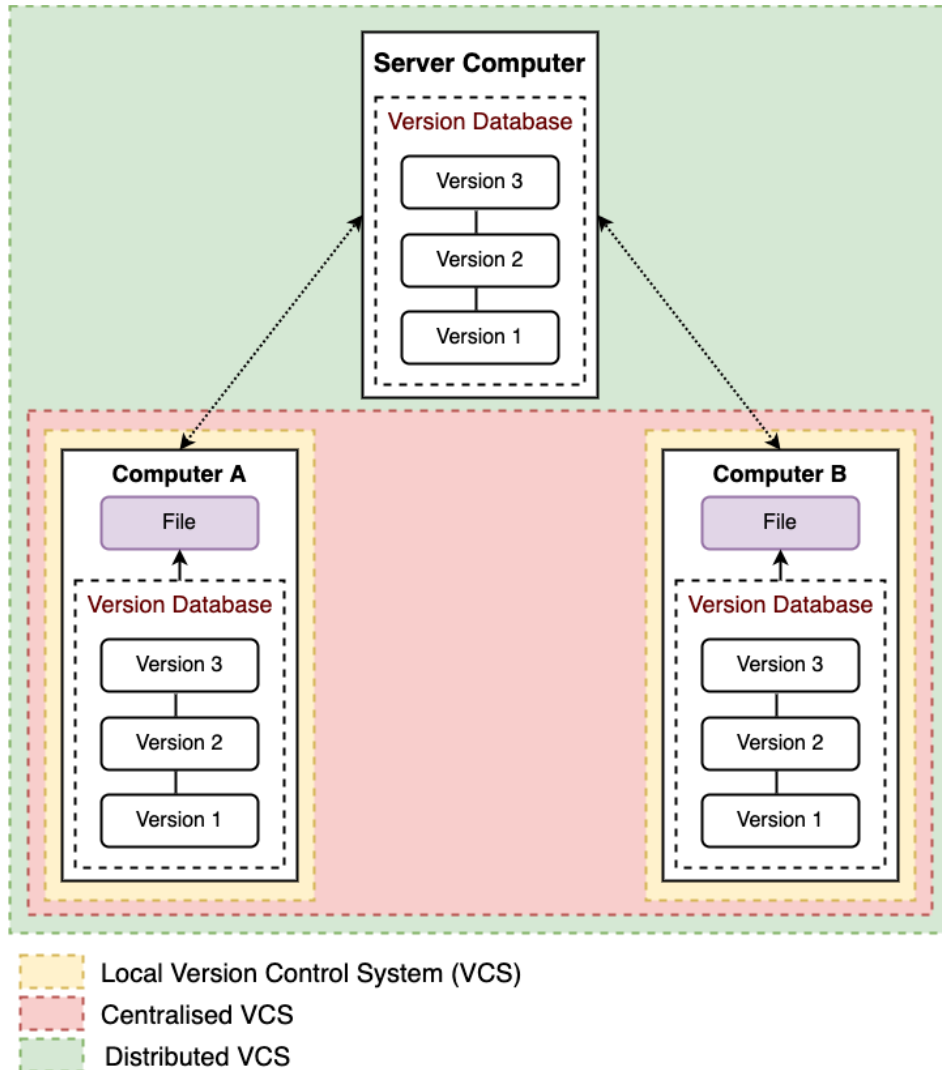


**Figure 6: Overview of version control system (VCS).** Adapted from (Chacon & Straub, 2021).

## Data analysis directory organization

ScienceCloud service of the University of Zurich was used for computing. On ScienceCloud, a data volume is mounted on my instance (virtual computer). In the data volume, two directories were created, namely “Data” and “Project”. The “Data” repository stores raw sequencing files, FASTQ files, and “gitfat” objects, while the Project directory stores all analysis and code and is version controlled with git. A schematic representation of this workflow can be seen in Figure 7. This is done for each dataset analysed.

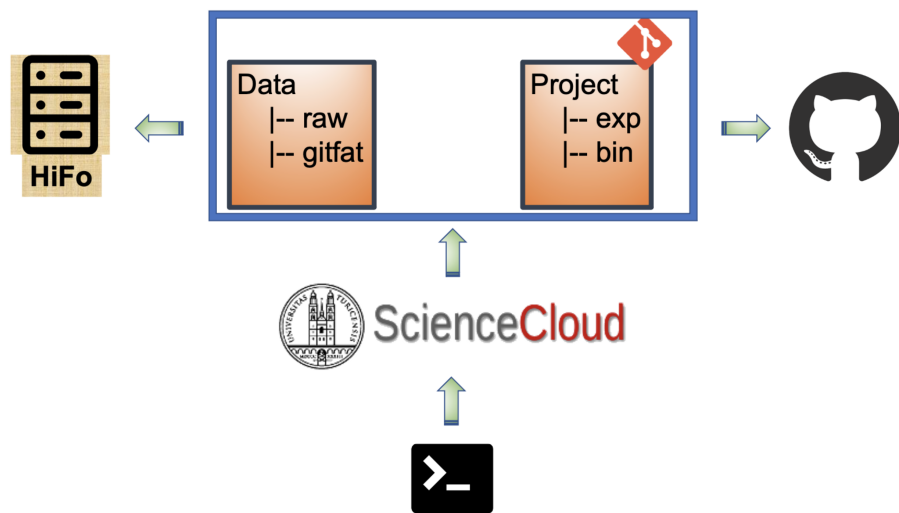


**Figure 7: Organization of data analysis projects.**

This organization of the data analysis projects ensures open and reproducible research. As all the analyses are version controlled, one can look at the analysis conducted back in time. Also, each analysis script has a log file, which stores the information of the tools version and any warnings or errors encountered during the analyses. Further, at the end of the project, the GitHub repository can be made public and all the code for intermediate data analysis are available to the research community.

## Pipelines for data analysis

I worked on multi-omics datasets for my doctoral research, which led to the development of data analysis pipelines for RNA sequencing (RNA-seq), Assay of Transposase Accessible Chromatin sequencing (ATAC-seq), Whole-genome bisulfite sequencing (WGBS), Reduced representation bisulfite sequencing (RRBS), Chromatin immunoprecipitation followed by sequencing (ChIP-seq), and short RNA sequencing (sRNA-seq).

## Quality check and trimming of sequencing datasets

The goal of data quality check and trimming is to find and clean any data quality issues in the dataset and possibly account for them. The sequencer determines the nucleotide bases in a DNA or RNA library during sequencing. A small sequence, known as a read, is created for each fragment in the library, which is a sequence of nucleotides. In a single experiment, sequencing technologies, such as Illumina, can generate a large number of sequence reads. The first step after receiving the sequenced data is to assess the data quality to determine the reliability of the sequenced reads. The FASTQ files are examined using **FastQC** (Andrews et al., 2012). **FastQC** provides a comprehensive view of the data, including the number of sequenced reads, base sequence quality, “N” content (if a sequencer cannot call a base, due to the technical limitations, it enters “N”; of each sequencing platform.), sequence duplication levels, and adapter information. A Hypertext Markup Language (HTML) report generated by the software, for each sample, helps to understand the pre-processing steps required. The quality assessment is done using the quality scores (Q-scores) in the FASTQ files, which are translated to quality statistics in **FastQC** reports and plotted as boxplots. Q score is defined as the base-calling error probabilities and is calculated by the formula:  $**Q = -\log_{10}(P)**$ . For instance, if a nucleotide base is assigned a Q score of 30, this is equivalent to the probability of an incorrect base call of 1/1000 times, which means that the accuracy of base calling is 99.9%. A Q score of 30 represents perfect base calling with no errors and ambiguities and is considered a benchmark for quality in high-throughput sequencing (HTS) (Ewing & Green, 1998).

(ref:mfc3) **Workflow for quality check and quality control for sequencing data.** QC: Quality Control. Adaptors are artificial DNA oligonucleotides and are required for sequencing by platforms like Illumina. During the process of Illumina library preparation, adaptors are ligated to the short DNA sequences. Because of the adapters (attached at the end of reads), the sequencing Q score is usually low, towards the end of the reads. Therefore, these are required to be removed before downstream processing of the data. Furthermore, the sequenced DNA reads could have trailing and leading ‘N’ (if a base caller fails to call a base at a genomic location, it will put ‘N’ instead of ‘A’, ‘T’, ‘G’ or ‘C’). Also, there is a chance that although long reads were sequenced, small reads appeared after sequencing, or they became shorter after removal of trailing or leading ‘N’. It is always better to get rid of small reads below a certain length, as they would be mapped to multiple locations and will lead to misinterpretation. Trimming is the process of modifying the ends of reads. Trimming can help to increase the number of reads that the aligner or assembler can successfully use, lowering the amount of unmapped or unassembled reads. **TrimGalore** is used to trim adapters and inferior ends of reads with a Phred score of less than 30 (`-q 30`), to remove Ns from both

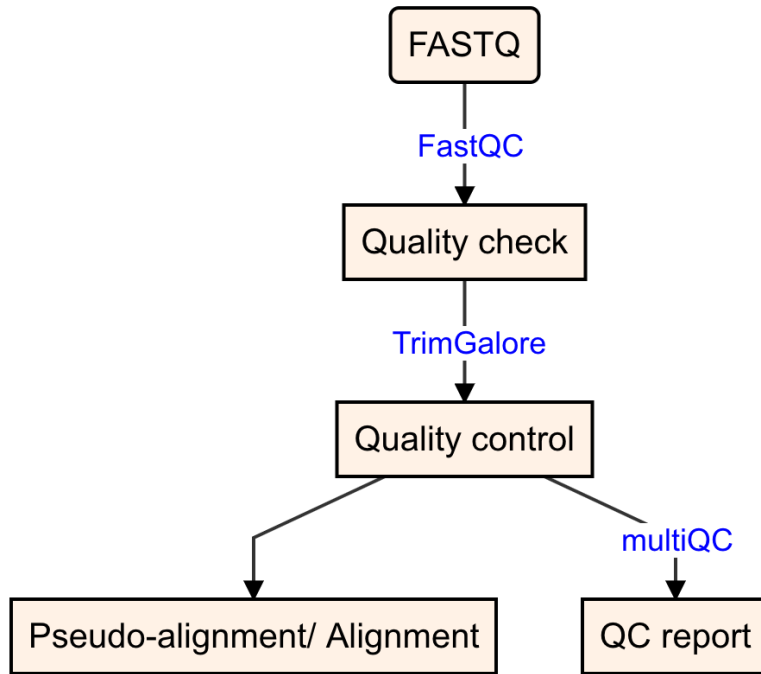


**Figure 8:** (ref:mfc3)

sides of reads (`--trim-n`), and to discard trimmed reads that are too short to be informative (e.g. `--length 30`, or 15 for small RNA-seq data). After this, all results are used to generate an overview report with `multiQC` (Ewels, Magnusson, Lundin, & Käller, 2016), which is a reporting tool that parses summary statistics from results of other bioinformatics data analysis tools. Finally, it is critical to recognize, identify, and rule out issues that may affect downstream analysis interpretation.

The trimmed data is then aligned to the reference genome, indexed with the specific tool needed for alignment. For example, for aligning WGBS data with the reference genome, the reference genome is first indexed with `Bismark`. This workflow is shown in Figure 8.

Some library preparation kits use the unique molecular identifier (UMI), which are complex indices and are added to the sequencing libraries before the polymerase chain reaction (PCR) amplification step. UMIs were first implemented in the iCLIP protocol (König et al., 2010) but has been implemented for RNA-seq, small RNA-seq, single-cell sequencing, ChIP-seq, and whole-genome sequencing (WGS).

## RNA sequencing

RNA sequencing (RNA-seq) is a technique that uses high-throughput sequencing (HTS) to investigate the quantity and sequences of RNA. It examines the transcriptome to determine, which of our DNA-encoded genes are turned on or off, and to what degree. RNA-seq pipeline

schematic is shown in Figure 9.

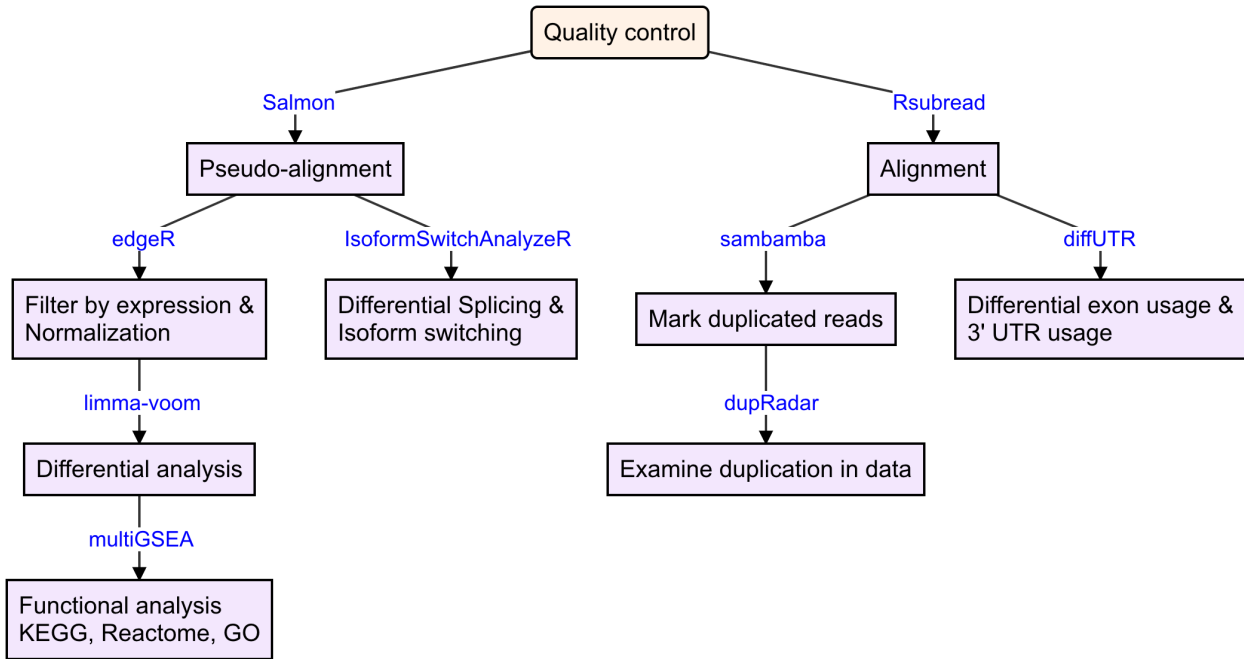


**Figure 9: Workflow for RNA sequencing data analysis.**

## Pseudo-alignment and alignment

Sequence alignment is used to determine where the sequences are similar to the reference genome and how similar they are. We can estimate where a read came from by aligning or “mapping” it to a reference genome or transcriptome. There are two families of methods for mapping reads in RNA-seq data: alignment and pseudo-alignment. For alignment, aligners such as **STAR** or **Rsusbread** are used. They align reads to a genome or transcriptome and perform spliced alignment. They return the reads’ base-level alignments. Transcript quantification tools such as **Salmon** (Patro, Duggal, Love, Irizarry, & Kingsford, 2017) and **Kallisto** (Bray, Pimentel, Melsted, & Pachter, 2016) instead perform pseudo-alignment. These tools use statistical inference to determine transcript abundances by mapping reads to the transcriptome. Alignments from the aligners can then be used for a variety of purposes, such as for feeding transcript assembly tools, for variant calling pipelines, or for transcript quantification tools.

Quality-controlled reads were pseudo-aligned using **Salmon** with automatic detection of the library type (`-l A`), correcting for sequence-specific bias (`--seqBias`), and correcting for fragment GC bias correction (`--gcBias`) on a `transcript` index prepared from GENCODE, with additional piRNA precursors and transposable elements (concatenated by family) from

Repeat Masker as in (K. Gapp et al., 2020). Downstream analyses including differential analysis; differential transcript usage and differential isoform switching; and functional analyses, are performed on the pseudo-alignment from **Salmon**.

Additionally, alignment is performed using the **Rsubread** package (Liao, Smyth, & Shi, 2019) using the **subjunc()** function, specific for RNA-seq data. Analysis of duplicates, differential exon usage, and differential 3' usage are performed on alignment obtained from **Rsubread**.

A direct comparison of genome alignment with transcriptome pseudo-alignment was performed in (Yi, Liu, Melsted, & Pachter, 2018) and the authors found that both approaches produce similar quantifications. However, (D. C. Wu, Yao, Ho, Lambowitz, & Wilke, 2018) suggested that it is not optimal to use alignment-free methods to analyze and quantify lowly expressed genes and small RNAs.

## Duplicated reads analysis

Duplicated reads are different copies of the exact same sequence. Unless a genomic region is highly expressed, most mRNA fragments are expected to be unique. A low degree of repetition may indicate that the target sequence is well-covered, whereas a high level of duplication is more likely to signal bias. Duplicate reads might be caused by PCR duplication or legitimately overrepresented sequences. Because PCR amplification is more efficient for some sequences than others, it can misrepresent the true proportion of sequences in the input, whereas truly overrepresented sequences are the result of very abundant transcripts in an RNA-Seq library and are an expected case and not of concern because they accurately represent the input.

Throughout the research, duplicated reads were marked in the aligned data using **sambamba** (Tarasov, Vilella, Cuppen, Nijman, & Prins, 2015), and further, the quality issues with PCR duplicates are analyzed using **dupRadar** (Sayols, Scherzinger, & Klein, 2016). **dupRadar** aids in separating the fraction of readings produced by artefacts from the fraction resulting from high expression.

## Differential expression analysis

Differential expression analysis (at the transcript or gene level) is the statistical examination of normalised read count data to find quantitative differences in expression levels between experimental groups.

Read counts at the transcript level are obtained from pseudo-aligned data and are aggregated at the gene level. Low counts of candidate genes/transcripts across samples give

minimal evidence for differential expression. When evaluating false discovery rates, they also add to the multiple testing burden, lowering the ability to find differentially expressed genes. A pre-filtering of counts is therefore performed using the `filterByExpr()` function from `edgeR` (Robinson, McCarthy, & Smyth, 2010) with a design matrix (matrix containing data about multiple characteristics of several samples, such as biological group, age, and batch for library preparation) and requiring at least 20 counts (`min.counts = 20`) (Germain, Sonrel, & Robinson, 2020). Next, the counts are normalized for different sequencing depths between samples and to eliminate composition biases between samples, for example, if there are a few highly expressed genes dominating in some samples, leading to fewer reads from other genes. Normalization factors are obtained using the `TMM` normalization method (Robinson et al., 2010) from the `edgeR` package, using the `calcNormFactors` function. `TMM` stands for Trimmed Mean of M values, in which the counts for the samples are scaled using a weighted trimmed mean of the log expression ratios. Differential expression analysis at gene and transcript level is performed using `limma-voom` (C. W. Law, Chen, Shi, & Smyth, 2014) pipeline from `limma` (Ritchie et al., 2015) package.

## Exploratory data analysis

Exploratory data analysis of counts (using principal component analysis, PCA), differential analysis results (volcano plot, MA plot, and heatmap), and assessment of library composition is performed using `plgINS`, a versatile R package, ([github.com/ETHZ-INS/plgINS](https://github.com/ETHZ-INS/plgINS)), under development by Dr. Pierre-Luc Germain. The package also comes with a shiny application.

## Differential transcript usage and differential isoform switching

Differential transcript usage (DTU) analysis looks for proportional differences in the makeup of a gene's transcripts between conditions.

DTU is performed using `IsoformSwitchAnalyzeR` (Vitting-Seerup & Sandelin, 2017, 2019). Isoforms are annotated via integration of a wide range of (predicted) annotations: Pfam was used for prediction of protein domains, CPC2 (version 2.0) for calculation of the coding potential, SignalP (version 5.0) for prediction of Signal Peptides, and IUPred2A was used to predict Intrinsically Disordered Region (IDRs) and Intrinsically Disordered Binding Regions (IDBRs). The results from Pfam, CPC2, IUPred2A, and SignalP are used with `IsoformSwitchAnalyzeR` for annotation and prediction of functional consequences for the identified isoform changes.

## Differential exon usage and differential 3' untranslated regions usage

Differential exon usage (DEU) analysis looks for variations in exon usage between experimental conditions. mRNAs' 3' untranslated regions (3' UTRs) are best recognized for regulating mRNA-based functions such as mRNA localization, stability, and translation (Mayr, 2019). Differential UTR usage looks for variations in 3' UTR usage between experimental conditions.

DEU and differential 3' UTR usage are performed using the diffUTR R package (Gerber, Schratt, & Germain, 2021).

## Functional analysis

The output of RNA-seq differential expression analysis is a list of significant differentially expressed genes (DEGs). The goal of functional analysis is to provide biological insight of DEGs. Functional analysis on Kyoto Encyclopedia of Genes and Genomes (KEGG) (Kanehisa, Furumichi, Sato, Ishiguro-Watanabe, & Tanabe, 2021), Reactome (Jassal et al., 2020), Gene Ontology (GO) (Consortium, 2021) and curated pathway list from the Gene Set Enrichment Analysis (GSEA) (Subramanian et al., 2005) databases is performed using multiGSEA ([github.com/lianos/multiGSEA](https://github.com/lianos/multiGSEA)), which facilitates the analysis with GOseq (Young, Wakefield, Smyth, & Oshlack, 2010), fGSEA (Korotkevich et al., 2016), Correlation Adjusted MEan RAnk gene set test (CAMERA) and camera pre-ranked (CAMERA-PR) (D. Wu & Smyth, 2012), ROtation testing using MEan Ranks (ROMER) and fry (Ritchie et al., 2015), and ROtAtion gene Set Testing (ROAST) (D. Wu et al., 2010). An advantage of using multiGSEA is that it has standardized input and output and provides a Shiny app for exploratory data analysis ([github.com/lianos/multiGSEA.shiny](https://github.com/lianos/multiGSEA.shiny)). With multiGSEA, it is easy to specify to use testing relative to a threshold (TREAT) method (McCarthy & Smyth, 2009), which takes a user-specified log fold change cut-off and recalculates the moderated t-statistics and p-values. Using TREAT only affects enrichment tests that first threshold the genes in the experiment as “significant” or not, like GOseq and not tests like the camera.

## Assay of Transposase Accessible Chromatin sequencing

The Assay of Transposase Accessible Chromatin sequencing (ATAC-seq) is widely used in studying chromatin biology to study chromatin accessibility and to identify open chromatin regions (OCRs). The nucleosome is the most basic component of chromatin. Each nucleosome is made up of about two turns of DNA wrapped around a set of eight proteins called histones known as histone octamer. With the help of nucleosomes, the genome is securely packed and structured, known as chromatin. The organization and accessibility of DNA are influenced by a number of factors, including chromatin structure, nucleosome location, transcription

factors, and histone modifications. As a result, these factors have a role in the activation and inactivation of genes. The genome is treated with a hyperactive version of the Tn5 transposase to insert sequencing adapters into OCRs (Buenrostro, Wu, Chang, & Greenleaf, 2015). Because it is easier, faster, and uses fewer cells than competing approaches like FAIRE-Seq and DNase-Seq, ATAC-Seq has become popular for discovering accessible regions of the genome. The schematic of the ATAC-seq pipeline is shown in Figure 10.

### **Alignment, post-alignment quality control, and peak calling**

Alignment of the ATAC-seq data is performed using `Bowtie2` (Langmead & Salzberg, 2012) with the following parameters: fragments up to 2 kb were allowed to align (`-X 2000`), entire read alignment (`-end-to-end`), suppressing unpaired alignments for paired reads (`-no-mixed`), suppressing discordant alignments for paired reads (`-no-discordant`) and minimum acceptable alignment score with respect to the read length (`-score-min L,-0.4,-0.4`). Tn5 inserts adapters separated by 9bp when it cuts an accessible chromatin region (Kia et al., 2017). This indicates that reads on the positive strand should be adjusted 4 bp to the right and reads on the negative strands should be shifted 5 bp to the left in order for the read start site to reflect the centre of where Tn5 binds as done in (Buenrostro, Giresi, Zaba, Chang, & Greenleaf, 2013), which is important for the footprint analysis. Using `alignmentSieve` from `deepTools` (Ramirez et al., 2016), aligned data (BAM files) are adjusted for the read start sites to represent the centre of the transposon cutting event (`-ATACshift`), and filtered for reads with a high mapping quality (`-minMappingQuality 30`). In addition, because the mitochondrial genome is devoid of chromatin packaging (Bogenhagen, 2012) a large number of mitochondrial reads can be a concern in ATAC-seq. Some ATAC-Seq samples have been found to include 80% mitochondrial reads, prompting the development of wet-lab approaches to address the problem (Corces et al., 2017). Also, because the open chromatin regions of interest are typically found in the nuclear genome, mitochondrial reads are typically excluded from the analysis. Hence, reads mapping to the mitochondrial chromosome and ENCODE blacklisted regions (regions where genome assembly results in erroneous signal) were filtered using `alignmentSieve`. Because ATAC-seq does not require rigorous size selection during library preparation, it can identify nucleosome positions using fragments representing nucleosome-free fragments (NFFs) nucleosome monomers, and multimers. There is approximately 147 bp of DNA wrapped around a nucleosome, and in order to obtain NFFs, which are indicative of transcription factor bindings, the fragments less than 147 bp must be extracted. To extract NFFs, all aligned files are merged within experimental groups, reads are sorted by left-most coordinates and indexed using `SAMtools` (H. Li et al., 2009), and NFFs were obtained by selecting alignments with a template length between 40 and 140 inclusively (Goodnight et al., 2019; Jung et

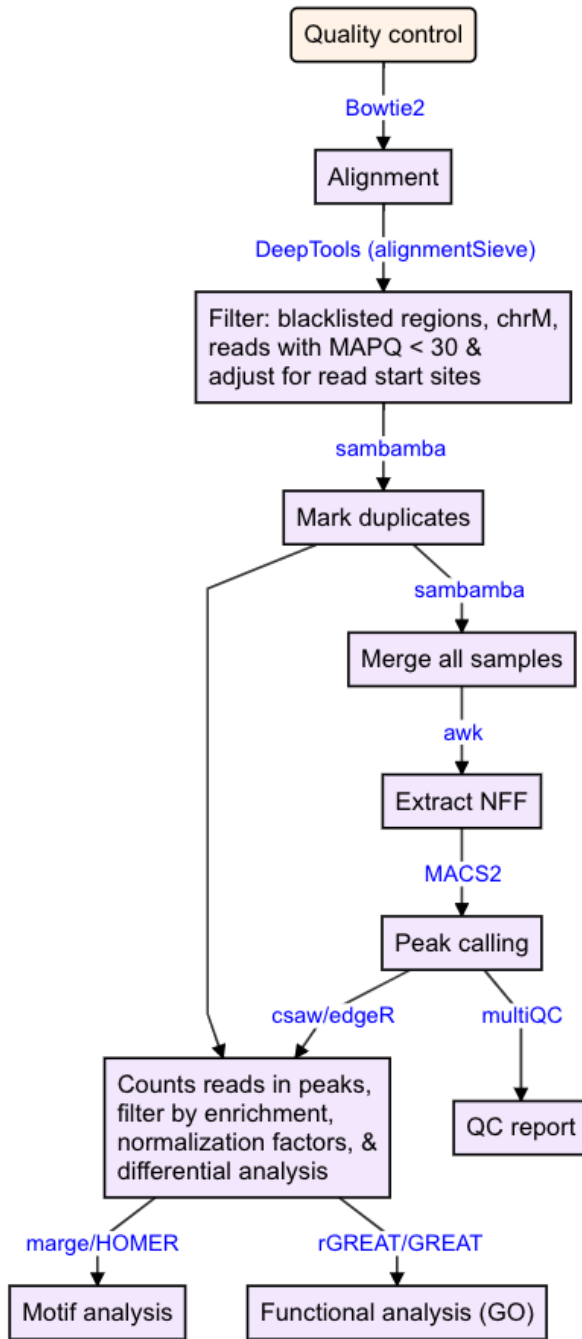


**Figure 10: Workflow for ATAC sequencing data analysis.** QC: Quality Control, NFF: Nucleosome Free Fragments.

al., 2017). Peak calling is a statistical approach that leverages data coverage properties to identify locations that are enriched as a result of protein/ transcription factor binding. To find regions corresponding to potential OCRs in the nucleosome-free regions, we want to identify regions where reads have piled up greater than the background read coverage. Peak calling on the NFFs is performed using MACS2 (Y. Zhang et al., 2008) with genome size in base-pair (-g genomeSize) and specifying the paired-end BAM file format (-f BAMPE).

### Peaks annotation and differential accessibility analysis

The goal of peak annotation is to map peaks to the regulatory elements. The peaks are annotated with transcript, and the distance to the nearest transcription start site, based on overlap with gene transfer format (GTF) file obtained from the GENCODE. The number of extended reads overlapping in the peak regions is calculated using the csaW package (Lun & Smyth, 2015). Peak regions that did not have at least 15 reads in at least 40% of the samples were filtered out. Normalization factors were obtained on the filtered peak regions using the TMM normalization method (Robinson et al., 2010) and differential accessibility analysis is performed using the Genewise Negative Binomial Generalized Linear Models with Quasi-likelihood (glmQLFit) test from the edgeR package. edgeR has recently been benchmarked and recommended for differential chromatin accessibility analysis (Gontarz et al., 2020).

### Functional analysis

GO analysis is performed on differentially accessible regions (DARs) with the rGREAT package ([github.com/jokergoo/rGREAT](https://github.com/jokergoo/rGREAT)), which is a wrapper around the Genomic Regions Enrichment of Annotations Tool (GREAT) (McLean et al., 2010). Transcription factor motif enrichment analysis is performed using the marge package (Amezquita, 2018), which is a wrapper around the Homer tool (Heinz et al., 2010).

### Differential accessibility analysis at transposable elements

Transposable elements (TEs) GTF file is obtained from [http://labshare.cshl.edu/shares/mhammelllab/www-data/TEtranscripts/TE\\_GTF/mm10\\_rmsk\\_TE.gtf.gz](http://labshare.cshl.edu/shares/mhammelllab/www-data/TEtranscripts/TE_GTF/mm10_rmsk_TE.gtf.gz). The GTF file provides hierarchical information about TEs: **Class** (level 1, eg. LTR), **Family** (level 2, eg. LTR L1), **Subtype** (level 3, eg. LTR L1 L1\_Rod), and **Locus** (level 4, eg. LTR L1 L1\_Rod L1\_Rod\_dup1). TE loci are annotated based on overlap with GENCODE as described above for ATAC-seq peaks. Filtered BAM files (without reads mapping to blacklisted or mitochondrial regions) are used for analyzing TEs. Mapped reads are assigned to TEs using featureCounts from the

R package `Rsubread` (Liao et al., 2019) and were summarized to Subtypes (level 3), allowing for multi-overlap with fractional counts, while ignoring duplicates. The number of extended reads overlapping at the TE loci is obtained using the `cshaw` package (Lun & Smyth, 2015). Subtypes that did not have at least 15 reads, and loci that did not have at least 5 reads in at least 40% of the samples, were filtered out. Normalization and differential accessibility analysis is performed as described above for the peaks. GO and motif enrichment analysis is performed as described above for the peak regions.

## Chromatin immunoprecipitation followed by sequencing

A substantial part of gene expression regulation is controlled by protein-DNA interactions. Proteins like transcription factors and histones influence how much and where genes are expressed. ChIP, followed by sequencing, can be used to investigate the interaction between a DNA sequence and a protein. There are two types of ChIP: cross-linked ChIP (X-ChIP) and native ChIP (N-ChIP). Formaldehyde is utilized to crosslink histones to DNA, and ultrasound sonication is used to fragment the DNA in X-ChIP, whereas the native covalent interaction between protein and DNA is exploited in N-ChIP (Park, 2009). The fundamental purpose of ChIP is to map global binding sites for any protein of interest, such as transcription factors (TF) and histones, in order to investigate specific modifications. *In vivo*, the approach generates a library of DNA locations bound to the protein of interest. Following ChIP on samples, library preparation, PCR amplification, and ultimately deep sequencing are performed. The schematic of the ChIP-seq pipeline is shown in Figure 11.

### Alignment and peak calling

Alignment is performed using `Bowtie2`. Reads with more than 3 mismatches are removed from the aligned data, as suggested in (Royo, Stadler, & Peters, 2016), and reads with low mapping quality (`-minMappingQuality 30`) or mapping to the mitochondrial chromosome or aforementioned blacklisted regions are also filtered out. Peak calling is performed using `MACS2` with mouse genome size in base-pair (`-g genomeSize`) and the BAM file format (`-f BAM/PEBAM`), together with the ChIP input sample.

### Peaks annotation, differential analysis, and functional analysis

These analyses are performed as described above for the ATAC-seq peaks.

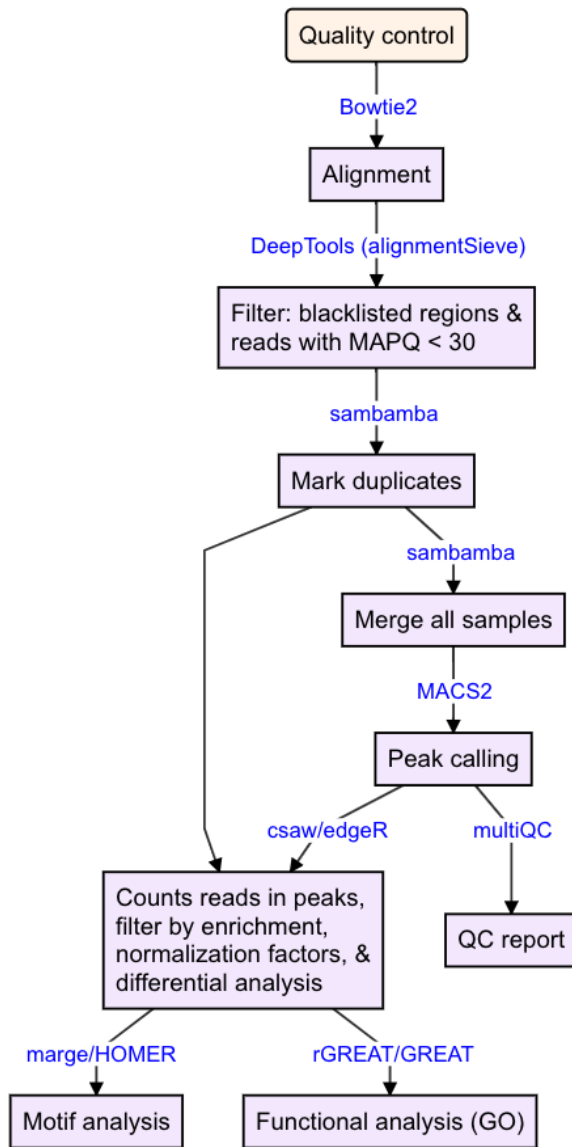


**Figure 11:** Workflow for ChIP sequencing data analysis. QC: Quality Control.

## Bisulfite sequencing

DNA methylation (DNAm) involves the addition of methyl groups to the DNA molecule. It most normally occurs at the C5 position of cytosines inside CpG dinucleotides, where it is stable during mitosis and meiosis. Methylation can change the activity of DNA without changing its sequence. DNAm is a reversible, cell-type-specific DNA modification that is usually persistent through cell division. It is not equally distributed across the genome, but rather is linked to CpG density. High-throughput bisulfite sequencing is one of the most reliable methods for measuring DNA methylation. In bisulfite conversion, unmethylated cytosine residues are converted to uracil, but methylated cytosines remain intact (Frommer et al., 1992), allowing methylation and unmethylated cytosine bases to be distinguished. Following PCR amplification, these uracils are converted to thymines. This is followed by the WGBS. WGBS is considered a gold-standard technology for DNA methylation detection as it provides a qualitative, quantitative, and efficient technique to identify 5-methylcytosine at single base-pair resolution. The cost of sequencing an entire genome is typically quite high. As a result, despite its use on huge genomes like the human genome, significant numbers of individual samples are rarely sequenced. For this reason, RRBS was developed, in which the bisulfite process occurs but only around 1% of the genome is sequenced. This makes it possible to sequence the genomes in greater numbers. The idea behind RRBS is to enrich the sequencing library with CpG-dense sections of the genome to boost the sequencing depth of cytosine-rich areas (Meissner et al., 2005). This is done by using CpG-specific restriction enzymes like MspI, which identifies the sequence 5'-CCGG-3'. MspI cleaves the complete genome in RRBS, leaving at least two cytosines per cleaved DNA fragment (one cytosine at either end of the MspI-MspI fragment). Sequencing libraries are made from size-selected MspI DNA fragments, followed by bisulfite conversion and sequencing of the converted library. The schematic of the BS-seq pipeline is shown in Figure 11.

## Alignment and methylation calling

Mismatches between the reads and the reference genome are introduced during bisulfite conversion, resulting in slow and imprecise mapping. Further, the DNA code's complexity is reduced. Hence, specialized tools are required for aligning the bisulfite sequencing data. Alignment of the bisulfite sequencing data is performed using **Bismark** (Krueger & Andrews, 2011) on a genome index built using **Bismark\_genome\_preparation**. Methylation information for individual cytosines (methylation calls) is extracted using the **Bismark\_methylation\_extractor** tool from the **Bismark** package.

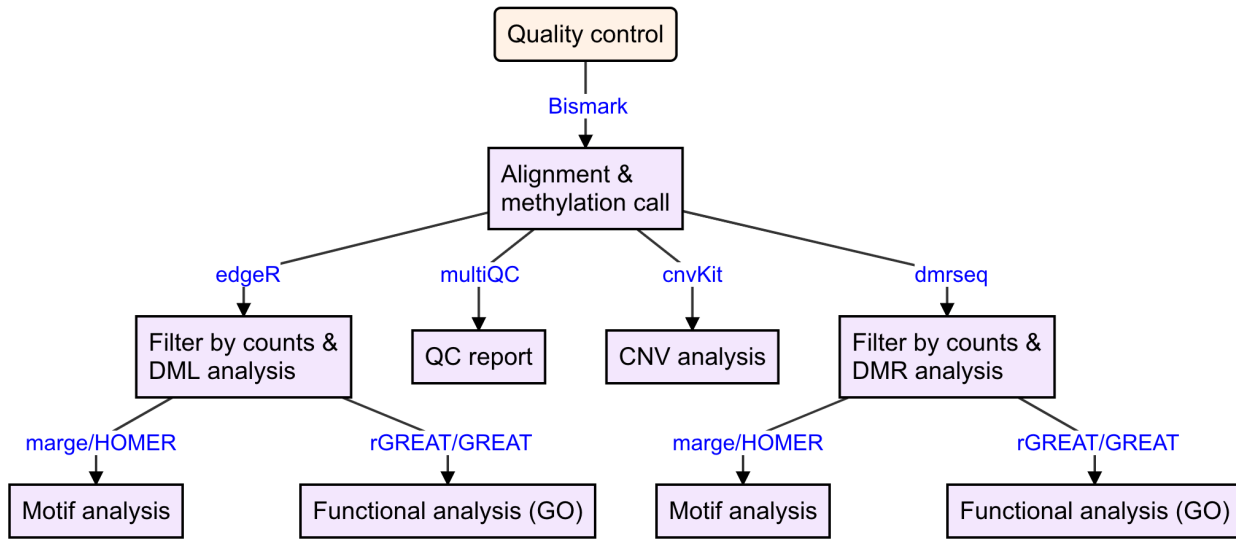


**Figure 12: Workflow for Bisulfite sequencing data analysis.** QC: Quality Control, DML: differentially methylated loci, DMR: differentially methylated regions, CNV: copy-number variation.

## Differential methylation analysis

Differential analysis can be performed at the loci level (differentially methylated loci, DML) or at the region's level (differentially methylated regions, DMRs). For the identification of DML and DMRs, the data is first filtered by the coverage among samples. DML are identified using `edgeR`. Identification of DMRs is not so straightforward, as defining regions boundaries is not easy the tool has to take into account correlation across loci of a region. Hence, during a course, we benchmarked different tools for detecting DMRs [dktanwar.github.io/sta426-project-dmr-comparison](https://dktanwar.github.io/sta426-project-dmr-comparison) and found `dmrseq` to outperform all other methods that we compared. DMRs from RRBS data are identified using the parameters recommended by Dr. Keegan Korthauer, author of `dmrseq` ([github.com/kdkorthauer/dmrseq/issues/14](https://github.com/kdkorthauer/dmrseq/issues/14)).

## Copy number variation analysis

The phenomenon of copy number variation (CNV) occurs when regions of the genome are repeated and the amount of repeats differs between individuals. CNV is a type of structural variation that occurs when a duplication or deletion event occurs that impacts a large number of base pairs. To infer and visualize CNV from WGBS data, we use the CNVkit (Talevich, Shain, Botton, & Bastian, 2016).

## DML and DMR annotation, and functional analysis

These analyses are performed as described above for the ATAC-seq data.

## Short RNA-seq

The short RNA-seq pipeline is not described in this section, as a method for analyzing small RNA-seq data has been developed and is discussed in detail in Chapter 3.

## Multi-omics analysis

Using different experiments, followed by sequencing, on the same samples or cells/tissues, such as RNA-seq, ATAC-seq, ChIP-seq, and BS-seq, results in multi-dimensional omics datasets that can be used to investigate relationships between different biological processes, such as gene expression, chromatin accessibility, histone modifications, and DNA methylation. Integrating multi-omics datasets is most challenging and is not straightforward to perform, as there are no standard recipes.

We present a straightforward and biologically useful approach for performing multi-omics analysis on RNA-seq, ATAC-seq, ChIP-seq, and BS-seq datasets. First, we overlap the DARs with ChIP-seq peaks enrichment, RNA-seq expression of overlapping genes with DARs, and methylation values of DARs overlapping loci from BS-seq data into one matrix, overlapMatrix. The DARs are initially divided into proximal (less than +/- 2.5 kb from a TSS) and distal (more than +/- 2.5 kb from a TSS) regions, as per the ENCODE guidelines (Harrow et al., 2012; Thurman et al., 2012); the proximal regions are further divided into active and inactive (proximal active and proximal inactive) groups based on nearby gene expression (if nearby gene expression is detected) (**step 1**). Next, these three groups are separated based on whether the biological groups are more or less accessible (**step 2**). This classification would reveal six separate clusters of DARs, each with its own biological profile. Further, proximally active genes are categorised based on their up/ down expression (**step 3**). Moreover, we categorised DARs depending on whether they had H3K4me3, which is a critical marker for the active transcription and developmentally stable genes (L. Fu & Zhang, 2019); H3K27ac, which is associated with the higher activation of transcription and therefore defined as an active enhancer mark (T. Zhang, Zhang, Dong, Xiong, & Zhu, 2020); or dual H3K4me3/H3K27ac enrichment (Beacon et al., 2021); as well as H3K27me3 enrichment, which is involved in transcriptional silencing (Bogliotti & Ross, 2012) (**step 4**). The schematic is shown in Figure 13. Furthermore, gene ontology and TF motif enrichment analysis can be done on these categorised DARs. For a more in-depth understanding, all of the regions can be further classified based on their methylation state (high or low). Please see Chapter 2 for an application of this multi-omics analysis.

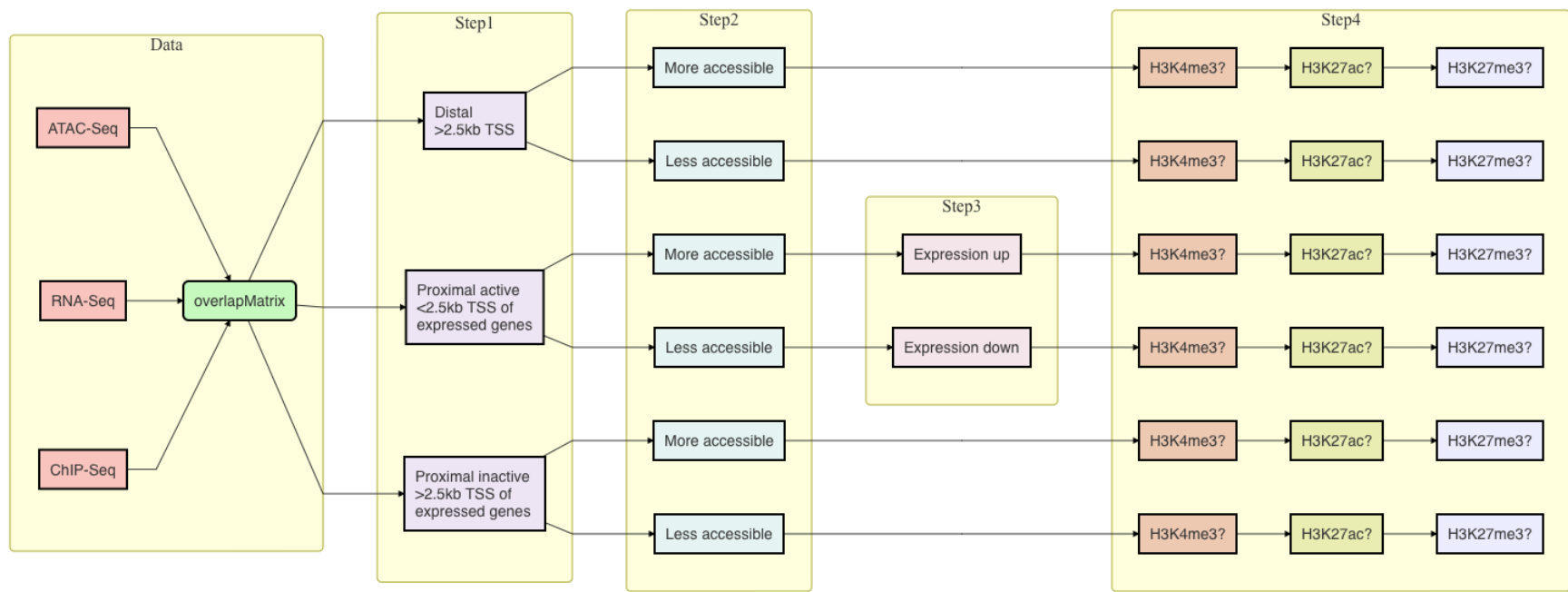


Figure 13: Workflow for multi-omics data integration.

Visualization of these regions is an essential step. We used EnrichedHeatmap (Gu, Eils, Schlesner, & Ishaque, 2018) and ComplexHeatmap (Gu, Eils, & Schlesner, 2016) packages for the visualization of categorized DARs.

**ATAC-seq:** ATAC-seq data is the starting point and we first find the middle of each DARs. After that, we obtain the coverage for 1kb upstream and downstream from the middle of DARs. We use the `normalizeToMatrix` function from the EnrichedHeatmap package and normalized the signal using the weighted mean between the intersected parts and un-intersected parts(`mean_mode = "w0"`) in a window of 50bp. In the normalized matrix, each row corresponds to DAR and each column corresponds to a window either on upstream or downstream of middle of the peak.

$$v_{w0} = \frac{\sum_{i=1}^n x_i w_i}{W + W'}$$

$W$  is the sum of width of the intersected parts ( $\sum_i^n w_i$ ) and  $W'$  is the sum of width for the non-intersected parts.

For visualization, DARs are ordered by the enriched scores. For each DAR in the matrix, values are denoted as  $x$ , indices as  $1, \dots, n_1$  for upstream windows, indices as  $n_1 + 1, \dots, n$  for downstream windows, and  $n_2 = n - n_1$  are the enriched score that are calculated as the sum of  $x$  weighted by distance to middle of the peak. DAR has a higher enriched score when there is more signal focused on it.

$$\sum_{i=1}^{n_1} x_i \cdot i / n_1 + \sum_{i=n_1+1}^n x_i \cdot (n - i + 1) / n_2$$

Moreover, we also plot the log[2]fold-changes of DARs using ComplexHeatmap.

**ChIP-seq:** ChIP-seq data coverage for 1kb upstream and downstream from the mid of DARs is obtained. We use the `normalizeToMatrix` function from the EnrichedHeatmap package and normalized the signal using the weighted mean between the intersected parts and un-intersected parts (`mean_mode = "w0"`) in a window of 50bp.

**BS-seq:** BS-seq data methylation values for 1kb upstream and downstream from the mid of DARs is obtained. We use the `normalizeToMatrix` function from the EnrichedHeatmap package and normalized the signal using the mean of all the signals (`mean_mode = "absolute"`) in a window of 50bp.

$$v_a = \frac{\sum_{i=1}^n x_i}{n}$$

**RNA-seq:** For RNA-seq data, we used ComplexHeatmap to plot the log[2]-fold-changes of expression values between the groups, and also the log[2]-fold-changes obtained after the

differential analysis.

# Chapter 1

## Dynamic chromatin accessibility in spermatogonial cells for transcriptional programings from early postnatal to adult stages

Deepak K Tanwar<sup>1,2,3,†</sup>, Irina Lazar-Contes<sup>1,2,3,†</sup>, Pierre-Luc Germain<sup>1,2,3,4</sup>, Isabelle M Mansuy<sup>1,2,3,#</sup>

<sup>1</sup>Laboratory of Neuroepigenetics, Brain Research Institute at the Medical Faculty of the University of Zurich.

<sup>2</sup>Institute for Neuroscience of the Department of Health Sciences and Technology, ETH Zurich, Zurich, Switzerland.

<sup>3</sup>Zurich Neuroscience Center, ETH and University of Zurich, Zurich, Switzerland.

<sup>4</sup>Statistical Bioinformatics Group, Swiss Institute of Bioinformatics, Zurich, Switzerland.

†Equal contributions

#Corresponding author

**Contributions:** *I performed data analysis, generated figures, wrote computational methods and figure captions, revised manuscript.*

## 1.1 Update on the new data analysis

This project has undergone two major changes as a result of the replacement of one of the spermatogonial cells (SCs) RNA-seq datasets by a better one.

### 1.1.1 Code availability

- BioRxiv version: bioRxiv\_v1
- This thesis version: thesis\_manuscript
- New analysis after inclusion of new RNA-seq data: deepak

### 1.1.2 Inclusion of RNA-seq data from the literature

Adult SCs RNA-seq data from the lab was excluded since it was obtained from polyA RNA-seq, as opposed to pups' RNA-seq, which was Total RNA-seq. In the preprint version of the manuscript (Lazar-Contes, Tanwar, Germain, Gaur, & Mansuy, 2020), we used RNA-seq data generated in the lab from SCs at the developmental stages postnatal day 8 (PND8), PND15, and postnatal week 21 (PNW21; also termed as adults in the manuscript). The RNA-seq datasets from PND8 and PND15 were generated using total RNA libraries, whereas the datasets from PNW21 were generated using polyA RNA libraries. Because polyA and total RNA-seq datasets are not directly comparable (Zhao, Zhang, Gamini, Zhang, & Schack, 2018), we obtained RNA-seq data from the PND7, PND14, and PNW8 stages from the literature (Hammoud et al., 2014, 2015) and compared it to the lab's RNA-seq data.

First, we compared the gene expression of lab PND8 samples to PND7 from literature and lab PND15 samples to PND14 from literature and discovered a strong correlation; however, data from PNW8 and PNW21 were not well correlated (result not shown). Following that, we performed differential analysis on data from the lab: PND15 vs PND8 and PNW21 vs PND15, as well as data from the literature: PND14 and PND7, and PNW8 and PND14. We compared the log<sub>2</sub> fold-changes from PND14 vs PND8 with PND15 vs PND8, and PNW8 vs PND14 with PNW21 vs PND15 after differential analysis. We discovered that the correlation between PND14 vs PND8 and PND15 vs PND8 was 52% ( $R = 0.52$ , Pearson method) and that most of the genes were changing in the same direction, whereas the correlation between PNW8 vs PND14 and PNW21 vs PND15 was negative 16% ( $R = -0.16$ ; Pearson method) and that around 50% of the genes were changing in the opposite direction, as shown in Figure 1.1A. As a result, we incorporated the PND14 and PNW8 datasets into our project to better compare developmental stages. We used differential analysis between PNW8 and PND14

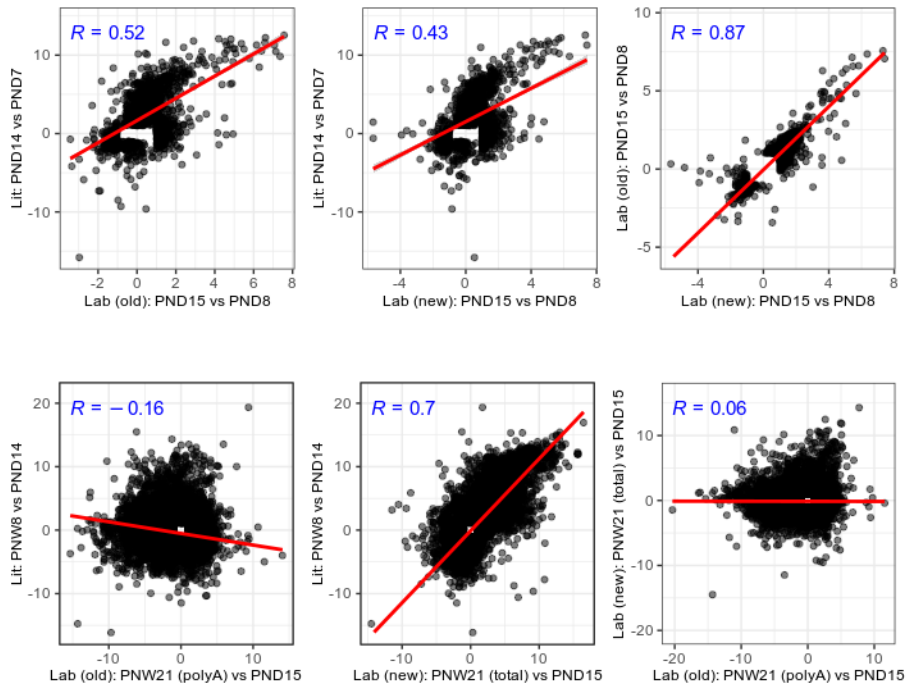


**Figure 1.1:** Log<sub>2</sub> fold-change comparison of RNA-seq data from the literature and lab (old and new).

rather than PNW8 and PND15 because the PND14 and PND15 samples were sequenced separately and could have unaccountable batch effects. These analyses were then updated in the manuscript and appear in Chapter 1.

### 1.1.3 New RNA-seq data from lab

Because of these limitations, we decided to generate new SCs data in the lab. Previously, the “Takara total RNA pico input mammalian kit v2” was used to generate libraries, but this kit is no longer available. The new RNA-seq dataset was obtained from the total RNA libraries prepared using the “Takara total RNA pico input mammalian kit v3.” Furthermore, PND8 and PND15 libraries were previously sequenced on the Illumina HiSeq 4000 platform, which is no longer available for sequencing at the Functional Genomics Center Zurich (FGCZ). To avoid any technical/ batch effects, we therefore re-sequenced the total RNA libraries from PND8 and PND15 on the Illumina NovaSeq platform using the “Takara total RNA pico input mammalian kit v3” along with the PNW21 total RNA libraries.

First, we compared the newly sequenced data to data generated previously in the lab and from the literature. We discovered that gene expression from newly generated PND8 data

was highly correlated with data generated in the lab previously and data from the literature. The data from the PNW21 stage is also well correlated with the literature (result not shown).

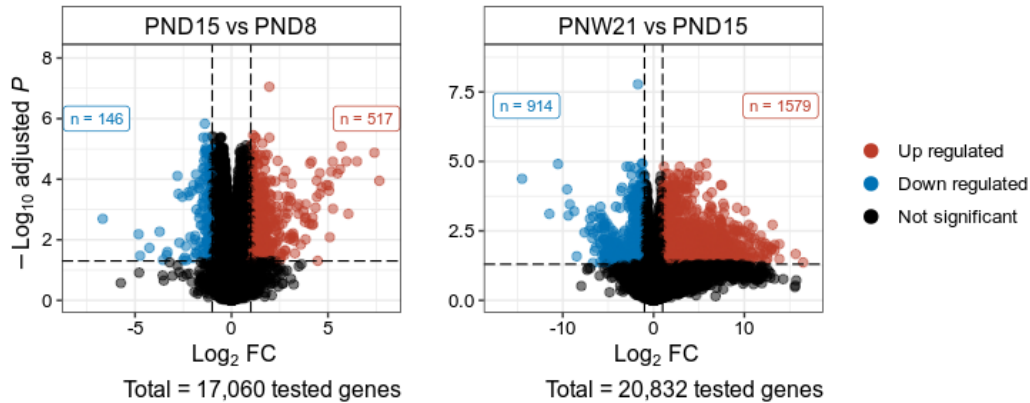


**Figure 1.2: Volcano plot of differentially expressed genes (adjusted  $P \leq 0.05$  and absolute  $\text{Log}_2\text{FC} \geq 1$ ).**

A: PND15 and PND8.

B: PNW21 and PND15.

We processed the RNA-seq data using the methods described in Chapter 1 and Methods. Following that, we conducted a differential analysis between PND15 and PND8, as well as PNW21 and PND15. Figure 1.2 shows that we found 663 genes that were differentially expressed between PND15 and PND8, and 2,493 genes that were differentially expressed between PNW21 and PND15.

We compared log2 fold-changes from new data PND15 vs PND8 to literature data PND14 vs PND8, and new data PNW21 vs PND15 to literature data PNW8 vs PND14. We discovered that the correlation between PND14 vs PND8 and PND15 vs PND8 was 43% ( $R = 0.43$ , Pearson method) and that most of the genes were changing in the same direction, and that the correlation between PNW8 vs PND14 and PNW21 vs PND15 was 70% ( $R = 0.7$ ; Pearson method) and that most of the genes were changing in the same direction, as shown in Figure 1.1C, 1.1D. Furthermore, we compared the lab's old data with the new data and discovered an 87% correlation ( $R = 0.87$ ; Pearson method) and nearly all the genes changing in the same direction for PND15 vs PND8, whereas the correlation for PNW21 vs PND15 was 6% ( $R = 0.06$ ; Pearson method) and nearly 50% genes changing in the opposite direction, Figure 1.1E, 1.1F. This is due to the fact that the previous PNW21 data were obtained from ployA libraries, whereas the new PNW21 data were obtained from total RNA libraries.

### 1.1.3.1 Identification of clusters of genes with distinct expression profiles

We discovered five clusters of genes that were differentially expressed. We have used the union of differentially expressed genes between PND15 and PND8, as well as PNW21 and PND15, and ran k-means clustering ( $k = 2$  to 10) on the log<sub>2</sub> fold-changes of normalized expression values, using PND8 samples as the baseline. Based on visual inspection, we select 7 clusters ( $k = 7$ ) and merge the clusters with visually observed similar expression profiles to obtain 5 clusters, Figure 1.3.

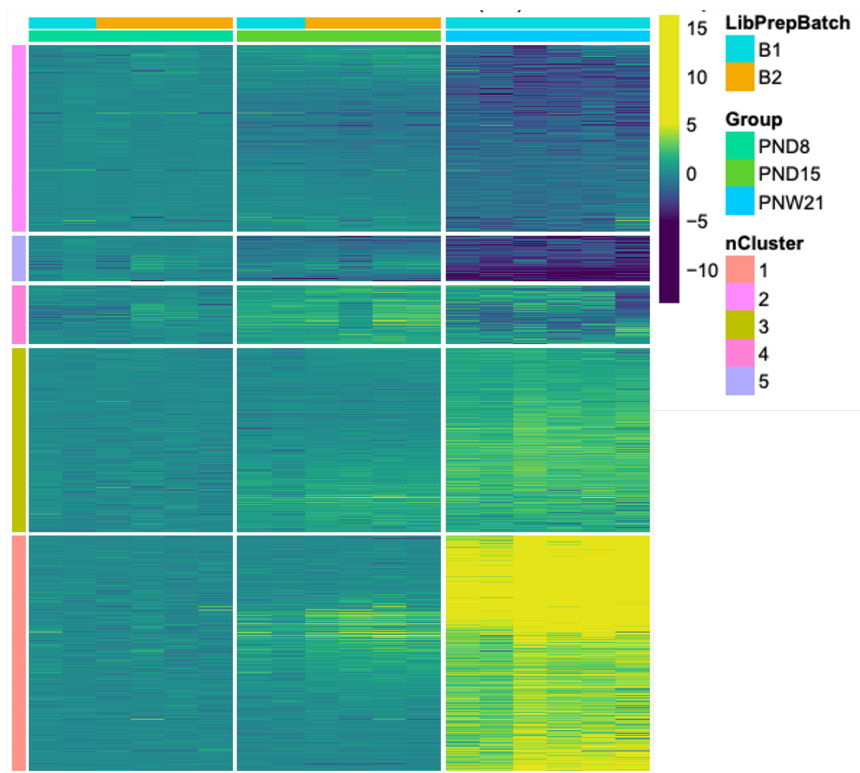


**Figure 1.3: K-means clustering ( $k = 5$ ) of genes with differential expression in postnatal versus adult spermatogonial cells.** Each row depicts a gene and each column depicts a sample. Gene expression fold-change is calculated by subtracting mean log<sub>2</sub> counts per million (CPM) of PND8 from PND15 and PNW21. Samples are clustered using Ward's method and genes are ordered by the “MDS\_angle method” using `seriation` (R package).

### 1.1.3.2 Multi-omics data integration

After combining data from ATAC-seq, RNA-seq, and ChIP-seq, we were able to generate clusters of distinct genome activity. We combined these datasets, with ATAC-seq as the starting point, Methods. We classified the differentially accessible regions (DARs) based on ATAC-seq and RNA-seq data into distal ( $> 2.5$  kb of the transcription start site, TSS)

and proximal (2.5kb of TSS). Following that, distal DARs were divided into two groups based on increased or decreased accessibility in PNW21, Figure 1.4,1.6, while proximal DARs were divided into six groups based on increased or decreased accessibility in PNW21 and up or down-regulation of nearby gene expression in PNW21 Figure 1.5, 1.7. Category 1: increased chromatin accessibility and upregulation of neighbouring genes; Category 2: increased chromatin accessibility and downregulation of neighbouring genes Category 3: decreased chromatin accessibility and downregulation of neighbouring genes, Category 4: decreased chromatin accessibility and upregulation of neighbouring genes, Category 5: increased chromatin accessibility with no detectable gene expression, and Category 6: decreased chromatin accessibility with no detectable gene expression. All such clusters had also been identified in the previous analysis (see Chapter 1 and (Lazar-Contes et al., 2020), however one of the original categories (Category 5 from Figure 1.5) disappeared in the new analysis. This category is related to TSS-proximal DARs which, against expectations, increase in expression despite a decrease in accessibility. Since expression implies promoter accessibility, it is safe to assume that this category was attributable to lack of comparability of the two RNAseq protocols.

To conclude, the results obtained from the newly generated RNA-seq data from the lab are quite similar to the results generated previously We have obtained similar results in terms of differential analysis and multi-omics data integrations. However, a number of analyses are still to be performed, for instance, gene-ontology analysis on differentially expressed genes, identified clusters of gene expression, and clusters obtained from multi-omics data integration; transcription factor motif analysis of clusters obtained from multi-omics data integration; and revision of figures and manuscript.

Figures 1.4, 1.5, 1.6, 1.7 are enriched heatmaps that show different clusters for distal and proximal regions. Each row represents a peak region, which is ordered by the ATAC signal. The mid-x-axis corresponds to the centre of a peak region and is extended to +/1 kbp. The ATAC heatmap's colour key represents the signal. For RNA-seq, the fold-change in gene expression is calculated by subtracting the mean  $\log_2$  CPM of PND8 from all samples.

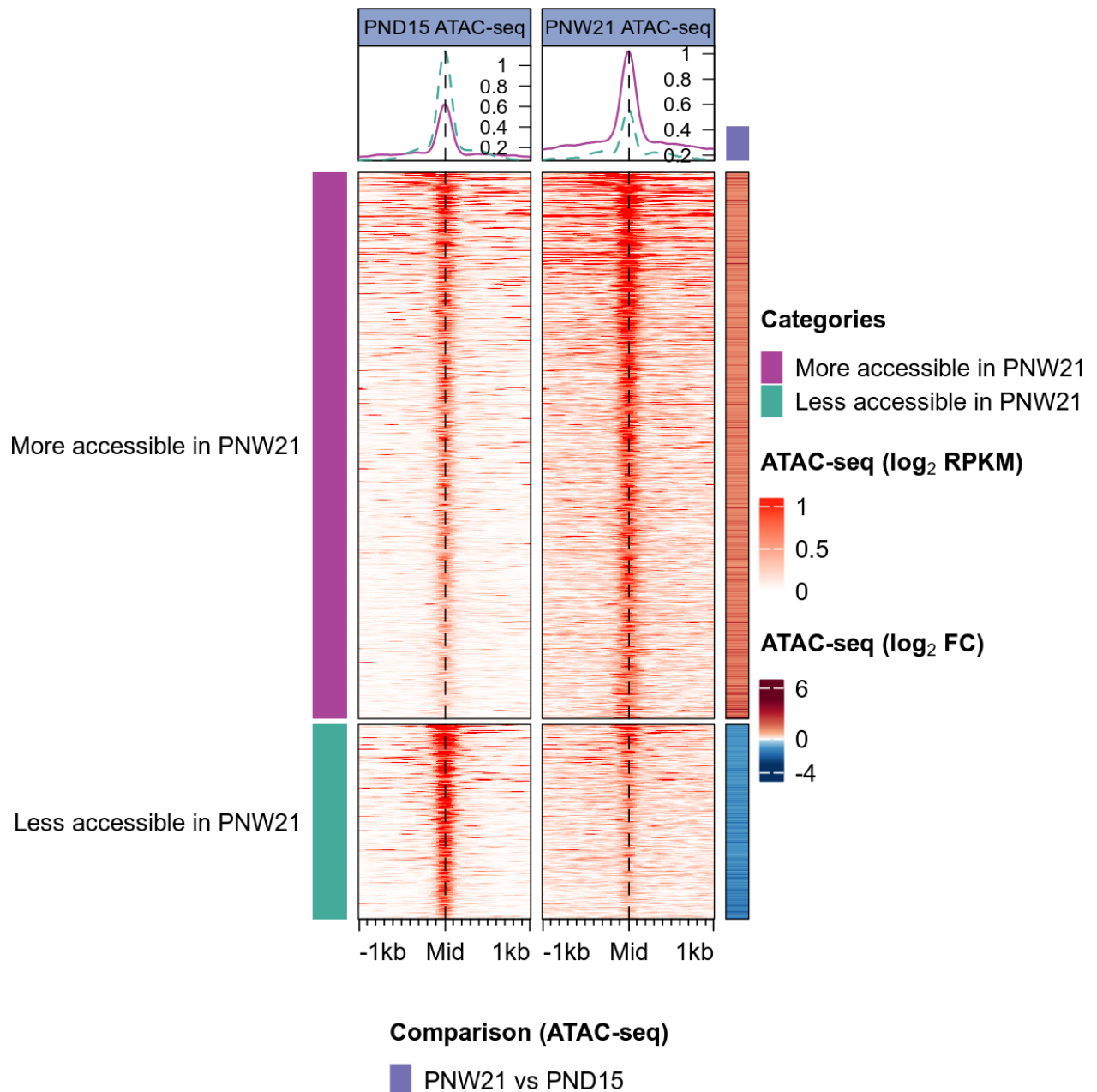


Figure 1.4: Enriched heatmap of distal differentially accessible regions.

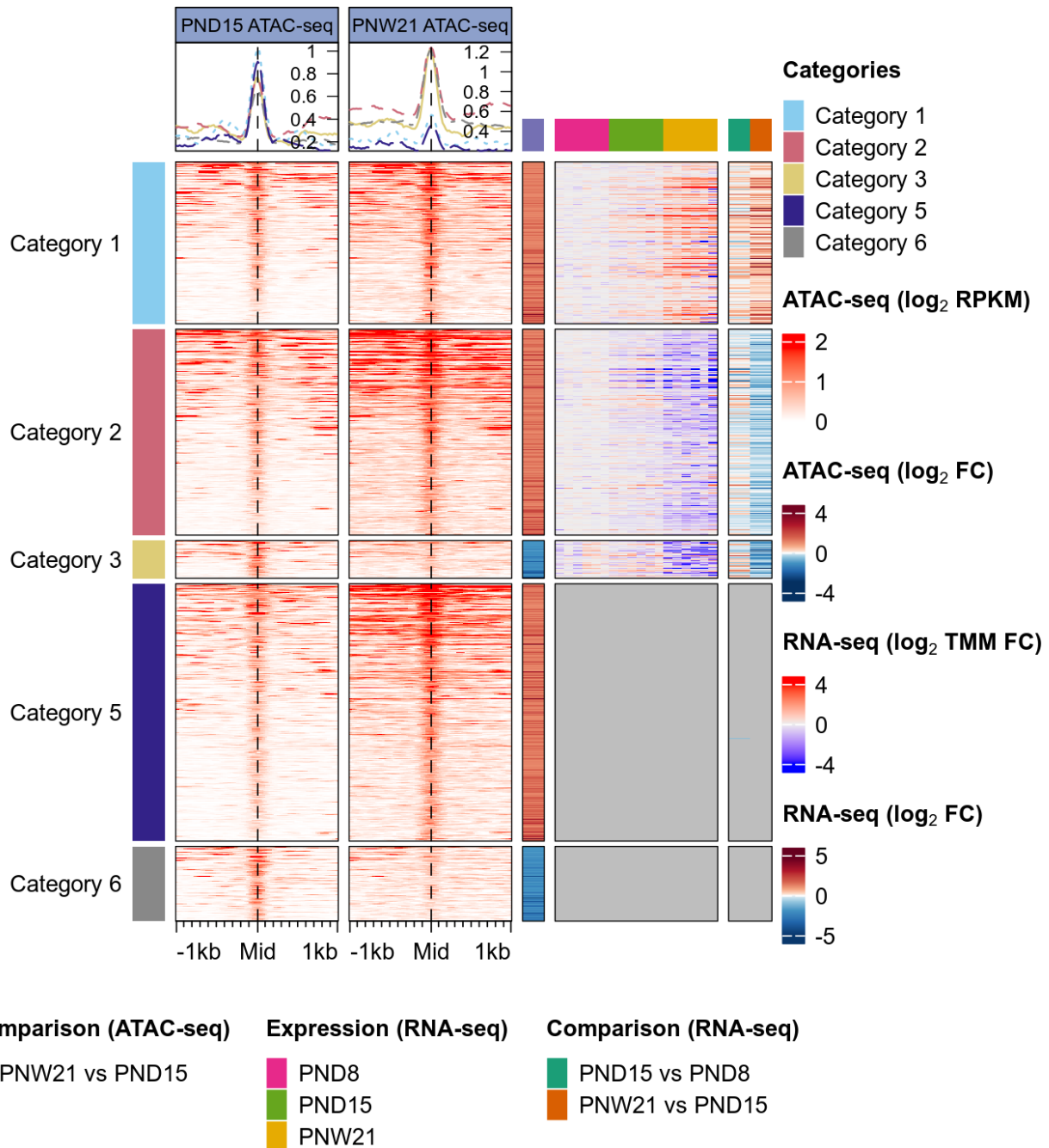
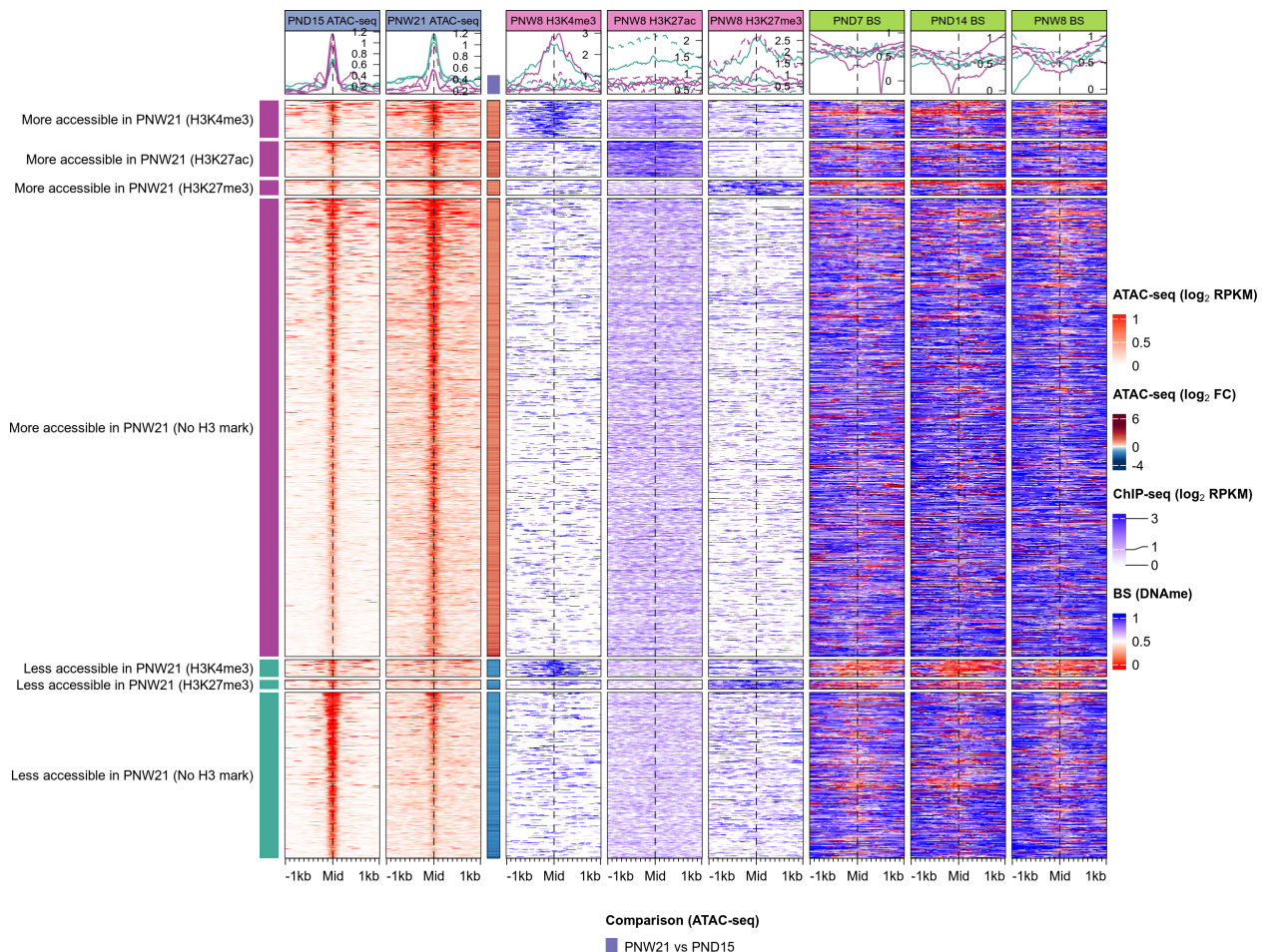


Figure 1.5: Enriched heatmap of proximal differentially accessible regions.



**Figure 1.6: Enriched heatmap of distal differentially accessible regions with ChIP-seq and BS-seq data.**

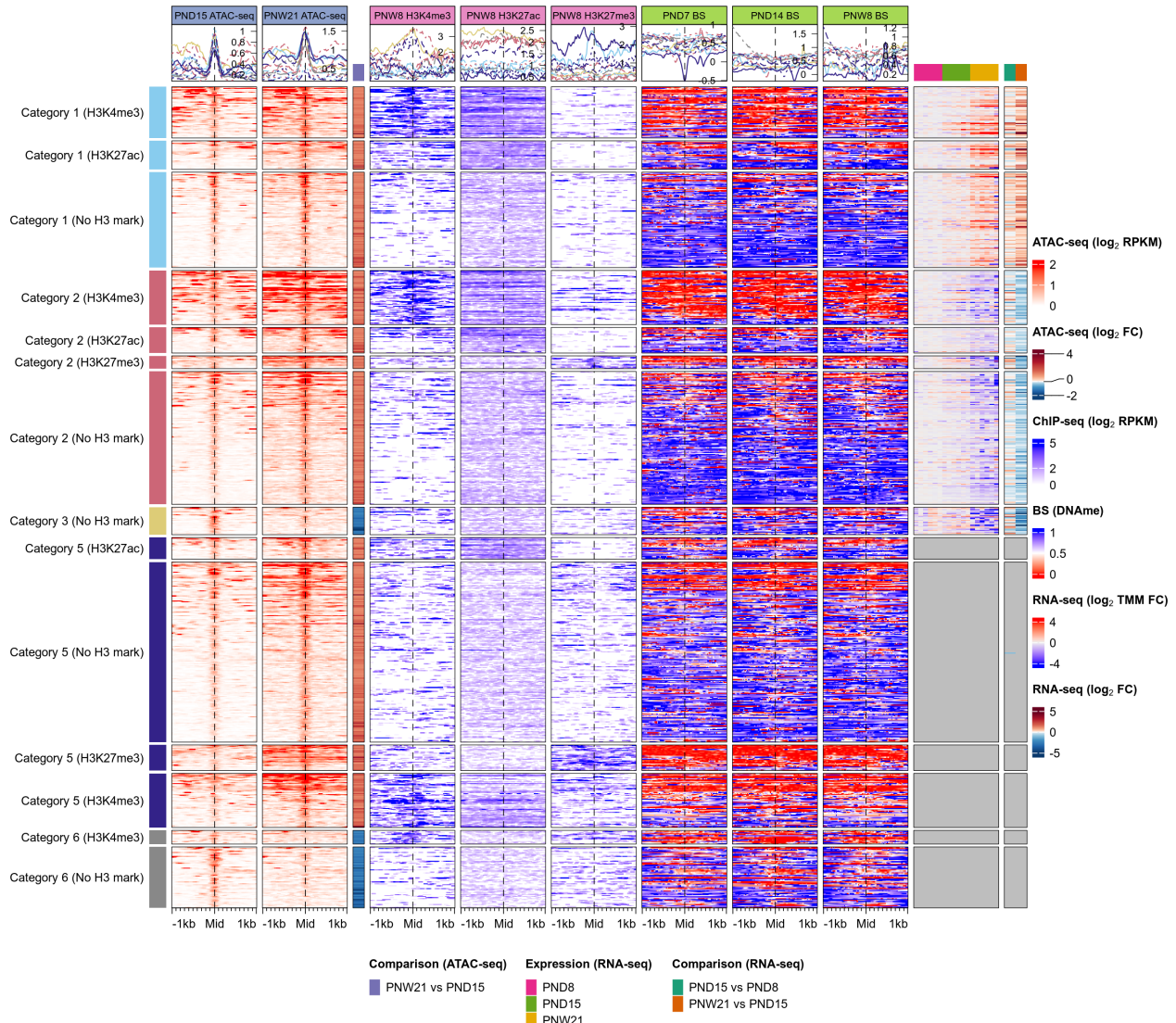


Figure 1.7: Enriched heatmap of proximal differentially accessible regions with ChIP-seq and BS-seq data.

## 1.2 Graphical Abstract

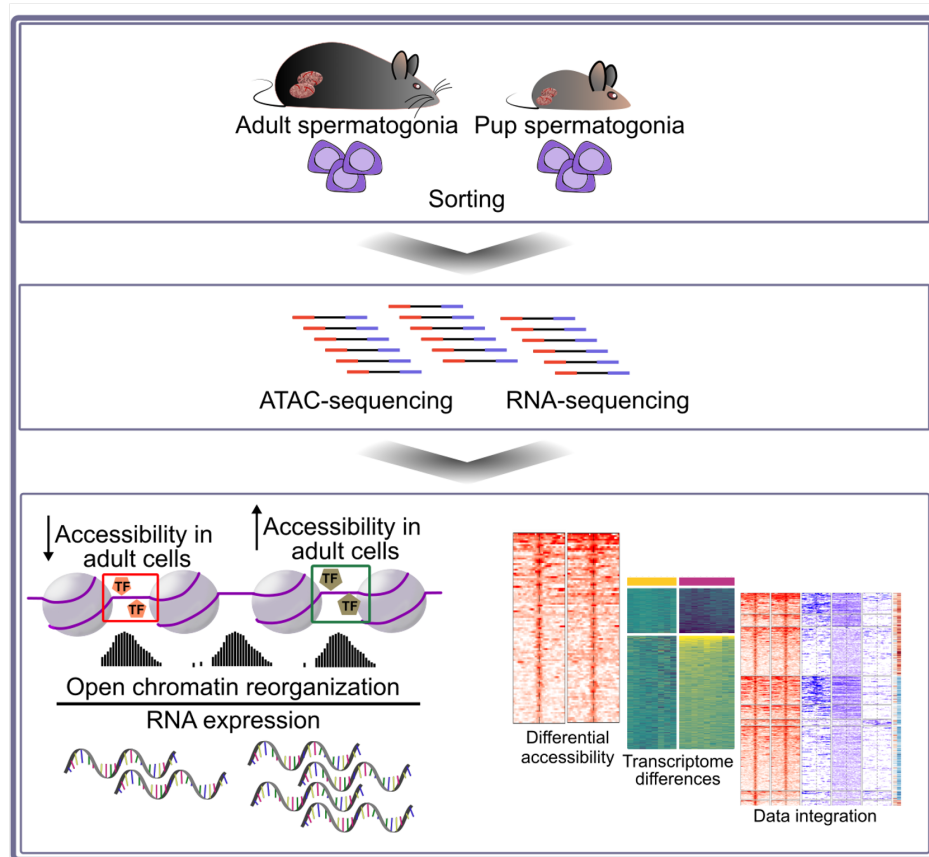


Figure 1.8: Graphical abstract.

### 1.3 Abstract

Stem cells have the capacity to self-renew and differentiate to give rise to tissues. In mammals, spermatogonial stem cells are unique undifferentiated cells in the male germline that are present throughout life and produce functional sperm. They have a remarkable dynamic transcriptome between postnatal life and adulthood, thought to allow adaptation to the maturing gonadal environment. To assess if chromatin remodelling is associated with this dynamic, we characterized chromatin accessibility in postnatal and adult spermatogonial cells in mice using ATAC-seq. Extensive changes in chromatin accessibility were observed in spermatogonial cells across postnatal development, that correlate with distinct gene expression profiles and transcription factor motif enrichment. We identify genomic regions with differential chromatin accessibility in adult spermatogonial cells, that are marked by distinct histone modifications and are situated in proximity to the transcription start site of genes important for cell maintenance and proliferation. Some of these regions correspond to transposable element subtypes enriched in multiple transcription factor motifs and with increased transcription. Together, our results reveal profiles of chromatin organization, histone modifications and gene expression in spermatogonial cells, and underscore the dynamic nature of the germline genome.

## 1.4 Introduction

Spermatogonial cells are cells in male gonads that actively self-renew and differentiate into spermatogenic cells to produce adult gametes. In mice, they become active one to two days after birth, when they exit mitotic arrest and start dividing, to populate the basement membrane of seminiferous tubules. During the first week of postnatal life, a population of spermatogonial cells continues to proliferate and gives rise to undifferentiated Asingle (As), Apaired (Apr) and Aaligned (Aal) cells. The remaining spermatogonia differentiate to form chains of daughter cells that become primary and secondary spermatocytes around postnatal day (PND) 10 to 12. Spermatocytes undergo meiosis and give rise to haploid spermatids that develop into spermatozoa. Spermatozoa are then released in the lumen of the seminiferous tubules and continue to mature in the epididymis until becoming capable of fertilization by PND 42-48 (Kubota & Brinster, 2018; Oatley & Griswold, 2017; Rooij, 2017).

Recent work using population or single-cell RNA sequencing (RNA-seq) showed that distinct transcriptional profiles characterize spermatogonial cells in postnatal and adult life (C. D. Green et al., 2018; Hammoud et al., 2014, 2015; Hermann et al., 2018; N. C. Law, Oatley, & Oatley, 2019). During the first week after birth, spermatogonia have unique features necessary for their rapid establishment and expansion along the basement membrane. This includes high expression of genes involved in cell cycle regulation, stem cell proliferation, transcription and RNA (Grive et al., 2019). In comparison, in the adult testis, genes are involved in the maintenance of a steady spermatogonial cells population, with a balance between proliferation and differentiation to ensure sperm formation predominates. This includes pathways related to paracrine signalling and niche communication, as well as mitochondrial function and oxidative phosphorylation (Grive et al., 2019; Hermann et al., 2018). Epigenetic changes such as histone tail posttranslational modifications and DNA methylation accompany transcriptional differences in spermatogonial cells across postnatal stages (Hammoud et al., 2014, 2015). However, little is known about the accessible chromatin landscape, during the transition from postnatal to the adult stage.

We examined chromatin reorganization in the transition from postnatal to adult spermatogonia and its functional relevance by profiling chromatin accessibility by ATAC-seq (assay for transposase-accessible chromatin with high-throughput sequencing) using an Omni-ATAC protocol (Corces et al., 2017) and integrating data with transcriptomic and epigenetic profiles. The results show that chromatin is extensively remodelled in spermatogonial cells during development, and its accessibility is increased at several genomic regions particularly transposable elements (TEs), that correlate with transcriptional and epigenetic signatures.

## 1.5 Results

### 1.5.1 Enrichment of spermatogonial cells from postnatal and adult mouse testis

We collected testes from mouse pups at postnatal days (PND) 8 and 15 and from males at postnatal week (PNW) 20, and prepared cell suspensions by enzymatic digestion. Spermatogonial cells were enriched by fluorescence-activated cell sorting (FACS) using surface markers (Supp. Figure 1.15aA) (Kubota, Avarbock, & Brinster, 2004a). Immunocytochemistry using PLZF, a well-established marker of undifferentiated spermatogonia (Costoya et al., 2004), confirmed that our preparation was enriched in spermatogonial cells, with 85-95% PLZF+ cells after FACS compared to 3-6% PLZF+ cells before (Supp. Figure 1.15aB). Transcriptomic analyses by RNA-seq validated the spermatogonial identity of the cells, showing high expression of stem cell and undifferentiated spermatogonial markers, and low expression of somatic cells (Leydig and Sertoli cells) markers both at PND 8 and 15 (Supp. Figure 1.15bC).

### 1.5.2 Chromatin is remodelled in spermatogonial cells during the development

We profiled chromatin accessibility in postnatal and adult spermatogonial cells using an Omni-ATAC protocol (Corces et al., 2017). Omni-ATAC has a higher signal-to-noise ratio than classical ATAC-seq and can be used with low input material (a few hundred cells). Accessible regions in the genome were identified by peak-calling on merged nucleosome-free fragments (NFF). Following the removal of lowly enriched regions, 158,978 regions were selected for downstream analyses (see Methods section for details). Most Tn5-accessible regions are intergenic (38%) and located in gene bodies (33%) or in the proximity of a transcription start site (TSS) (28% +/- 1 kb from TSS) (Supp. Figure 1.16aA). 3212 differentially accessible regions were identified between PND15 and adult spermatogonia with the majority showing a gain in accessibility in adult cells (Figure 1.9aA and Table S1). Regions of differential accessibility are predominantly intergenic (45%) and intronic (34%), and 15% of all differentially accessible regions are +/- 1kb from a TSS (Figure 1.9aB). Gene ontology (GO) analysis, showed that regions with increased accessibility in adult spermatogonia are associated with cell fate and stem cell population maintenance, protein metabolism and RNA metabolic processes (Figure 1.9bC and Table S1). Separate GO analyses depending on genomic location showed that regions located in gene bodies (mainly introns) are enriched for terms related to reproduction and protein metabolism, whilst regions close to or overlapping with a TSS relate to cell fate specification and tissue morphogenesis (Supp. Figure 1.16bB and Table

S1). Regions with decreased accessibility in adult spermatogonia are predominantly located in intergenic regions and associated with multiple terms related to embryonic development (Figure 1.9bC and Table S1).

### 1.5.3 Differentially accessible chromatin regions associated with distinct gene expression dynamics

To assess the relevance of changes in chromatin accessibility, we first integrated our ATAC-Seq data with transcriptomic datasets and examined the correlation between chromatin states and transcriptome. We conducted RNA-seq analyses on postnatal spermatogonial cells and used published data from Thy1+ adult spermatogonial cells. We found that 719 genes are differentially expressed in spermatogonial cells between PND8 and PND15, with 515 being upregulated and 212 downregulated (Figure 1.10aA and Table S2). Fast Gene Set Enrichment Analysis (FGSEA) showed that pathways related to RNA processing and splicing, cell cycle, redox homeostasis and protein catabolism are downregulated between PND8 and PND15 while pathways associated with cellular transport, exocytosis and signal transduction are upregulated (Figure 1.10aB and Table S2). Comparable analyses using published RNA-seq data from PND14 and adult spermatogonia cells (Hammoud et al., 2014, 2015) similarly identified transcriptional changes between postnatal and adult stages (Fig. S?A and Table S2) and downregulation of pathways related to RNA processing, ribosome biogenesis and cell cycle in adults compared to postnatal cells. Pathways related to developmental programs and mitochondrial functions were also downregulated and those related to spermatogenesis or involving cytokine signalling were upregulated (Fig. S? and Table S2).

To integrate chromatin accessibility and transcriptomic datasets, we first divided differentially-accessible regions into proximal (situated less than +/- 2.5 kb from a TSS) and distal (situated more than +/- 2.5 kb from a TSS) following ENCODE practice (Becker, 2011; Harrow et al., 2012; Thurman et al., 2012). For proximal regions, we further defined 6 different categories based on the change in expression of the nearest gene. The first two include proximal regions with increased chromatin accessibility and upregulated (Category 1) or downregulated (Category 2) expression of the nearest gene. Category 3 and 4 include regions of less chromatin accessibility with the nearest gene either downregulated or upregulated, respectively. Category 5 and 6 include regions with increased or decreased chromatin accessibility respectively, whose nearest gene is not expressed in spermatogonial cells (Figure 1.11aA and Table S3)).

### 1.5.4 Differentially accessible chromatin regions associated with distinct epigenetic profiles

Next, we examined the relationship between chromatin accessibility and epigenetic marks using published ChIP-seq and bisulfite sequencing (BS) datasets from Thy1+ spermatogonia (Hammoud et al., 2014, 2015). Profiles of histone marks including H3K4me3, H3K27ac and H3K27me3 in adult spermatogonial cells, and DNA methylation in PND7, PND14 and adult spermatogonial cells were used. ....analyses showed that for a subset of regions in Category 1, there is an overlap with active H3K4me3, H3K27ac or dual H3K4me3/K27ac modifications, and an overall lack of H3K27me3 (Figure 1.11aB and Table S3). Notably, several of the genes in Category 1 with chromatin opening marked by histone modification(s) are known regulators of stem cell potency. *Pdk1* promoter region was marked by dual H3K4me3/K27ac, while *Pdk1* mRNA was upregulated in adult spermatogonia (Supp. Figure 1.17A). *Pdk1* (phosphoinositide-dependent protein kinase 1) is a glycolysis factor important for stem cell self-renewal (W. Chen et al., 2020; Kanatsu-Shinohara et al., 2016). In contrast, the *Gata2* promoter region was marked by the bivalent H3K4me3/K27me3 mark, while *Gata2* expression showed an upregulation across testis maturation (Supp. Figure 1.17). *Gata2* (GATA-binding factor 2) is a known target of *NANOS2*, an essential regulator of spermatogonial stem cell potential (Barrios et al., 2010; Sada, Suzuki, Suzuki, & Saga, 2009). Other exemplary genes in Category 1 include pyruvate cellular carriers *Slc25a18*, *Slc23a1* and *Slc2a5*, suggesting differences in glycolysis regulation in adult spermatogonial cells (Table S3). Notably, we found increased chromatin accessibility at the TSS of GDNF receptor *Gfra2* (Figure 1.11bC). At the mRNA level, *Gfra2* displayed a marked upregulation in adult spermatogonial cells, indicating an increased utilization of GFRA2 receptors in adult spermatogonial cells compared to early postnatal stages, in which GFRA1-mediated signalling is dominant (Figure 1.11bC) (Grive et al., 2019; Hammoud et al., 2015). We also observed increased chromatin accessibility and upregulation of DNA damage responsive gene *Fus*, and the multifunctional redox gene *Prdx4* (Table S3).

Interestingly, the highest number of differentially accessible chromatin regions were in Category 2, and included proximal regions with increased chromatin accessibility and decreased expression of nearby genes in adult spermatogonia, indicative of active repression taking place (Fig. 3A and Table S3). A subset of Category 2 regions was marked by H3K27me3 together with H3K4me3 and mainly associated with developmental genes such as *Satb1* and *Hmx1*, (Supp. Figure 1.17B). Other developmental genes such as *Tbx4* also displayed a decreased accessibility and an increase in mRNA expression (Figure 1.11bC). GO enrichment analysis revealed that regions in Category 2 are associated with regulation of

cell cycle, RNA processing, DNA repair and cell division (Table S4). Such an example is Fgf8, important for Fgf8-Fgfr1 mediated maintenance of undifferentiated spermatogonia (Hasegawa & Saga, 2014). Fgf8 showed increased chromatin accessibility close to its TSS and a downregulated expression in adult spermatogonia, in agreement with recent findings from scRNA-seq data suggesting downregulation of Fgfr1-mediated signalling with age (Fig. S3B) (Grive et al., 2019; Hasegawa & Saga, 2014).

Regions in Category 3 displayed decreased chromatin accessibility and downregulation of nearby genes in adult spermatogonia and were mostly depleted of any of the 3 histone marks investigated (Figure 1.11aA and 1.11aB). GO enrichment on the nearby genes revealed an association with developmental processes and WNT signalling (Table S4). A notable example we identified in this category is Pdgfra, a gene involved in the hepatic stellate cell activation pathway, which was recently identified by scRNA-seq to be upregulated in spermatogonial stem cells in the immature testis compared to the adult stage (Hermann et al., 2018). Pdgfra displayed a marked downregulation in adult spermatogonia, and a decrease in chromatin accessibility overlapping its TSS (Figure 1.11bC). Another example of a gene important for early postnatal spermatogonial cell establishment is Dap2ip, which we also found to carry a marked decrease in chromatin accessibility at its TSS and lower expression in adult spermatogonial cells (Supp. Figure 1.17C). Surprisingly, we also identified a category of proximal regions (Category 4) with decreased accessibility (<20 regions) at genes that were upregulated in adult spermatogonial cells and with a previously uncharacterized role in spermatogonial cells (Figure 1.11aA). Notably, DNAm profiles across postnatal stages did not show any significant change across any of the 6 categories of proximal regions, suggesting a relatively stable DNAm profile in the transition from early postnatal to adult stage (Supp. Figure 1.17D). Aside from proximal regions, we also identified numerous distal regions with differential chromatin accessibility between PND15 and adult spermatogonial cells (Supp. Figure 1.18A). Similar to proximal regions, accessibility in distal regions mainly increased in adult spermatogonial cells compared to the early postnatal stage. When integrating the literature ChIP-seq data, we observed enrichment for H3K4me3, H3K27ac and H3K27me3 at a small number of the differentially accessible distal regions, indicative of potential regulatory roles (Supp. Figure 1.18B and Table S3). Similar to proximal regions, DNAm levels did not display major changes in the transition from early postnatal to adult stage (Supp. Figure 1.18B). Taken together, our data integration reveals novel associations between chromatin regions of differential accessibility, histone marks and gene transcription in spermatogonial cells from postnatal to adult stages of development. They suggest that chromatin accessibility is a mechanism of control of transcriptional programs and of certain signalling pathways during development.

### 1.5.5 Accessibility changes at open chromatin regions carry binding sites for distinct families of transcription factors

Transcription factors (TFs) are essential for establishing and maintaining transcriptional programs across developmental stages in cells Fushan et al. (2015). To examine if regions of different chromatin accessibility between PND15 and adult spermatogonia are enriched in regulatory elements such as TF binding motifs, we performed motif enrichment analysis using the Hypergeometric Optimization of Motif EnRichment (HOMER) tool (Heinz et al., 2010). In regions with increased chromatin accessibility, we identified 41 enriched TF motifs ( $q\text{-value} \leq 0.05$ ) (Figure 1.12aA). Top candidates by significance ( $q\text{-value} \leq 0.0001$ ) are members of the Fos/Jun family (FOS, FOSB, FOSL1 and FOSL2, JUN, JUNB and JUND) (Figure 1.12aB). Notably, at the mRNA level, some of the TFs displayed age-specific differences ( $\log_2\text{CPM} \geq 1$  and  $\text{abs } \log_2 \text{ fold change} \geq 1$ ): Fos, Junb and Jund were downregulated in adult spermatogonial cells (Figure 1.12bC). JUN, FOS and CREB are all part of the AP-1 (activating protein-1) superfamily, and play an important role in regulating cell proliferation and death, by mediating the senescence-associated chromatin and transcriptional landscape (Martínez-Zamudio et al., 2020; Shaulian & Karin, 2002). JUND and c-FOS specifically promote the proliferative potential of spermatogonial stem cells (He et al., 2008; M. Wang et al., 2018). USF1 and POU3F1, 2 factors important in the maintenance of the spermatogonial stem cell pool also displayed enriched binding motifs in the more accessible regions. However, their mRNA levels were downregulated in adult spermatogonial cells (Figure 1.12bC) [(Faisal et al., 2019, 2019)]. POU3F1 is a GDNF-regulated TF, which has been shown to play an important role in promoting spermatogonial cell self-renewal capacity (Niu et al., 2011; Xin Wu et al., 2010). Notably, Pou3f1 downregulation in adult spermatogonial cells coincides with marked downregulation of Gfra1 and upregulation of Gfra2 (Figure 1.11bC and Table S2). TF motif analysis using HOMER also revealed enriched binding sites for retinoic acid receptors such as RXRa and RARa (Figure 1.12aA). Recently, expression of RA receptors Rxra and Rara was reported in the stem cell-containing population of spermatogonial cells in both pup and adult testis, together with evidence that their utilization in spermatogonial cells is vastly dependent on the niche microenvironment (Lord, Oatley, & Oatley, 2018).

To check if some TF binding motifs are preferentially enriched in certain genomic locations, we performed motif enrichment analysis for more accessible chromatin regions situated in gene bodies, intergenic regions and in regions  $+/- 1\text{kb}$  from TSS. We identified several TF motifs specifically enriched in intergenic regions, specifically members of the ubiquitously expressed NF-Y complex, NF-YA, NF-YB and NF-YC (Figure 1.12bD). In mESCs, NF-Y TF family members located in distal regions facilitate a permissive chromatin conformation

and play an important role in the expression of core ESC pluripotency genes (Oldfield et al., 2014). Furthermore, NF-YA/B motif enrichment has also been found in regions of open chromatin in human spermatogonial cells (Guo et al., 2017).

Although regions of more accessible chromatin encompass the majority of the differentially accessible regions in adult spermatogonia compared to PND15, less accessible chromatin also displayed a high number of enriched TF binding motifs (Figure 1.12aA). Notably, almost all of these TF motifs were uniquely enriched in the regions of decreased chromatin accessibility and predominantly associated with developmental factors. Top hits included members of the FOX family (FOXO1, FOXO3, FOXP2, FOXK1, FOXA2) and members of the ETS and ETS-related families (ETS1, GABPA, ETV4, ELF1, ELF3) (Figure 1.12aB). The gene expression levels of most of these TFs were decreased in adult spermatogonial cells (Figure 1.12aA). FOXO1 is a pivotal regulator of the self-renewal and differentiation of spermatogonial stem cells in both pup and adult testis, via the PI3K-Akt signalling pathway (F. Chan et al., 2014; Goertz, Wu, Gallardo, Hamra, & Castrillon, 2011). The roles of the various ETS-related TFs in spermatogonial cells have not been clarified, however recently published data found ETV4 in the stem-cell enriched fraction of the spermatogonial population, particularly during the spermatogonial stem cell pool establishment immediately after birth (Cheng et al., 2020; N. C. Law et al., 2019). Motif enrichment analysis on the regions with decreased chromatin accessibility situated in the gene body and intergenic regions revealed that TFs are important in numerous developmental processes (FOXC1, FOXJ2, FOXM1, LHX6) were specifically enriched in intergenic regions of decreased chromatin accessibility (Figure 1.12bD). This is consistent with the association of intergenic regions with embryonic development-related GO terms that we previously detected (Figure 1.9bC). Our findings provide a detailed characterization of the enriched TF motifs present at the regions of dynamic accessibility between PND15 and adult spermatogonial populations and point towards novel candidate regulators of the differential transcriptome of the pup and adult mouse spermatogonia.

### **1.5.6 Chromatin accessibility at transposable elements undergoes significant remodelling in the transition from postnatal to adult spermatogonia**

Transposable elements (TEs) are under tight control in the germline, through coordinated epigenetic mechanisms involving DNA methylation, chromatin silencing and PIWI proteins – piRNA pathway (Deniz, Frost, & Branco, 2019; Thompson, Macfarlan, & Lorincz, 2016). Recent evidence suggests an important role for long terminal repeat (LTR) - type elements, specifically for ERVKs, the youngest class of endogenous retroviruses (ERVs), in the transcri-

tional regulation of mRNAs and long non-coding RNAs (lncRNAs) during mitosis-to-meiosis transition (Davis et al., 2017; Sakashita et al., 2020). Furthermore, accessibility analysis at LTRs in mitotic and meiotic germ cells, revealed a unique chromatin accessibility landscape in spermatogonial cells, compared to the rest of the germ cells in the testis (Sakashita et al., 2020). To explore potential differences in TEs regulation driven by postnatal age, we compared the accessibility of TEs in PND15 and adult spermatogonia. For this purpose, we quantified the ATAC-seq reads overlapping TEs defined by UCSC RepeatMasker and performed differential accessibility analysis at the subtype level (see Methods section). Our results revealed that the transition from PND15 to the adult stage is accompanied by significant chromatin accessibility differences at 135 TE subtypes (Figure 1.13aA and 5B and Table S5). Although most of the differentially accessible TE subtypes displayed a decrease in chromatin accessibility between PND15 and adult stages (68,9%, 93/135) (Figure 1.13aA), we also observed 42 TE subtypes which increased in accessibility in adult spermatogonia (Figure 1.13aB). Of note, more accessible subtypes also displayed an increased expression in adult spermatogonia compared to the early postnatal stage (Figure 1.13aB). TE loci within the subtypes harbouring changes in chromatin accessibility were situated in intergenic and intronic regions (68% intergenic and 25% intronic), and around 6% were located in the proximity of a gene (+/- 1kb from a TSS) (Figure 1.13aC). LTRs were the most abundant TEs to display changes in chromatin accessibility, specifically ERVK and ERV1 subtypes (Figure 1.13aA and 5B). Exemplary ERVK subtypes harbouring less accessible chromatin included RLTR17, RLTR9A3, RLTR12B and RMER17B (Table S5). Enrichment of RLTR17 and RLTR9 repeats have been reported previously in mESCs, specifically at TFs important for pluripotency maintenance such as Oct4 and Nanog (Fort et al., 2014). Interestingly, we identified the promoter region of the lncRNA Lncenc1, an important regulator of pluripotency in mESCs (Fort et al., 2014; Sun et al., 2018), harboring several LTR loci with decreased accessibility in our adult spermatogonia, with the RLTR17 locus falling within the TSS of Lncenc1. This decrease in accessibility correlated with a marked decrease in expression of Lncenc1 in adult spermatogonia (Figure 1.13aD). Lncenc1 (also known as Platr18) is part of the pluripotency-associated transcript (Platr) family of lncRNAs which were recently identified as potential regulators of the pluripotency-associated genes Oct4, Nanog and Zfp42 in mESCs (Bergmann et al., 2015; Dann et al., 2008; D. C. Wu et al., 2018). We were also able to identify several other Platr genes, such as Platr27 and Platr14, for which the TSS overlapped LTRs with reduced accessibility, RLTR17 and RLTR16B\_MM, respectively (Figure 1.13aD and Table S5). These 2 pluripotency-associated transcripts also showed a decrease in mRNA expression in adult spermatogonia, while their expression was unchanged between PND8 and PND15 (Figure 1.13aD and Table S5). The remaining LTR subtypes

with decreased accessibility in adult spermatogonia belonged to the ERV1, ERVL and MaLR families (Figure 1.13aA). Only very few other non-LTR TEs showed a decrease in chromatin accessibility, with 7 DNA element subtypes, 2 Satellite subtypes and 1 LINE subtype, respectively (Figure 1.13aA and Table S5). Emerging evidence suggests an important contribution of TEs in providing tissue-specific substrates for TF binding (Fort et al., 2014; Sundaram et al., 2014; Sundaram & Wysocka, 2020). To investigate the regulatory potential of the less accessible LTR subtypes, we assessed the enrichment of TF motifs in these regions using HOMER. To do so, we focused on the family level and grouped together all LTR subtypes coming from one family (EVK, ERV1, ERVL and ERVL-MaLR families). Among the less accessible LTR families, ERVKs showed the highest number of enriched TF motifs in adult spermatogonial cells. Top hits included TFs with known regulatory roles in cell proliferation and differentiation such as FOXL1 and FOXQ1, stem cell maintenance factors ELF1, EBF1 and THAP11 and TFs important in spermatogenesis PBX3, ZNF143 and NFYA/B (Figure 1.13bE and S6A). ERVLs displayed motif enrichment for very few TFs, among which the previously undescribed ETV2, newly reported spermatogonial stem cell factor ZBTB7A and the testis-specific CTCF paralog CTCFL (Figure 1.13bE) (C. D. Green et al., 2018).

Among the TE subtypes which increased in chromatin accessibility, members of the ERVK, ERVL and ERV1 families were predominant (57.1%, 24/42) (Figure 1.13aB). Interestingly, we also found a considerable number of LINE L1 subtypes with increased chromatin accessibility in adult spermatogonial cells (Figure 1.13aB). When parsing the data for more accessible loci within the L1 subtypes, we found several L1 loci situated less than +/- 5 kb from the TSS of numerous olfactory (Olfr) genes. Most of them were located in Olfr gene clusters on chromosomes 2, 7 and 11 (Table S5). Furthermore, the increase in accessibility of the L1 loci correlated with an increase in mRNA expression of the nearby Olfr gene in adult spermatogonial cells (Figure 1.14A). Representative examples were Olfr362 and Olfr1307, both situated in the Olfr gene cluster on Chr2 (Figure 1.14B). Interestingly, when visualizing the data in IGV, we also observed that the Olfr gene cluster on chromosome 2 exhibited a higher density of L1 loci compared to neighbouring regions (Supp. Figure 1.20B). Similar to before, we performed TF motif enrichment analysis at the family level by grouping together all differentially accessible TE subtypes coming from one family. More accessible LINE L1s were highly enriched in TF motifs, particularly in multiple members of the ETS, E2F and FOX families (Figure 1.14C). The most significant motifs belonged to spermatogonial stem cell maintenance and stem cell potential regulators FOXO1 and ZEB1, as well as TFs which have been recently associated with active enhancers of the stem cell-enriched population of spermatogonia such as ZBTB17 and KLF5 (Figure 1.14C and S6C) (Cheng et al., 2020). More accessible ERV1s also displayed enrichment of several TF binding sites,

including spermatogenesis-related TFs (PBX3, PRDM1, NFYA/B), hypoxia-inducible HIF1A and cytokine regulators STAT5A/B, suggestive of different spermatogonial cell metabolic demands between early postnatal and adult stage (Figure 1.14C and S6C). Overall, we provide an extensive characterization of the chromatin accessibility landscape of TEs in PND15 and adult spermatogonia, reveal differences in accessibility and TF motif landscape at distinct subtypes of TEs between these 2-time points, and suggest potential gene programs that may be regulated by these changes.

## 1.6 Discussion

As initiators of the spermatogenic cascade, spermatogonial cells are essential in germ cell proliferation and differentiation throughout postnatal life. Although recent studies employing bulk and scRNA-seq have revealed distinct transcriptional signatures of spermatogonial cells across postnatal life, very few have focused on describing the underlying landscape of open chromatin, and the extent to which it can contribute to the gene expression dynamics (Grive et al., 2019; Hammoud et al., 2015; Hermann et al., 2018).

Our ATAC-seq revealed a reorganization of open chromatin in adult spermatogonia compared to the PND15 cell population. This striking reorganization of accessible chromatin, which we detected mainly in intergenic and intronic regions, may be indicative of novel regulatory regions governing at least in part the vast transcriptome changes that spermatogonial cells undergo in their transition from early postnatal to adult stage (Grive et al., 2019; Hammoud et al., 2015). Indeed, we found that the regions of differential accessibility were associated with distinct gene pathways, with morphogenesis and developmental pathways associated to the regions of decreased chromatin accessibility, while regions of increased chromatin openness were enriched for DNA repair pathways, stem cell maintenance, RNA processing and protein metabolic processes. Furthermore, we identified numerous enriched TF motifs in the regions of differential accessibility, indicative of their potential regulatory role. AP-1 TFs with previously described roles in spermatogonial cell proliferation such as JUND and c-FOS, and pluripotency factors such as POU3F1, displayed enriched binding sites in the regions of increased chromatin accessibility. In contrast, FOX and ETS TF motifs, known regulators of developmental pathways, mainly mapped to regions that decreased in accessibility in adult spermatogonial cells. For some of the enriched TF motifs, a preference for certain genomic locations was evident: NF-YA and B binding sites exhibited enrichment specifically in intergenic regions of more accessible chromatin which interestingly, were also associated with spermatogenesis-related pathways. NF-YA/B is also localized in intergenic regions of open chromatin in humans spermatogonial cells (Guo et al., 2017), prompting

an additional investigation of their roles in regulating spermatogonial cell programs, with potential consequences for sperm formation.

Our comparison of the gene expression changes from PND8 to PND15 spermatogonial cells confirmed the dynamic transcriptome associated with developing spermatogonial cell states (Grive et al., 2019; Hammoud et al., 2015). Notably, PND15 corresponds to the maturation of the Sertoli cell niche in the mouse testis (Flickinger, 1967; Shinohara, Orwig, Avarbock, & Brinster, 2001). Upregulation of pathways associated with signal transduction and cellular transport in PND15 spermatogonia suggests an increased cellular communication with the somatic niche, compared to the first week of postnatal development. We complemented these findings with literature RNA-seq data from PND14 and adult spermatogonia and confirmed further transcriptome changes in signalling pathways related to mitochondria, developmental processes and cell-to-cell signalling. Furthermore, we revealed numerous pathways related to cytokine signalling upregulated in adult spermatogonia, which point to the recently suggested role of testis resident macrophages in maintaining and regulating spermatogonial proliferation (DeFalco et al., 2015; Garbuzov et al., 2018). These findings suggest that, as the testis matures and the somatic niche develops, spermatogonial cells rely more on paracrine signalling and undergo vast changes in gene expression programs.

To obtain a comprehensive profile of the chromatin and the transcriptome differences between early postnatal and adult spermatogonial cells, we have integrated the chromatin accessibility and gene expression, with known histone H3 modifications and global DNAm patterns of THY1+ spermatogonial cells from (Hammoud et al., 2014, 2015). This allowed us to identify 4 distinct categories of differentially accessible chromatin regions for which the nearest gene was dynamically expressed between early postnatal and adult stages. Interestingly, we found a similar number of genes with increased chromatin accessibility around their TSS which exhibited either an up- or a downregulated expression between pup and adult spermatogonia. In the category of upregulated genes with increased nearby chromatin accessibility, we identified several factors associated with redox processes, mitochondria function and cell proliferation. In contrast, genes marked by an increase in chromatin accessibility and downregulated expression in adult spermatogonia comprised factors important for cell cycle, RNA processing and developmental genes, suggesting that active repression is taking place at these genes (Starks, Biswas, Jain, & Tuteja, 2019). For some of the developmental genes, more accessible chromatin was also marked by a bivalent H3K4me3/H3K27me3, indicative of a poised state. Notably, previous findings in THY1+ adult spermatogonial cells and in sperm also revealed a poised state at promoters of developmental genes (Erkek et al., 2013; Hammoud et al., 2014; Jung et al., 2017). Therefore, our findings suggest that open chromatin reorganization may contribute to the poised status that is already established at

the spermatogonial cell stage for certain developmental genes. We also identified a category of regions for which the decrease in chromatin accessibility correlated with a decreased expression, the category which also included developmental factors. The stable methylation patterns we detected at the differentially accessible chromatin regions, in both distal and proximal genomic regions, suggest a minimal impact for DNAm in regulating gene expression dynamics of spermatogonial cells across postnatal age.

Lastly, by investigating chromatin accessibility specifically at TEs, we revealed that distinct TE subtypes undergo changes in chromatin accessibility between PND15 and adult spermatogonial populations. ERVK and ERV1 subtypes were the most abundant categories of TEs to become less accessible in adult spermatogonia, whilst LINE L1 subtypes gained in accessibility. Although the majority of these TEs resided in intergenic and intronic regions, we were able to detect specific loci belonging to the differentially accessible ERVK and LINE L1 subtypes, which localized nearby TSS of distinct gene families. RLTR17, one of the LTR subtypes with decreased chromatin accessibility in adult spermatogonial cells, overlapped the TSS of several downregulated long-non coding RNAs from the Platr family. Platr genes, including the ones identified in our study, Lncenc1 and Platr14, are LTR-associated long non-coding RNAs important for embryonic stem cell gene expression programs (Bergmann et al., 2015). Interestingly, RLTR17 has also been previously linked to pluripotency maintenance. In mouse embryonic stem cells, RLTR17 is highly expressed and enriched in open chromatin regions and has been shown to provide binding sites for pluripotency factors Oct4 and Nanog (Fort et al., 2014). On the basis of these findings, we suggest that RLTR17 chromatin organization may play a significant role in regulating pluripotency programs between early postnatal and adult spermatogonial cells. In contrast to the decreased accessibility of LTRs, LINE L1 subtypes displayed an increase in chromatin accessibility in adult spermatogonial cells. Some of these L1 loci were situated in the vicinity of olfactory receptor genes with upregulated mRNA expression in adult spermatogonia. Recent findings in mouse and human embryonic stem cells have suggested a non-random genomic localization for L1 elements, specifically at genes that encode proteins with specialized functions (Lu et al., 2020). Among these, the Olfr gene family was the most enriched in L1 elements (Lu et al., 2020). Although their role in spermatogonial cells is currently not established, Olfr proteins have been implicated in the swimming behaviour of sperm (Fukuda & Touhara, 2005; Vanderhaeghen, Schurmans, Vassart, & Parmentier, 1997). Given their dynamic regulation across age in spermatogonial cells, we speculate that Olfr genes could play additional roles in spermatogenesis, other than in sperm physiology. This data together with the high number of enriched TF motifs identified at the differentially accessible ERVKs and LINE L1 elements underscores previously undescribed regulatory roles for chromatin

organization of TEs in spermatogonial cells during the transition from developing to adult stages (Sundaram et al., 2014; Sundaram & Wysocka, 2020).

One limitation of our study is the incomplete purification achieved using FACS, which doesn't fully remove other testis cell types from our cell preparations. Therefore, we cannot entirely exclude the influence of contaminating cells on some of the transcriptome and chromatin accessibility data interpretation. Secondly, differences can also stem from the literature datasets which involve similar but not identically enriched populations of spermatogonial cells. Nevertheless, by comparing open chromatin landscape between developing and adult spermatogonial cells, our results reveal for the first time that there is an age-dependent dynamic reorganization of chromatin accessibility in spermatogonial cells. By integrating this newly generated data with gene expression profiles and known histone modifications, we provide novel insight into the chromatin - transcriptome dynamics of mouse spermatogonial cells between developing and adult stages and compile an information-rich resource for further germline studies.

## 1.7 Methods

### 1.7.1 Mouse husbandry

Male C57Bl/6J mice were purchased from Janvier Laboratories (France) and bred in-house to generate male mice used for experiments. All animals were kept on a reversed 12-h light/12-h dark cycle in a temperature- and humidity-controlled facility, with food (M/R Haltung Extrudat, Provimi Kliba SA, Switzerland) and water provided ad libitum. Cages were changed once weekly. Animals from 2 independent breedings were used for the experiments.

### 1.7.2 Germ cells isolation

Germ cells were isolated from male mice at postnatal day (PND) 8 or 15 for RNA-seq and ATAC-seq experiments, and adults at 20 weeks of age (PNW20) for ATAC-seq. Testicular single-cell suspensions were prepared as previously described with slight modifications (Kubota et al., 2004a, 2004b). For preparations using PND8 and PND15 pups, testes from 2 animals were pooled for each sample. Pup testes were collected in sterile HBSS on ice. Tunica albuginea was gently removed from each testis, making sure to keep the seminiferous tubules as intact as possible. Tubules were enzymatically digested in 0.25% trypsin-EDTA (ThermoFisher Scientific) and 7mg/ml DNase I (Sigma-Aldrich) solution for 5 min at 37°C. The suspension was vigorously pipetted up and down 10 times and incubated again for 3 min at 37°C. The digestion was stopped by adding 10% fetal bovine serum (ThermoFisher Scientific) and the cells were passed through a 20µm-pore-size cell strainer (Miltenyi Biotec) and pelleted by centrifugation at 600g for 7 min at 4°C. Cells were resuspended in PBS-S (PBS with 1% PBS, 10 mM HEPES, 1 mM pyruvate, 1mg/ml glucose, 50 units/ml penicillin and 50 µg/ml streptomycin) and used for sorting. For preparations from adult testis, one adult male was used for each sample. The tunica was removed and seminiferous tubules were digested in 2 steps. The first consisted of incubation in 1mg/ml collagenase type IV (Sigma-Aldrich) for 5 min at 37°C and vigorous swirling until the tubules were completely separated. Then tubules were placed on ice for 5 min to sediment, the supernatant was removed and washed with HBSS. Washing/sedimentation steps were repeated 3 times and were necessary to remove interstitial cells. After the last washing step, sedimented tubule fragments were digested again with 0.25% trypsin-EDTA and 7mg/ml DNase I solution, and the digestion was stopped by adding 10% FBS. The resulting single-cell suspension was filtered through a 20µm strainer (Corning Life Sciences) and washed with HBSS. After centrifugation at 600g for 7 min at 4°C, the cells were resuspended in PBS-S, layered on a 30% Percoll solution (Sigma-Aldrich) and centrifuged at 600g for 8 min at 4°C without braking. The top 2 layers (HBSS and Percoll)

were removed and the cell pellets were resuspended in PBS-S and used for sorting.

### 1.7.3 Spermatogonial cells enrichment by FACS

For pup testis, dissociated cells were stained with BV421-conjugated anti-b2M, biotin-conjugated anti-THY1 (53-2.1), and PE-conjugated anti-av-integrin (RMV-7) antibodies. THY1 was detected by staining with Alexa Fluor 488-Sav. For adult testes, cells were stained with anti-a6-integrin (CD49f; GoH3), BV421-conjugated anti-b2 microglobulin (b2M; S19.8), and R-phycoerythrin (PE)-conjugated anti-THY1 (CD90.2; 30H-12) antibodies. a6-Integrin was detected by Alexa Fluor 488-SAv after staining with biotin-conjugated rat anti-mouse IgG1/2a (G28-5) antibody. Prior to FACS, 1 µg/ml propidium iodide (Sigma) was added to the cell suspensions to discriminate dead cells. All antibody incubations were performed in PBS-S for at least 30 min at 4oC followed by washing in PBS-S. Antibodies were obtained from BD Biosciences (San Jose, United States) unless otherwise stated. Cell sorting was performed at 4oC on a FACS Aria III 5L using an 85µm nozzle at the Cytometry Facility of the University of Zurich. For RNA-seq on PND8 and PND15 spermatogonia, cells were collected in 1.5 ml Eppendorf tubes in 500 µL PBS-S, immediately pelleted by centrifugation and snap-frozen in liquid N2. Cell pellets were stored at -80oC until RNA extraction. For OmniATAC on PND15 spermatogonia, 25'000 cells were collected in a separate tube, pelleted by centrifugation and immediately processed using the OmniATAC library preparation protocol 10. For OmniATAC on adult spermatogonia, 5000 cells from each animal were collected in a separate tube and further processed using the same protocol.

### 1.7.4 Immunocytochemistry

The protocol used for assessing spermatogonial cell enrichment after sorting was kindly provided by the Oatley Lab at Washington State University, Pullman, USA (Yang, Racicot, Kaucher, Oatley, & Oatley, 2013). Briefly, 30,000-50,000 cells adhered to poly-L-Lysine coated coverslips (Corning Life Sciences) in 24-well plates for 1 h. Cells were fixed in freshly prepared 4% PFA for 10 min at room temperature then washed in PBS with 0.1% Triton X-100 (PBS-T). Non-specific antibody binding was blocked by incubation with 10% normal goat serum for 1 h at room temperature. Cells were incubated overnight at 4oC with mouse anti-PLZF (0.2 µg/ml, Active Motif, clone 2A9) primary antibody. Alexa488 goat anti-mouse IgG (1 µg/mL, ThermoFisher Scientific) was used for secondary labelling at 4oC for 1 h. Coverslips were washed 3x and mounted onto glass slides with VectaShield mounting medium containing DAPI (Vector Laboratories) and examined by fluorescence microscopy. Stem cell enrichment was determined by counting PLZF+ cells in 10 random fields of view from each

coverslip and dividing by the total number of cells present in the field of view (DAPI-stained nuclei).

### 1.7.5 RNA extraction and library preparation for RNA-seq

For RNA-seq on PND8 and PND15 spermatogonial cells, total RNA was extracted from sorted cells using AllPrep RNA/DNA Micro kit (Qiagen). RNA quality was assessed using a Bioanalyzer 2100 (Agilent Technologies). Samples were quantified using Qubit RNA HS Assay (ThermoFisher Scientific). 10 ng of total RNA from each sample were used to prepare total long RNA sequencing libraries using SMARTer® Stranded Total RNA-Seq Kit v2 - Pico Input Mammalian (Takara Bio USA, Inc.) at the Functional Genomics Center Zurich (FGCZ) according to the manufacturer's instructions.

### 1.7.6 Library preparation for Omni-ATAC

Chromatin accessibility was profiled in PND15 and adult spermatogonial cells. Libraries were prepared starting from 25 000 PND15 and 5000 adults sorted spermatogonia, respectively 10. Briefly, sorted cells were lysed in cold lysis buffer (10 mM Tris-HCl pH 7.4, 10 mM NaCl, 3 mM MgCl<sub>2</sub>, 0.1% NP40, 0.1% Tween-20, and 0.01% digitonin) and nuclei were pelleted and transposed using Nextera Tn5 (Illumina) for 30 min at 37°C in a thermomixer with shaking at 1000 rpm. Transposed fragments were purified using the MinElute Reaction Cleanup Kit (Qiagen). Following purification, libraries were generated by PCR amplification using the NEBNext High-Fidelity 2X PCR Master Mix (New England Biolabs), and purified using Agencourt AMPure XP magnetic beads (Beckman Coulter) to remove primer dimers (78bp) and fragments >1000bp. Library quality was assessed on an Agilent High Sensitivity DNA chip using the Bioanalyzer 2100 (Agilent Technologies).

### 1.7.7 RNA sequencing

Quality control and alignment: Single-end (SE) sequencing was performed using an Illumina HiSeq4000 at the FGCZ. PND8 raw data (FASTQ files) was merged from two individual runs. For analysis of published RNA-seq data (PND14 and PNW8 spermatogonia), FASTQ files were obtained using fastq-dump (version 2.10.8), quality-controlled using FastQC (Andrews et al., 2012) (version 0.11.8). TrimGalore (Krueger, 2015) (version 0.6.2) was used to trim adapters and low-quality ends from reads with Phred score less than 30 (-q 30), and for discarding trimmed reads shorter than 30 bp (-length 30). Trimmed reads were pseudo-aligned using Salmon (Patro et al., 2017) (version 0.9.1) with automatic detection of the library

type (-l A), correcting for sequence-specific bias (`-seqBias`) and correcting for fragment GC bias correction (`-gcBias`) on a transcript index prepared for the Mouse genome (GRCm38) from GENCODE (version M18) (Harrow et al., 2012), with additional piRNA precursors and transposable elements (concatenated by family) from Repeat Masker as in (K. Gapp et al., 2020).

Downstream analysis: Analysis was conducted with R(R Core Team, 2019) (version 3.6.2) using packages from The Comprehensive R Archive Network (CRAN) (`%5Bcran.r-project.org%5D`(<https://cran.r-project.org/>)) and Bioconductor (Huber et al., 2015). Pre-filtering of genes was performed using the `filterByExpr` function from edgeR (Robinson et al., 2010) (version 3.28.1) with a design matrix and requiring at least 15 counts (`min.counts = 15`). Normalization factors were obtained using TMM normalization (Robinson & Oshlack, 2010) from edgeR package and differential gene expression (DGE) analysis was performed using limma-voom (C. W. Law et al., 2014) pipeline from limma (Ritchie et al., 2015) (version 3.42.2).  $\log_2$  fold change between samples was calculated by subtracting  $\log_2$  normalized expression values. Gene ontology (GO) analysis was performed on expressed genes with fGSEA (version 1.15.2) using `fGSEAMultilevel` function on sets with 10 to 1000 annotated genes (`minSize = 10`, `maxSize = 1000`), and p-values boundary of 1E-100 (`eps = 1e-100`) (Korotkevich et al., 2016). For PND8 versus PND15 comparison, genes were pre-ranked using t-statistic; for PND14 versus PNW8 comparison,  $\log_2$  fold change was used due to the lack of multiple replicates for each time point. REVIGO was used to summarize GO terms obtained following fGSEA (Supek, Bošnjak, Škunca, & Šmuc, 2011).

### 1.7.8 Omni-ATAC

Quality control, alignment, and peak calling: Paired-end (PE) sequencing was performed on PND15 and adult spermatogonial cells samples on an Illumina HiSeq2500 platform (FGCZ). FASTQ files were assessed for quality using FastQC (Andrews et al., 2012) (version 0.11.8). Quality control (QC) was performed using TrimGalore (Krueger, 2015) (version 0.6.2) in PE mode (`-paired`), trimming adapters, low-quality ends (`-q 30`) and discarding reads  $< 30$  bp after trimming (`-length 30`). Alignment on the GRCm38 genome was performed using Bowtie2 (Langmead & Salzberg, 2012) (version 2.3.5) with the following parameters: fragments up to 2 kb were allowed to align (`-X 2000`), entire read alignment (`-end-to-end`), suppressing unpaired alignments for paired reads (`-no-mixed`), suppressing discordant alignments for paired reads (`-no-discordant`) and minimum acceptable alignment score with respect to the read length (`-score-min L,-0.4,-0.4`). Using alignmentSieve (version 3.3.1) from deepTools (Ramirez et al., 2016) (version 3.4.3), aligned data (BAM files) were adjusted for the read start sites to

represent the centre of the transposon cutting event (-ATACshift), and filtered for reads with a high mapping quality (-minMappingQuality 30). Reads mapping to the mitochondrial chromosome and ENCODE blacklisted regions were filtered out. To call nucleosome-free regions, all aligned files were merged within groups (PND15 and adult), sorted, and indexed using SAMtools (H. Li et al., 2009) (version 0.1.19), and nucleosome-free fragments (NFFs) were obtained by selecting alignments with a template length between 40 and 140 inclusively. Peak calling (identifying areas in a genome that have been enriched for transcription factors) on the NFFs was performed using MACS2 (Y. Zhang et al., 2008) (version 2.2.7.1) with mouse genome size (-g 2744254612) and PE BAM file format (-f BAMPE).

Differential accessibility analysis: The downstream analysis was performed in R(version 3.6.2), using packages from CRAN and Bioconductor (Huber et al., 2015). The peaks were annotated based on overlap with GENCODE (version M18) (Harrow et al., 2012) transcript, and/or the distance to the nearest transcription start site (available at the following link: [https://github.com/mansuylab/SC\\_postnatal\\_adult/bin/annoPeaks.R](https://github.com/mansuylab/SC_postnatal_adult/bin/annoPeaks.R)). The number of extended reads overlapping in the peak regions was calculated using the csaw package (Lun & Smyth, 2015) (version 1.20.0). Peak regions that did not have at least 15 reads in at least 40% of the samples were filtered out. Normalization factors were obtained on the filtered peak regions using the TMM normalization method (Robinson & Oshlack, 2010) and differential analysis on the peaks (adults vs PND15) was performed using the Genewise Negative Binomial Generalized Linear Models with Quasi-likelihood (glmQLFit) Tests from the edgeR package (Robinson et al., 2010) (version 3.28.1). Peak regions that had an absolute  $\log_2$  fold change  $\geq 1$  and an FDR  $\leq 0.05$  were categorized as differentially accessible regions. GO analysis was performed on DARs with the rGREAT package (Gu, 2021) (version 1.18.0), which is a wrapper around the GREAT tool (McLean et al., 2010) (version 4.0). Transcription factor motif enrichment analysis was performed using the marge package (Amezquita, 2018) (version 0.0.4.9999), which is a wrapper around the Homer tool (Heinz et al., 2010) (version 4.11.1).

Differential accessibility analysis at transposable elements: TE gene transfer format (GTF) file was obtained from [labshare.cshl.edu/shares/mhammelllab/www-data/TEtranscripts/TE\_GTF/mm10\_rmsk\_TE.gtf.gz%20on%2003.02.2020] ([http://labshare.cshl.edu/shares/TEtranscripts/TE\\_GTF/mm10\\_rmsk\\_TE.gtf.gz](http://labshare.cshl.edu/shares/TEtranscripts/TE_GTF/mm10_rmsk_TE.gtf.gz)) on 03.02.2020. The GTF file provides hierarchical information about TEs: **Class** (level 1, eg. LTR), **Family** (level 2, eg. LTR L1), **Subtype** (level 3, eg. LTR L1 L1\_Rod), and **Locus** (level 4, eg. LTR L1 L1\_Rod L1\_Rod\_dup1). TE loci were annotated based on overlap with GENCODE (version M18) as described above for ATAC-seq peaks. Filtered BAM files (without reads mapping to blacklisted or mitochondrial regions) were used for analyzing TEs. Mapped reads

were assigned to TEs using featureCounts from the R package Rsubread (Liao et al., 2019) (version 2.0.1) and were summarized to Subtypes (level 3), allowing for multi-overlap with fractional counts, while ignoring duplicates. The number of extended reads overlapping at the TE loci were obtained using the csaw package (Lun & Smyth, 2015) (version 1.20.0). Subtypes which did not have at least 15 reads, and loci that did not have at least 5 reads in at least 40% of the samples, were filtered out. Normalization and differential accessibility analysis were performed as described above. Subtypes that had an absolute  $\log_2$ fold change  $\geq 0.5$  and an FDR  $\leq 0.05$  were categorized as differentially accessible subtypes and the loci with an absolute  $\log_2$  fold change  $\geq 1$  and an FDR  $\leq 0.05$  were categorized as differentially accessible loci. For further downstream data analysis, only the differentially accessible loci of differentially accessible subtypes were considered. GO and motif enrichment analysis were performed as described above.

### 1.7.9 Chromatin immunoprecipitation sequencing

Quality control, alignment, and peak calling:ChIP-Seq SE data for PNDW8 (adults) were obtained from GEO accession GSE49621 (Hammoud et al., 2014). FASTQ files were obtained using fastq-dump (version 2.10.8), and different runs were merged. The FASTQ files were assessed for quality using FastQC (Andrews et al., 2012) (version 0.11.8). Quality control (QC) was performed using TrimGalore (Krueger, 2015) (version 0.6.0), trimming adapters, low-quality ends (-q 30) and discarding trimmed reads shorter than 30 bp (-length 30). Alignment to the GRCh38 genome was performed using Bowtie2 (Langmead & Salzberg, 2012) (version 2.3.5). Reads with low mapping quality (-minMappingQuality 30) or mapping to the mitochondrial chromosome or aforementioned blacklisted regions were filtered out. Peak calling was performed using MACS2 (Y. Zhang et al., 2008) (version 2.2.7.1) with mouse genome size (-g 2744254612) and SE BAM file format (-f BAM).

### 1.7.10 Bisulfite sequencing (BS)

Quality control and alignment:BS paired-end data for PND7, PND14, and PNW8 (adults) were obtained from GEO accession GSE49623 (Hammoud et al., 2015). FASTQ files were obtained using fastq-dump (version 2.10.8), and different runs were merged. FASTQ files were assessed for quality using FastQC (Andrews et al., 2012) (version 0.11.8). QC was performed using TrimGalore (Krueger, 2015) (version 0.6.4\_dev) in PE mode (-paired), trimming adapters, low-quality ends (-q 30) and discarding trimmed reads shorter than 30 bp (-length 30). Alignment of the QC data was performed using Bismark (Krueger & Andrews, 2011) (version 0.22.3) on a GRCh38 index built using bismark\_genome\_preparation

(version 0.17.0). Methylation information for individual cytosines was extracted using the bismark\_methylation\_extractor tool from the Bismark package (version 0.22.3).

### 1.7.11 High-throughput sequencing data analysis

Data availability: the datasets used in this study are available from the following GEO accessions: \*\*GSE\_\_\_\_\_\*\*, GSE49621, GSE49622, GSE62355, and GSE49623. An overview of the datasets included in the study is shown in Table 1.1

**Table 1.1:** Datasets used in this manuscript

Source	Sequencing	Stages (n)
GSE	RNA-seq	PND8 (8), PND15 (9)
GSM1525703	RNA-seq	PND14 (1)
GSM1415671	RNA-seq	PNW8 (1)
GSE	ATAC-seq	PND15 (6), PNW20 (5)
GSM1202705	ChIP-seq (H3K4me3)	PNW8 (1)
GSM1202708	ChIP-seq (H3K27me3)	PNW8 (1)
GSM1202713	ChIP-seq (H3K27ac)	PNW8 (1)
GSM1202723	ChIP-seq (Input)	PNW8 (1)
GSE49623	BS-seq	PND7 (1), PND14 (1), PNW8 (7)

### 1.7.12 Figures

All figures in this study were generated using ggplot2 (Wickham, 2016), EnrichedHeatmap (Gu et al., 2018), and ComplexHeatmap (Gu et al., 2016) packages, and using base plotting functions in R. Genomic tracks were generated in IGV and colour coded in Inkscape.

## 1.8 Authors contribution

ILC and IMM conceived and designed the study. ILC prepared samples, performed all RNA-seq, ICC and ATAC-seq experiments. DKT analyzed RNA-seq, ATAC-seq, ChIP-seq and BS data, with significant support from PLG. ILC and DKT prepared figures. ILC interpreted the data with significant input from DKT, PLG and IMM. ILC wrote the manuscript with significant help from DKT, PLG and IMM. All authors read and accepted the final version of the manuscript.

## 1.9 Acknowledgements

We thank Francesca Manuella and Martin Roszkowski for taking care of animal breeding, Yvonne Zipfel for animal care, Andrew McDonald for assistance with basic lab needs, Silvia Schelbert and Alberto Corcoba for taking care of the animal licenses and lab organization. We thank Rodrigo Arzate for conceptual support and critical reading of the manuscript. We thank Catherine Aquino and Emilio Yángüez from the Functional Genomics Center Zurich for support and advice with library preparation and sequencing. We are very grateful to Jon Oatley, Melissa Oatley, Tessa Lord and Nathan Law for conceptual advice, hands-on training, and for providing detailed protocols for testis dissection and preparation, and immunocytochemistry of spermatogonial cells. We thank Zuguang Gu for support with heatmaps. We thank Service and Support for Science IT ([www.s3it.uzh.ch](http://www.s3it.uzh.ch)) for computational infrastructure.

## 1.10 Competing interest

The authors declare that they have no competing interests.

## 1.11 Funding

The lab is funded by the University Zurich, ETH Zurich, the Swiss National Science Foundation Grant No. 31003A\_175742 / 1, ETH fellowship ETH-25 19-2. DKT is supported by a Swiss Government Excellence Scholarship.

## 1.12 Data and materials availability

Repository accession numbers will be available at publication or by request to the corresponding author. The code employed for the data analysis is available from [https://github.com/mansuylab/SC\\_postnatal\\_adult](https://github.com/mansuylab/SC_postnatal_adult).

## 1.13 Figures

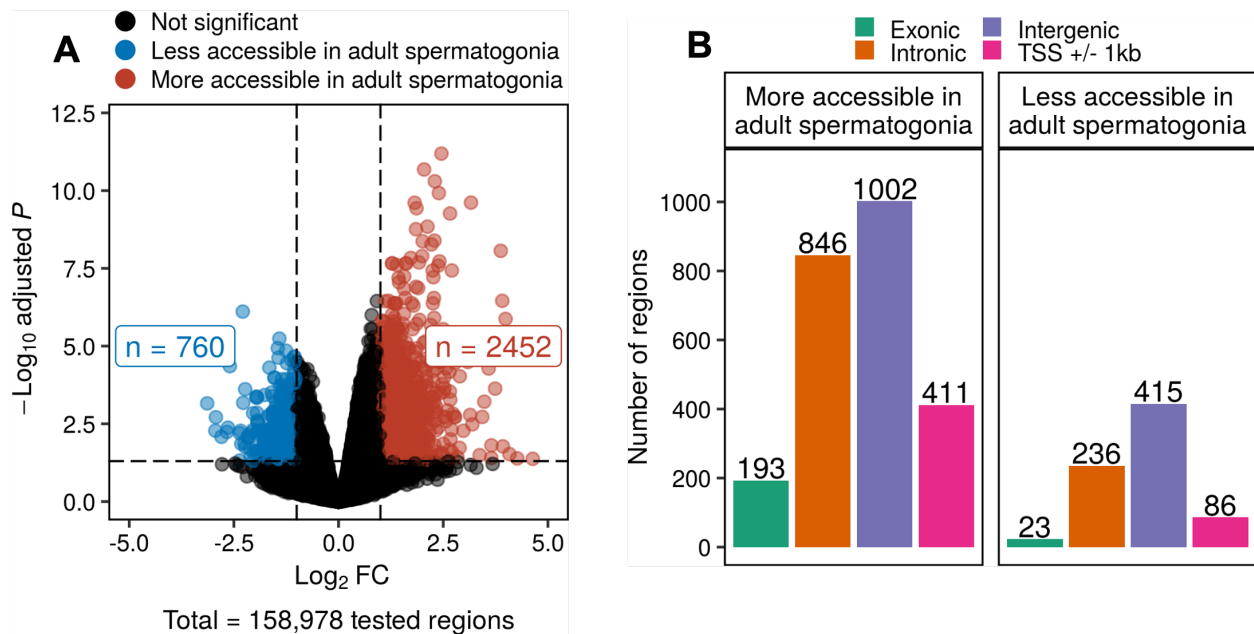


**Figure 1.9a:** Regions of differential chromatin accessibility in spermatogonial cells between postnatal and adult stages associate with distinct biological processes.

**A:** Volcano plot of differentially accessible regions (adjusted  $P \leq 0.05$  and absolute  $\log_2 FC \geq 1$ ) between PND15 ( $n = 6$ ) and adult ( $n = 5$ ) spermatogonial cells identified by ATAC-seq.

**B:** Bar plot illustrating the genomic distribution of differentially accessible chromatin regions in PND15 and adult spermatogonial cells. Genomic regions are categorized in exonic, intronic, intergenic and +/- 1kb from the TSS of a gene.

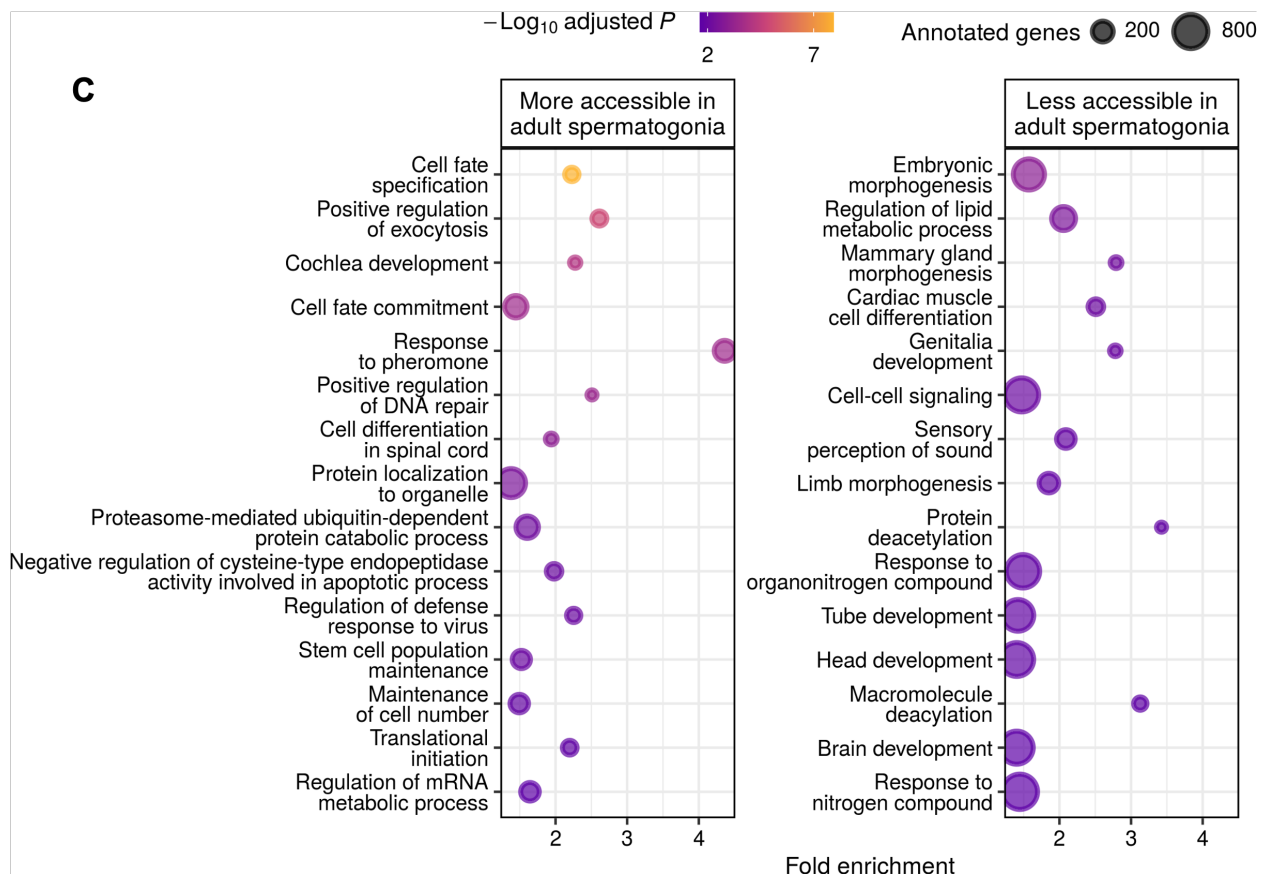


**Figure 1.9b: Regions of differential chromatin accessibility in spermatogonial cells between postnatal and adult stages associate with distinct biological processes.**

**C:** Dot plots of top enriched GO biological processes for regions with increased or decreased chromatin accessibility in adult spermatogonia. Dots size indicates the number of genes in the term, and their colour corresponds to the adjusted P-value of the term's enrichment.

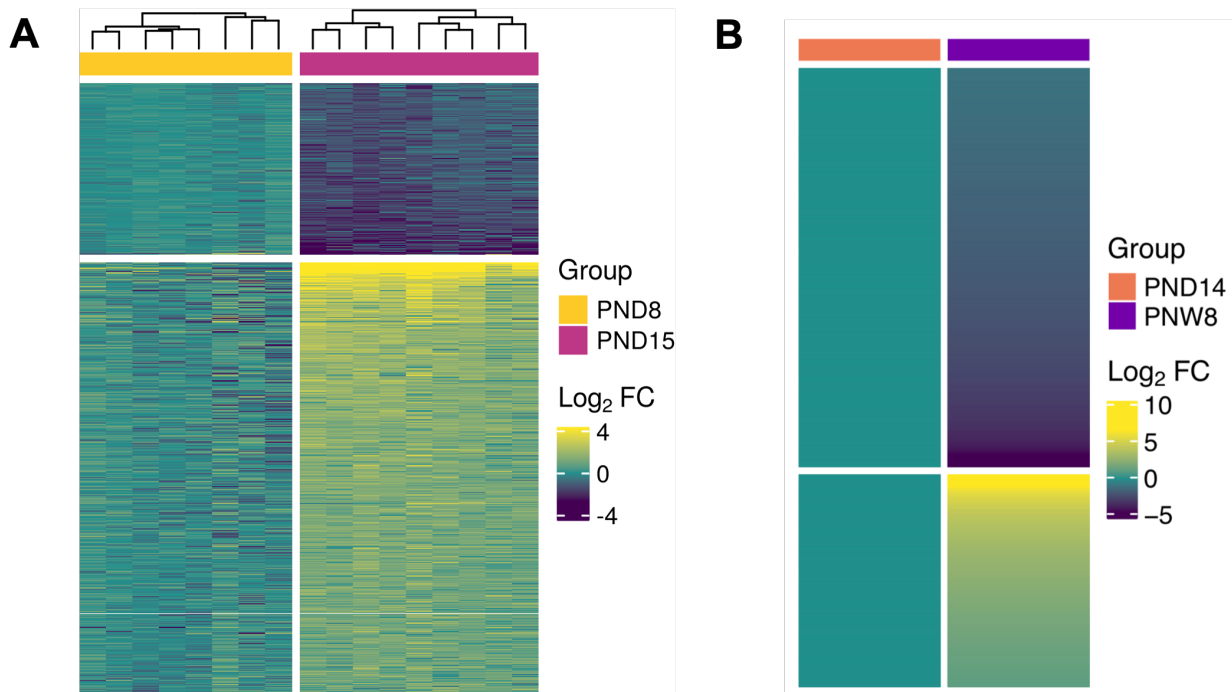


**Figure 1.10a: Transcriptomic profile in postnatal and adult spermatogonial cells.**

**A:** Heatmap of differentially expressed genes (coding and non-coding) (adjusted  $P \leq 0.05$  and absolute Log<sub>2</sub> FC  $\geq 1$ ) between PND8 ( $n = 9$ ) and PND15 ( $n = 8$ ) spermatogonial cells. Shown are Log<sub>2</sub> FC with respect to the average of PND8 data. Samples are clustered using Ward's method. Genes are ordered by principal component analysis (PCA) method using seriation (R package).

**B:** Dot plots of top 20 enriched GO biological processes (adjusted  $P \leq 0.05$ ) from GSEA analysis of PND8 versus PND15. GO terms are summarized by REVIGO and ordered by their normalized enrichment scores (NES). The size of the dot indicates the number of expressed genes annotated in the GO term, and the colour corresponds to the adjusted P-value.

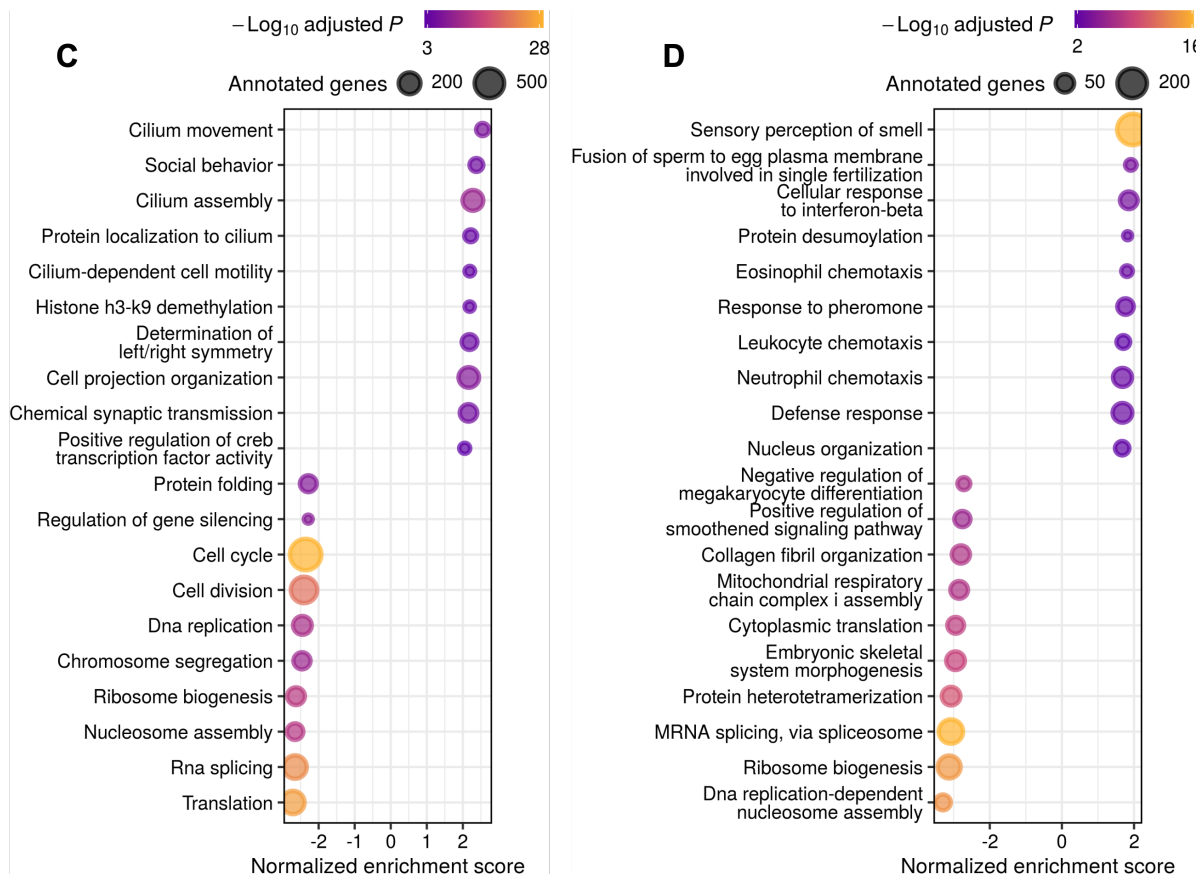


**Figure 1.10b: Transcriptomic profile in postnatal and adult spermatogonial cells.**

**C,D:** Dot plots of top 10 enriched GO BP terms ( $\text{adjusted } P \leq 0.05$ ) from GSEA analysis of PND15 vs PND8 and PNW8 vs PND14 comparison, respectively. GO terms are summarized by REVIGO and ordered by their normalized enrichment scores (NES). The size of the dot indicates the number of expressed genes annotated in the GO term, and the colour corresponds to the adjusted  $P$  value.

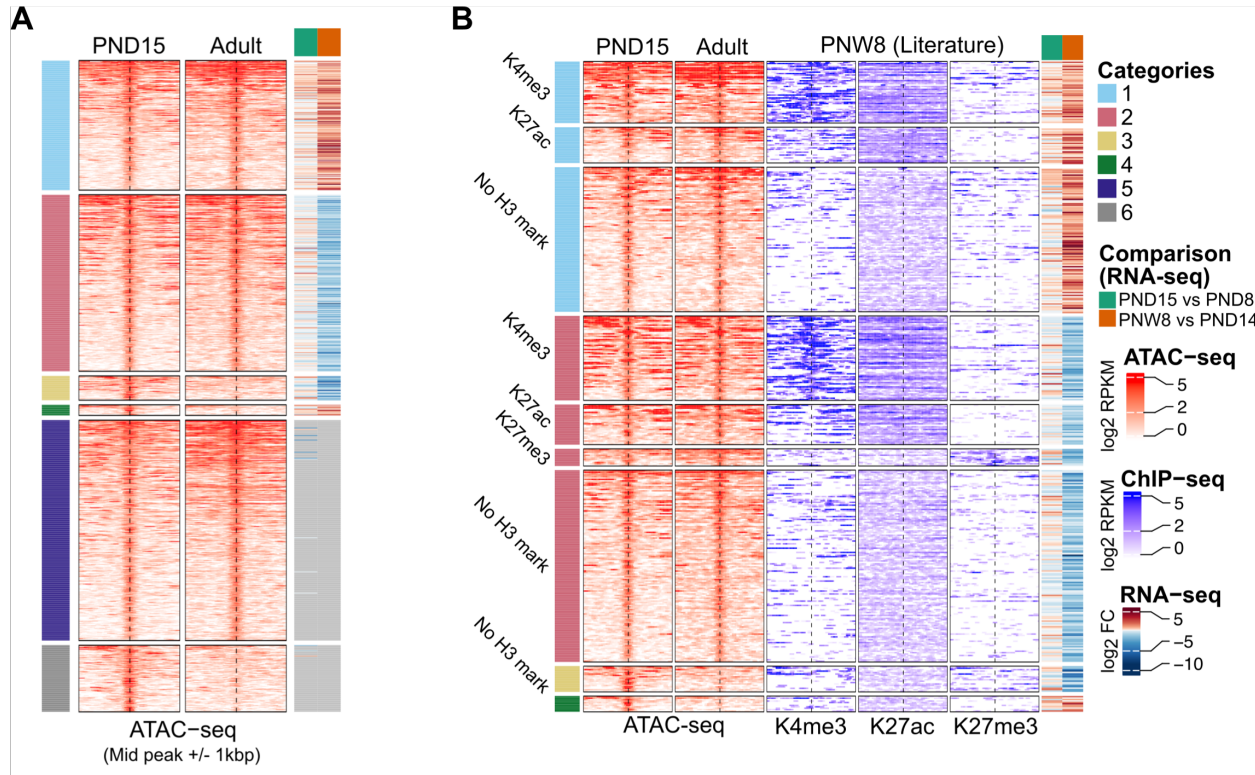


**Figure 1.11a: Chromatin accessibility and histone modifications at proximal regions of genes dynamically expressed between PND15 and adult spermatogonial cells.**

**A:** Heatmap of mean coverage across conditions showing proximal regions of increased chromatin accessibility and increased (Category 1, n = 171) or decreased (Category 2, n = 233) gene expression, decreased chromatin accessibility and decreased (Category 3, n = 32) or increased (Category 4, n = 14) gene expression when comparing PND15 with adult spermatogonia. Proximal inactive regions were defined as regions with increased (Category 5, n = 291) or decreased (Category 6, n = 88) accessibility for which no expression of the nearest gene could be detected by RNA-seq.

**B:** Heatmap showing the overlap between Category 1-4 regions and ChIP-seq data in PNW8 spermatogonia for H3K4me3, H3K27ac and H3K27me3. For each of the Category 1-4, the following sub-categorization was applied: regions enriched for H3K4me3 (with or w/o H3K27ac and/or H3K27me3), regions enriched for H3K27ac (and lack both H3K4me3 and H3K27me3) and regions enriched for H3K27me3 (and lack both H3K4me3 and H3K27ac). For (A, B), each line represents a peak region and regions are ordered within a category by the ATAC-seq signal. Mid-x-axis corresponds to the middle of a peak region and is extended to +/- 1 kb. The colour-key of the ATAC-seq heatmap represents the ATAC-seq signal in Log<sub>2</sub> Reads Per Kilobase per Million (RPKM) reads sequenced. For RNA-seq, Log<sub>2</sub> FC is shown from PND8 versus PND15 and PND14 versus PNW8 comparisons. Rows are ordered by the enriched scores of ATAC-seq data.

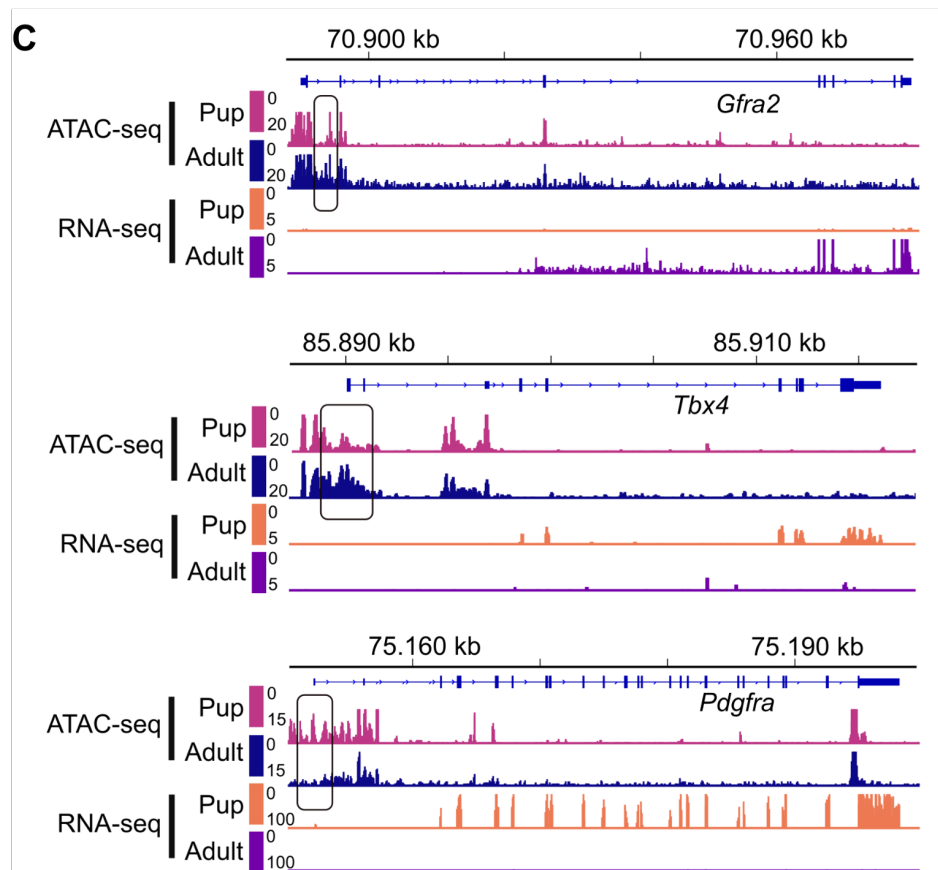


**Figure 1.11b: Chromatin accessibility and histone modifications at proximal regions of genes dynamically expressed between PND15 and adult spermatogonial cells.**

**C:** Genomic snapshots from the Integrative Genomics Viewer (IGV, Broad Institute) of exemplary genes from Category 1 (*Gfra2*), category 2 (*Hmx1*) and category 3 (*Pdgfra*) showing the relative abundance of transcripts from RNA-seq and chromatin accessibility from ATAC-seq. RNA-seq data correspond to literature PND14 and PNW8 spermatogonial cells and ATAC-seq data to PND15 and adult spermatogonial cells. Genomic snapshots from the Integrative Genomics Viewer (IGV, Broad Institute) of exemplary genes from Category 1 (*Gfra2*), Category 2 (*Hmx1*) and Category 3 (*Pdgfra*) showing the relative abundance of transcripts from RNA-seq, chromatin accessibility from ATAC-seq and enrichment of 3 different histone marks (H3K27ac, H3K4me3 and H3K27me3) from ChIP-seq. Pup (PND15 ATAC-seq or PND14 RNA-seq samples) spermatogonia are represented in green and adult (PNW20 ATAC-seq samples or PNW8 RNA-seq and ChIP-seq samples) spermatogonia are represented in orange and overlaid in each of the IGV tracks.

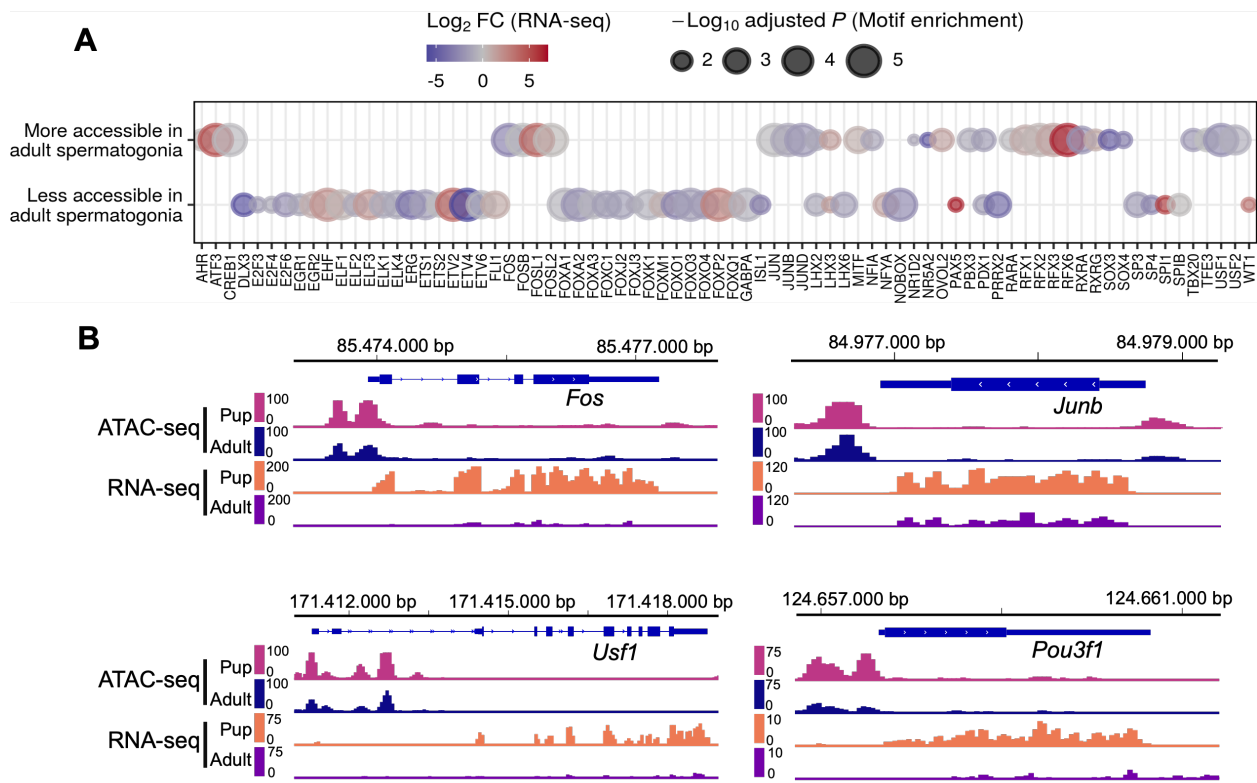


**Figure 1.12a: Transcription factor dynamics at differentially accessible regions is predicted by motif enrichment in adult spermatogonial cells.**

**A:** Dot plot of all transcription factor motifs enriched in the regions of decreased and increased accessibility between adult and PND15 spermatogonia. Each dot corresponds to a motif. The differential gene expression of each transcription factor was extracted from the PND14 and PNW8 literature RNA-seq and is shown as colour-coded Log<sub>2</sub> FC. The size of the dot indicates the HOMER motif enrichment adjusted P of each motif.

**B:** Genomic snapshots from the Integrative Genomics Viewer (IGV, Broad Institute) of mRNA expression levels of representative enriched TFs in the regions of increased chromatin accessibility. RNA-seq data corresponds to literature PND14 and adult (PNW8) spermatogonial cells and ATAC-seq data to PND15 and adult (PNW20) spermatogonial cells, respectively.

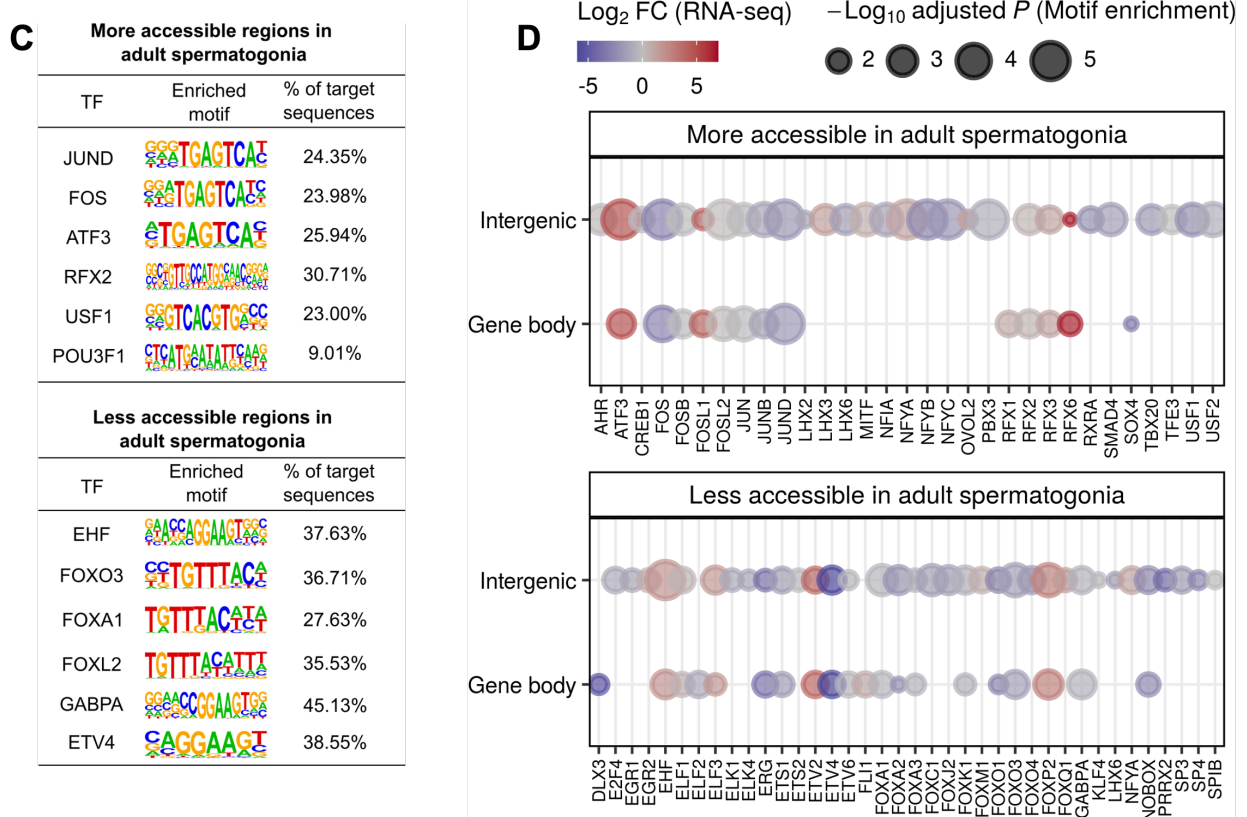


**Figure 1.12b: Transcription factor dynamics at differentially accessible regions is predicted by motif enrichment in adult spermatogonial cells.**

**C:** HOMER extracted consensus sequences for each transcription factor motif. Representative examples from the most enriched transcription factor families are depicted.

**D:** Dot plots of top transcription factor motifs enriched in differentially accessible chromatin regions situated in gene bodies and in intergenic areas of the genome. Each dot corresponds to a motif. The differential gene expression of each transcription factor was extracted from the PND14 and PNW8 literature RNA-seq and is shown as colour-coded Log<sub>2</sub> FC. The size of the dot indicates the HOMER motif enrichment adjusted P of each motif.

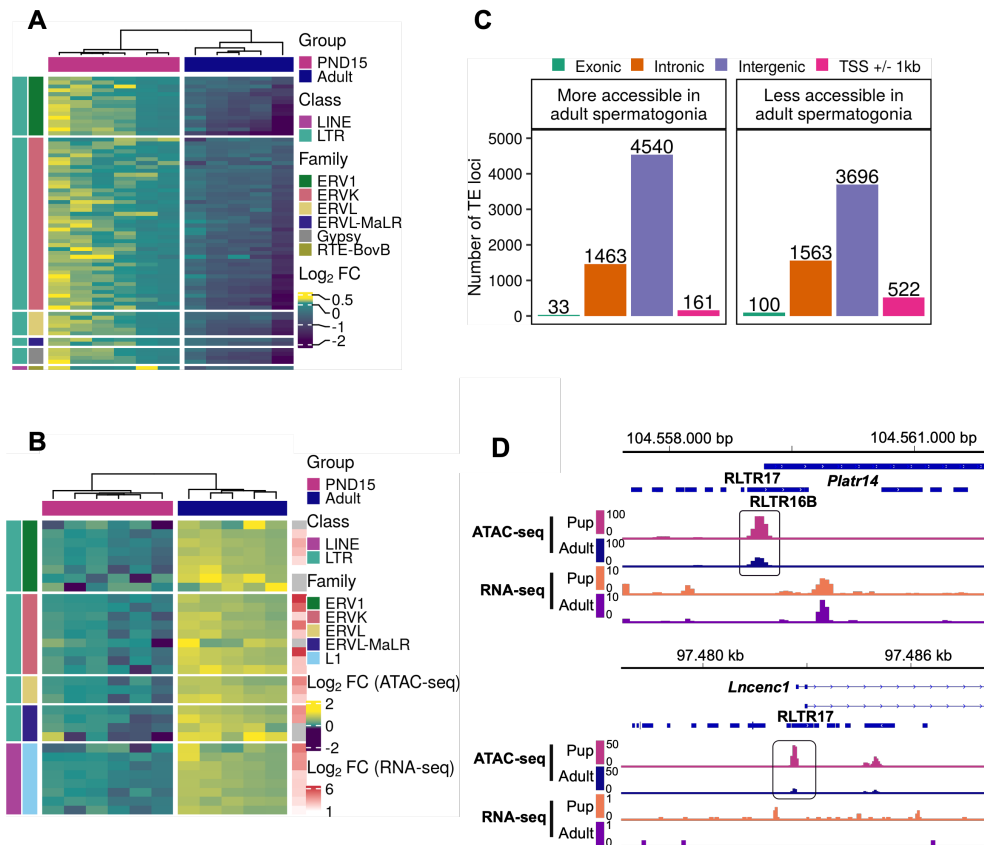


**Figure 1.13a: Differential chromatin accessibility at transposable elements (TEs) in adult spermatogonial cells compared to PND15.**

**A:** Heatmap of the LTR and LINE subtypes with decreased accessibility between adult and PND15 spermatogonia (adjusted  $P \leq 0.05$  and  $\text{Log}_2 \text{ FC} \geq 0.5$ ).

**B:** Heatmap of the LTR and LINE subtypes with increased accessibility between adult and PND15 spermatogonia (adjusted  $P \leq 0.05$  and  $\text{Log}_2 \text{ FC} \geq 0.5$ ). Expression changes of these subtypes between PNW8 and PND14 spermatogonia literature RNA-seq is represented as Log<sub>2</sub> FC.

(**A, B**) Log<sub>2</sub> FC are shown with respect to the average of the PND15 samples. Samples are clustered using Ward's method. Subtypes are ordered by principal component analysis (PCA) method using seriation (R package).

**C:** Bar plot illustrating the genomic distribution of differentially accessible TEs between adult and PND15 spermatogonial cells.

**D:** Genomic snapshots from the Integrative Genomics Viewer (IGV, Broad Institute) of Lncenc1 and Platr14 showing LTRs from RepeatMasker and the average normalized RNA-seq and ATAC-seq coverage (RPKM). LTR loci were extracted using RepeatMasker. RNA-seq data corresponds to literature PND14 and adult (PNW8) spermatogonial cells and ATAC-seq data to PND15 and adult (PNW20) spermatogonial cells, respectively.

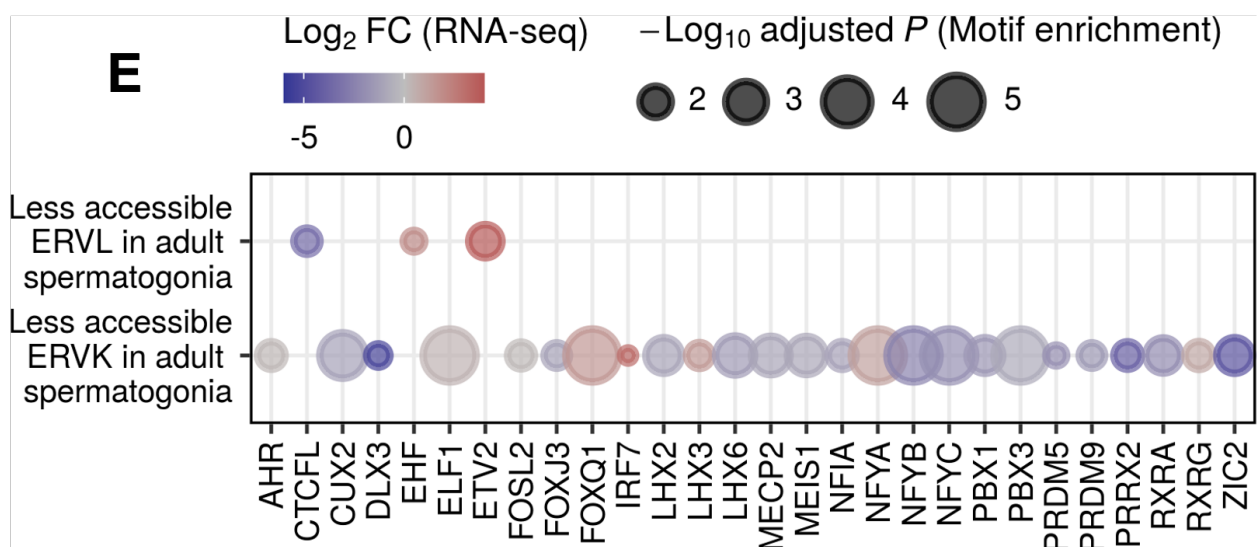


**Figure 1.13b: Differential chromatin accessibility at transposable elements (TEs) in adult spermatogonial cells compared to PND15.**

**E:** Dot plots of top transcription factor motifs enriched in the less accessible ERVKs and ERVL subtypes. Each dot corresponds to a motif. The differential gene expression of each transcription factor was extracted from the PNW8 vs PND14 comparison from literature RNA-seq and is shown as colour-coded  $\text{Log}_2 \text{FC}$ . The size of the dot indicates the HOMER motif enrichment adjusted P of each motif.

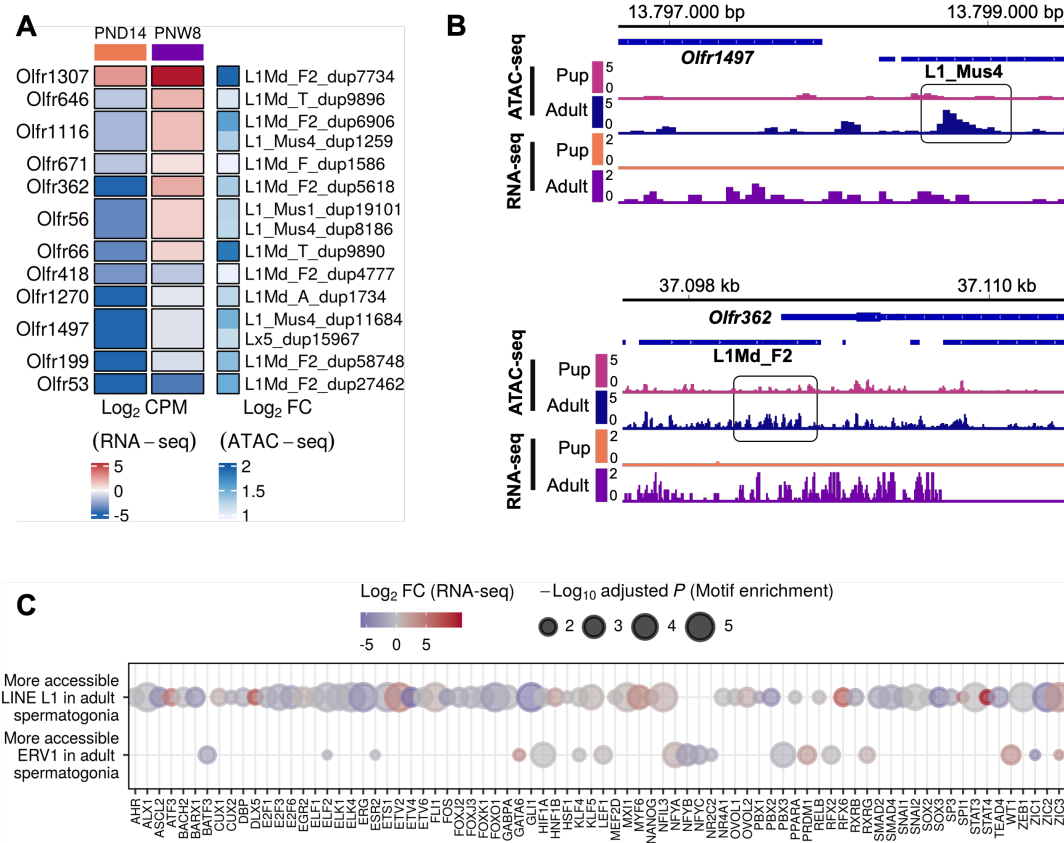


**Figure 1.14: Increased accessibility at LINE L1 subtypes located near Olfr gene clusters.**

**A:** Heatmap of the *Olfr* genes for which we identified an upregulated expression from PND14 to PNW8 timepoints and an increase in accessibility at a nearby L1 locus. RNA expression levels are expressed as Log<sub>2</sub> CPM at each timepoint. Accessibility changes at each of the corresponding L1 locus situated within +/- 5kbp from the gene are expressed as Log<sub>2</sub> FC calculated from the ATAC-seq analysis of the differentially accessible TEs between adult and PND15 spermatogonial cells. Locus are ordered by PCA method using seriation (R package).

**B:** Genomic snapshots from the Integrative Genomics Viewer (IGV, Broad Institute) of exemplary genes *Olfr1497* and *Olfr362* showing relative abundance of transcripts from RNA-seq and chromatin accessibility from ATAC-seq. LINE loci were extracted using Repeat Masker. RNA-seq data corresponds to literature PND14 and adult (PNW8) spermatogonial cells and ATAC-seq data to PND15 and adult (PNW20) spermatogonial cells, respectively.

**C:** Dot plots of top transcription factor motifs enriched in the more accessible L1 and ERV1 subtypes. Each dot corresponds to a motif. The differential gene expression of each transcription factor was extracted from the PNW8 vs PND14 comparison from literature RNA-seq and is shown as colour-coded Log<sub>2</sub> FC. The size of the dot indicates the HOMER motif enrichment adjusted P of each motif.

## 1.14 Supplementary Figures

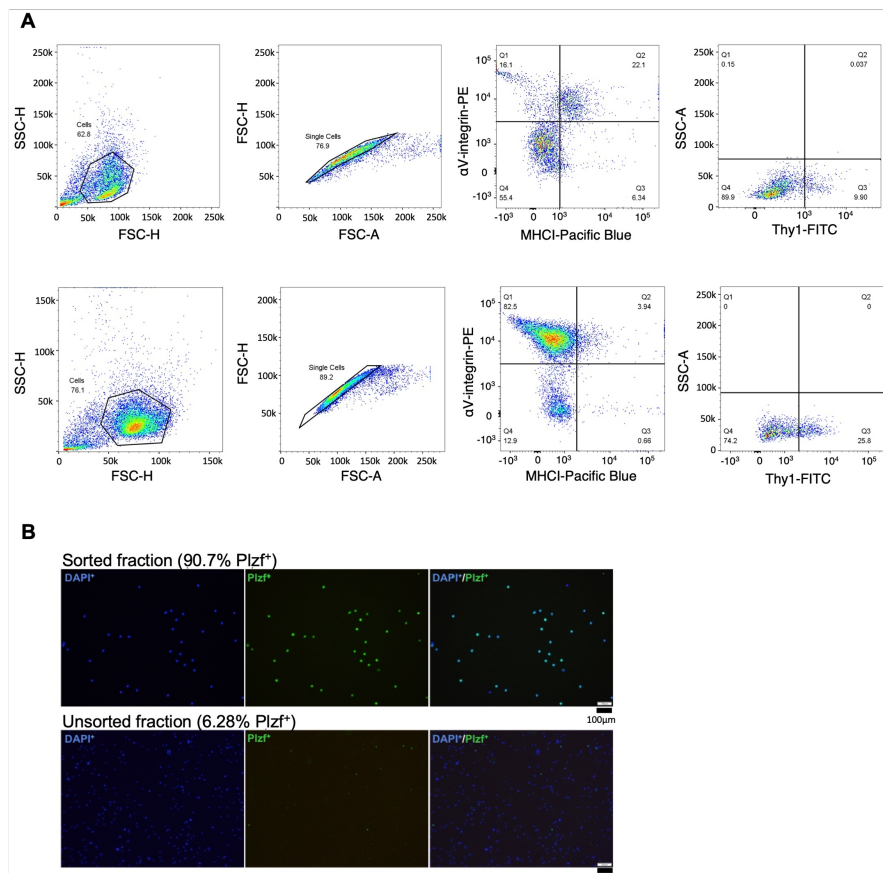


**Figure 1.15a: FACS leads to enrichment of PLZF+ cells in testicular preparations from mouse.**

**A:** Representative dot plots of the sorting strategy for spermatogonial cell enrichment. Gating based on side scatter/forward scatter (SSC-A/FSC-A) and forward scatter – height/ forward scatter – area (FSC-H/FSC-A) was performed to exclude cell debris and cell clumps.

**B:** PLZF+ cells are enriched following FACS, illustrated by immunocytochemistry on unsorted and sorted cell preparations. Immunocytochemistry of PND15 unsorted and the sorted testis cell suspension was performed by fixing cells on poly-L-lysine coated slides. Cells were stained with anti-PLZF antibody (S19 clone, Active Motif) and VECTASHIELD (with DAPI) antifade mounting medium was used for mounting. Cells were visualized with a fluorescence microscope and counted in 10 different fields of view/slide. The number of PLZF+ and PLZF- cells from 10 different fields of view were averaged.

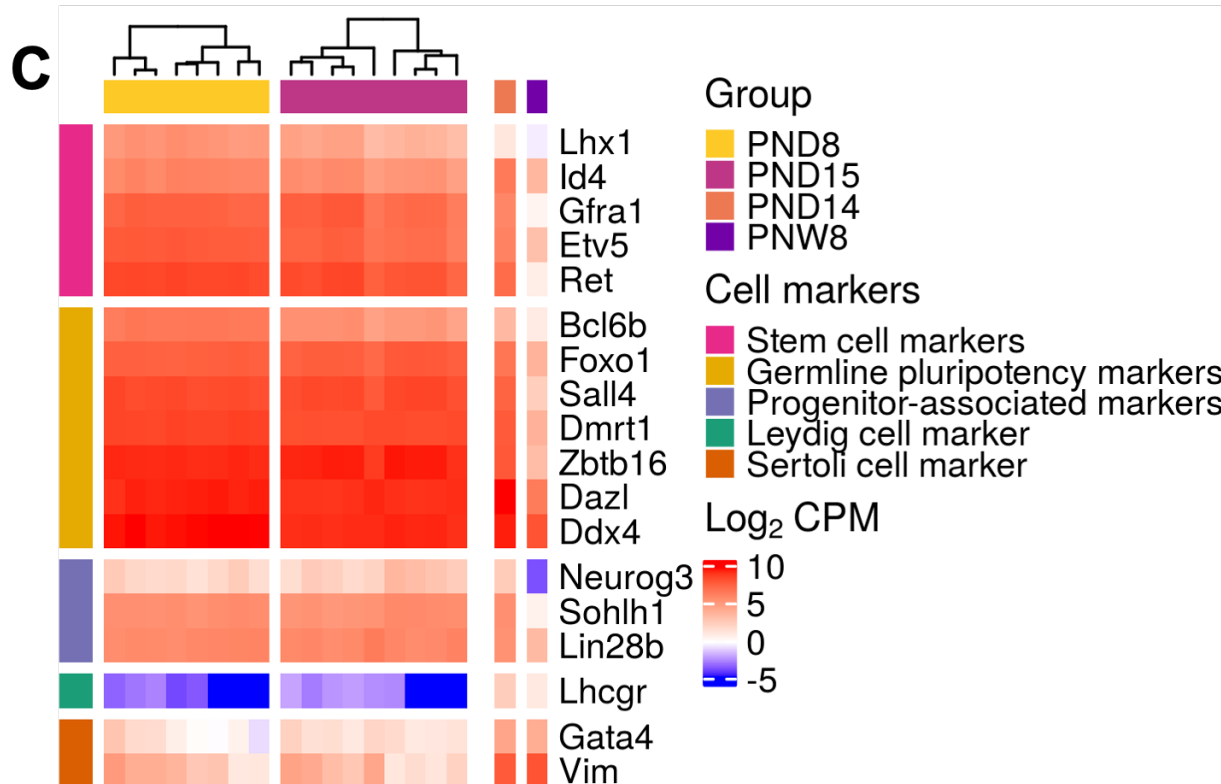


**Figure 1.15b: FACS leads to enrichment of PLZF+ cells in testicular preparations from mouse.**

C Heatmap of the expression profile of selected markers for spermatogonial and different testicular somatic cells from our PND8 and PND15 RNA-seq data, and PND14 and PNW8 datasets from the literature. Key genes for stem cell potential, stem and progenitor spermatogonia, and Leydig and Sertoli cells were chosen to evaluate spermatogonial cells enrichment in the populations. Gene expression is represented in Log<sub>2</sub>CPM (counts per million).

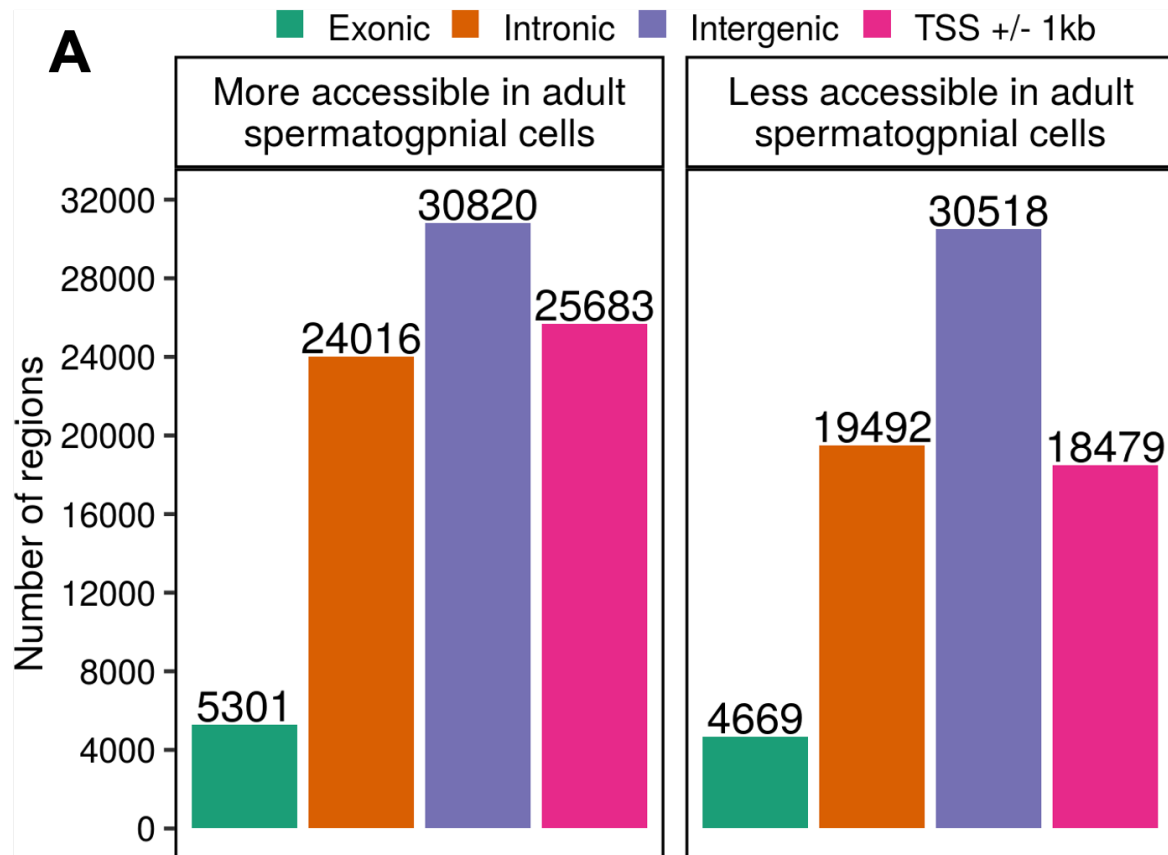


**Figure 1.16a: Omni-ATAC profiles of PND15 and adult spermatogonial cells and their genomic distribution.**

**A:** Genomic distribution of the 158, 978 identified Omni-ATAC regions in between exonic, intronic, intergenic and located +/- 1kb of a transcriptional start site (TSS).

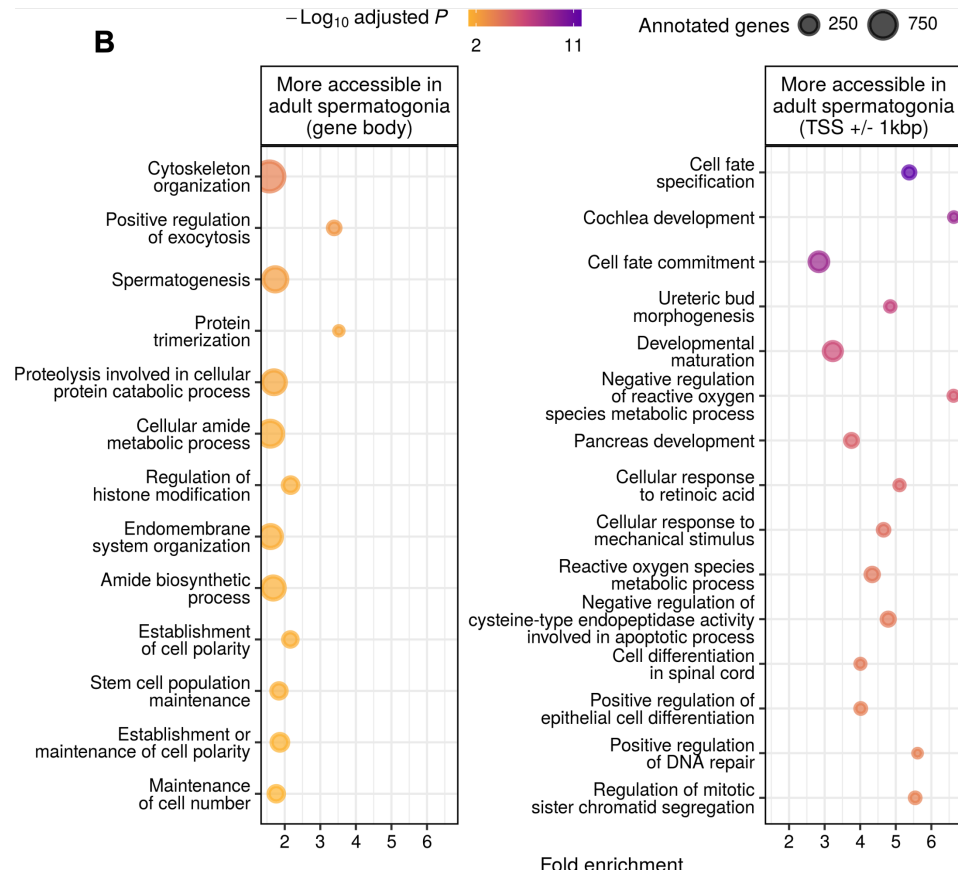


**Figure 1.16b: Omni-ATAC profiles of PND15 and adult spermatogonial cells and their genomic distribution.**

**B:** Dot plots of top enriched GO biological processes for regions with increased chromatin accessibility in adult spermatogonia, within gene bodies and around TSS of nearby genes (TSS +/- 1kb). The size of dots indicates the number of genes in the term and the colour of each dot corresponds to the adjusted *P*-value of the term's enrichment.

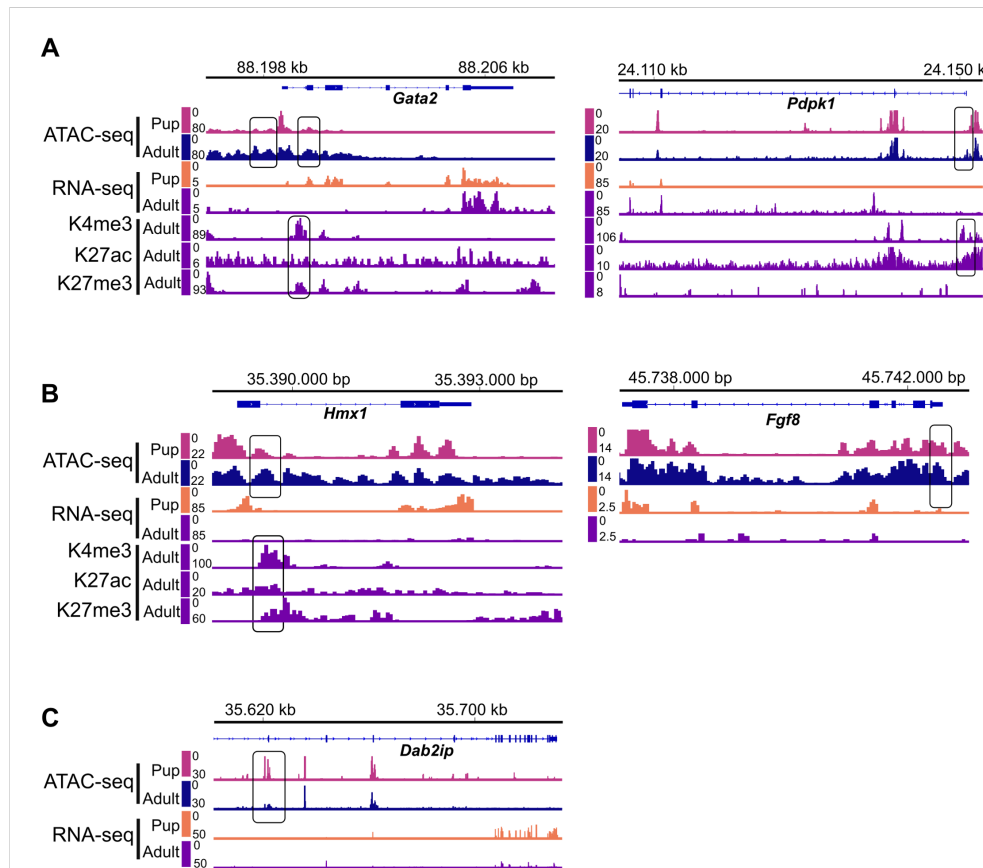


**Figure 1.17: Representative examples from Categories 1-3 resulted from the overlap of chromatin accessibility, gene expression and histone profiling datasets.** Genomic snapshots from the Integrative Genomics Viewer (IGV, Broad Institute) of exemplary genes from **A:** Category 1 (*Pdpk1* and *Gata2*), **B:** Category 2 (*Hmx1* and *Fgf8*), and **C:** Category 3 (*Dab2ip*) showing the relative abundance of transcripts from RNA-seq, chromatin accessibility from ATAC-seq and enrichment of H3K27ac, H3K4me3 and H3K27me3 from ChIP-seq. RNA-seq data correspond to literature PND14 and PNW8 spermatogonial cells and ATAC-seq data to PND15 and adult spermatogonial cells.

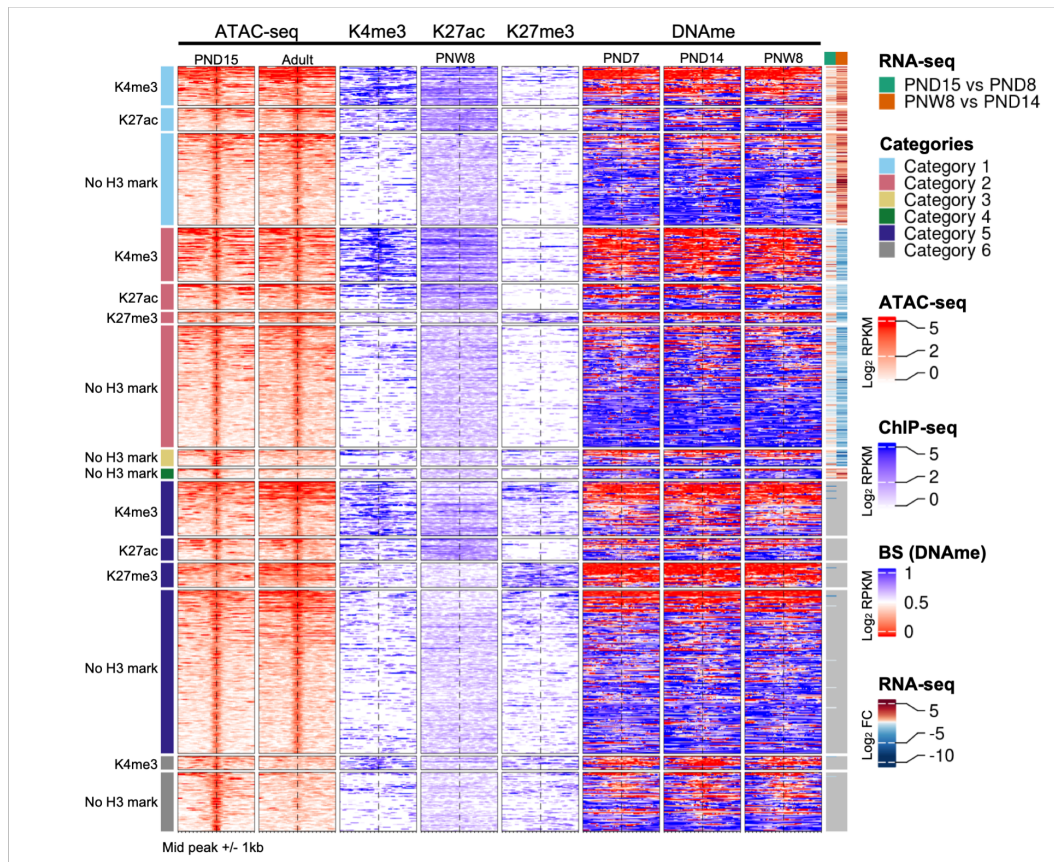


**Figure 1.18: DNAme profiles of spermatogonial cells do not show major changes over the period of testis postnatal maturation.** Enriched heatmaps showing the overlap between Category 1-4 regions, literature ChIP-seq data in PNW8 spermatogonia for H3K4me3, H3K27ac and H3K27me3, and DNAme data from BS in PND7, PND14 and PNW8 spermatogonia. For each of the Category 1-4 the following sub-categorization was applied: regions that are enriched for H3K4me3 (with or w/o H3K27ac and/or H3K27me3), regions that are enriched for H3K27ac (and lack both H3K4me3 and H3K27me3) and regions that are enriched for H3K27me3 (and lack both H3K4me3 and H3K27ac). Each line represents a peak region and the regions are ordered by the ATAC-seq signal. Mid-x-axis corresponds to the middle of a peak region and is extended to +/- 1 kbp. The colour-key of the ATAC-seq, ChIP-seq and BS heatmaps represent ATAC-seq, ChIP-seq and BS signal, respectively. For RNA-seq, Log<sub>2</sub> FC is shown from PND8 vs PND15 and PND14 vs PNW8 comparisons. For BS, the level of DNAme is between 0 and 1, with 0 representing completely unmethylated loci and 1 fully methylated loci, respectively.

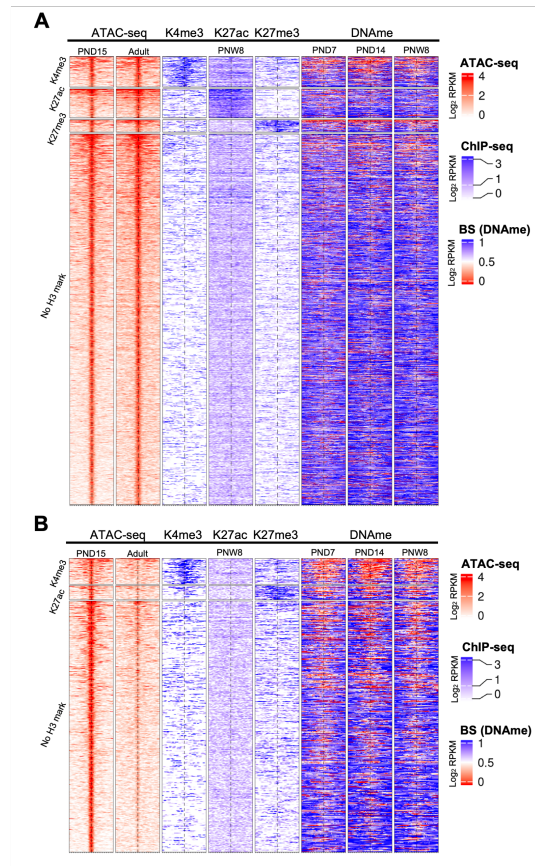


**Figure 1.19: Distinct chromatin profiles between PND15 and adult spermatogonia are present at distal regions across the genome.** (A-B) Enriched heatmaps showing the overlap between more accessible regions (A) and less accessible regions (B) situated in distal regions in spermatogonial cells, and literature ChIP-seq and DNAme data in PNW8 spermatogonia. The following sub-categorization was applied: regions that are enriched for H3K4me3 (with or w/o H3K27ac and/or H3K27me3), regions that are enriched for H3K27ac (and lack both H3K4me3 and H3K27me3) and regions that are enriched for H3K27me3 (and lack both H3K4me3 and H3K27ac). Each line represents a peak region and the regions are ordered by the ATAC-seq signal. Mid-x-axis corresponds to the middle of a peak region and is extended to +/- 1 kbp. The colour-key of the ATAC-seq, ChIP-seq and BS heatmaps represent ATAC-seq, ChIP-seq and BS signal, respectively. For BS, the level of DNAme is between 0 and 1, with 0 representing completely unmethylated loci and 1 fully methylated loci, respectively.

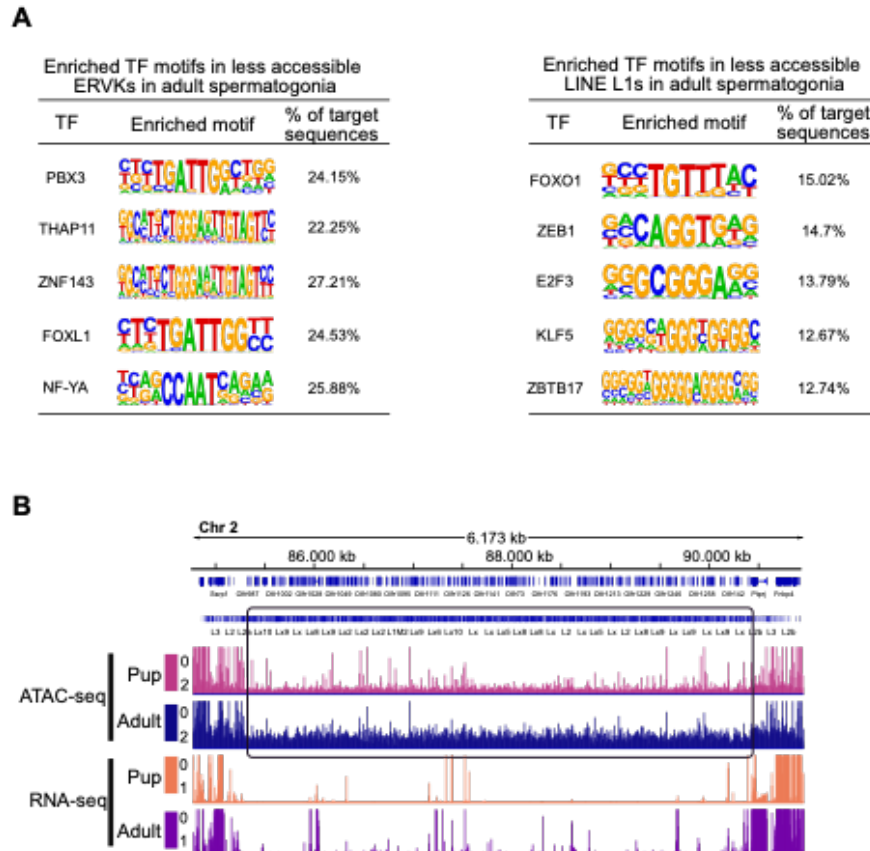


**Figure 1.20: Differentially accessible TEs exhibit enriched TF motifs and correspond to regions nearby non-random gene families.** **A:** HOMER extracted consensus sequences for TF motifs enriched in less accessible ERVK subtypes. Representative examples from the most enriched transcription factor families are depicted. **B:** Genomic snapshots from the Integrative Genomics Viewer (IGV, Broad Institute) of a cluster of Olfr genes on Chr2 overlapping an increased density of LINE elements relative to the neighbouring regions. The relative abundance of transcripts from RNA-seq and chromatin accessibility from ATAC-seq are shown. RNA-seq data corresponds to literature PND14 and adult (PNW8) spermatogonial cells and ATAC-seq data to PND15 and adult (PNW20) spermatogonial cells, respectively.

## 1.15 Supplementary tables

Supplementary tables are too big to be included in the thesis, hence they are provided as links

1. Supplementary table 1
2. Supplementary table 1
3. Supplementary table 1
4. Supplementary table 1
5. Supplementary table 1
6. Supplementary table 1



# Chapter 2

## Early life stress affects the miRNA cargo of epididymal extracellular vesicles in mouse

Anar Alshanbayeva<sup>1,2,3</sup>, Deepak K Tanwar<sup>1,2,3</sup>, Martin Roszkowski<sup>1,2,3</sup>, Francesca Manuella<sup>1,2,3</sup>, Isabelle M Mansuy<sup>1,2,3,#</sup>

<sup>1</sup>Laboratory of Neuroepigenetics, Brain Research Institute at the Medical Faculty of the University of Zurich.

<sup>2</sup>Institute for Neuroscience of the Department of Health Sciences and Technology, ETH Zurich, Zurich, Switzerland.

<sup>3</sup>Zurich Neuroscience Center, ETH and University of Zurich, Zurich, Switzerland.

#Corresponding author

**Journal:** *Biology of Reproduction*

**DOI:** 10.1093/biolre/ioab156

**Contributions:** I performed data analysis with Anar Alshanbayeva, generated figures with Anar Alshanbayeva, assisted Anar Alshanbayeva in writing the manuscript, and revised manuscript with Anar Alshanbayeva.

## 2.1 Graphical Abstract

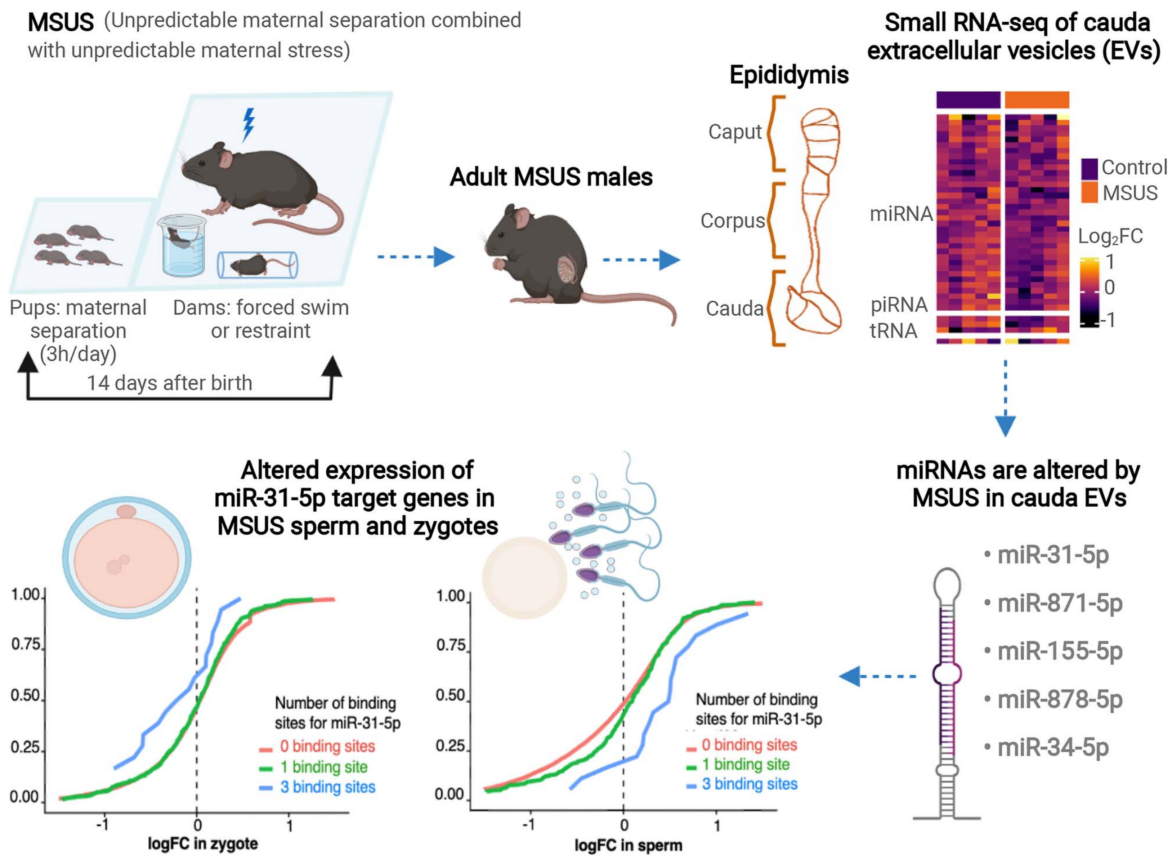


Figure 2.1: Graphical abstract.

## 2.2 Abstract

Sperm RNA can be modified by environmental factors and has been implicated in communicating signals about changes in a father's environment to the offspring. The small RNA composition of sperm could be changed during its final stage of maturation in the epididymis by extracellular vesicles (EVs) released by epididymal cells. We studied the effect of exposure to stress in early postnatal life on the transcriptome of epididymal EVs using a mouse model of transgenerational transmission. We found that the small RNA signature of epididymal EVs, particularly miRNAs, is altered in adult males exposed to postnatal stress. In some cases, these miRNA changes correlate with differences in the expression of their target genes in sperm and zygotes generated from that sperm. These results suggest that stressful experiences in early life can have persistent biological effects on the male reproductive tract that may in part be responsible for the transmission of the effects of exposure to the offspring.

## 2.3 Summary sentence

miRNA cargo of extracellular vesicles in cauda epididymis is altered by paternal exposure to early life stress. This correlates with changes in the expression of target genes in sperm and in zygotes generated from that sperm.

## 2.4 Key words

epigenetics, epididymis, epididymosomes, early life stress, extracellular vesicles, miRNAs, sperm.

## 2.5 Introduction

Post-testicular maturation of spermatozoa in the epididymis is an elaborate process that involves modifications of sperm RNA, protein, and lipid content (**nixon\_2015?**; **re-jraji\_2006?**; **sharma\_2016?**; **skerget\_2015?**; **tamessar\_2021?**). The epididymis is segmented into different parts, including the initial segment, caput, corpus, and cauda. Each segment has a distinct gene expression profile, and different protein and lipid composition. Some modifications in epididymal spermatozoa are conserved across species (**sellem\_2020?**). For example, ~50% of miRNAs, a class of small RNAs that are modified during caput to cauda epididymis transit, is identical in mouse and bovine spermatozoa (**sellem\_2020?**). One mechanism by which small RNA load in spermatozoa is modified along the epididymis is by uptake of extracellular vesicles (EVs), also known as epididymosomes, which are produced by epididymal epithelial cells (**reilly\_2016?**). Studies have shown that epididymosomes can be taken up by maturing sperm through proteins present on the sperm head such as dynamin in mice and tetraspanins or syntenins in humans (**caballero\_2013?**; **reilly\_2016?**; **thimon\_2008?**; **zhou\_2019?**). Co-incubation experiments provided evidence for epididymosome-mediated transfer of miRNAs to spermatozoa (**reilly\_2016?**). Exogenous DNA and RNA can also be directly taken up by spermatozoa via artificial liposomes (**bachiller\_1991?**).

However, it is still not clear if changes in small RNA composition of spermatozoa occurring during epididymal transit are required for embryonic development, and studies on the subject have been conflicting (**conine\_2018?**; **suganuma\_2005?**). Changes in sperm small RNA have nevertheless been suggested to play a role in the transmission of information about paternal experiences to the progeny and can influence their developmental trajectory (**chan\_2020?**; **gapp\_2014?**; **sharma\_2016?**). Epididymosomal small RNA content can also be altered by exposure, for instance, to dietary insult and stress (**chan\_2020?**; **sharma\_2016?**). For instance, epididymosomal miRNAs are changed by exposure to chronic stress (**chan\_2020?**) and low-protein diet (**sharma\_2016?**) in mice.

Transmission of information about paternal exposure to the offspring depends on the type of exposure, its duration and the developmental window at which it is applied. To date, little is known about the long-term effects of early life stress, particularly stress experienced after birth, on epididymosomal small RNA composition in adulthood, and whether any changes to this composition can influence gene expression in sperm and in zygotes generated from that sperm. Using a transgenerational mouse model of postnatal stress induced by unpredictable maternal separation combined with unpredictable maternal stress, unpredictable maternal separation combined with unpredictable maternal stress (MSUS) (**franklin\_2010?**), we show that the miRNA signature of cauda epididymosomes in adult males is altered by exposure,

and that this alteration, correlates with changes in the expression of their target genes in sperm and in zygotes.

## 2.6 Results

### 2.6.1 Isolation of cauda epididymosomes confirmed by several methods

To characterize the RNA composition of cauda epididymosomes, epididymosomes were isolated by high-speed ultracentrifugation from adult control males and males exposed to MSUS (Figure 2.2A). MSUS consists of exposing newborn pups to unpredictable maternal separation for 3h daily and subjecting dams to unpredictable maternal stress during separation ([franklin\\_2010?](#)). Adult MSUS-exposed and control males were euthanized and cauda epididymis was collected. Successful isolation of cauda epididymosomes was confirmed by electron microscopy, immunoblotting, and nanoparticle-tracking analyses (Figure 2.2). The presence and purity of epididymosomes was further validated by staining with the EV-specific marker CD9 and confirmation of the absence of the cellular marker Glyceraldehyde 3-phosphate dehydrogenase (GAPDH) (Figure 2.2B). Size analysis by nanoparticle-tracking indicated that the collected particles are 50–300nm in diameter (Figure 2.2D). Imaging by transmission electron microscopy showed the typical cup-shaped structures of epididymosomes (Figure 2.2C, Supplementary Figure 2.6A) ([choi\\_2017?](#)). RNA profiling by high-resolution automated electrophoresis showed enrichment for small RNAs of different length, similar to previous studies on cauda epididymosomal RNA (Supplementary Figure 2.6B) ([sharma\\_2016?](#); [conine\\_2018?](#)).

### 2.6.2 The number and size of epididymosomes in adult males are not altered by postnatal stress

We next examined the number and size of cauda epididymosomes in adult MSUS and control males by dynamic light scattering. No significant difference could be detected between MSUS and control males (Figure 2.3A and B). Since most epididymosomal production occurs via apocrine secretion from principal cells located in caput epididymis, we also examined the expression of genes involved in EVs exocytosis. We chose Ras-related protein Rab-5A (*Rab5*) and Ras-related protein Rab-7A (*Rab7*), which are involved in vesicle trafficking, the soluble NSF attachment protein (SNARE) family protein vesicle-associated membrane protein 7 (*Vamp7*) and SNARE recognition molecule synaptobrevin homolog YKT6 (*Ykt6*), involved

in vesicle fusion. No significant change in the expression of these genes could be detected in caput epididymis between MSUS and control adult males (Figure 2.3C). However, we observed a consistent trend (not statistically significant) for decreased expression of all genes involved in EVs secretion in caput epididymis of MSUS mice (Figure 2.3C).

### 2.6.3 miRNAs are persistently altered by postnatal stress in cauda epididymosomes

Epididymosomal small RNAs are known to be affected by changing environmental conditions in rodents. Small RNAs, like tRNA-derived fragments (tRFs), miRNAs and more recently rRNA-derived small RNA fragments are believed to act as messengers of a father's experiences that can be transferred to the offspring ([sharma\\_2016?](#); [chan\\_2020?](#); [wang\\_2021?](#); [zhang\\_2018?](#)). Our previous work showed that early postnatal stress alters small and long RNA content in sperm of adult males ([gapp\\_2014?](#); [gapp\\_2020?](#)). Since caudal sperm and epididymosomal small RNA profiles are highly similar ([sharma\\_2016?](#)), we examined whether small RNA content of cauda epididymosomes is also altered by postnatal stress. We extracted RNA from cauda epididymosomes of adult MSUS and control males and prepared small RNA-seq (sRNA-seq) libraries. RNAs of different size were observed in cauda epididymosomes, with the majority of small RNA reads mapping to tRNAs as previously observed (Figure 2.4A) ([sharma\\_2016?](#)). When plotting the results of differential expression analysis of small RNAs ( $P < 0.05$ ) between MSUS and control sample, the majority of nonsignificant differences in small RNAs appeared to be in miRNAs, although some differences in tRNAs and piRNAs were also detected (Figure 2.4B). We next performed size-selection on the same libraries to enrich for miRNAs and then, we re-sequenced the libraries (Supplementary Figure 2.7A and C). As expected, size-selection did not alter the abundance of miRNAs and uniformly enriched the miRNA fraction in all samples (Supplementary Figure 2.7B–D). Differential expression analysis of miRNAs biotypes from the combined sequencing datasets after batch effect correction revealed changes in several miRNAs in MSUS cauda epididymosomes (Supplementary Table S2.1). These include upregulation of miR-878-5p, miR34c-5p, miR-881-3p and downregulation of miR-31-5p and miR-155-5p (adjusted  $P \geq 0.1$ ). Differential expression analysis on all small RNA biotypes from the combined datasets showed that 70% of all significantly altered small RNAs correspond to miRNAs, 15% to tRNAs, 15% to piRNAs and snoRNAs, while rRNAs are not changed (Supplementary Table S2.4). Pathway analysis of top candidate RNAs from miRNA-based analysis after size-selection revealed that the most up- and down-regulated miRNAs ( $P < 0.05$ ) have target mRNAs that encode proteins involved in fatty acid metabolism, steroid biosynthesis, lysine degradation,

and thyroid hormone signaling (Figure 2.4C). Notably, similar pathways are altered in plasma of MSUS males during postnatal life and adulthood as shown by metabolomic analysis ([vansteenwyk\\_2020?](#)). In particular, metabolites implicated in polyunsaturated fatty acid biogenesis were up-regulated, whereas steroidogenesis and the steroidogenic ligand aldosterone were down-regulated ([vansteenwyk\\_2020?](#)). Steroidogenesis was already altered at postnatal day 28 in MSUS males, with total cholesterol significantly decreased in testis (Figure 2.4D) and HDL cholesterol significantly increased in liver (Figure 2.4F). Since the primary role of HDL cholesterol in blood is to transport excess cholesterol from peripheral tissues to liver, an increase in HDL in liver is consistent with a decrease in testis. However, cholesterol was no longer altered in testis of adult MSUS males (Figure 2.4E), suggesting a transient alteration. The androgen receptor, which the cholesterol derivatives, androgens bind to, was decreased in adult caput epididymis (Figure 2.4G), suggesting potential secondary effects of lower cholesterol in testis when occurring in early postnatal life.

#### 2.6.4 mRNA targets of miRNAs from cauda epididymosomes are altered by postnatal stress in sperm and in zygotes

The relative abundance of miRNAs in cauda epididymosomes and mature sperm significantly correlated (Figure 2.5C), consistent with prior findings ([sharma\\_2016?](#); [chan\\_2020?](#)). Since cauda epididymosomes carry small RNA payloads matching those of mature sperm and are part of the ejaculate ([frenette\\_2005?](#); [belleanne\\_2013a?](#)), they may contribute to the information delivered to the oocyte upon fertilization. Therefore, we looked at the mRNA targets of miRNAs significantly changed in MSUS cauda epididymosomes in two previously published analysis of genes identified in MSUS sperm and in zygotes derived from MSUS males ( $P < 0.05$ ) ([gapp\\_2020?](#)). For this, we plotted the cumulative log fold-change distribution of all genes from differential expression analysis of sperm or zygotes versus the number of conserved binding sites for miRNAs significantly changed by MSUS in cauda epididymosomes (Figure 2.5A and B, Supplementary Figure 2.10). Target genes with three binding sites for miR-31-5p, a miRNA differentially expressed in MSUS cauda epididymosomes, had increased expression in sperm and decreased expression in zygotes from MSUS males (Figure 2.5A and B, Supplementary Table S2.2 and S2.3). However, not all targets of miRNAs significantly altered in MSUS cauda epididymosomes showed corresponding changes in expression in sperm and zygotes (Supplementary Figure 2.10). We then conducted miRNA-gene interaction analysis based on experimentally validated data from Tarbase ([vlachos\\_2017?](#)). This analysis showed that, overall, the five miRNAs significantly changed in MSUS cauda epididymosomes target genes that are part of pathways involved

in steroid biosynthesis, extracellular matrix (ECM)–receptor interaction, and cell-adhesion molecules (Figure 2.5D).

## 2.7 Discussion

The effects of environmental factors on RNA in the male reproductive tract, in particular, the epididymis have been examined in rodent models. Until now, most models have used invasive exposure such as dietary insult or injection of endocrine disruptors, applied prenatally and sometimes before conception. Few studies have examined the effects of non-invasive psychological/emotional exposure such as stress in early life and the effects on epididymal RNA in adulthood ([chan\\_2020?](#)). This study examines if postnatal stress affects RNAs in EVs released from the cauda epididymis and whether this has consequences for mature sperm and zygotes generated from that sperm.

Using a transgenerational mouse model of early postnatal stress, we show that several miRNAs, including miR-871-3p, miR-31-5p, miR-155-5p, miR-878-5p, and miR-34c-5p are altered in cauda epididymosomes in adult males exposed to postnatal stress, and that the targets of some of these miRNAs are affected in mature sperm and zygotes. Particularly, miR-31-5p is significantly decreased in cauda epididymosomes and its target genes are up-regulated in sperm but down-regulated in zygotes generated from that sperm, suggesting an over-compensation during early development. This may also be due to the heterogeneity of epididymosomes which have different size, biogenesis, and cellular targeting ([sullivan\\_2015?](#)), leading to a dissociation between the RNA content of epididymosomes and transcriptional changes in zygotes. It has been suggested that different subsets of epididymosomes have different roles. While a subset communicates with spermatozoa during sperm epididymal transit ([reilly\\_2016?](#); [sharma\\_2016?](#)), another subset serves in the communication within epididymal epithelial cells ([belleanne\\_2013a?](#)), and a third one is delivered as part of seminal fluid during fertilization ([belleanne\\_2013?](#); [frenette\\_2005?](#)). Thus owing to their heterogeneity, not all cauda epididymosomes or their cargo is delivered to the oocyte upon fertilization, which may explain the differences in miRNAs targets that are affected in sperm and zygotes.

Several of the differentially expressed miRNAs in MSUS cauda epididymosomes play a role in metabolic processes and early development ([reza\\_2019?](#)). For instance, miR-31-5p is involved in glucose metabolism and fatty acid oxidation ([reza\\_2019?](#)). In humans, its target complement C1q Tumor Necrosis Factor-Related Protein 9A (CTRP9) protein is negatively correlated with the amount of visceral fat and positively associated with a beneficial glucose and metabolic phenotype ([shao\\_2017?](#)). This is consistent with the observation that glucose

and insulin metabolism are also affected by MSUS (**franklin\_2010?**; **gapp\_2014?**). The level of other miRNAs is significantly increased or decreased in MSUS epididymosomes, such as miR-155-5p, which facilitates differentiation of mouse embryonic stem cells, or miR-34c-5p that initiates the first embryonic cleavage in mice (**reza\_2019?**).

The first days after birth are a sensitive period for the development and the establishment of cellular niches in tissues. Epithelial cells in the epididymis, which are the source of epididymosomes, undergo differentiation and expansion postnatally until puberty (**na\_2002?**). Once their expansion is completed, epididymal epithelial cells remain at a nearly constant number in adulthood. If they can be modified by prior exposure, they may therefore carry a memory of exposure into adulthood. The postnatal development and differentiation of epididymal epithelial cells primarily depend on testicular signals (**biliska\_2006?**; **na\_2002?**; **robaire\_2011?**; **zhu\_2000?**). Since chronic stress affects the coupling of the hypothalamus–pituitary and hypothalamus–gonadal axes, stress-related decrease in steroidogenesis can profoundly affect the differentiation and expansion of epididymal epithelial cells in early postnatal life. A number of studies have shown the importance of the abundance of androgens during postnatal life for epididymal development (**na\_2002?**). Thus, the availability of testicular cholesterol during epididymal cells differentiation has implications for these cells. Systemic alteration in cholesterol metabolism seen in young MSUS males (decreased total cholesterol in testis and increased HDL cholesterol in liver) may contribute to metabolic changes seen in adult animals, for instance in plasma steroidogenesis and fatty acid pathways, and to alterations in glucose and insulin metabolism in adult MSUS males. Moreover, androgen-dependent miRNAs miR-878-5p and miR-871-3p are significantly increased in cauda epididymosomes in MSUS.

In conclusion, our results provide evidence that chronic stress in early postnatal life alters miRNAs in EVs of the male reproductive tract in adulthood, with effects in mature sperm and zygotes. These persistent and intergenerational effects *in vivo* point to the sensitivity of the reproductive system to stress exposure and the detrimental consequences for descendants. These consequences may differ depending on the time window and severity of paternal stress exposure. Further studies are necessary to more precisely define these effects and the source of vesicles and their cargo miRNAs.

## 2.8 Materials and methods

### 2.8.1 Animals

Animal experiments were conducted according to the Swiss Law for Animal Protection and were approved by the cantonal veterinary office in Zürich under license number 83/2018. C57Bl/6 J mice were obtained from Janvier (France) and bred in-house to generate animals for the experiments. Animals were maintained under a reverse light–dark cycle in a temperature and humidity-controlled environment with constant access to food and water. Nine months old age-matched MSUS and control males were used for small RNA-sequencing (sRNA-seq) of cauda epididymosomes, tissue collection for RT-qPCR, nanoparticle-tracking analysis, and total cholesterol measurements. HDL cholesterol and total cholesterol measurements were performed on MSUS and control males at postnatal day 28. Datasets from previous publication ([gapp\\_2020?](#)): caudal sperm RNA-seq was performed on 5-months old males, and zygote RNA-seq was performed on zygotes from 3-months old males.

### 2.8.2 MSUS

To obtain MSUS mice, 3-months old C57Bl/6 J females and their litters were subjected to daily 3 h separation unpredictably and females were exposed to an unpredictable stressor during separation as previously described ([franklin\\_2010?](#)). Control dams and pups were left undisturbed. After weaning at postnatal day 21, pups from different litters were randomly assigned to cages of 4–5 mice, in corresponding treatment groups to avoid litter effects.

### 2.8.3 Tissue collection

After decapitation and blood collection, mice were pinned on a dissection board and cleaned with alcohol. Epididymis and testis were excised and separated from surrounding adipose tissue. The epididymis was separated into caput, corpus, and cauda. Cauda was excised with several incisions and sperm collected with a swim-up protocol. The supernatant was collected to isolate epididymosomes. The whole testis and caput epididymis were crushed with stainless steel beads in a tissue crusher in cold PBS, centrifuged at 3000 rcf for 10 min to pellet the tissue and cells and used for total cholesterol and HDL cholesterol measurements.

### 2.8.4 Electron microscopy images

Negative staining of cauda epididymosomes was performed with methylcellulose. Briefly, the carrier grid was glow-discharged in plasma for 10 min and washed with a drop of PBS,

then incubated in 1% glutaraldehyde (GA) in water for 5 min and washed with water five times for 2 min each. Afterwards the grid was incubated in 1% UAc (uranyl acetate) for 5 min and then kept on ice in methylcellulose/UAc (900  $\mu$ l methylcellulose 2% and 100  $\mu$ l 3% UAc) solution. After incubation with methylcellulose/UAc, the excess liquid was removed by dipping onto a filter paper. The grid was air-dried on ice for 5 min. Imaging was performed with a transmission electron microscope.

### 2.8.5 Epididymosomes isolation by ultracentrifugation

After pelleting sperm following the sperm swim-up protocol in M2 medium (Sigma, M7167), the supernatant was centrifuged at 2000 rcf for 10 min, 10 000 rcf for 30 min and then ultracentrifuged at 120 000 rcf at 4 °C for 2 h (TH 64.1 rotor, Thermo Fisher Scientific). The epididymosomal pellet was then washed in PBS at 4 °C and ultracentrifuged at 120 000 rcf at 4 °C for 2 h. The resulting pellet was resuspended in 60  $\mu$ l of PBS for all downstream analysis.

### 2.8.6 Immunoblotting

PBS-resuspended pellet containing epididymosomes was lysed in 10x RIPA buffer for 5 min at 4 °C. Equal amounts of protein were mixed with 4x Laemmli Sample Buffer (Bio-Rad Laboratories, USA) and loaded on 4–20% Tris-Glycine polyacrylamide gels (Bio-Rad Laboratories, USA). The membranes were blocked in 5% SureBlock (in Tris-buffer with 0.05% Tween-20) for 1 h at room temperature and incubated with overnight at 4 °C with primary anti-Cd9 ([1:3000; System Biosciences, USA] and anti-Gapdh [1:5000; Cell Signaling, USA; 14C10]) antibodies.

### 2.8.7 Nanoparticle tracking analysis

Particle number and size of epididymosomes were measured using a Nanosight NS300 (Malvern, UK) at 20 °C, according to the manufacturer's instructions and lots were generated using a published method ([dragovic\\_2011?](#)). The following parameters were kept constant for all samples: “Camera level” = 14 and “Detection threshold” = 7. For measurements with Nanosight, the resuspended pellet from ultracentrifugation was diluted to a 1:1000 concentration.

### 2.8.8 RNA isolation and epididymosomes profiling

To lyse purified epididymosomes, 33 µl of lysis buffer (6.4 M guanidine HCl, 5% Tween 20, 5% Triton, 120 mM EDTA, and 120 mM Tris pH 8.0) per 60 µl of PBS resuspended pellet was added to each sample, together with 1 µl Proteinase K and 3.3 µl water. Samples were incubated at 60 °C for 15 min with shaking. A total of 40 µl water were added and RNA was extracted using Trizol LS protocol, according to the manufacturer's instructions. Profiling of extracted RNA was done using high-resolution automated electrophoresis on a 2100 Bioanalyzer (Agilent, G2939BA), according to instructions for the RNA 6000 Pico Kit (Agilent, 5067-1513) reagent.

### 2.8.9 Preparation and sequencing of sRNA-seq libraries from epididymosomes

sRNA-seq libraries were prepared using the NEB Next Small RNA-sequencing kit (NEB #E7300, New England BioLabs), according to the manufacturer's instructions. About 80–90 ng of total RNA per sample was used to prepare the libraries. The same libraries were sequenced before and after size-selection (target peak 150 bp) with the BluePippin System. 200 million reads were obtained for 10 samples, with 125 bp single-stranded read-length on a HiSeq2500 sequencer.

### 2.8.10 RT-qPCR

For gene expression analysis in caput epididymis, RNA was extracted using the phenol/chloroform extraction method (TRIzol; Thermo Fisher Scientific). Reverse transcription was performed using miScript II RT reagents (Qiagen) - HiFlex buffer, and RT qPCR was performed with QuantiTect SYBR (Qiagen) on the Light-Cycler II 480 (Roche). All samples were run in cycles as follows: 95 °C for 15 min, 45 cycles of 15 s at 94 °C, 30 s at 55 °C and 30 s at 70 °C, followed by gradual increase of temperature to °C. The endogenous control *Gapdh* was used for normalization. The expression level of genes was analyzed using two-tailed Student's *t*-test.

### 2.8.11 Cholesterol measurements

Testicular and epididymal total cholesterol and HDL cholesterol levels were measured using the CHOL reagent, in conjunction with SYNCHRON LX System(s), UniCel DxC 600/800 System(s) and Synchron Systems Multi Calibrator (Beckman Coulter), according to the

manufacturer's instructions at the Zurich Integrative Rodent Physiology (ZIRP) facility of the University of Zurich.

### 2.8.12 Bioinformatics data analysis

sRNA-sequencing FASTQ files were processed using the `ExceRpt` pipeline, previously established for EV small RNA data analysis ([rozowsky\\_2019?](#)). Briefly, `ExceRpt` first automatically identifies and removes known 3' adapter sequences, then aligns against known spike-in sequences used for library construction, filters low-quality reads and aligns them to annotated sequences in the UniVec database. Reads not filtered out in pre-processing steps are then aligned to the mouse genome and transcriptome using `STAR` aligner ([dobin\\_2013?](#)). The annotations were performed in the following order: miRbase, tRNAscan, piRNA, GENCODE, and circRNA. rRNA counts were obtained using `Oasis` 2 tool. Reads mapped to miRNAs were combined from sequencing obtained before and after size-selection and corrected for batch effect using `RUVSeq` ([leek\\_2014?](#)). Normalization factors were calculated using TMM ([robinson\\_2010?](#)) method and differential expression was performed using `edgeR` package ([robinson\\_2010a?](#)) in R. For cumulative distribution plots, miRNA targets (all and conserved) were downloaded from TargetScan release 7.2 ([agarwal\\_2015?](#)). When using context++ scores, targets were split into three same-frequency groups according to their scores.  $P$ -values were calculated using a Kolmogorov-Smirnov test between the first and last groups (i.e. strongest and weakest targets). The miRNA pathway analysis was conducted using a web-server tool DIANA-mirPath ([vlachos\\_2017?](#)), where targets were predicted-derived from DIANA-TarBase v6.0, a database of experimentally validated miRNA targets. The adjusted  $P$  cutoff value of 0.05 was used for the identification of expressed pathways. The miRNAs and their corresponding target pathways information was extracted and plots were generated in R. `ggplot2` ([wickham\\_2016?](#)) and `ComplexHeatmap` ([gu\\_2016?](#)) R packages were used for generation of figures.

## 2.9 Data availability

The datasets collected for this study are available as follows:

- sRNA-seq dataset of cauda epididymosomes before and after sizeselection: NCBI GEO under accession number GSE175976.
- Codes for bioinformatics analysis of RNA-sequencing datasets and all corresponding differential expression analyses: Github repository [mansuylab/alshanbayeva\\_et\\_al\\_2021](#).

- Sperm and zygote sequencing datasets from previous publications can be found in ArrayExpress database at EMBL-EBI ([www.ebi.ac.uk/arrayexpress](http://www.ebi.ac.uk/arrayexpress)) with the accession number E-MTAB-5834 (sperm) and E-MTAB-6589 (zygotes).

## 2.10 Authors' contributions

AA and IMM conceived and designed the study. FM and MR performed the MSUS breeding and collected tissue samples. AA and DKT performed data analysis and generated figures. AA wrote the manuscript with input from DKT and IMM. AA performed all experiments for RNA sequencing and all molecular analyses. IMM supervised the project and raised funds.

## 2.11 Grant Support

The work was supported by Swiss National Science Foundation (31003A-135715), ETH grants (ETH-10 15-2 and ETH-17 13-2), the Slack-Gyr Foundation, the Escher Foundation. The Mansuy lab is funded by the University Zürich, the Swiss Federal Institute of Technology, the Swiss National Science Foundation (31003A-135715), ETH grants (ETH-10 15-2 and ETH-17 13-2), the Slack-Gyr foundation, the Escher Foundation. Deepak K. Tanwar is supported by the Swiss Government Excellence Scholarship. Martin Roszkowski was funded by the ETH Zurich Fellowship (ETH-10 15-2).

## 2.12 Acknowledgements

We thank Pierre-Luc Germain for advice on data analysis and for generating cumulative distribution plots, Irina Lazar-Contes for help with MSUS breeding, Silvia Schelbert for work on the animal license, Emilio Yandez at Function Genomics Center Zurich (FGCZ) for advice on the sRNA sequencing, Alekhya Mazumkhar for help with nanoparticle-tracking analysis, Yvonne Zipfel for animal care, Zurich Integrative Rodent Physiology facility for performing cholesterol measurements. We also thank Eloise Kremer, Ali Jawaid, and Mea Holmes for their initial contributions to the project.

**Conflict of interest:** The authors declare no conflict of interest.

## 2.13 Figures

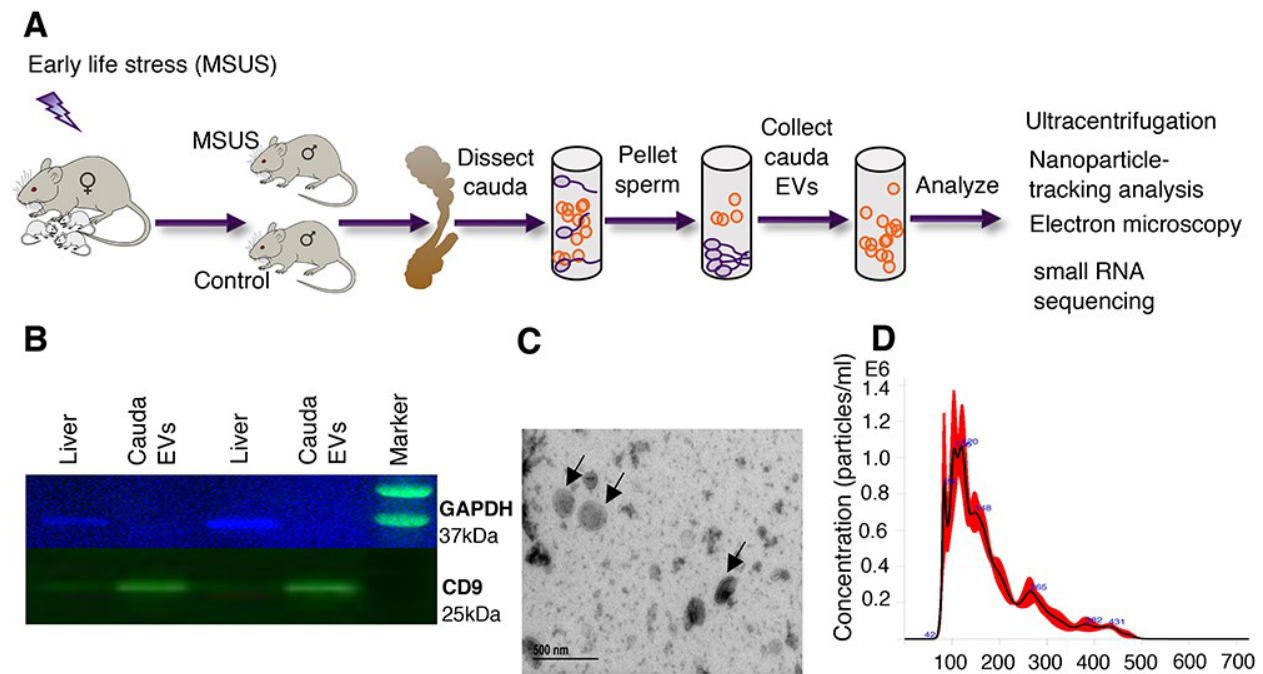


**Figure 2.2: Isolation and characterization of cauda epididymosomes.**

**A:** Schematic representation of cauda epididymosomes preparation.

**B:** Immunoblot analysis was used to confirm the purity of isolation by staining with epididymosomal marker CD9 and absence of cellular marker GAPDH in the ultracentrifuged pellet.

**C:** Electron microscopy images of the preparations were used to assess the size and heterogeneity of the isolated populations. Arrows indicate cauda epididymosomes.

**D:** Nanoparticle-tracking analysis by dynamic light scattering showed particles of expected size of 50–300 nm.

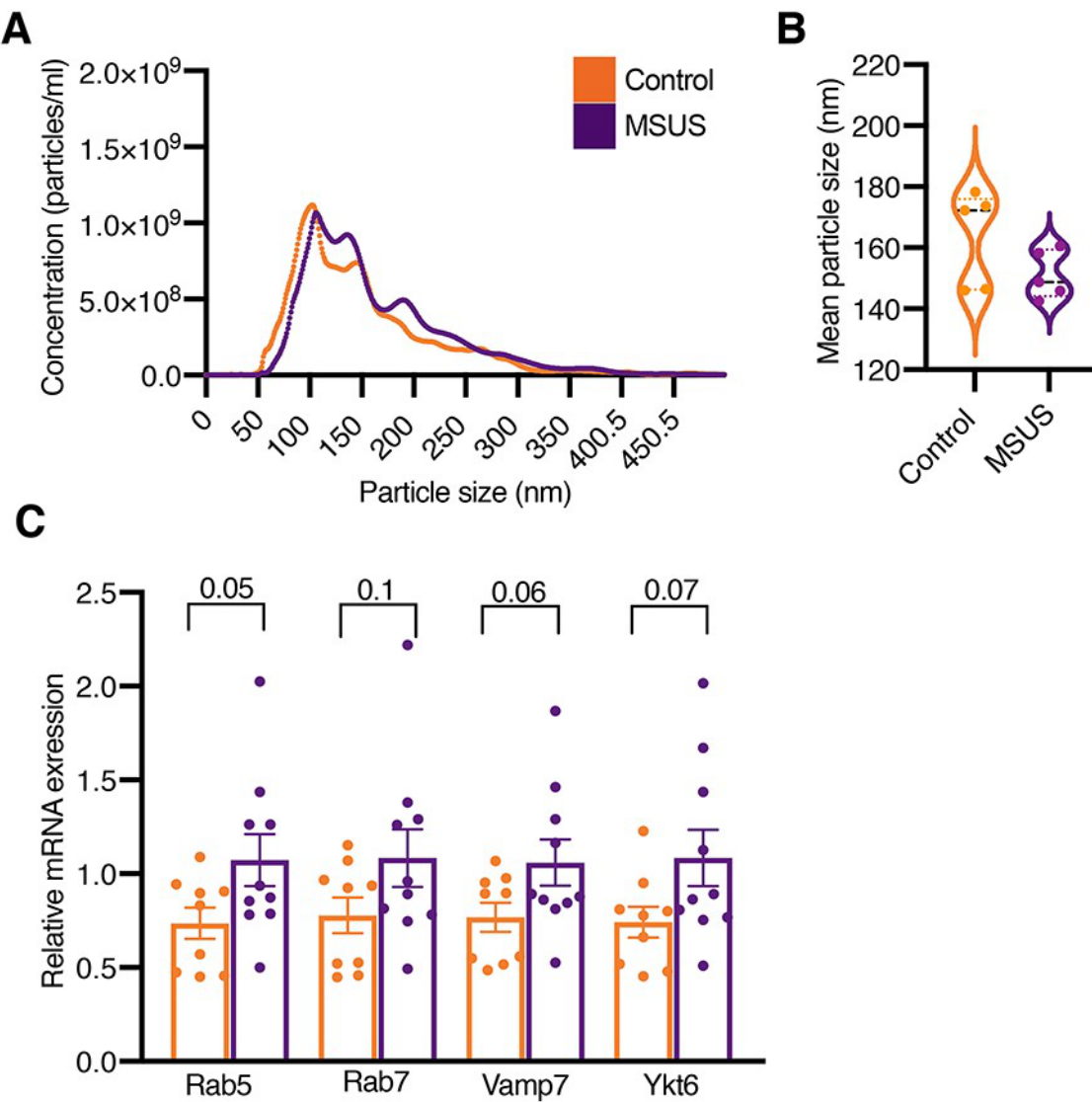


**Figure 2.3: Comparison of epididymosomal number, size, and release machinery in adult MSUS and control males.**

**A:** Nanoparticle-tracking analysis showed no difference in the number of cauda epididymosomes between MSUS and control males. The plots were generated from average values across replicates ( $N = 5$  animals/group). Data are presented as mean  $\pm$  standard error of the mean (SEM).  $P < 0.05$ .

**B:** Quantification of nanoparticle-tracking analysis showed the mean size of cauda epididymosomes was not changed between the two groups ( $N = 5$  animals/group). Data are presented as mean  $\pm$  SEM.  $P < 0.05$ .

**C** Expression of genes involved in vesicular secretion in the caput epididymis from adult males measured by qRT-PCR. The experiments were performed in triplicates without pooling ( $N = 8$  animals/group).

Expression of GAPDH was used as endogenous control to normalize the expression level of the target genes. Data are presented as mean  $\pm$  SEM.  $P < 0.05$ .

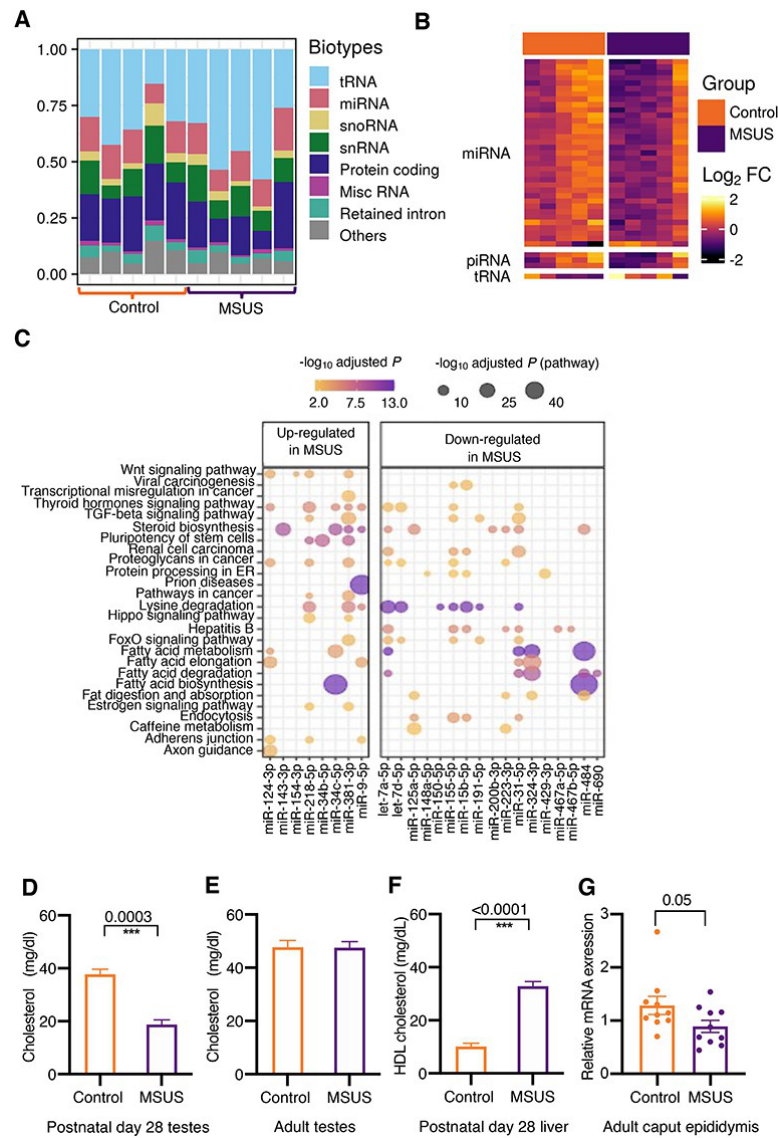


**Figure 2.4: Target pathways of up- and down-regulated miRNAs in adult MSUS cauda epididymosomes and alterations in steroidogenesis in postnatal and adult MSUS males.**

**A:** Representative distribution of RNA biotypes from cauda epididymosomal sequencing ( $N = 10$  animals, 5 animals/group).

**B:** Heatmap of the most abundant small RNAs ( $n = 39$ ). Expression fold-change ( $\log_2 FC$ ) was calculated by subtracting  $\log_2$  counts per million of MSUS from controls. Each row depicts a small RNA and each column depicts a sample. Samples and RNAs are ordered by “PCA” method using **seriation** (R package).

**C:** Dot plot of miRNAs and pathways. Color-scale of the dot represents  $-\log_{10}$  adjusted  $P$  of miRNA in a pathway and size of the dot represents  $-\log_{10}$  adjusted  $P$  of the pathway.

Total cholesterol measurements in whole testes of males at postnatal day 28 ( $N = 4$  males/group) **D** and adulthood ( $N = 10$  controls,  $N = 7$  MSUS) **E**. **F:** HDL cholesterol level in the liver of males at postnatal day 28 ( $N = 6$  males/group).

**G:** Relative expression level of the androgen receptor in adult caput epididymis measured by qRT-PCR. qRT-PCR experiments were performed in triplicates, without pooling ( $N = 10$  animals/group).

(D–G) Data are presented as mean  $\pm$  SEM.  $P < 0.05$ .

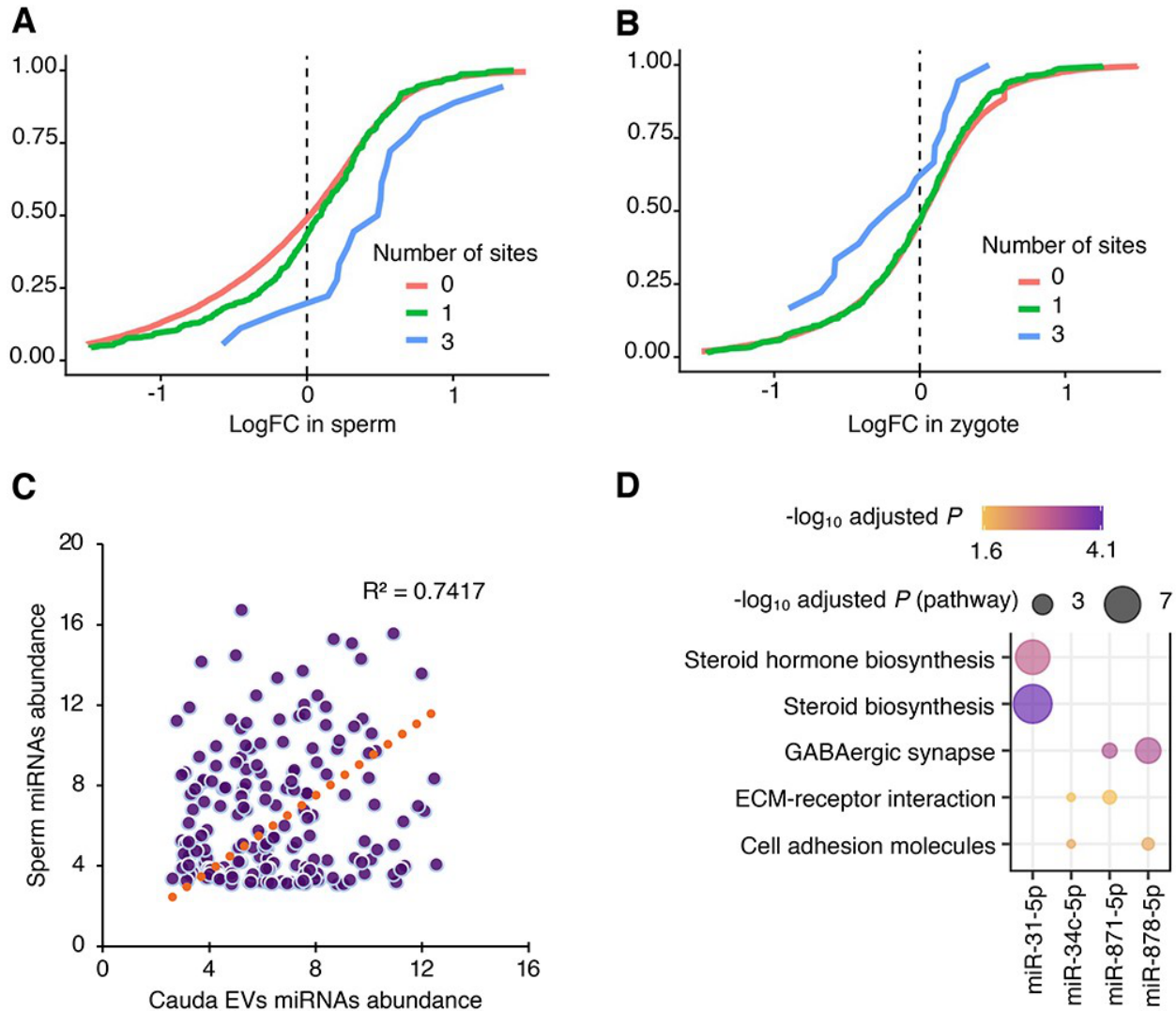


**Figure 2.5:** Targets of miRNAs from cauda epididymosomes are altered by MSUS in sperm and zygotes.

Cumulative distribution plots of miR-31-5p targets from 5-months old MSUS and control caudal sperm RNA-seq **A** and from RNA-seq of zygotes originating from 3-months old MSUS and control males **B**.

**C:** miRNA abundance of sperm plotted against abundance in cauda epididymosomes. Coefficient of determination ( $R^2=0.74$ ).

**D:** Dot plot of the top target pathways ( $\text{adjusted } P < 0.05$ ) of miRNAs differentially expressed ( $\text{adjusted } P \leq 0.1$ ) in adult MSUS cauda epididymosomes. Color-scale of the dot represents  $-\log_{10}$  adjusted  $P$  of miRNA in a pathway and size of the dot represents  $-\log_{10}$  adjusted  $P$  of the pathway.

## 2.14 Supplementary figures

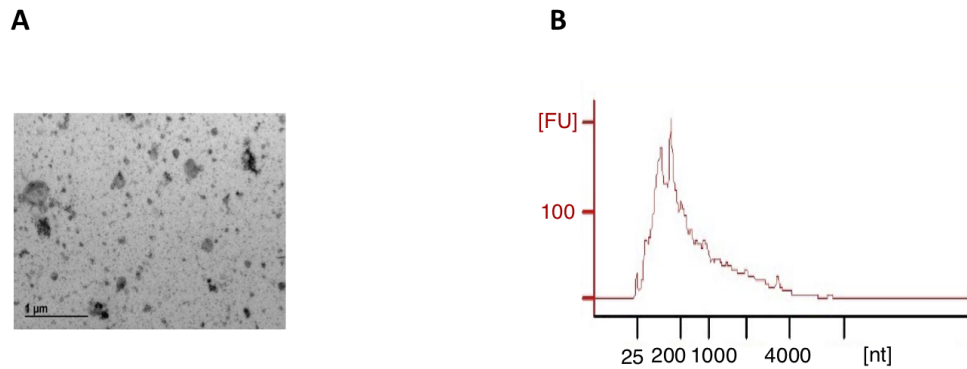


**Figure 2.6: Electron microscopy image and electrophoresis.**

**A:** Electron microscopy image of the preparations were used to access the size and heterogeneity of the isolated populations.

**B:** The RNA amount of epididymosomes preparations was assessed by high-resolution automated electrophoresis.

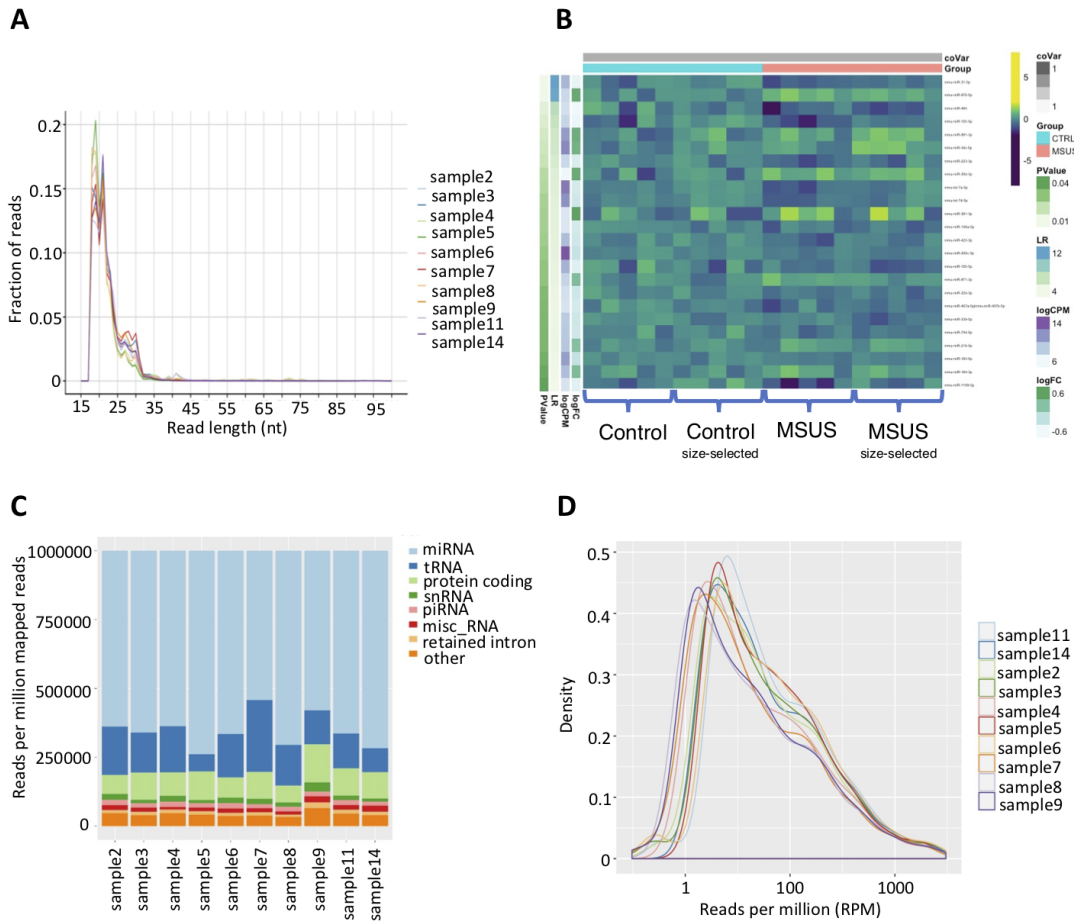


**Figure 2.7: Data overview.**

**A:** RNA read-length distributions of cauda epididymosomal small RNAs after size-selection.

**B:** Heatmap of top miRNAs of cauda epididymosomal small RNA-seq before and after size-selection. Each row depicts a miRNA and each column depicts a sample. ( $N = 10$  Controls,  $N = 10$  MSUS).

**C:** Representative distribution of RNA biotypes from cauda epididymosomal small RNA-seq after size-selection. ( $N = 5$  Controls,  $N = 5$  MSUS).

**D:** miRNA abundance distributions plot of cauda epididymosomal small RNA-seq. ( $N = 10$  Controls,  $N = 10$  MSUS)

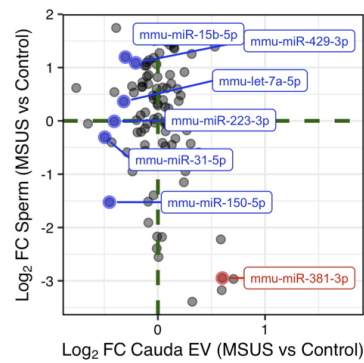


**Figure 2.8: Scatterplot of log fold-change of miRNAs in sperm and cauda epididymosomes.** miRNAs down-regulated (blue) and up-regulated (red) in MSUS cauda epididymosomes.

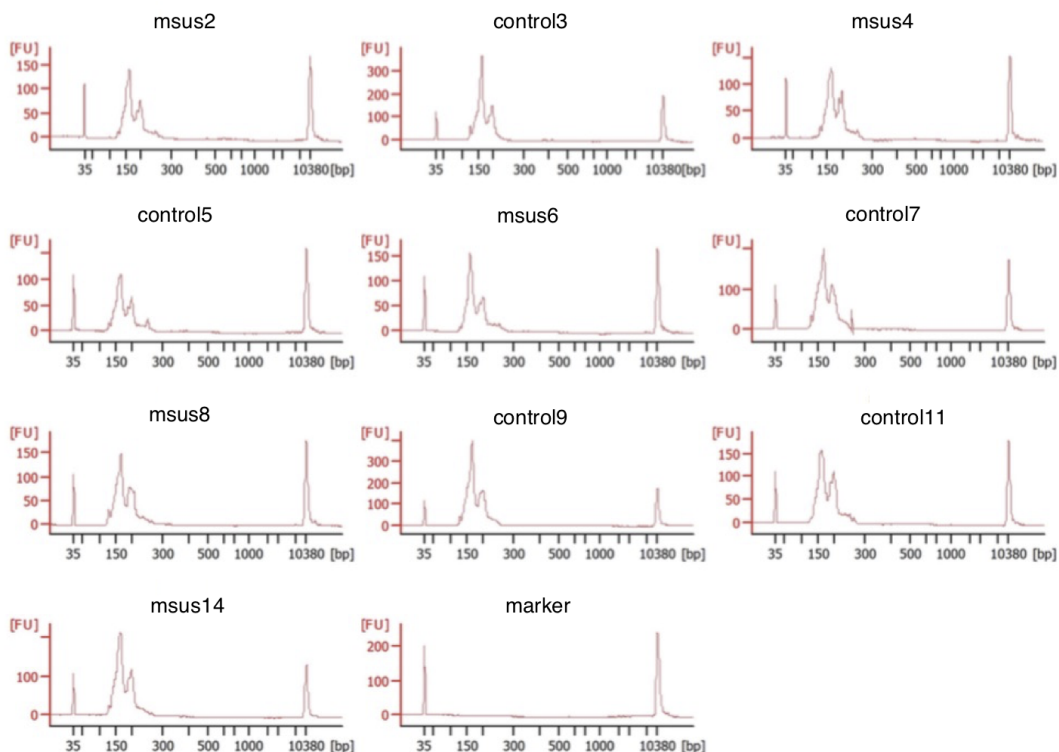


**Figure 2.9: Profiles of cauda epididymosomal small RNAs by high-resolution automated electrophoresis.** ( $N = 10$  Controls,  $N = 10$  MSUS).

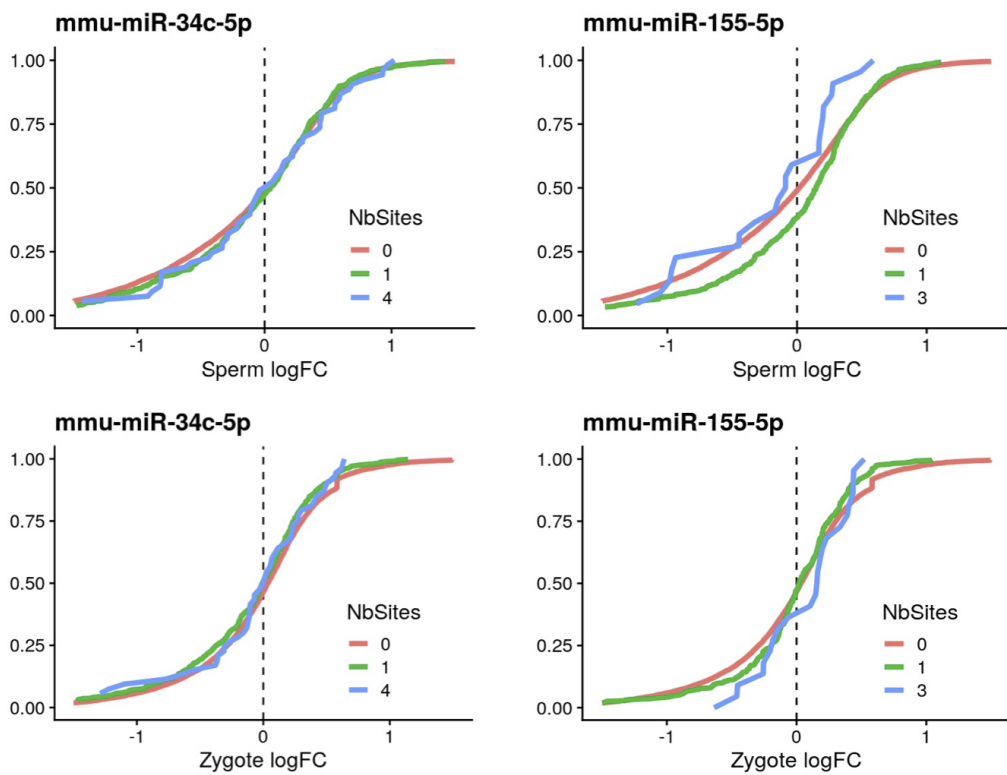


**Figure 2.10:** Cumulative distribution plots of miR-34c-5p, miR-155-5p targets in differentially expressed genes ( $P \leq 0.05$ ) from MSUS sperm and zygote RNA-sequencing.

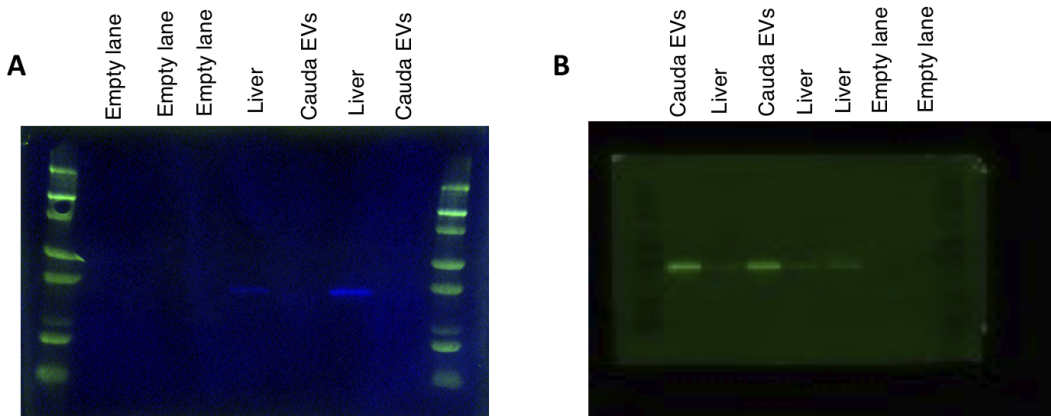


**Figure 2.11:** Immunoblot images of cauda epididymosomes and liver cell lysate, stained with cellular marker GAPDH (37kDa) and extracellular vesicle marker CD9 (25kDa). Same membrane was incubated and imaged separately.

## 2.15 Supplementary Tables

**Table 2.1:** Supplementary table 1

microRNA	logFC	logCPM	LR	PValue	FDR
mmu-miR-871-3p	0.4224445	7.865090	11.917353	0.0005560	0.0721259
mmu-miR-31-5p	-0.3876365	9.998799	11.067851	0.0008780	0.0721259
mmu-miR-155-5p	-0.4509784	7.903016	10.270414	0.0013518	0.0721259
mmu-miR-881-3p	0.2898815	11.465624	9.947026	0.0016111	0.0721259
mmu-miR-878-5p	0.4517734	7.616360	9.829572	0.0017173	0.0721259
mmu-let-7f-5p	-0.2539420	15.094684	8.265118	0.0040414	0.1414491
mmu-let-7a-5p	-0.3252566	13.378699	7.854573	0.0050692	0.1507945
mmu-miR-34c-5p	0.3699764	12.490816	7.628736	0.0057446	0.1507945
mmu-let-7c-5p	-0.2660684	14.170724	6.590841	0.0102505	0.2391777
mmu-let-7d-5p	-0.2957245	12.060525	6.254407	0.0123885	0.2514734
mmu-miR-148a-5p	-0.3860498	6.582776	6.099744	0.0135201	0.2514734
mmu-miR-486a-5p mmu-miR-486b-5p	0.4242328	9.175211	5.992121	0.0143699	0.2514734
mmu-miR-223-3p	-0.3918551	7.627599	5.758552	0.0164086	0.2650618
mmu-miR-142a-5p	-0.3388176	7.860399	5.331804	0.0209397	0.2995186
mmu-miR-484	-0.4464519	7.035887	5.294393	0.0213942	0.2995186
mmu-miR-182-5p	-0.1858805	11.537582	5.084665	0.0241383	0.3168156
mmu-miR-183-5p	-0.2106265	11.356649	4.759219	0.0291418	0.3395679
mmu-let-7g-5p	-0.1769275	14.499171	4.704360	0.0300862	0.3395679
mmu-miR-181d-5p	0.2729988	7.492399	4.642132	0.0311962	0.3395679
mmu-miR-467a-5p mmu-miR-467b-5p	-0.3391907	6.822511	4.509472	0.0337076	0.3395679

**Table 2.2:** Supplementary table 2

Glul	logFC 1.00	meanExpr 7.7	PValue 2.4e-06	FDR 0.0042	sites 2	targetscan .score -0.60	...8	conserved.sites 1
Pik3c2a	1.00	4.2	3.0e-06	0.0048	2	-0.36	NA	2
Trankl	0.93	4.7	6.9e-05	0.0240	3	-0.53	NA	1
Wdr5	1.00	1.8	2.le-03	0.1000	2	-0.65	NA	1
Eif5	0.93	5.2	8.4e-05	0.0260	1	-0.39	NA	1
Bicdl	1.10	3.7	1.le-04	0.0280	2	-0.23	NA	1

**Table 2.3:** Supplementary table 3

Hsf2bp	logFC -2.30	meanExpr -1.60	PValue 0.0300	FDR 0.12	sites 1	targetscan .score -0.460	...8	conserved.sites 1
Satb2	-1.90	-1.60	0.0110	0.12	2	-0.380	NA	2
Dpep3	-2.50	-2.90	0.0029	0.12	1	-0.019	NA	1
Jazf1	-1.20	-0.23	0.0015	0.12	2	-0.640	NA	1
Ret	-1.90	-1.80	0.0100	0.12	2	-0.250	NA	1
Wdr5	-0.93	2.50	0.0360	0.12	2	-0.650	NA	1
Snx22	-1.70	-1.30	0.0067	0.12	2	-0.250	NA	2
Rab9b	-1.20	-4.30	0.0380	0.12	2	-0.490	NA	1
Nr5a2	-1.50	1.30	0.0140	0.12	1	-0.320	NA	1
Plinl	-2.70	-0.62	0.0290	0.12	1	-0.210	NA	0

**Table 2.4:** Supplementary table 4

RNA	logFC	logCPM	LR	PValue	FDR
Prr15:protein_coding	-0.7873999	4.547372	30.18055	0.0000000	0.0001084
Gm15806:processed_pseudogene	-0.6498672	6.510597	25.26703	0.0000005	0.0006874
mmu-miR-34c-5p	0.7802879	11.007007	17.68464	0.0000261	0.0184327
mmu_piR_004086	0.9769300	6.282539	17.63425	0.0000268	0.0184327
Gm42427:TEC	-0.6134632	8.603910	16.67736	0.0000443	0.0244041
Gata3:protein_coding	-0.4928509	6.189582	16.11356	0.0000597	0.0273818
mmu-miR-878-5p	0.8891784	6.148635	15.77038	0.0000715	0.0281354
Hpgd:protein_coding	-0.5320409	8.066485	15.16616	0.0000985	0.0338922
Ccdc136:protein_coding	0.6987606	4.387168	14.00494	0.0001823	0.0472578
mmu-miR-181d-5p	0.6157888	5.694342	13.85633	0.0001973	0.0472578
Tacc2:protein_coding	-0.5657623	4.398129	13.69020	0.0002156	0.0472578
mmu-miR-871-3p	0.6763168	6.446751	13.66182	0.0002189	0.0472578
mmu-miR-9-5p	0.7204504	6.140215	13.49688	0.0002390	0.0472578
Gm26168:misc_RNA	0.6325019	4.872739	13.22844	0.0002757	0.0472578
Gm23921:misc_RNA	0.5727151	6.650877	13.21883	0.0002772	0.0472578
Abcg2:nonsense-mediated_decay	-0.5214647	6.638810	13.19591	0.0002806	0.0472578
Hipk3:protein_coding	-0.4861401	4.791792	12.68259	0.0003691	0.0472578
Odf1:protein_coding	0.5552237	6.042366	12.63222	0.0003792	0.0472578
mmu-miR-881-3p	0.8813852	10.064670	12.60867	0.0003840	0.0472578
mmu-miR-455-5p	0.6872305	5.255313	12.60016	0.0003857	0.0472578
Snord88a:snoRNA	0.6180176	5.030322	12.50995	0.0004048	0.0472578
His	1.1442782	10.636565	12.47395	0.0004127	0.0472578
Rnf2:protein_coding	-0.4823013	4.596362	12.32996	0.0004457	0.0472578
Gm10524:TEC	-0.4943310	5.296549	12.29409	0.0004544	0.0472578
Ptgr1:protein_coding	-0.4927718	6.068551	12.28196	0.0004574	0.0472578
Abcg2:protein_coding	-0.5283684	7.721448	12.26538	0.0004614	0.0472578
mmu-miR-218-5p	0.6591410	7.439262	12.23378	0.0004693	0.0472578
iMet	0.8698821	9.497592	12.18997	0.0004805	0.0472578



# Chapter 3

## shortRNA

**shortRNA**: a flexible framework for the analysis of short RNA sequencing data

**Contributions:** *I worked towards the tool development, data analysis, results interpretation. This has been done together with Pierre-Luc Germain.*

### 3.1 Abstract

Short RNA are important molecules that play key functional roles in the regulation of the genome. Several classes of short RNAs, such as miRNA, tRNA and tRNA fragments, and piRNAs have been characterized and have complex biogenesis. Short RNA sequencing is becoming increasingly relevant in the research of regulatory mechanisms in a wide range of biological functions. From an analysis point of view, each type of RNA has its own features, and hence, specialized methods have been developed focused on particular types, which not only multiply the work needed for a comprehensive analysis but potentially create misassignment problems. In addition, methods are typically divided into genome-based methods that do not deal adequately with post-transcriptional modifications, and transcript-based methods that are blind to unannotated features. Finally, there are several outstanding issues in the analysis of short RNAs, which are critical in the analysis of some samples. There is, therefore, a need for an analysis framework that is: sufficiently tailored to consider the specificities of different classes of short RNA and their biogenesis, and sufficiently general and exhaustive to perform global analyses. We developed a user-friendly, highly flexible and comprehensive R package for a thorough end-to-end analysis of short RNA sequencing data (planned submission to Bioconductor). Our package is appropriately adapted to take into account the differences between different types of short RNA and their biogenesis and is seamlessly expandable to include additional annotation. We use a customized genome

annotation with artificial chromosomes to account for post-transcriptional modifications, and a flexible rule-based approach to assign reads along a tree of hierarchically organized features. This enables the systematic querying, exploration, and differential expression analysis of short RNAs at various degrees of granularity, from specific sequences to RNA classes. We also include various normalization and experimental-bias correction methods. The **shortRNA** R package is developed to perform all the steps from within R and is platform-independent.

## 3.2 Introduction and background

Previous decades have revealed a number of RNAs that are distinct from the messenger RNAs. Short-RNAs are non-coding RNA molecules that are fewer than 200 nucleotides long and play an important role in genome regulation. Several types of short RNAs, of different lengths, have been discovered including microRNA (miRNA; 18-24 nt); small interfering RNA (siRNA; 21-27 nt); small nucleolar RNA (snoRNA; 60-170 nt); small nuclear RNA (snRNA/ U-RNA; 10-300 nt); Small temporal RNA (stRNA; 18-24 nt); tRNA-derived small RNA (tsRNA), including tRNA halves (tsRNA; 28-36 nt) and tRNA fragments (tRFs; 14-22 nt); small rDNA-derived RNA (srRNA; 18-30 nt); repeat-associated small interfering RNA (rasiRNA; 24-27 nt); and Piwi-interacting RNA [piRNA; 26-31 nt, present in animals in the germline cells and also in the brain (Zuo, Wang, Tan, Chen, & Luo, 2016)]. Some short RNAs, for instance, miRNA and siRNA, are known to suppress gene expression by sequence-specific interactions with regulatory regions during transcription, RNA processing and translation (J. Zhu et al., 2016), and by forming the core with RNA-induced silencing complex (RISC) (Pratt & MacRae, 2009). In addition, short-RNAs have been related to cancer, Parkinson’s disease, Alzheimer’s disease, and prion disease (Gong, Liu, Liu, & Liang, 2005), and hence, are used as biomarkers.

Several methods have been developed for the analyses of short RNA sequencing data. The development of high-throughput sequencing (HTS) techniques allows researchers to study short RNAs in diverse tissues or cells. HTS not only allows for the quantification of known short RNAs but also for the identification and quantification of novel short RNAs. The small RNA sequencing (sRNA-Seq) bears challenges and biases that researchers need to be informed of in order to properly analyze the data. First, most of the methods concentrate on a specific type of short RNA, such as **MINTmap** (Loher, Telonis, & Rigoutsos, 2017) focus on analyzing tRFs, **TAM 2.0** (J. Li et al., 2018), **Prost!** (Desvignes, Batzel, Sydes, Eames, & Postlethwait, 2019), **Chimira** (Vitsios & Enright, 2015), and **mirTools 2.0** (J. Wu et al., 2013) focus on miRNAs. Next, a few tools concentrate on most types of short RNAs (not all), such as **ncPRO-seq** (C.-J. Chen et al., 2012), **sRNAtoolbox** (Rueda et al., 2015), **SPAR** (Kukša

et al., 2018), **Threshold-seq** (Magee, Loher, Londin, & Rigoutsos, 2017), **sRNAAnalyzer** (Xiaogang Wu et al., 2017), **UEA sRNA Workbench** (Stocks et al., 2012), **Sports1** (Shi, Ko, Sanders, Chen, & Zhou, 2018), and **Oasis2** (Rahman et al., 2018). Tools that concentrate on many types of short RNAs, such as **Oasis2** and **Sports1**, perform sequential mapping, for example, they perform sequential mapping by first assigning the reads to miRNAs, then assigning the leftover to tRNAs, and then the remaining ones to mRNAs, which can create a misassignment problem as short reads can map to multiple locations. But this information is lost because only unmapped reads are aligned against the next annotation. In addition, although the libraries for sequencing are tailored to short RNAs, other long RNAs are also often detected in the sequencing data, and also because short RNAs often overlap with other features, prioritization between the biotypes is crucial. Further, there are quite a high number of sequenced reads left that map to the reference genome but are not assigned to the known features. Moreover, although most of the tools do not consider assignment rules for reads assignment, few tools such as **Prost!** have a set of defined rules for reads assignment. But, the rules are only for the miRNAs. Furthermore, the multi-mapping reads are either excluded or randomly assigned to the multi-mapping positions in the genome. As well as, not all the tools deal with the post-transcriptional modifications, such as the addition of “CCA” towards the 3’ end of tRNAs (Barraud & Tisné, 2019; Hou, 2010; Ibba & Soll, 2000), which is important for the recognition of tRNA by enzymes and translation (R. Green & Noller, 1997; Sprinzl & Cramer, 1979); and the addition of “G” towards the 5’ end in histidine tRNAs (Cooley et al., 1982; Cozen et al., 2015), this is critical for histidyl-tRNA synthetase (HisRS) recognition (Fromant, Plateau, & Blanquet, 2000), which is responsible for the integration of histidine into proteins (Freist, Verhey, Rühlmann, Gauss, & Arnez, 1999). On top of these limitations, most of the tools are written in different programming languages, are platform-dependent and depend on external tools, which can create a barrier for installation for the user; and the tools are either web-based, which restrict the user for additional downstream analysis or command-line based, which creates a restriction for the non-computational researchers. Besides, the available tools use feature-based counting (number of reads, counts, associated with each feature), except for **seqpac** (Skog et al., 2021), a recently published tool, which uses sequence-based counting (number of reads, counts, associated with each unique sequence). Sequence-based counting would prevent the same sequence from being annotated multiple times within and across samples, hence increasing the efficiency for alignment and reads assignment. Also, it directly enables looking at specific variations in sequences or their boundaries. However, due to this complexity, it can be challenging to explore data at the level of individual sequences, which calls for methods that can afford different levels of granularity. Hence, specialized tools are required with specialized pipelines to analyze sRNA-seq data.

We developed **shortRNA**, an R tool that addresses all of the issues listed above for processing sRNA-seq data. Our tool is cross-platform (it may run on any operating system) and built on the Bioconductor framework, in particular making use of efficient data structures (e.g., `DataFrame`, `FactorList`, and `TreeSummarizedExperiment`) enabling interoperability with other Bioconductor packages. Users can use **shortRNA** to conduct a thorough analysis of their data, from quality control (trimming, adapter removal, UMI compressing) and alignment to quantification and downstream analysis. **shortRNA** also has a set of customizable criteria for assigning reads to various types of short RNAs and seamlessly enables querying features at the level of individual fragments. We have tested our tool using a published mouse dataset from sperm, simulated data from sperm, and human data from peripheral blood mononuclear cells (PBMC; unpublished).

## 3.3 Methods

### 3.3.1 Development and testing environment

The **shortRNA** package is developed and tested on the Linux (GNU/Linux 4.4.0-210-generic x86\_64) operating system, Ubuntu (version 16.04.7 LTS) with 16 processors and 124 GB of RAM, using R 3.6.3 and R 4.0.5. As the **shortRNA** tool is developed as an R package, it is platform-independent (can easily be installed and run on other operating systems).

### 3.3.2 Backbone data structures of **shortRNA**

The **shortRNA** package is developed around four main data structures from Bioconductor: `phylo`, `FactorList`, `DataFrame`, and `TreeSummarizedExperiment`. These four data structures store the data and results in the most efficient manner and enable fast computation.

#### 3.3.2.1 `phylo`

The phylogenetic tree is a branching diagram used to depict evolutionary relationships. In R, the `phylo` class stores the phylogenetic relationship. In **shortRNA**, we save the relationship between RNA biotypes, features, and reads as a `phylo` object, section Features Tree.

#### 3.3.2.2 `FactorList`

In the case of a long vector of repeated characters, R takes more memory to store them and also the computation could be quite slow. These repeated character vectors could be stored as factors, where levels are provided to each unique character in the

vector (<https://datascience.stackexchange.com/questions/12018/when-to-choose-character-instead-of-factor-in-r>). However, when factors are stored in a list, the levels are traditionally defined for each element of the list, which can be very inefficient memory-wise. The **FactorList**, a class from the IRanges Bioconductor package, instead stores lists of factors as a single factor vector with added list membership information. In addition, like other AtomicList objects, it enables list operations without iteration. This is helpful for efficiently saving the object in R memory and for fast computations.

### 3.3.2.3 **DataFrame**

Rectangular data can be stored as **data.frame** class object in R. **DataFrame** functions from S4Vectors Bioconductor package and behaves similar to **data.frame** in terms of construction and subsetting. An advantage of using **DataFrame** is that it can store any type of object in a column, for example, a **FactorList**, or even another **DataFrame**, while retaining all the methods and functionalities of traditional **data.frames**.

### 3.3.2.4 **TreeSummarizedExperiment**

**TreeSummarizedExperiment** is a Bioconductor package extending the classical **SummarizedExperiment** (Morgan, Obenchain, Hester, & Pagès, 2020) and with additional hierarchy data and operations (R. Huang et al., 2020). The **SummarizedExperiment** class holds rectangular matrices of experiment data, accompanied by row and column annotation data. There are two classes in the **SummarizedExperiment** package: **SummarizedExperiment** and **RangedSummarizedExperiment**. Instead of a **DataFrame** of features, **RangedSummarizedExperiment** objects represent genomic ranges of interest. Figure 3.1A depicts the structure of the **SummarizedExperiment**. The rectangular data matrices are stored as assays, **rowData** stores annotation for corresponding rows in the assays, **colData** stores annotation for corresponding columns in the assays, ranges are described by a **GRanges** or a **GRangesList** object, which are stored as **rowRanges**, and metadata can be used to store additional data-related information.

In extension to the **SummarizedExperiment**, **TreeSummarizedExperiment** has **rowTree**, which stores the hierarchical structure of rows of assays; **colTree**, which stores hierarchical structure of columns of the assays; **rowLinks**, which stores the link information between the rows of the assays and **rowTree**; **colLinks**, which stores the link information between the columns of the assays; and **referenceSeq**, which stores the reference sequence for the features, depicted in Figure 3.1B.

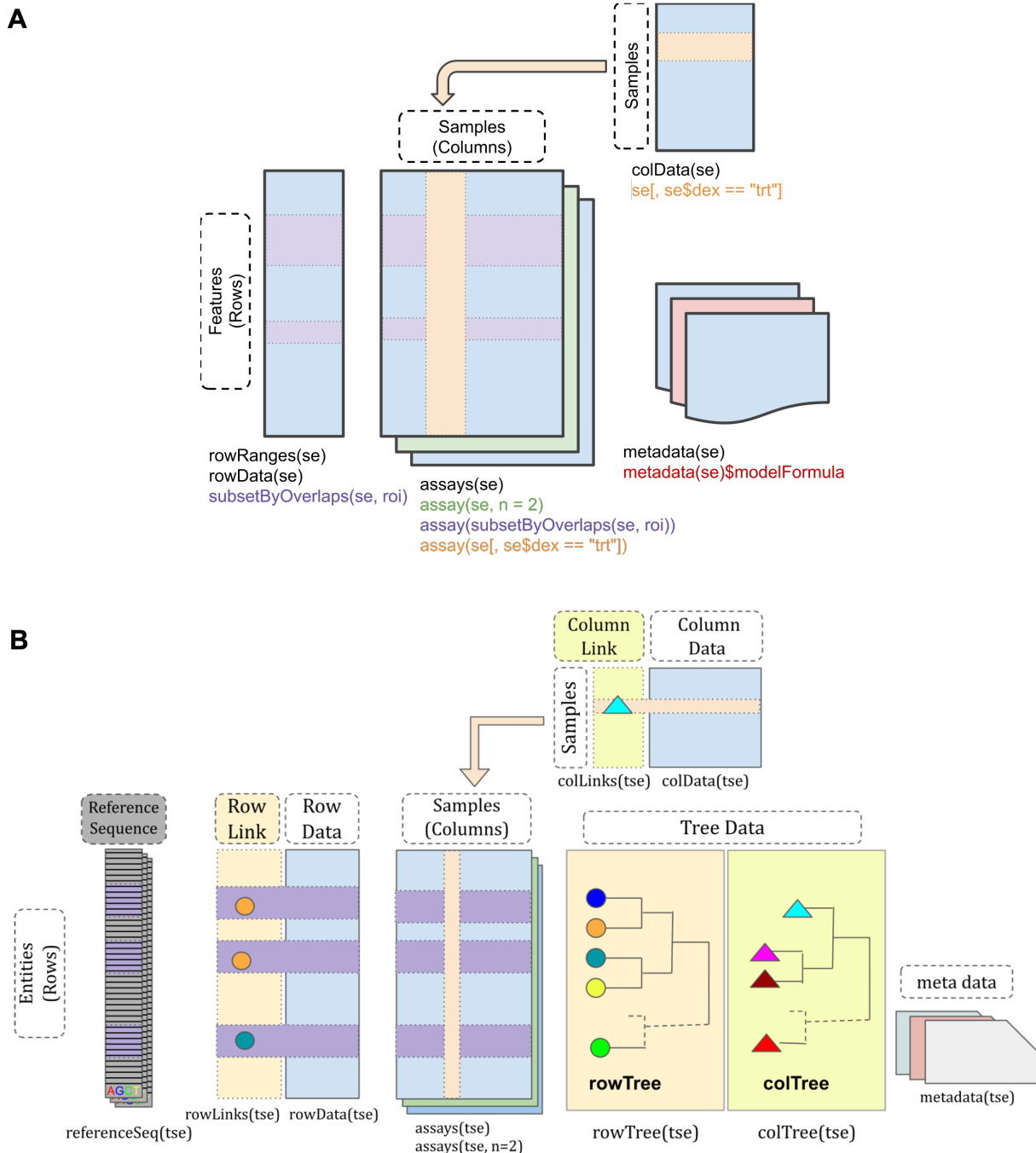


**Figure 3.1:** Schematic of A: `SummarizedExperiment` (Morgan et al., 2020), B: `TreeSummarizedExperiment` (R. Huang et al., 2020)

### 3.3.3 Pipeline

The `shortRNA` pipeline includes three major data analysis steps: preprocessing of data, alignment and reads assignment with the customisable assignment rules, and statistical analysis and visualization. Figure 3.2 shows the outline of the pipeline. First, the data goes through the preprocessing steps that consist of filtering and alignment of unique sequenced reads. The raw data undergo quality assessment and then the quality control steps are performed. The data is then aligned to a custom genome containing, in addition to the reference genome, extra pseudo-chromosomes for handling post-transcriptional modifications. Aligned reads are then overlapped with the features annotation and reads are assigned to the features using customisable assignment rules, which is an important part of this pipeline, after that, a features tree is formed. After the reads assignment, the data goes through the statistical analysis steps that consist of normalization and differential analysis. The quality controlled data are normalized and then the test for differential expression of short RNAs is performed in the user-defined biological groups.

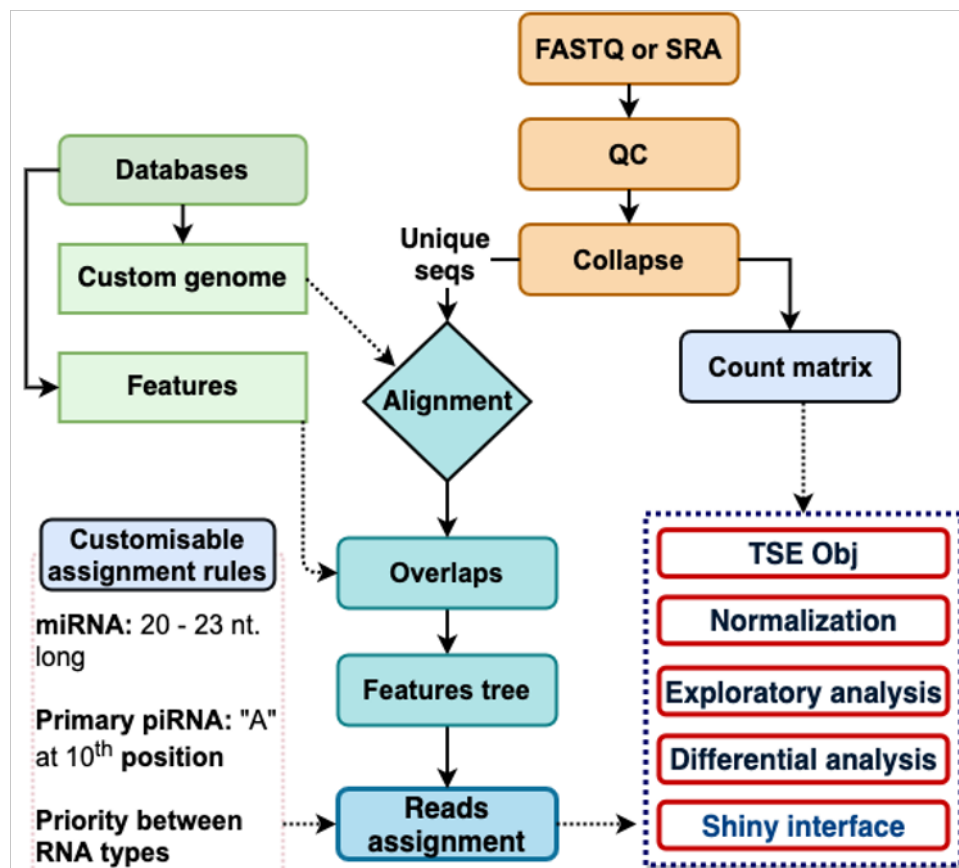
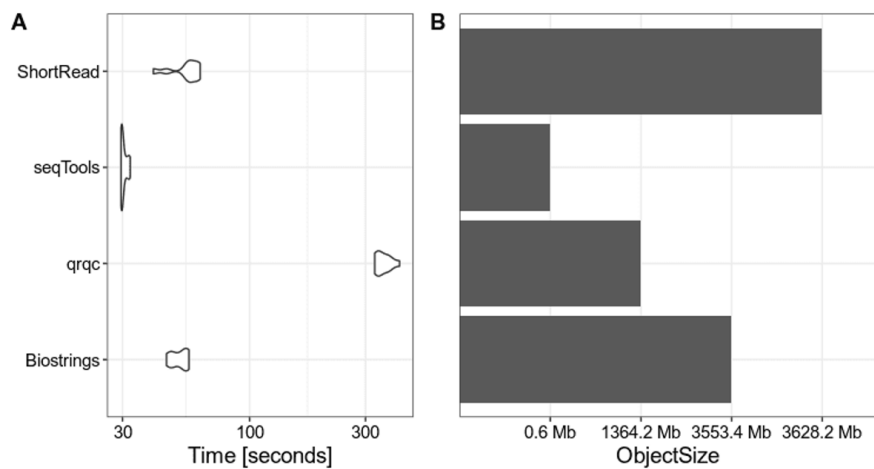


Figure 3.2: Overview of `shortRNA` pipeline

### 3.3.3.1 Quality control and trimming

Quality control (QC) and trimming is a vital step in HTS data analysis. To assess and control the quality of sRNA-Seq data, we adapted the functionalities from two R packages: `Rfastp` (W. Wang & Carroll, 2020) and `seqTools` (Kaisers, 2020). `Rfastp` is used for trimming the low-quality reads and adapter trimming. Further, with the summary files from `Rfastp`, the functions in our tool could be used for making a table of comparison for before and after QC, plots for duplicated reads, reads quality plot, and base-content plots. We benchmarked `Biostrings` (Pagès, Aboyoun, Gentleman, & DebRoy, 2020), `qrqc` (Buffalo, 2020), `ShortRead` (Morgan et al., 2009), and `seqTools` for reading and storing FASTQ files quality data in R, using an 863 MB FASTQ file. `seqTools` outperformed the other three tools in terms of reading and storing the FASTQ file quality data, as shown in Figure 3.3. Hence, we used it for reading the FASTQ files quality data, before and after QC, to make reads length distribution plots. To summarize, the QC functions provide information about sequencing depth, reads quality, possible adapter sequences, duplicated reads, and sequence length distribution, both before and after QC. The interactive plots provide users with greater insight into their data. Exemplary plots and tables from the QC report of a sample are shown in Figure 3.4.



**Figure 3.3:** Benchmark of four different Bioconductor tools for reading and storing FASTQ file quality data. Performance of four tools is measured in **A**: the amount of time they take for reading the file, **B**: the amount of memory they take to store the data.

Unique Molecular Identifiers (UMIs) are complex indices of 8-16 nucleotide lengths that are introduced to sequencing libraries before PCR amplification steps. Researchers can use UMI to evaluate the efficiency with which they collect input molecules, identify sampling bias, and, most importantly, identify and compensate for the effects of PCR amplification bias (Y. Fu, Wu, Beane, Zamore, & Weng, 2018). Preprocessing of data sequenced with

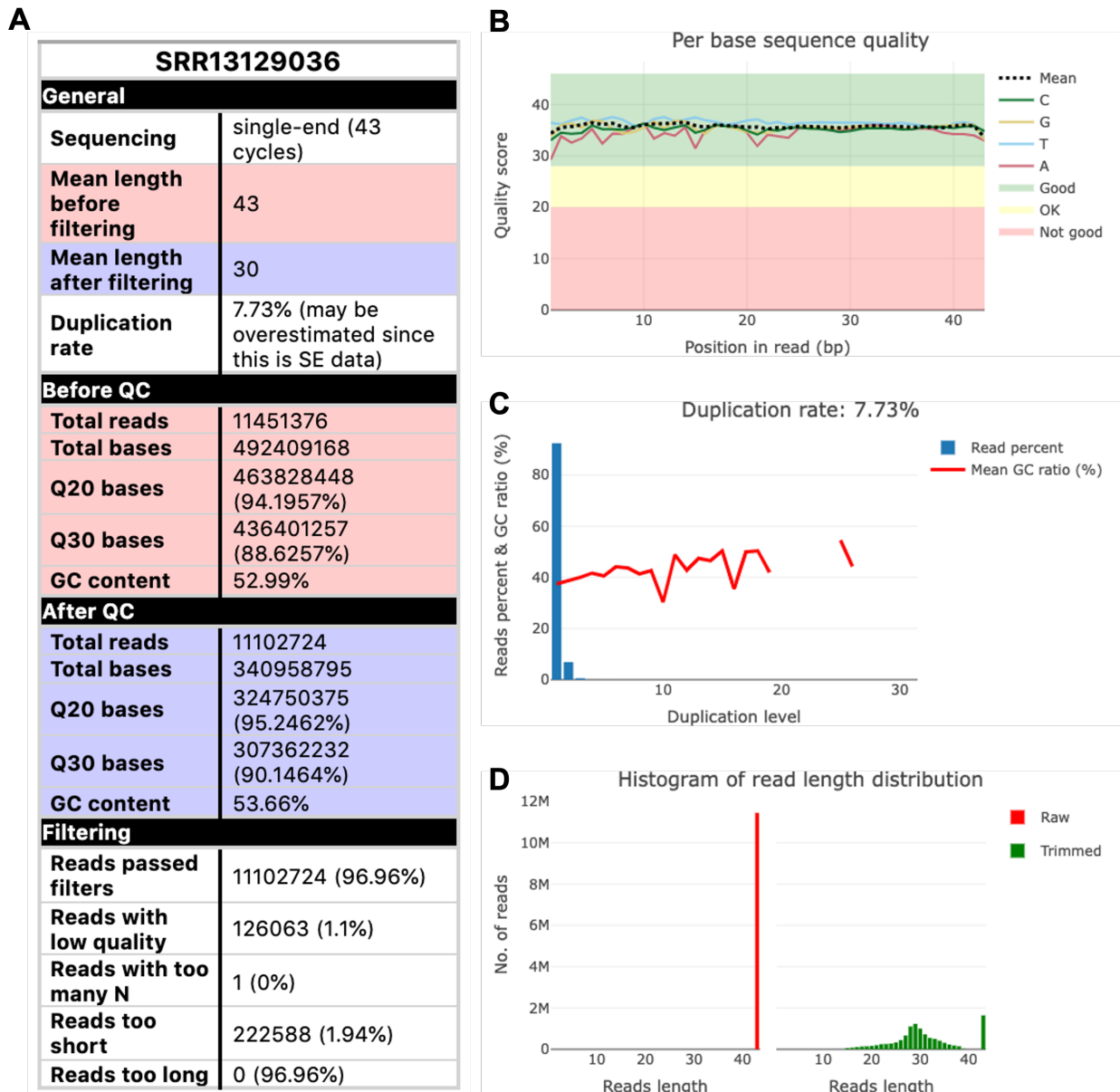


**Figure 3.4:** Exemplary QC report plots of a sperm sample from (Katharina Gapp et al., 2021). **A:** Quality control table, **B:** Quality score lines plot at each nucleotide in the sequencing reads, **C:** Barplot of reads duplication level with the mean GC ratio represented as lines, **D:** Histogram of reads distribution, before and after quality control

UMIs is required for reads deduplication and correction, as well as the creation of consensus sequences from each UMI. In `shortRNA`, we have adapted the `UMIc` tool for UMIs collapsing (Tsagiopoulou et al., 2021), which takes into account the frequency and the Phred quality of nucleotides and the distances between the UMIs and the actual sequences for collapsing the sequences.

Schematic of quality checks and quality control is shown in Figure 3.5.

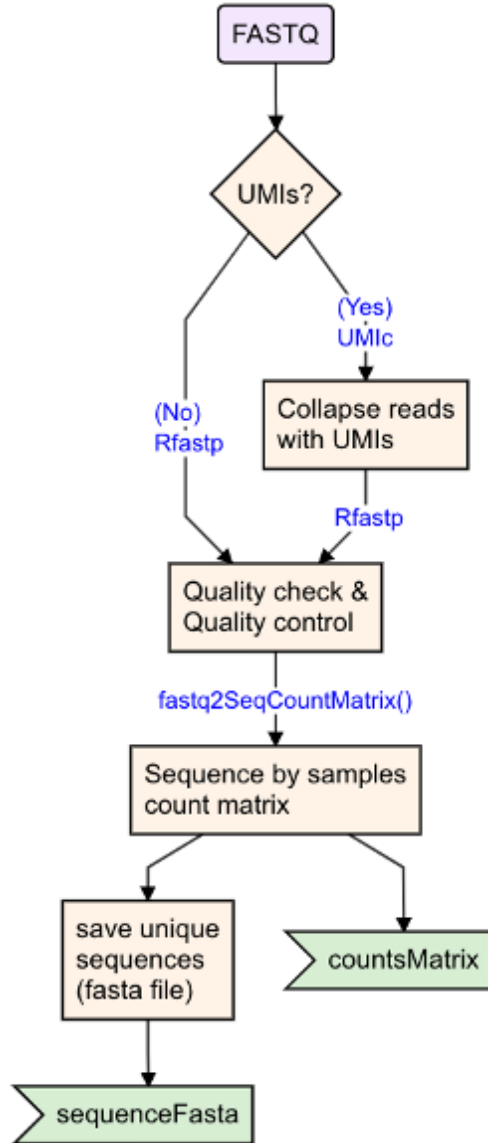


**Figure 3.5:** Schematic of quality check and quality control of FASTQ files, UMIs collapsing (if present), and collapsing FASTQ files to obtain unique sequences for alignment and making a sequence by samples counts matrix

### 3.3.3.2 Sequence count matrix

From the trimmed FASTQ files, we extract the unique reads sequences and make a sample by sequence count matrix. This matrix represents the counts of sequences in each sample, keeping only sequences occurring more than once. This is done by the `fastq2SeqCountMatrix()` function from `shortRNA`. Further, we export these sequences as a fasta file. An overview of this step is shown in Figure 3.5. The two main outputs from this step are `sequenceFasta`, which would be used for alignment, and `countsMatrix`.

### 3.3.3.3 Annotation preparation

Sequencing generates nucleotide sequences with unknown functions, while sequence annotation provides descriptive information about sequenced DNA sequences. Several databases are available for the annotation of the sequences. In `shortRNA`, we used miRBase (Griffiths-Jones, Saini, van Dongen, & Enright, 2008) for miRNAs; GtRNADb (P. P. Chan & Lowe, 2016) for tRNAs; mitoRNADb (Jühling et al., 2009) for mitochondrial tRNAs; for mouse, we use piRNA precursors from (X. Z. Li et al., 2013), rRNAs from SILVA (Quast et al., 2013), and mRNAs and other biotypes from Ensembl (Howe et al., 2021). It is possible for users to have additional databases of their choice.

The miRBase database is a collection of miRNA sequences and annotations. In miRBase, miRNAs are named as, for example, org-mir-20a. The first 3 letters signify the organism, “20” tell us that it was an early-discovered family (20th family that was named), “20a” tell us that there is possibly another related miRNA, for example, org-mir-20a. Here, org-mir-20a is a precursor. The mature miRNA species may be derived from both the 5’ and 3’ arms of the precursor duplex, and are called the miRNA-5p and -3p species, respectively. In this example, it would be org-mir20a-5p and org-mir20a-3p. All the miRNAs overlapping between Ensembl and miRBase were removed from Ensembl and the remaining one from Ensembl, not overlapping, were renamed to match the nomenclature of miRBase. For example, Mir7679 is renamed to org-miR-7679. Further, if the length of Ensembl miRNAs were more than 25bp, we labelled them as precursors.

A miRNA cluster is a group of two or more miRNA hairpins that are transcribed from miRNA genes that are physically adjacent, transcribed in the same direction, and are not separated by a transcription unit or a miRNA in the opposite orientation. There are mostly 2-3 mature miRNAs in a miRNA cluster, but there is an existence of a bigger miRNA cluster, which is found in humans on chromosome 13: miR-17 to miR-92, involved in tumour formation, and development of heart lungs and immune systems (Lai & Vera, 2013). Researchers group the miRNAs to form a miRNA cluster by the distance between them. For example, (Baumgart

et al., 2017; Griffiths-Jones et al., 2008) call a group of miRNA as clusters if miRNAs are within 10kb and (Yuan et al., 2009) used a distance of 50kb. In **shortRNA**, we use a distance of 10kb for clustering miRNAs as more than 40% of experimentally validated human miRNA cluster genes have been identified within 10kb (Griffiths-Jones et al., 2008; Lai & Vera, 2013).

The genomic tRNA database (GtRNADb) is a database of tRNA gene predictions created by tRNAscan-SE (P. Chan, Lin, Mak, & Lowe, 2021) on whole or almost complete genomes. In GtRNADb, tRNAs symbols consist of 5 parts, separated by a “-”, for example, tRNA-Ala-AGC-9-2. In this example, tRNA (prefix) represents tRNA genes that are high scoring and not predicted as pseudogenes. If it was a pseudogene, it would have been represented as “tRX”. At the second position, we have three-letter amino acids (isotype), which stand for tRNA isotype. At the third position, we have anticodon detected in the gene sequence. At the fourth position, there is a unique ID (transcript ID) of a tRNA transcript or “isodecoder” with a particular isotype and anticodon. The fifth position represents the gene locus ID and for tRNA genes with multiple identical copies, this gene locus ID represents the particular gene copy in the genome. For the mitochondrial tRNAs, we obtained the sequences from mitotRNADb (Jühling et al., 2009) using the tRNADbImport (GM, 2018) R package. Further, we removed all the duplicated sequences and renamed the mitochondrial tRNAs as per the naming convention of GtRNADb, adding “mt” as a prefix. Mature tRNAs receive a post-transcriptional addition of “CCA” (Barraud & Tisné, 2019), hence, we added “CCA” to all the tRNA/ mt-tRNA sequences at the 3’ end. All histidine tRNAs of known sequence are one nucleotide longer at the 5’ end than are other tRNA species(Cozen et al., 2015),hence we added “G” at the 5’ end of the sequences of Histidine tRNAs/ mt-tRNAs to account for this post-translational modification, as also done in (Cozen et al., 2015; Shi et al., 2018). Because of these post-transcriptional modifications, we add the sequences of tRNA into the genome FASTA file as pseudo chromosomes. For example:

```
>pseudoChr_tRNA-Thr-CGT-1-1
GGCGCGGTGGCCAAGTGGTAAGGCCTGGTCTCGTAAACCGAAGATCACGGGTTCGAACCCCGTCCGTGCCTCCA

>pseudoChr_mt_tRNA-His-GTG-1-1
GGTGAATATAGTTACAAAAAACATTAGACTGTGAATCTGACAACAGGAAATAACCTCCTGTTACCCCCA
```

All the tRNAs overlapping between Ensembl and GtRNADb were removed from Ensembl and the remaining tRNA from Ensembl, not overlapping, were labelled as pseudo tRNAs.

SILVA is an rRNA database, which provides extensive, quality-checked, and regularly updated datasets of aligned short (16S/18S, SSU) and large subunit (23S/28S, LSU) ribosomal RNA sequences. rRNAs are repeated sequences and are masked in the genomes in the Ensembl

database, and are not listed in the features annotation. Hence, we add them as well as pseudo chromosomes to the genome FASTA file, similar to tRNAs.

`getDB()`, Figure 3.6, function retrieve the databases, account for the post-translational modifications of tRNAs, alter mitochondrial tRNA database, and create miRNA clusters and assign miRNAs and miRNA precursors to miRNA clusters. The output from `getDB()` is then parsed to the `prepareAnnotation()` function, which prepares features annotation as `GRanges()`, save the genome and pseudo-genomes and index that for alignment. Features annotation are then converted to `FactorList` using `featuresAnnoToFL()`. The main three outputs from the annotation preparation are features as `GRanges()` and `FactorList()`, and indexed `customGenome`.

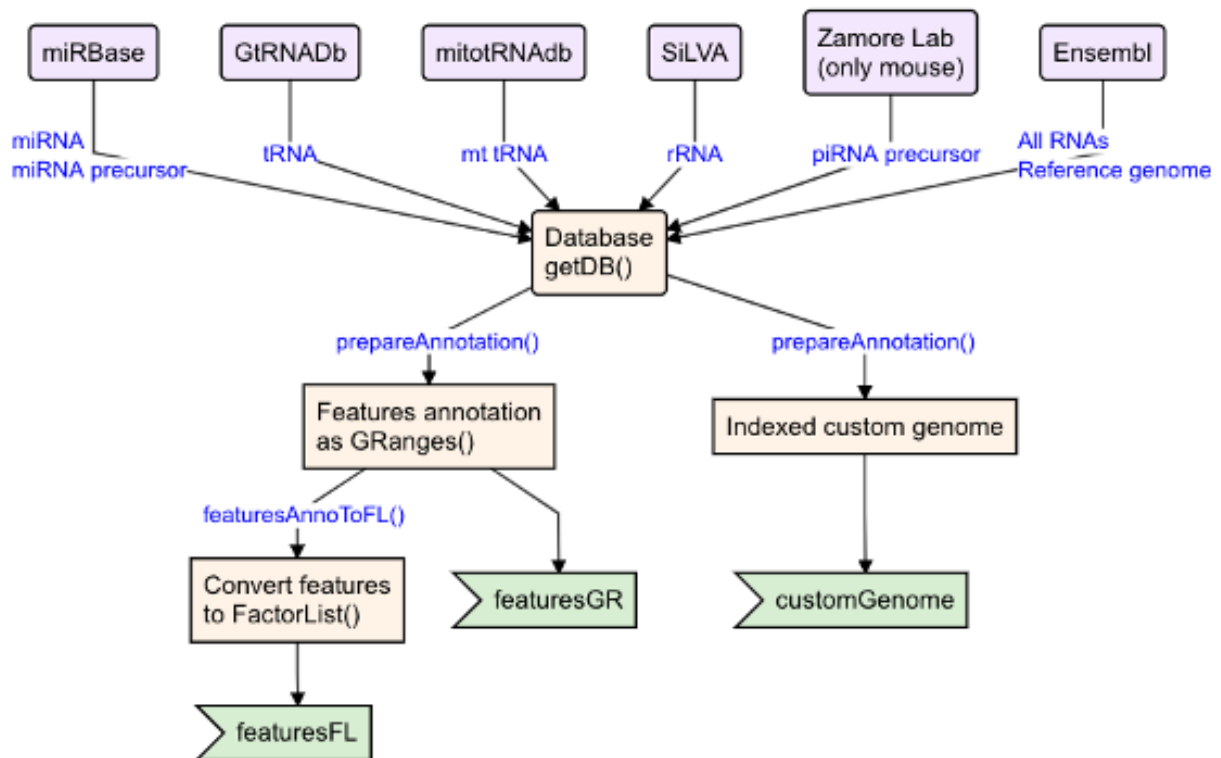


**Figure 3.6:** Schematic of obtaining database, preparing annotations and custom genome indexes for alignment

### 3.3.3.4 Alignment

Alignment is necessary to know where in the genome reads belong. The alignment of short RNA remains a persistent under-recognized problem. We align the FASTA file of sequences with the custom genome prepared in the annotation step. For alignment, we use the `Rsubread` R package (Liao et al., 2019) with the index of custom genome generated on the genome and

pseudo-chromosomes (`index = "customGenome"`), with the GTF from Ensembl database obtained from `getDB()` of `shortRNA` (`GTF = exonsBy(db$ensdb)`), and allowing to report the maximal number of equally-best mapping locations (`nBestLocations = 16`). Please refer to the schematic in Figure 3.7.

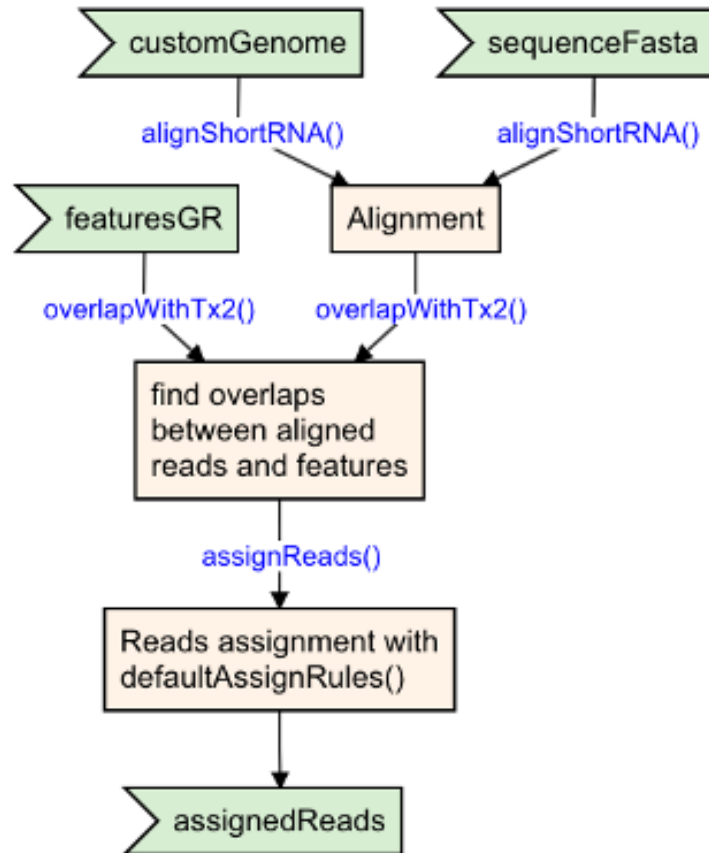


**Figure 3.7:** Schematic of alignment, overlapping features and aligned sequences, and assigning reads to features using assignment rules

### 3.3.3.5 Reads annotation and assignment

After alignment, the aligned file (BAM file) is overlapped with the features annotation (`featuresGR`) using the `overlapWithTx2()` function. It is possible that a read overlaps with multiple features. Next, the overlaps are parsed with the `assignReads()` function with the assignment rules, `defaultAssignRules()`, for validating the overlap and finding assignment of multi mapping reads. Please refer to the schematic in Figure 3.7.

### 3.3.3.6 Assignment rules

A sequence read can be mapped to multiple locations in the genome. It is critical to ensure that the reads are properly mapped to the feature and that they are assigned to one or more features. In the `shortRNA` package, we defined a set of customizable rules for this purpose. The output of the function `defaultAssignRules()` is described below:

We consider reads with at least 50% overlap to the features to be valid read assignments.

```
$overlapBy
[1] 0.5
```

By default, we do not prioritize the assignment based on the size of the overlap between reads and features (when a read overlaps multiple features); however this option is available to users.

```
$prioritizeByOverlapSize
[1] FALSE
```

We prioritize overlap in the same strand, but enable overlaps from the opposite strand if there is no known feature on the same strand.

```
$sameStrand
[1] "prioritize"
```

We give priority to known features in our assignments.

```
$prioritizeKnown
[1] TRUE
```

Next come validation rules specific to RNA types. For example, in order to be assigned to primary piRNAs, the read should be 26-32 nucleotides long, with the first nucleotide being a T.

```
$typeValidation$primary_piRNA
$typeValidation$primary_piRNA$fun
function(src, allowRevComp=FALSE, length=26:32){
  length <- as.integer(length)
  valid <- src$length >= min(length) & src$length <= max(length)
  if(length(w <- which(valid))==0) return(valid)
```

```

seqs <- as.character(src$seq[w])
valid[w] <- sapply(strsplit(seqs,""),FUN=function(x){ x[[1]]=="T" })
if(allowRevComp){
  revcomp <- as.character(reverseComplement(DNAStringSet(seqs)))
  valid[w] <- valid[w] |
    sapply(strsplit(seqs,""),FUN=function(x){ x[[1]]=="T" })
}
valid
}

```

If the read cannot be identified as a primary piRNA, it is referred to as a piRNA precursor.

```

$typeValidation$primary_piRNA$fallback
[1] "piRNA_precursor"

```

Secondary piRNA sequences should be 26 to 32 nucleotides long, with A in the 10th position (Brennecke et al., 2007).

```

$typeValidation$secondary_piRNA
$typeValidation$secondary_piRNA$fun
function(src, allowRevComp=FALSE, length=26:32){
  length <- as.integer(length)
  valid <- src$length >= min(length) & src$length <= max(length)
  if(length(w <- which(valid))==0) return(valid)
  seqs <- as.character(src$seq[w])
  valid[w] <- sapply(strsplit(seqs,""),FUN=function(x){ x[[10]]=="A" })
  if(allowRevComp){
    revcomp <- as.character(reverseComplement(DNAStringSet(seqs)))
    valid[w] <- valid[w] |
      sapply(strsplit(seqs,""),FUN=function(x){ x[[10]]=="A" })
  }
  valid
}

```

If a read cannot be identified as secondary piRNA, it is referred to as a piRNA precursor.

```
$typeValidation$secondary_piRNA$fallback
[1] "piRNA_precursor"
```

For miRNAs, the length should be between 19 and 24 nucleotides, and the read should overlap the feature by at least 16 bp. The maximum number of non-overlapping nucleotides allowed is three.

```
$typeValidation$miRNA
$typeValidation$miRNA$fun
function (src, length = 19:24, minOverlap = 16L, maxNonOverlap = 3L)
{
  src$length %in% length & src$overlap >= minOverlap & (src$length -
    src$overlap) <= maxNonOverlap
}

$typeValidation$miRNA$length
[1] 19 20 21 22 23 24
```

If a read cannot be assigned to a mature miRNA, it is assigned to a miRNA precursor.

```
$typeValidation$miRNA$fallback
[1] "miRNA_precursor"
```

Reads that are assigned to tRNAs (or pseudo tRNAs) undergo additional classification. tRNA 5p fragments are less than 30 bp long and begin in the feature's 5bp. tRNA 3p fragments are less than 50 bp long, with a distance to the feature end of 5bp. Starts at  $+/- 1$ bp of the feature and has a length of 30 to 34 nucleotides for 5p half. The 3p half begins at  $+/- 1$ bp of the feature, has a length of 34 to 50 nucleotides, and ends with CCA.

```
$reclassify
$reclassify$tRNA
function(srcts, rules=list(
  "tRNA_internal_fragment"=function(x){ rep(TRUE, nrow(x)) },
  "tRNA_5p_fragment"=function(x){ x$startInFeature < 5L & x$length < 30L },
  "tRNA_3p_fragment"=function(x){ x$distanceToFeatureEnd < 5L & x$length < 50L },
  "tRNA_5p_half"=function(x){ x$startInFeature %in% -1:1 & x$length %in% 30:34 },
  "tRNA_3p_half"=function(x){ x$distanceToFeatureEnd %in% -1:1 & x$length >= 34L &
```

```

x$length <= 50L & grepl("CCA$",x$seq) }
)) {
  valids <- vapply(rules, FUN.VALUE=logical(nrow(srcs)), FUN=function(fn){
    fn(srcs)
  })
  if(nrow(srcs) == 1) valids <- t(valids)
  factor(apply(valids, 1, FUN=function(x) max(which(x))),
         seq_len(ncol(valids)), colnames(valids))
}

```

We also assign priorities to different types of RNA. Priorities can be changed by increasing or decreasing the numbers; for example, in the case of only miRNA sequencing, users can set higher priorities for miRNAs by changing the number from 1 to 2 or higher.

\$priorities				
miRNA	tRNA	tRNAP	Mt_tRNA	snRNA
1	1	1	1	1
snoRNA	antisense	primary_piRNA	secondary_piRNA	
1	1	1	1	
precursor	long_RNA	longRNA		
-1	-1	-1		

### 3.3.3.7 Features tree

We organized the features and reads in the form of a rooted phylogenetic tree in a hierarchical fashion. This is done by the function `assignReadsToTree()` in `shortRNA`, Figure 3.12. From the root, we have two main branches: `shortRNA` and long RNA, Figure 3.8C. We keep the features that are longer than 200 bp in long RNA and the features that are shorter than 200 bp in short RNA. Each branch is then further divided into RNA types. The miRNAs and tRNAs are further divided into sub-branches to account for the multi-mapping problems, Figure 3.9 and Figure 3.10. Sequence quality and a follow up trimming, may result in one nucleotide shorter sequence. Because of the hierarchical organization, unique reads mapping to a feature are kept in the hierarchy, Figure 3.8. If the user would like to include an additional database for short RNAs, an additional branch can be added to the tree while preparing annotation, `prepareAnnotation()`.

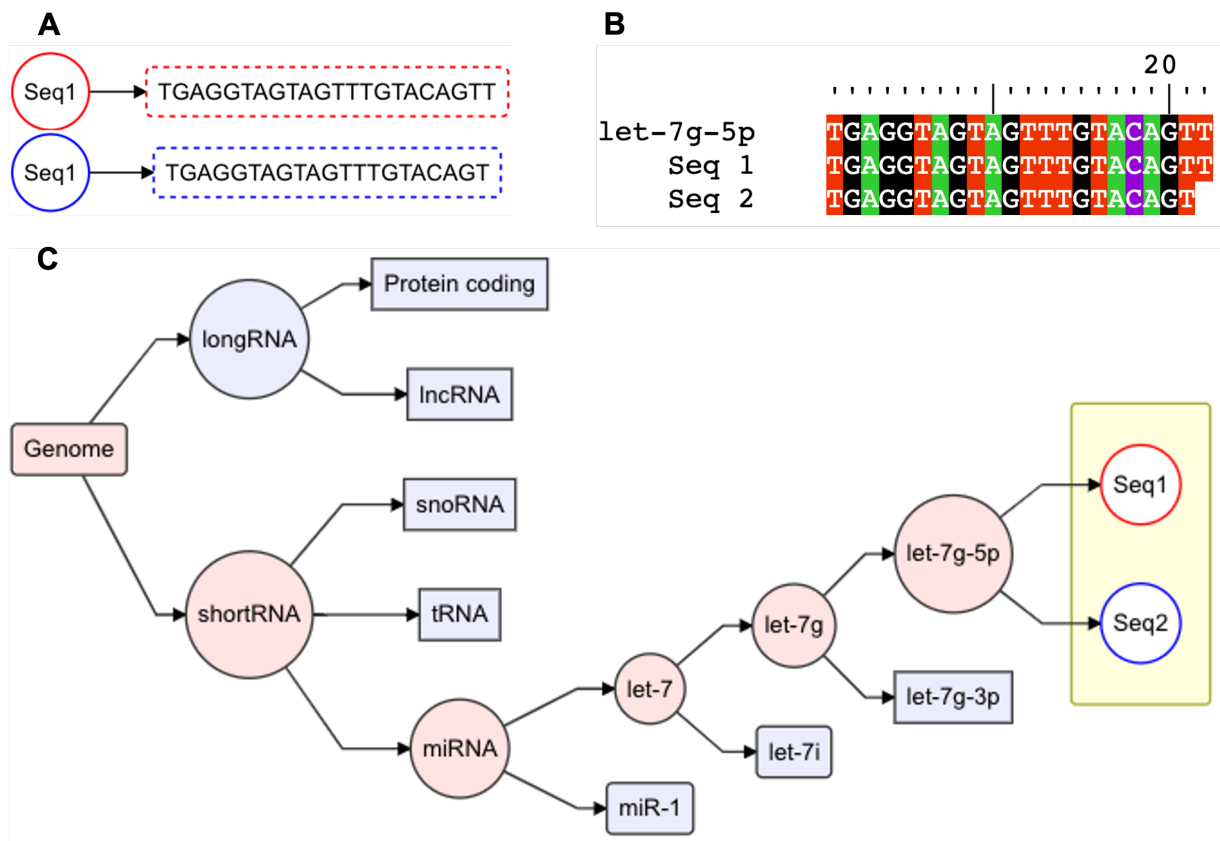


**Figure 3.8:** General framework of feature tree and assignment of sequences to the tree. **A:** Example of two sequences. **B:** Alignment of both the sequences to miRNA. **C:** General outline of the feature tree and assignment of both the sequences to the tree

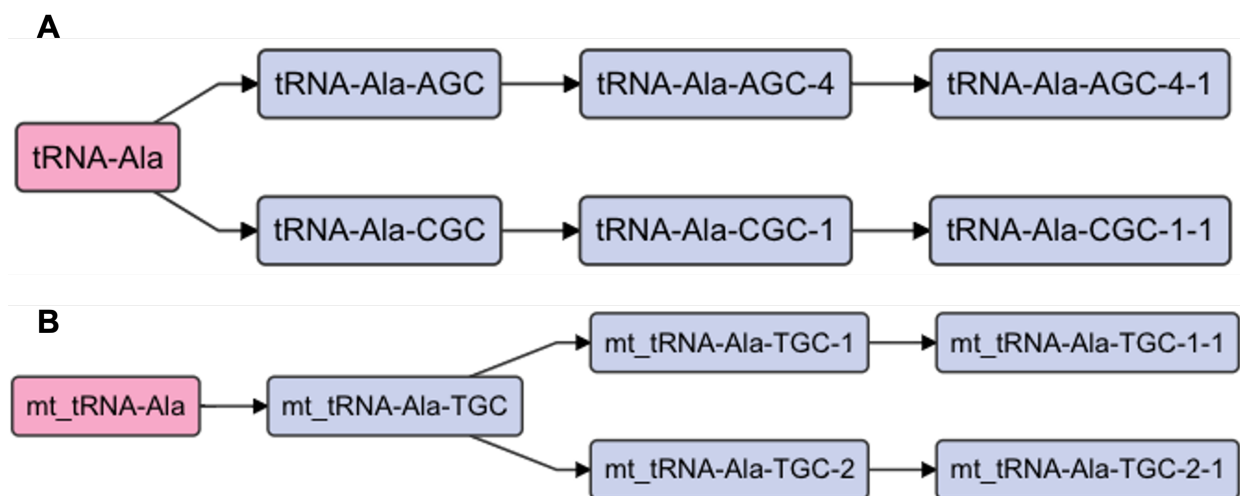


**Figure 3.9:** Hierarchical organization of **A:** tRNA features and **B:** mitochondrial tRNA features.

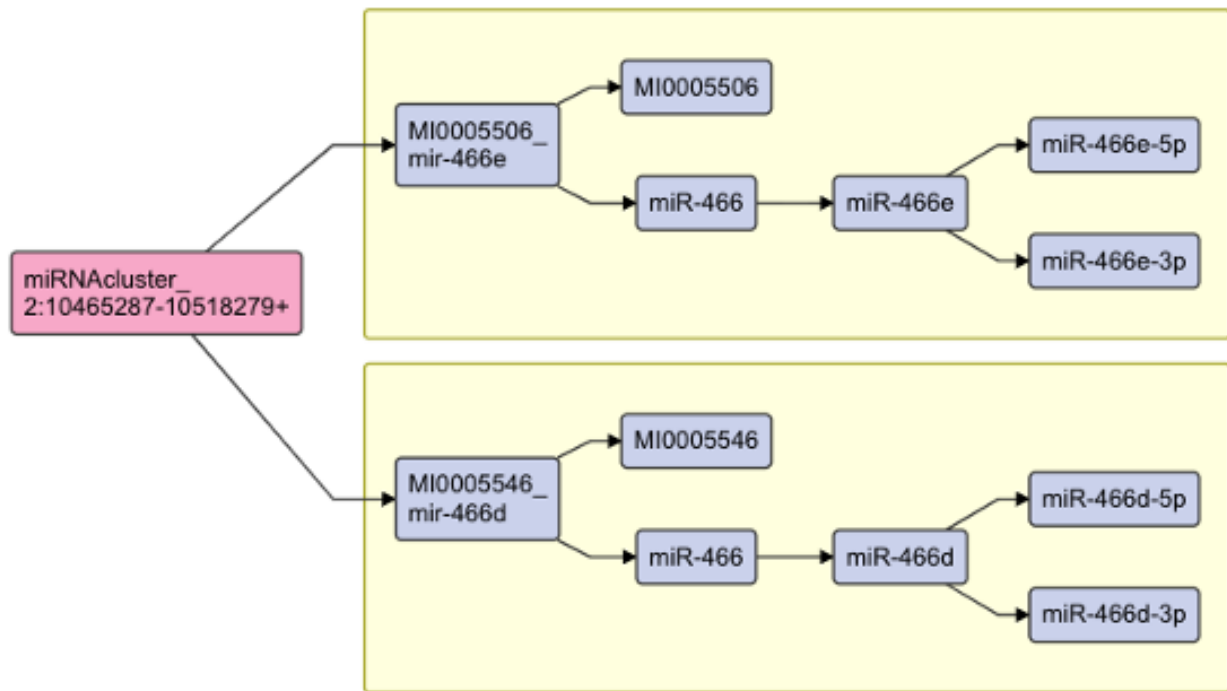


**Figure 3.10:** Hierarchical organization of miRNA features

### 3.3.3.8 Reads assignment ambiguity

Reads can align to multiple locations in the genome, and when this is the case, typical workflows will either randomly align to one location or not report any alignment. We allow for multi-mapping during alignment, and address ambiguities when we assign reads to features. Specifically, we assign it to the parent of all the features to which the read maps. Figure 3.11A depicts a read that can be mapped to multiple tRNAs, Figure 3.11B. While assigning reads to the features tree, we assign this read as an ambiguous read to the parent of all the features it is mapping to; in this case, tRNA-Leu-CAG, Figure 3.11C.

### 3.3.3.9 Construction of TreeSummarizedExperiment object

The feature tree and the assigned reads DataFrame is then used for the construction of the TreeSummarizedExperiment object, which is then used for all the downstream analysis, including differential analysis. This is depicted in Figure 3.12.

### 3.3.3.10 Differential analysis

The hierarchical structure of the features implies that differential expression analysis could be performed at different levels of the hierarchy, which would however increase the multiple testing problem. We, therefore, rely on the method for dynamic testing of hierarchical

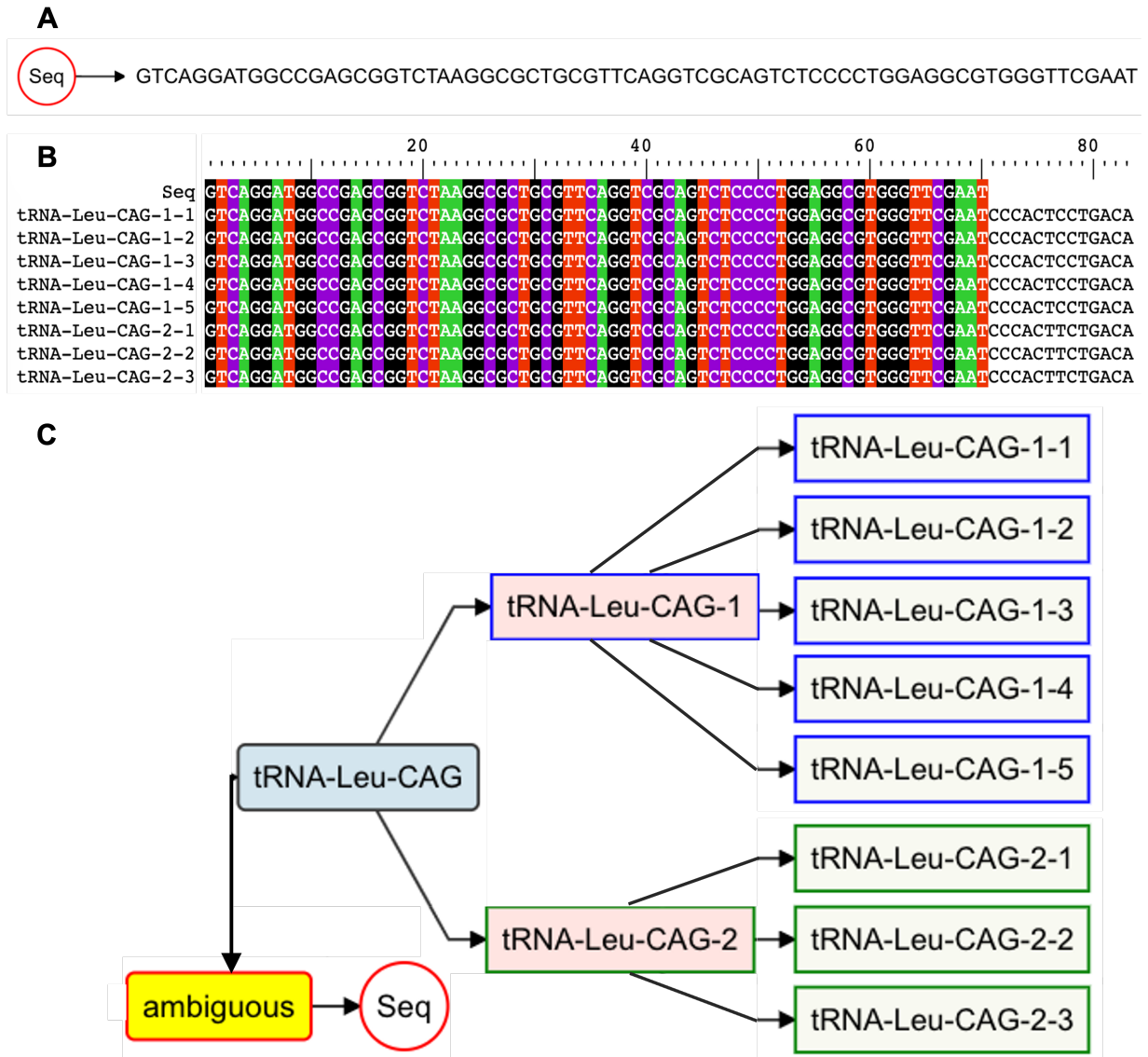


**Figure 3.11:** Multiple assignments of a sequence mapping to a tRNA. **A:** Exemplary sequence. **B:** Multiple sequence alignment plot of the sequence and the features to which it is mapping. **C:** Assignment of the reads to the tRNA feature tree

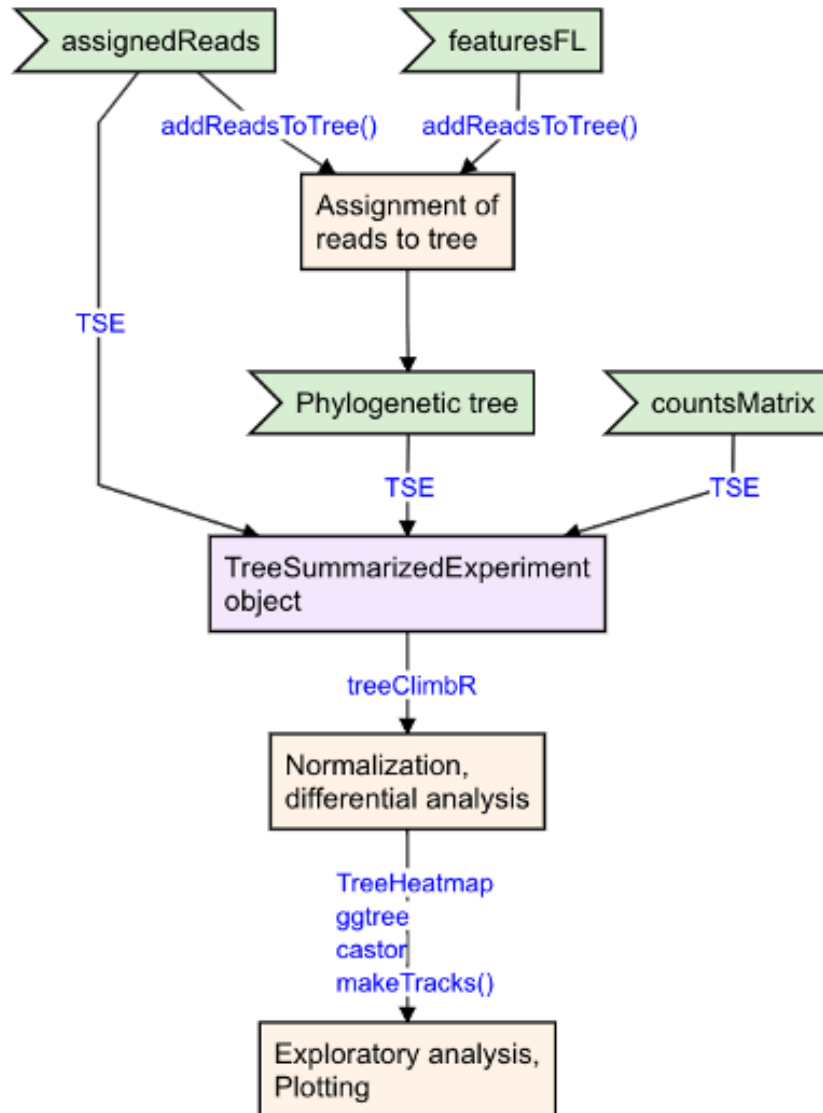


**Figure 3.12:** Schematic of assigning reads to the features tree of features, creation of `TreeSummarizedExperiment` object, and downstream analysis and plotting

hypotheses implemented in `treeclimbR` (R. Huang et al., 2021) for differential analysis of features.

Following normalization and differential analysis, users can use the `TreeHeatmap`, `ggtree`, and `castro` R packages for exploratory data analysis and figure creation. The `shortRNA makeTracks()` function can be used to create genomic tracks, as shown in Figures 3.15, 3.18a, and 3.18b. We intend to expand our package by writing wrappers for these packages in order to generate plots from within `shortRNA`.

### 3.3.3.11 Table of important functions

Table 3.1 shows some of the most important functions of the `shortRNA` package. In the table, the functions are organized in the chronological order of data analysis.

**Table 3.1:** Important functions from shortRNA

Function name	Function description
<code>generateQCreport</code>	Perform quality check, quality control, provide trimmed files and generates an HTML report
<code>fastq2SeqCountMatrix</code>	Generates a sequence by sample count matrix
<code>getDB</code>	Obtain databases for annotation of desired genome
<code>prepareAnnotation</code>	Using the databases provided, create a features GRanges object and index the genome
<code>alignShortRNA</code>	Align the sequences with custom genome index built using <code>prepareAnnotation</code>
<code>overlapWithTx2</code>	Find overlaps between read alignments and a feature annotation
<code>assignReads</code>	Assign overlapped reads from <code>overlapWithTx2</code> as per the assignment rules
<code>defaultAssignRules</code>	Display default reads assignment rules
<code>featuresAnnoToFL</code>	Convert the features GRanges object to a FactorList
<code>addReadsToTree</code>	Assign reads to the FactorList of features as per output of <code>assignReads</code>
<code>makeTracks</code>	Make a genomic track of aligned data for given genomic location

## 3.4 Results

### 3.4.1 Datasets used for testing the pipeline

We used a previously published sperm sRNA-seq dataset from (Katharina Gapp et al., 2021) (GEO accession: GSE162112), in which we additionally spiked simulated reads. We also used an unpublished PBMC human dataset from the Schratt Lab (<https://schrattlab.ethz.ch/>) at the ETH Zurich, on which qPCR were additionally performed for 5 miRNAs (miR-30b-5p, miR-30e-5p, miR-30d-5p, miR-499-5p, and miR-1248). We used these human data to correlate quantifications from `shortRNA`, `seqpac`, `Sports1`, and `Oasis2` with delta Ct values from qPCR. We analyzed both of these datasets with `shortRNA`, `seqpac`, `Sports1`,

and `Oasis2` tools to compare the quantification of miRNAs. Further, we used the simulated reads from miRNAs to test the reads assignment and to assess differential analysis.

For both datasets, we used miRBase (miRNA), GtRNADB (tRNA), MttRNADB (mitochondrial tRNA), SiLVA (rRNA), and Ensemble. For the sperm dataset from the mouse, we also used piRNA precursors.

### 3.4.2 Comparison of quantification and identification of miRNAs

#### 3.4.2.1 shortRNA quantification is positively correlated with `Oasis2` and `Sports1`

We used `Sports1`, `seqpac`, `Oasis2`, and `shortRNA` with the default parameters to analyze the sperm dataset. Following the data analysis, we limited our assessment to miRNAs for comparison across tools. We found 1970 miRNAs using `Oasis2`, 1137 using `Sports1`, 1024 using `seqpac`, and 503 using `shortRNA`. We began by examining the quantification with all four tools. Figure 3.13 shows a comparison of the quantification of miRNAs from `Sports1`, `Oasis2`, and `seqpac` with `shortRNA`. We discovered that the quantifications of `shortRNA` and `Oasis2`, as well as `shortRNA` and `Sports1`, are highly correlated. In contrast, the correlation of quantification between `shortRNA` and `seqpac` was negative. We investigated this discrepancy and discovered a large number of short reads (length: less than 15 nucleotides) mapping to miRNAs and assigned by `seqpac`, but which were considered invalid overlaps in light of our assignment rules.

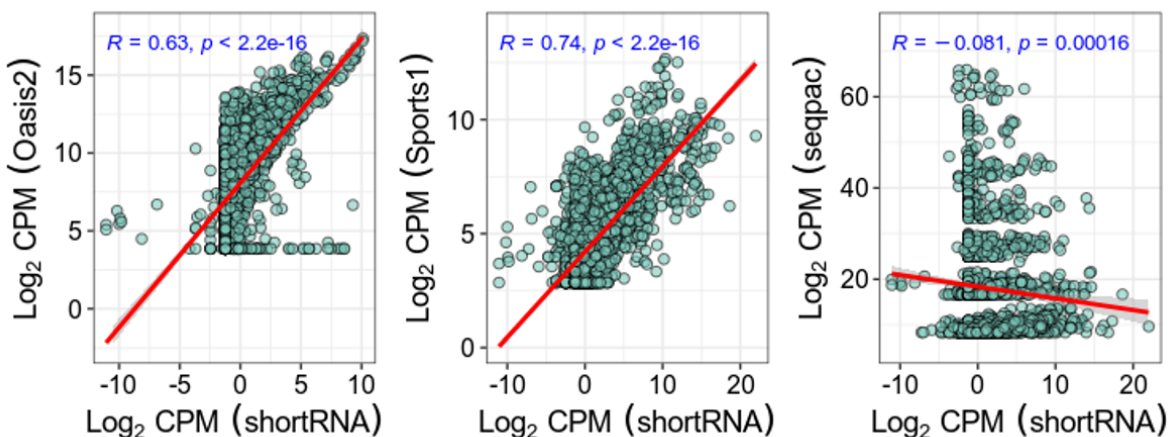


**Figure 3.13:** Comparison of Log2 TMM normalized quantification of miRNAs from `shortRNA` with `Oasis2`, `Sports1`, and `seqpac`

### 3.4.2.2 **shortRNA** accurately identify miRNAs

Following that, we examined the overlaps of identified miRNAs between four tools. Despite the fact that all of the tools use miRBase, we discovered that only 44 miRNAs were commonly detected by all of the tools, Figure 3.14. One possible explanation is that the miRBase for mouse genome contains approximately 2000 mature miRNAs and approximately 1300 miRNA precursors, and **seqpac** and **Sports1** only use miRNA precursors in the data analysis pipeline, whereas **Oasis2** and **shortRNA** use both mature and miRNA precursors. Figure 3.14 shows that there were 231 miRNAs that were commonly detected by **Oasis2**, **Sports1**, and **seqpac**, but not by **shortRNA**. Next, we looked into these miRNAs and discovered that three were removed from the most recent version of miRBase; for the other 228, we did not find alignment in the genome using **shortRNA**, despite accepting mismatches and soft-clipping. Based on our findings, we believe that these miRNAs are the result of misalignment or sequential alignment by the other three tools. When we examined the sequences mapping to these miRNAs according to **seqpac**, we discovered that all of the reads mapping to these miRNAs were shorter than 15 bp, and as a result, are very unlikely to represent functional miRNAs. In conclusion, we discovered that **shortRNA** can accurately identify miRNAs.

### 3.4.3 Data simulation to check the alignment and reads assignment by **shortRNA**

We validated the alignment and reads assignment by spiking the reads in the sperm dataset (Appendix C). In brief, we simulated reads for a miRNA cluster containing mmu-miR-125a-5p, mmu-miR-99b-5p, mmu-let-7e-5p, mmu-let-7e-3p, mmu-miR-99b-3p, and mmu-miR-125a-3p, as well as reads from a miRNA precursor, mmu-miR-144. To test for differential analysis, the sequences from these miRNAs were spiked while also creating differences between groups. Three invalid sequences were also simulated for the precursor to test the accuracy of read assignment and were properly aligned to miRNA precursors, as shown in Figure 3.15.

Further, the reads were assigned accurately to miRNAs, Table 3.2.

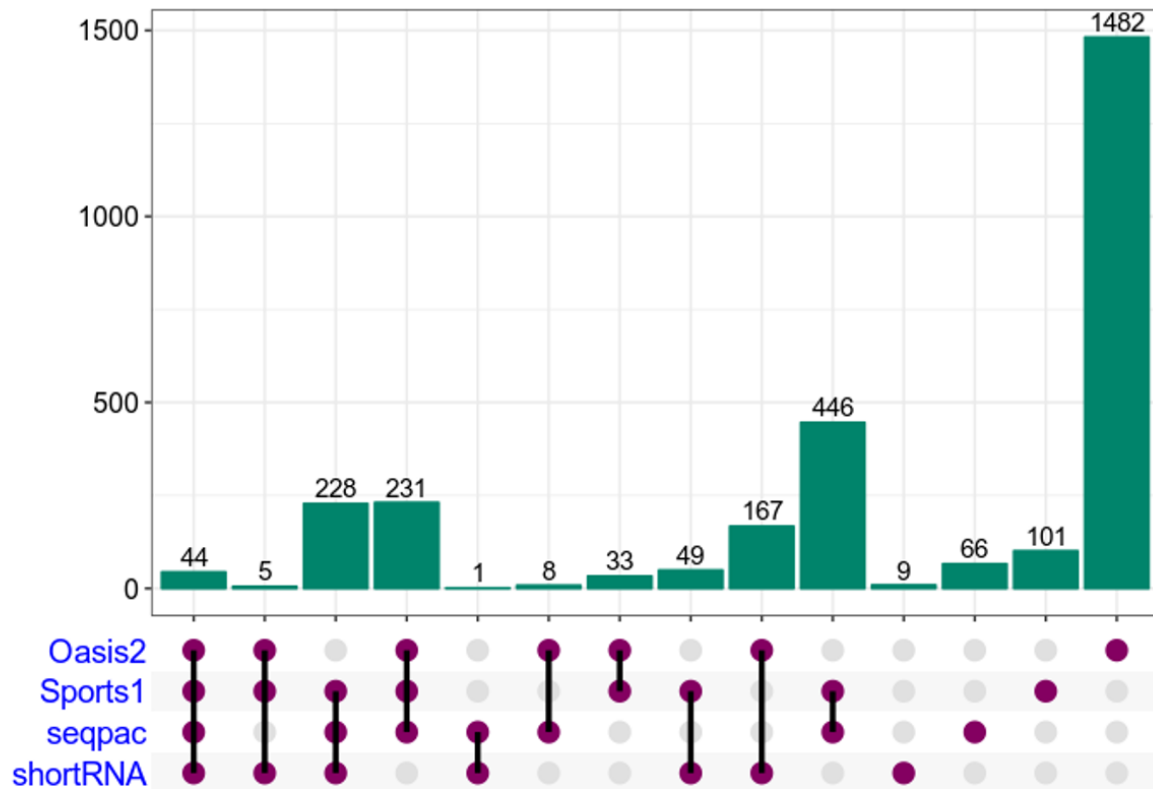


**Figure 3.14:** Upset plot of overlaps of detected features between four methods: shortRNA, Oasis2, Sports1, and seqpac

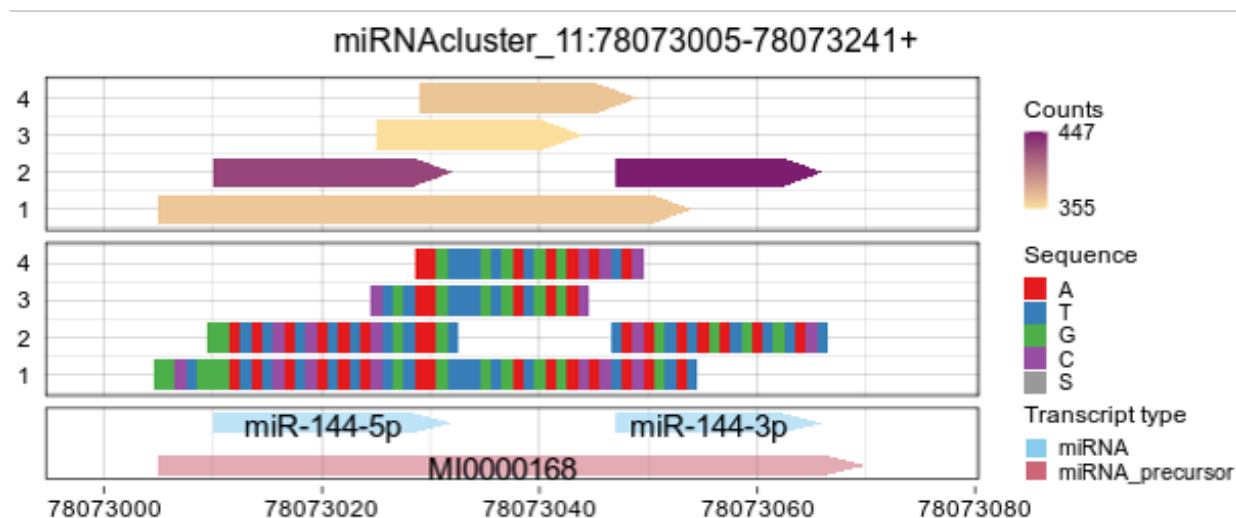


**Figure 3.15:** Genomic plots of simulated reads from miRNA precursor.

**Table 3.2:** Assignment of simulated reads by shortRNA

Sequence	Overlap	Transcript ID	Transcript type	Transcript length	valid	Valid miRNA
AAGTTTGTGATGAGACACTAC	21	MI0000168	miRNA_precursor	66	TRUE	FALSE
ACAGGTGAGGTCTTGGGAGCC	22	miR-125a-3p	miRNA	22	TRUE	TRUE
CAAGCTCGTGTCTGTGGGTCGG	22	miR-99b-3p	miRNA	22	TRUE	TRUE
CACCGTAGAACCGACCTTGCG	22	miR-99b-5p	miRNA	22	TRUE	TRUE
CTATACGGCCTCCTAGCTTCC	22	let-7e-3p	miRNA	22	TRUE	TRUE
CTGTAAGTTGTGATGAGAC	20	MI0000168	miRNA_precursor	66	TRUE	FALSE
GGATATCATCATATACTGTAAGT	23	miR-144-5p	miRNA	23	TRUE	TRUE
GGCTGGATATCATCATATACTGTAAGTTGTGATGAGACACTACAGTAT	50	MI0000168	miRNA_precursor	66	TRUE	FALSE
TACAGTATAGATGATGTACT	20	miR-144-3p	miRNA	20	TRUE	TRUE
TCCCTGAGACCCCTTAACCTGTGA	24	miR-125a-5p	miRNA	24	TRUE	TRUE
TGAGGTAGGAGGTTGTAGTT	22	let-7e-5p	miRNA	22	TRUE	TRUE

### 3.4.4 Differential expression analysis

We performed differential analysis using the `treeClimbR` package. Through differential analysis, candidate proposal, multiple testing correction, and candidate evaluation, `treeclimbR` integrates the observations with a tree that reflects the hierarchical relationship between entities and finds an appropriate resolution on the tree to interpret the association. During simulations, we spiked the mature miRNAs miR-99b-5p and miR-99b-3p to be different. After differential analysis, because both miR-99b-5p and miR-99b-3p were simulated to be different, we found that miR-99b was called to be differentially expressed, Figure 3.16. Looking at the cluster, miRNAcluster\_17:17830188-17830879, the full cluster would have been differentially expressed if one read mapping to miR-125a-5p, in grey, would also have been significantly different.

### 3.4.5 Validation using human data and quantitative real-time PCR

To validate the `Oasis2`, `Sports1`, `seqpac`, and `shortRNA` quantifications, we used an unpublished PBMC human dataset and corresponding quantitative real-time PCR (qPCR) quantifications. The PBMC dataset was analyzed using the default parameters from `Oasis2`, `Sports1`, `seqpac`, and `shortRNA`. Then, we correlated the qPCR quantification of five miRNAs with the quantification using all four tools, Figure 3.17. Because `Sports1` and `seqpac` only report miRNA quantification at the level of precursors, the precursor of mature miRNAs quantification was used for the correlation of these tools with the qPCR. When we looked at the overall correlation of miRNAs with qPCR quantifications, we discovered that except `seqpac`, all tools have a good correlation, Figure 3.17A. Overall, we found a low correlation of quantifications between four tools and qPCR. We found that `Oasis2` quantification was negatively correlated with qPCR Ct values for miRNAs miR-30d-5p and miR-30e-5p, as shown in Figure ??B. The quantification of miRNAs using short RNAs was found to be posi-

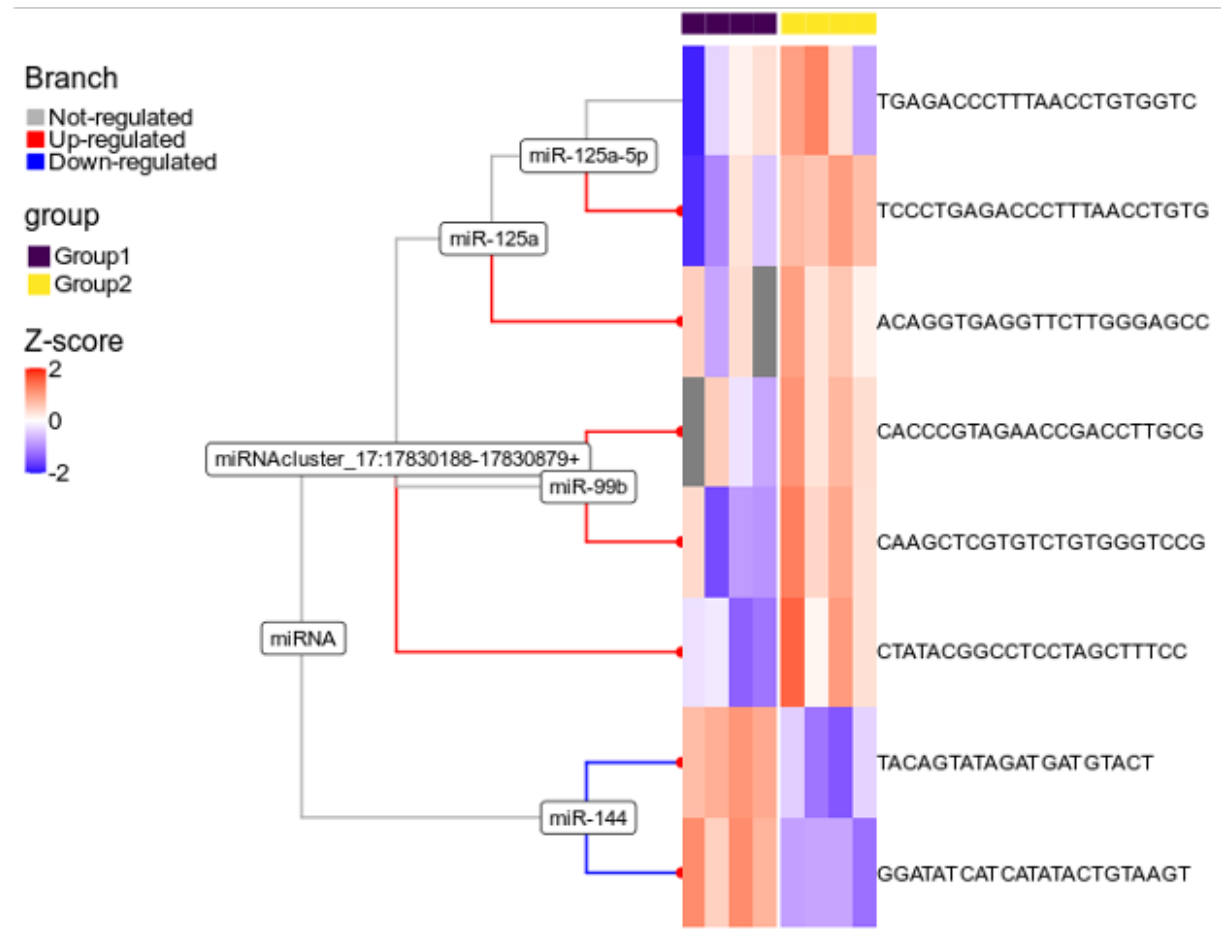


**Figure 3.16:** Hierarchical representation of features and assigned reads to them. Differential expression analysis of features from two miRNA clusters. Simulated read nodes are highlighted in orange colour

tively correlated with the quantification of miRNAs using qPCR. In addition, we performed a visual inspection of the reads mapping to these miRNAs by creating genomic tracks, as shown in Figures 3.18a and 3.18b. As a result, while `shortRNA` quantifications were visually observed to correctly count reads, they were not substantially correlated with qPCR, but were generally better correlated with qPCR quantifications than the other methods.

### 3.4.6 Qualitative comparison with other tools

There are several tools published for analyzing the sRNA-seq data. In Table: Qualitative comparison, we made a qualitative comparison of 20 other tools. Table is too big to be displayed here.

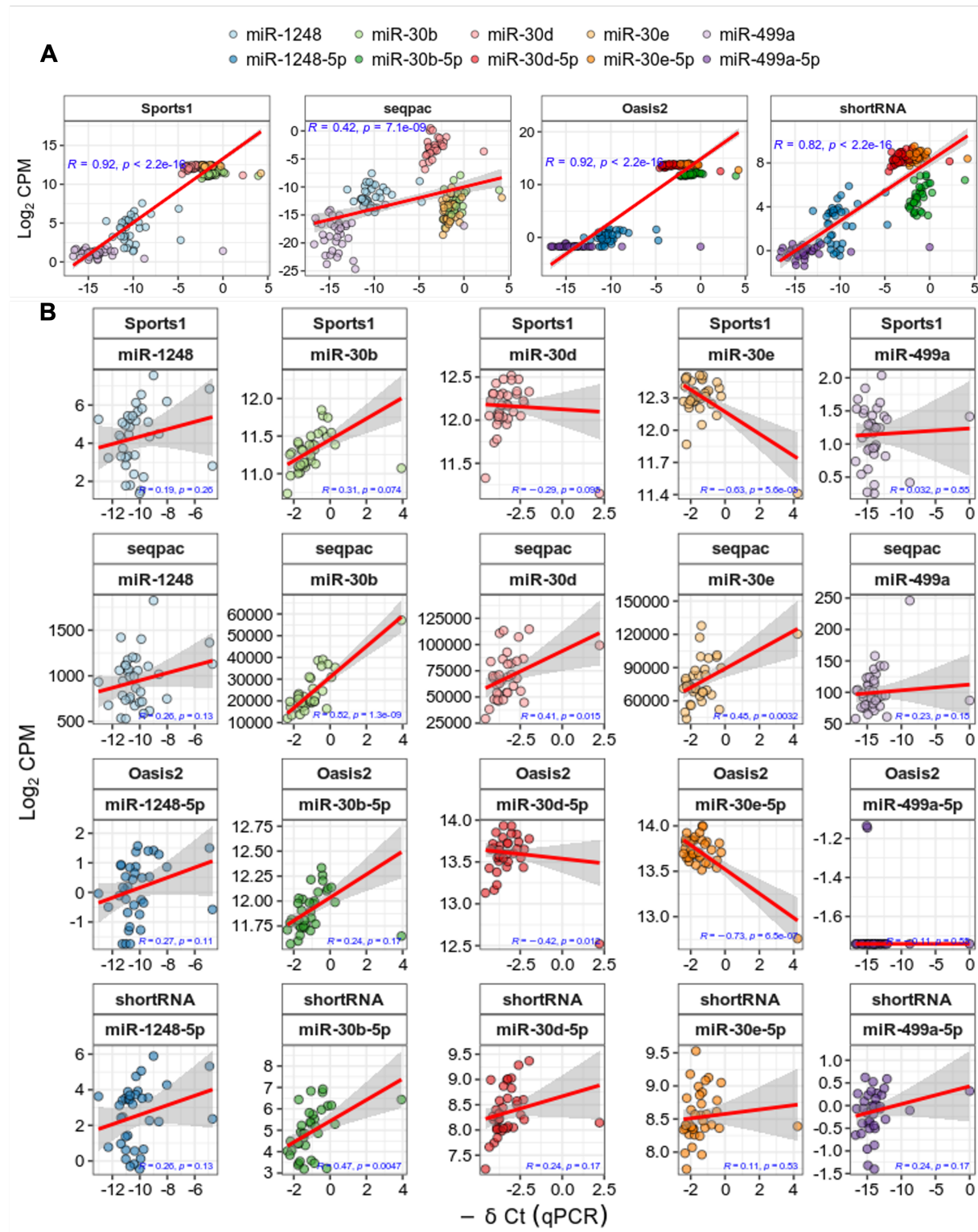


**Figure 3.17:** Comparison of quantifications of five miRNAs from four different tools with -Delta Ct values from qPCR. **A:** Overall correlation. **B:** Correlation at individual miRNA

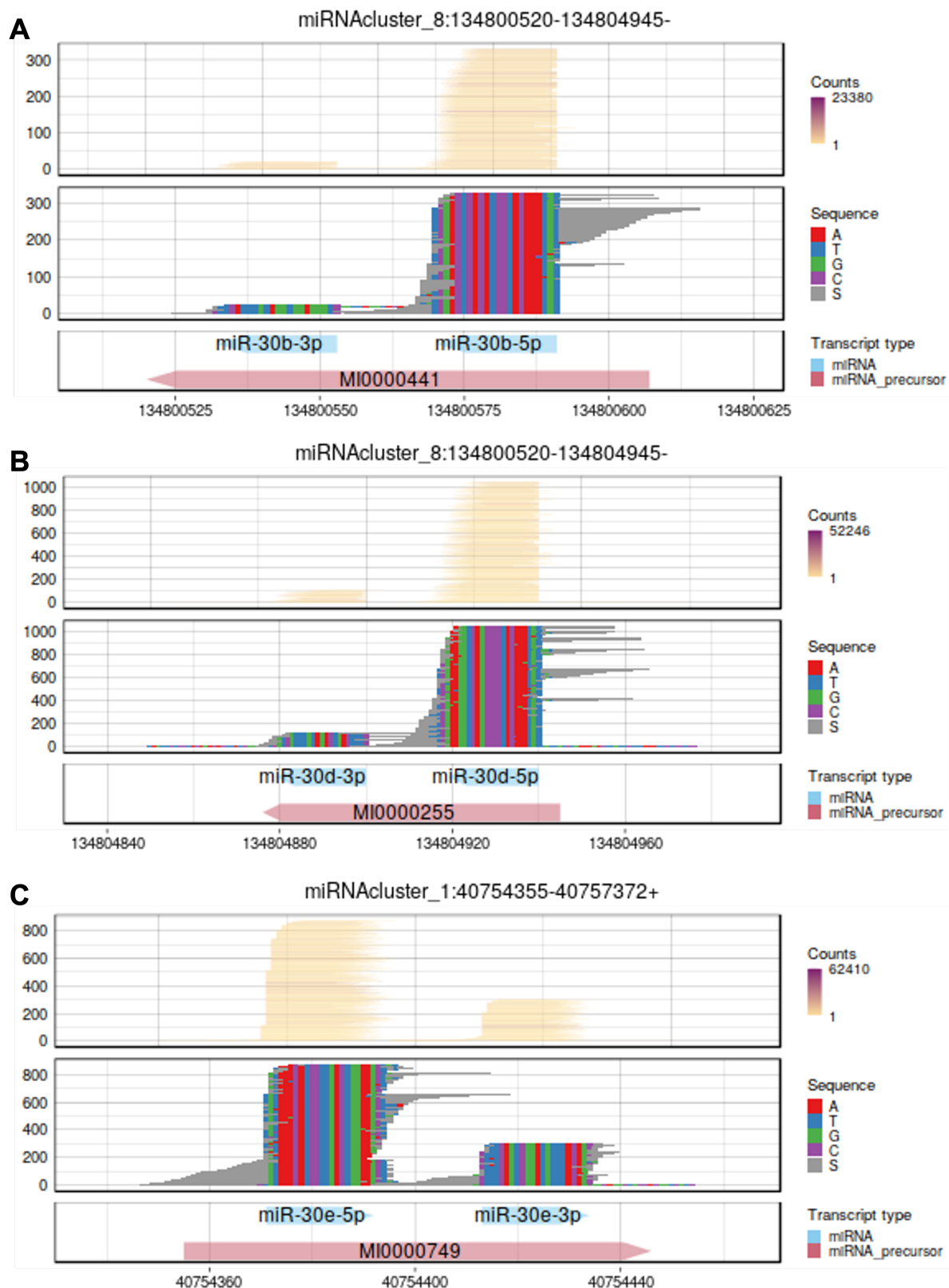


Figure 3.18a: Genomic plots of validated miRNAs

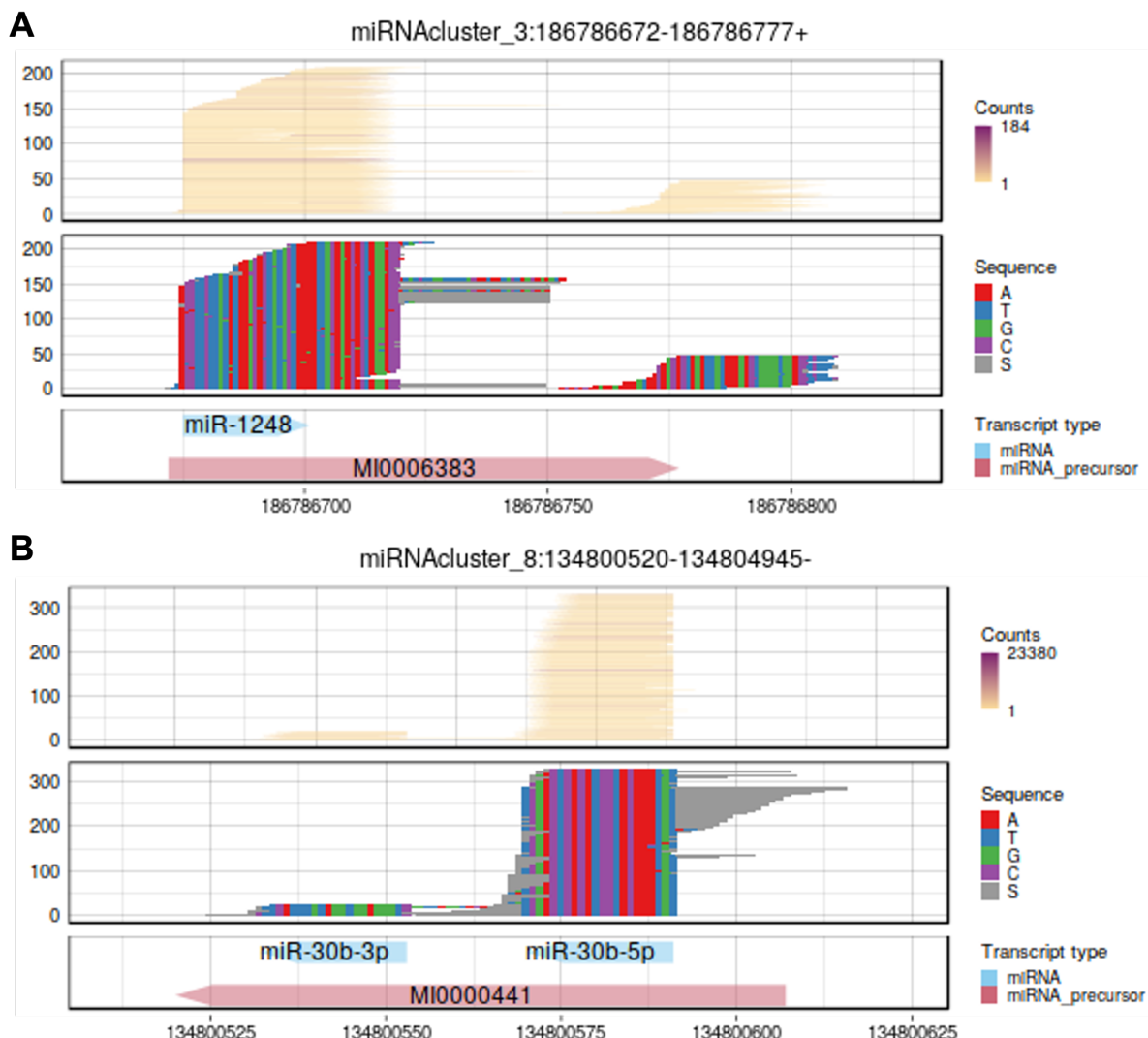


Figure 3.18b: Genomic plots of validated miRNAs

## 3.5 Discussion & Outlook

Due to the non-unique genomic origin, short length, and numerous post-transcriptional modifications of short RNA species, data processing of sRNA-Seq has proven to be difficult. Moreover, from a bioinformatics point of view, there are several challenges in analyzing data generated from small RNA sequencing techniques, including alignment, reads assignment, normalization, and differential analysis. Importantly, quantifying small RNAs correctly is a computational challenge. To a large extent, different tools provide varying quantification. This is startling, and it highlights the need for further research and better tools in the field.

We present **shortRNA**, an R package, a novel tool, for analyzing sRNA-seq data, which can reduce the likelihood of false discoveries from the sRNA-seq data. **shortRNA** is available from [github.com/mansuylab/shortRNA](https://github.com/mansuylab/shortRNA) and is planned to be submitted to the Bioconductor. The **shortRNA** R package is developed around the existing frameworks of Bioconductor: **phylo**, **FactorList**, **DataFrame**, and **TreeSummarizedExperiment**. Hence, it is expected to be able to interact seamlessly with many other tools, such as **ggtree**, **castor**, and **TreeHeatmap**. **shortRNA** performs preprocessing, alignment, and downstream analysis of the sRNA-seq data. Moreover, **shortRNA** is able to deal with the sequencing data with UMIs using **UMIc**. Further, if an adapter sequence is unknown, it is possible to detect the adapter sequence using **shortRNA**.

We tested the package on various human and mouse datasets and demonstrated it using the mouse sperm dataset, simulated mouse sperm dataset, and human dataset from PBMCs. We compared the quantifications of miRNAs from **shortRNA** to those of three other tools: **Sports1**, **Oasis2**, and **seqpac** and found them to be well correlated with **Sports1** and **Oasis2**. We demonstrated **shortRNA**'s ability to assign reads to features in a meaningful way by customisable assignment rules. **shortRNA** uses a considerable proportion of reads, multi-mapping reads, that are either discarded by other methods or aligned randomly. We demonstrated that **shortRNA** correctly annotates reads to features using simulated reads from the sperm dataset. In addition, we demonstrated that **shortRNA** correctly identifies differentially expressed reads. Finally, using the human PBMC data and corresponding qPCR quantifications from five mature miRNAs, we demonstrated that **shortRNA** quantification is better correlated with qPCR data than the other three tools.

In general, however, we observed a very low correlation of all methods against qPCR in terms of the relative miRNA expression across samples. There are a number of potential explanations for this discrepancy. First, the lack of normalization of miRNA quantifications with U6 expression. In several investigations, including in this dataset, RNU6B (U6) is used to normalize circulating miRNA data (Donati, Ciuffi, & Brandi, 2019). Although

qPCR is used to measure mature miRNA levels, its great sensitivity necessitates proper normalization to account for non-biological variance. This is naturally different from the RNA sequencing analysis, where the normalization is based on the whole distribution of RNAs. This discrepancy could therefore be one reason for the low correlations. On the contrary, it has been advised that U6 should not be utilized for data normalization of circulating miRNAs (Benz et al., 2013; Donati et al., 2019). Next, the lack of UMIs in the data. UMIs make it possible to eliminate PCR amplification biases(Y. Fu et al., 2018). The lack of UMIs in human PBMC data might have resulted in technical duplication, and hence affecting the correlation with the qPCR data.

Most tools for the sRNA-seq data analysis, including **Sports1** and **Oasis2**, use feature-based counting, whereas **seqpac** uses sequence-based counting for sRNA-seq data analysis. The benefit of sequence-based counting is that it preserves sequence integrity and allows users to BLAST (Altschul, Gish, Miller, Myers, & Lipman, 1990) candidate sequences to confirm classification and obtain additional information. In addition, sequence-based counting allows for the examination of sequence-specific variations or their boundaries. Further, when using sequence-based counting, users can choose to remove sequences that have low evidence and do not replicate across samples in their data. **shortRNA**, on the other hand, has the advantage of both sequence-based and feature-based counting due to the hierarchical organization of features and mapping sequences. Because of the short lengths of the reads and their proclivity to originate from higher-copy number regions of the genome, multi-mapping reads are much more common in sRNA-seq data. Commonly used sRNA-seq alignment methods for multi-mapping reads are either very low precision (choosing an alignment at random and make it difficult to determine their true origins) or sensibility (ignoring multi-mapping reads, which result in losing a high proportion of reads). **shortRNA** allows these reads to be aligned multiple times and then assign them, using a set of customisable rules, either to a specific feature or to a position in the feature tree which makes it usable while preserving knowledge of eventual ambiguities.

**shortRNA** makes use of miRBase, GtRNADb, MtTRNADb, SILVA and Ensembl databases, but it is possible to manually add databases and extend the list. We used adaptable assignment rules to identify the correct assignment of a read. For example, if the data comes only from miRNAs, the user can set higher priority for mapping the reads with miRNAs by changing the number from 1 to 2 or higher. Further, we used a phylogenetic tree structure to organize the features and to assign the reads to features. If a sequence is overlapped with multiple features, we assign the read to the parent of both features. This helps in solving the problem of multi-mapping.

## 3.6 Limitations

**shortRNA** has not been thoroughly tested across multiple platforms. Although we anticipate that the **shortRNA** will be platform independent, it has not yet been tested on other operating systems. We intend to do so at a later date. In addition, we also intend to extensively benchmark **shortRNA** with existing tools and strategies for reads assignment.

Simulations for other types of RNA are necessary to benchmark the read assignment. We have only simulated reads from miRNAs and miRNA precursors and demonstrated the proper assignment of reads using **shortRNA**. Simulations of reads mapping to tRNAs, reads mapping to piRNAs and reads mapping to rRNAs will be performed to better assess the reads assignment.

The ambiguous assignment of multi-mapping reads to the parent of all mappable features is not always biologically meaningful. If a read is assigned to multiple tRNAs, Figure 3.11, it is still meaningful to assign it to the parent of all mapping tRNAs. In contrast, if a read maps to both a tRNA and a protein-coding gene, assigning it to the parent of both protein coding and tRNA provides less biological insight. Hence, we plan to compare **shortRNA** to other read assignment strategies for multi-mapping reads in depth. Other strategies for assigning multi-mapping reads exist (Handzlik, Tatsoglou, Vlachos, & Hatzigeorgiou, 2020; Johnson, Yeoh, Coruh, & Axtell, 2016), and a benchmark with simulations would be required to assess the **shortRNA** assignment of multi-mapping reads. Instead of assigning reads to the parent of all mappable features, this would aid in the proper assignment and provide more biological insight for the reads mapping to multiple biotypes.

The current implementation of **UMIc** for dealing with sRNA-seq data based on UMIs is extremely slow. There are several for-loops for running analysis, as well as a non-parallel implementation of the code by the authors of **UMIc**. We intend to optimize the code for speed by parallelizing it and replacing for-loops with parallel apply functions.

**shortRNA** has limited user-friendly plotting capabilities. Users can currently use data visualization packages developed for **TreeSummarizedExperiment**, such as **TreeHeatmap**, directly. However, we intend to create wrappers for otheR packages in order to facilitate the visualization of data and results. Also, we will be creating a Shiny app for exploratory analysis of the data and results.

IsomiRs analysis could be implemented in **shortRNA**. IsomiRs are miRNAs that vary slightly in sequence, which result from variations in the cleavage site during miRNA biogenesis (5'-trimming and 3'-trimming variants), nucleotide additions to the 3'-end of the mature miRNA (3'-addition variants) and nucleotide modifications (substitution variants). While in principle our hierarchical and sequence-based approach is ideal for their investigation,

tailored functions would make this more straightforward for the users. We plan to extend our package to include isoMiRs analysis by adapting functionalities of the **isomiR** R package (Lorena Pantano [Aut, Cre], Georgia Escaramis [Aut], ChristosArgyropoulos [Aut], 2017).

**shortRNA** is developed to work with single-end sRNA-seq data. We plan to extend our package to work with paired-end sRNA-seq data.

## 3.7 Conclusion

In conclusion, we developed an R package, platform-independent, for analysis of the sRNA-seq data. This package provides a great overview of the quality, performs QC, aligns the data to custom made genome, performs reads annotation and assignment with adaptable assignment rules, organizes reads and features as a phylogenetic tree, performs differential analysis, and provides interactive plots for exploratory data analysis. **shortRNA** currently works with single-end sequencing data.

## 3.8 Data and code availability

**shortRNA** is available from: [github.com/mansuylab/shortRNA](https://github.com/mansuylab/shortRNA)

No sequencing data were generated during this study. Code for simulating reads is presented in Appendix D.

Data analysis steps for sRNA-seq data with **shortRNA** is available in Appendix C.

# Conclusion and outlook

## Overall conclusion

In this Doctoral thesis, first, the work is presented on the development of pipelines for multi-omics high-throughput sequencing data, Methods, and data analysis pipelines have been used to analyze multi-omics data from the lab and literature, Appendix A. Next as summarized in Chapter 1, we compare the open chromatin landscape of developing and adult spermatogonial cells to explore the development of spermatogonial cells in postnatal development. We discovered and characterized genomic regions with differential genomic activity in spermatogonial cells by combining the data generated by the host lab with the data available from the literature. After that, as summarized in Chapter 2, we studied the impact of early postnatal stress on the transcriptome of epididymal extracellular vesicles. Our findings show that chronic stress in early postnatal life affects miRNAs in adult male reproductive tract extracellular vesicles, with consequences for mature sperm and zygotes. Finally, in Chapter 3 we created an R package, `shortRNA`, for analyzing short RNA sequencing data that is platform-independent, provides a good overview of the quality, performs quality control, aligns the data to a custom-made genome, performs read annotation and assignment with adaptable assignment rules, organizes reads and features as a phylogenetic tree, performs differential analysis, and provides interactive plots for exploratory data analysis. However, there are a number of changes or further investigations that might be needed, which we will explore in this section.

## MSUS-associated differences

The MSUS model is appropriate for examining epigenetic inheritance owing to environmental perturbations, but low effect sizes make it difficult to discover candidates that passed multiple testing corrections. The costs associated with sample creation and sequencing, makes it challenging to have a higher number of replicates in the experimental designs. After multiple testing correction, obtaining significant p-values requires either appropriate data distribution

assumptions or a high number of replicates. Clipper, a new statistical framework for reducing false discovery rates without relying on p-values or specific data distributions, was published recently (Ge et al. 2021). Clipper has been shown to outperform conventional methods for limiting false discoveries, thus pipelines can be updated to implement it.

## RNA sequencing data analysis pipeline

Data analysis pipelines for RNA sequencing could be adapted. **Salmon**, a tool for obtaining quantifications from RNA-seq data, is used for pseudo-alignment while accounting for GC biases at the fragment level, sequence-specific biases, and position-specific fragment starts distribution. **Salmon Anomaly Detection** (SAD) tool can be incorporated into the RNA sequencing data analysis pipeline in addition to **Salmon** quantifications. SAD identifies probable misquantifications in **Salmon**'s RNA-seq transcript expression estimation. However, due to several external dependencies, implementing this tool may be difficult (<https://github.com/Kingsford-Group/sad/issues>), and this will almost certainly necessitate containerization from the authors, either via **conda** or **Docker**. Also, while evaluating and quantifying lowly-expressed genes and small RNAs with alignment-free pipelines, such as **Salmon**, potential pitfalls have been recognized, particularly when the small RNAs contain biological variability. As a result, when the analysis isn't limited to simply protein-coding genes, an alignment-based technique like **Rsubread** or **STAR** can be used (Wu et al. 2018). Further, for differential transcript usage and isoform switching, we employed **IsoformSwitchAnalyzeR**. Under the hood, **IsoformSwitchAnalyzeR** employs **DEXseq** for differential transcript usage. However, **DEXseq** has the drawback of not being able to account for blocking variables. **BANDITS** could also be used instead of **DEXseq** in the **IsoformSwitchAnalyzeR** pipeline because it outperforms **DEXseq** (Tiberi and Robinson 2020).

## ATAC sequencing data analysis pipeline

In recent years, ATAC-seq has grown in popularity as a tool for investigating chromatin accessibility. Despite improvements in protocols, bioinformatics analysis tools are still in their development, with no comprehensive analytical pipeline defined. The interpretation of ATAC-seq results is currently hampered by this. The majority of the tools used to analyze ATAC-seq data are from the ChIP-seq or DNA-seq fields. For example, **MACS2**, the peak caller we used for ATAC-seq, was designed originally for ChIP-seq data. **HMMRATAC** is a peak calling method for ATAC-seq data that combines the nucleosome-free and nucleosome-enriched signals from a single ATAC-seq dataset to find open chromatin regions (Tarbell and Liu 2019).

Our strategy was instead to use the nucleosome-free fragments (which are indicative of TF binding) for peak calling. Because we only looked into nucleosome-free fragments, HMMRATAC was not used. Also, HMMRATAC's authors advise against using it on ATAC-seq datasets that have undergone physical or computational size selection. But, HMMRATC could be employed for investigating outside the nucleosome-free fragments.

The ATAC-seq pipeline can also be extended to include tools for nucleosome positioning and transcription factor footprinting analysis. However, nucleosome detection is problematic due to an inherent shortcoming of ATAC-seq data, which typically has inadequate read coverage beyond peaks (Yan et al. 2020). Based on empirical and computational estimates, the recommended minimum number of mapped reads for open chromatin detection and differential analysis in mammalian species is 50 million, and 200 million for TF footprinting (Yan et al. 2020). Due to the reduced read coverage outside the open chromatin regions, nucleosome detection in ATAC-seq data was shown to be more difficult than in MNase-seq data (Yan et al. 2020). Because we did not sequence this deep, we did not include TF footprinting in the pipeline, which would necessitate a thorough investigation of tools. These drawbacks necessitate a detailed study of the tools employed in ATAC-seq for normalization, peak calling on NFFs, and TF footprinting.

## Updating manuscript from Chapter 1 in light of latest RNA-seq data

The datasets used for the study of spermatogonial cell development were not initially designed for that purpose, but to investigate the changes at different developmental stages because of the MSUS paradigm. As a result, the datasets were not ideal for this new purpose: the study originally employed polyA RNA sequencing data from the PNW21 stage, while RNA sequencing data from the stages PND8 and PND15 came from Total RNA sequencing. We, therefore, used data from the literature but determined to re-generate the data from the PNW21 stage in the lab in order to have more impactful research and accurate findings. Because of these changes, the entire downstream analysis, including functional analysis, motif analysis, data integration, and re-creation of the figures, will have to be repeated. Some of these analyses have been completed and are included in Chapter 1 as an update. In general, however, given the high consistency of the results across the two analyses, we are confident that the main results will remain unchanged.

## Low correlations of quantification between **shortRNA** and qPCR

In terms of relative miRNA expression across samples, we found a low correlation between sequencing-based quantifications (with **shortRNA** as well as with other tools) and qPCR. We covered a variety of possible explanations for this mismatch in Chapter 3, including normalizing the data with U6 RNA expression and the lack of UMIs. We don't have an exact explanation for the poor correlations, but we want to look into them further using a variety of techniques, including testing the **shortRNA** tool with UMI-based data with corresponding qPCR quantifications and creating a more extended simulation dataset.

# Appendix A

## Datasets analyzed from lab's MSUS model

Tissue	Cells	Model/Time/Age	HTS techniques	Generations	CTRL	MSUS	Data availability	DOI	GitHub
Sperm	Sperm	NA	RNA-Seq (Riboo)	F1	6	7	E-MTAB-5834	NA	mansuylab/sperm_kathi
Sperm	Sperm	NA	short RNA-Seq	F1	4	3	GSE50132	10.1038/mn.3695	dktanwar/sperm_GSE50132
Sperm	Sperm	NA	RNA-Seq (Riboo)	F1	10	10	NA	Not published	mansuylab/sperm_martin mansuylab/omnisperm
Sperm	Sperm	NA	WGBS	F1	10	10	NA	Not published	mansuylab/sperm_WGBS mansuylab/omnisperm
Sperm	Sperm	PPAR injected (24 hours)	RNA-Seq (polyA)	F1	4	4	GSE154369	10.15252/embj.2020104579	mansuylab/tesa_sperm_1 mansuylab/gretchen
Sperm	Sperm	PPAR injected (46 days)	RNA-Seq (Riboo)	F1	7	7	GSE154369	10.15252/embj.2020104579	mansuylab/tesa_sperm_2 mansuylab/gretchen
Testis	Spermatogonial Cells	PND8	RNA-Seq (Riboo)	F1	8	7	NA	Not published	mansuylab/SC_postnatal_adult mansuylab/SC_longRNA
Testis	Spermatogonial Cells	PND8	RNA-Seq (Riboo)	F1	6	NA	NA	Not published	mansuylab/SC_postnatal_adult
Testis	Spermatogonial Cells	PND15	RNA-Seq (Riboo)	F1	9	8	NA	Not published	mansuylab/SC_postnatal_adult mansuylab/SC_longRNA
Testis	Spermatogonial Cells	PND15	RNA-Seq (Riboo)	F1	6	NA	NA	Not published	mansuylab/SC_postnatal_adult
Testis	Spermatogonial Cells	PNW21	RNA-Seq (polyA)	F1	6	6	NA	Not published	mansuylab/SC_postnatal_adult mansuylab/SC_adult
Testis	Spermatogonial Cells	PNW21	RNA-Seq (Riboo)	F1	6	NA	NA	Not published	mansuylab/SC_postnatal_adult
Testis	Spermatogonial Cells	PND8	short RNA-Seq	F1	8	7	NA	Not published	mansuylab/SC_postnatal_adult
Testis	Spermatogonial Cells	PND15	short RNA-Seq	F1	6	6	NA	Not published	mansuylab/SC_postnatal_adult
Testis	Spermatogonial Cells	PND8	RRBS	F1	6	5	NA	Not published	mansuylab/SC_postnatal_adult mansuylab/ssc_pnd8_RRBS
Testis	Spermatogonial Cells	PND15	ATAC-Seq	F1	6	6	NA	Not published	mansuylab/SC_postnatal_adult mansuylab/SC_atac
Testis	Spermatogonial Cells	PNW21	ATAC-Seq	F1	5	5	NA	Not published	mansuylab/SC_postnatal_adult mansuylab/SC_atac
Testis	Sertoli	NA	RNA-Seq (Riboo)	F1	6	7	NA	Not published	NA
Testis	Testis	NA	RNA-Seq (polyA)	F1	5	5	NA	Not published	mansuylab/MSUS23_tissue_RNASeq
Testis	Testis	NA	RNA-Seq (polyA)	F3	5	6	NA	Not published	mansuylab/MSUS23_tissue_RNASeq
Liver	Liver	NA	RNA-Seq (polyA)	F1	5	5	NA	Not published	mansuylab/MSUS23_tissue_RNASeq
Liver	Liver	NA	RNA-Seq (polyA)	F3	5	6	NA	Not published	mansuylab/MSUS23_tissue_RNASeq
Brain	Hippocampus	NA	RNA-Seq (polyA)	F1	5	5	NA	Not published	mansuylab/MSUS23_tissue_RNASeq
Brain	Hippocampus	NA	RNA-Seq (polyA)	F3	5	6	NA	Not published	mansuylab/MSUS23_tissue_RNASeq
Brain	Hypothalamus	NA	RNA-Seq (polyA)	F1	17	7	NA	Not published	NA
Zygote	Zygote	NA	RNA-Seq (Riboo)	F1	4	4	E-MTAB-6589	10.1038/s41380-018-0271-6	mansuylab/zygote_kathi
Embryo	Embryo	4.6.8 cell	RNA-Seq (polyA)	F1	41	36	NA	Not published	mansuylab/embryos_martin
Ovum	Ovum	NA	short RNA-Seq	F1	7	8	NA	Not published	mansuylab/anastasia_ocyto_shortRNA
Cauda	Epididymosmes	NA	short RNA-Seq	F1	5	5	GSE175976	10.1093/biolre/ioab156	mansuylab/alsharabayeva_et_al_2021
HSC	HSC	NA	RNA-Seq (Riboo)	F1	4	5	NA	Not published	mansuylab/HSC_RNA-Seq
Uterosomes	Uterosomes	NA	short RNA-Seq	F1	6	6	NA	Not published	mansuylab/uterosomes

## Human dataset from the Schratt lab

Tissue	Cells	HTS techniques	Data availability	Source	GitHub
Blood	PBMC	short RNA-Seq	Not published	Schratt Lab (INS, ETHZ)	ETHZ-INS/schratt_PBMC

## Mouse datasets analyzed from literature

Tissue	Cells	Age/Time	HTS techniques	Generations	Group	nsamples	Data availability	DOI	Source	GitHub
Brain	mPFC	NA	RNA-Seq (Ribod0)	F1	Control	3	From author	10.1038/s41386-020-0727-7	Literature	dktanwar/mPFC_MSUS
Brain	mPFC	NA	RNA-Seq (Ribod0)	F1	MSUS	3	From author	10.1038/s41386-020-0727-7	Literature	dktanwar/mPFC_MSUS
Sperm	Sperm	NA	short RNA-Seq	F1	Control	8	GSE162112	10.1016/j.isci.2021.102870	Literature	dktanwar/sperm_GSE162112
Testis	Spermatogonial Cells	PND7	RNA-Seq (Ribod0)	F1	Control	2	GSE62355	10.1101/gad.261925.115	Literature	mansuylab/SC_postnatal_adult
Testis	Spermatogonial Cells	PND14	RNA-Seq (Ribod0)	F1	Control	1	GSM1525703	10.1101/gad.261925.115	Literature	mansuylab/SC_postnatal_adult
Testis	Spermatogonial Cells	PNW8	RNA-Seq (Ribod0)	F1	Control	1	GSM1415671	10.1016/j.stem.2014.04.006	Literature	mansuylab/SC_postnatal_adult
Testis	Spermatogonial Cells	PND7	WGBS	F1	Control	1	GSE49623	10.1016/j.stem.2014.04.006	Literature	mansuylab/SC_postnatal_adult
Testis	Spermatogonial Cells	PND14	WGBS	F1	Control	1	GSE49623	10.1016/j.stem.2014.04.006	Literature	mansuylab/SC_postnatal_adult
Testis	Spermatogonial Cells	PNW8	WGBS	F1	Control	7	GSE49623	10.1016/j.stem.2014.04.006	Literature	mansuylab/SC_postnatal_adult
Testis	Spermatogonial Cells	PNW8	ChIP-Seq (H3K4me3)	F1	Control	1	GSM1202705	10.1016/j.stem.2014.04.006	Literature	mansuylab/SC_postnatal_adult
Testis	Spermatogonial Cells	PNW8	ChIP-Seq (H3K27me3)	F1	Control	1	GSM1202708	10.1016/j.stem.2014.04.006	Literature	mansuylab/SC_postnatal_adult
Testis	Spermatogonial Cells	PNW8	ChIP-Seq (H3K27ac)	F1	Control	1	GSM1202713	10.1016/j.stem.2014.04.006	Literature	mansuylab/SC_postnatal_adult
Sperm	Sperm	PNW 10-13	WGBS	F1	Control	6	GSE75323	10.1016/j.devcel.2015.11.024	Literature	dktanwar/GSE75323_reanalysis
Sperm	Sperm	PNW 10-13	WGBS	F1	Low protein	5	GSE75323	10.1016/j.devcel.2015.11.024	Literature	dktanwar/GSE75323_reanalysis
Sperm	Sperm	PNW 10-13	WGBS	F1	High-fat	5	GSE75323	10.1016/j.devcel.2015.11.024	Literature	dktanwar/GSE75323_reanalysis
Testis	Spermatogonial Cells	PND6	ATAC-seq	F1	ID4-eGFP-Bright	3	GSE131657	10.1016/j.isci.2020.101596	Literature	mansuylab/SC_postnatal_adult
Testis	Spermatogonial Cells	PND6	ATAC-seq	F1	ID4-eGFP-Dim	3	GSE131657	10.1016/j.isci.2020.101596	Literature	mansuylab/SC_postnatal_adult

# Appendix B

## Other publications and manuscripts during doctoral thesis work

### Involvement of circulating factors in the transmission of paternal experiences through the germline

Gretchen van Steenwyk<sup>†</sup>, Katharina Gapp<sup>†</sup>, Ali Jawaid, Pierre-Luc Germain, Francesca Manuella, **Deepak K Tanwar**, Nicola Zamboni, Niharika Gaur, Anastasiia Efimova, Kristina M Thumfart, Eric A Miska, Isabelle Mansuy<sup>#</sup>

<sup>†</sup>Equal contributions

<sup>#</sup>Corresponding author

**Journal:** *The EMBO Journal*

**DOI:** 10.15252/embj.2020104579

**Contributions:** *Analysis of RNA-seq data.*

### Symposium summary: Epigenetic inheritance-impact for biology and society 26–28 August 2019, Zurich, Switzerland

Irina Lazar-Contes, Martin Roszkowski, **Deepak K Tanwar** and Isabelle M Mansuy<sup>#</sup>

<sup>#</sup>Corresponding author

**Journal:** *Environmental Epigenetics*

**DOI:** 10.15252/embj.2020104579

**Contributions:** *Writing manuscript.*

## **OmniSperm: Multiomic analyses of sperm and offspring production from a single male**

Martin Roszkowski, Irina Lazar-Contes, Pierre-Luc Germain, **Deepak K Tanwar**, Anara Alshanbayeva, Niharika Obrist, Ali Jawaid, Gretchen van Steenwyk, Eloise Kremer, Dalila Korkmaz, Mark Ormiston, Francesca Manuella, Johannes vom Berg, Jorg Tost, Johannes Bohacek, Isabelle M Mansuy<sup>#</sup>

#Corresponding author

**DOI:** 10.3929/ethz-b-000489446 (Doctoral thesis, Chapter 2)

**Contributions:** *Analysis of RNA-seq from sperm and embryos, and WGBS data from sperm.*

## **Early life stress alters chromatin accessibility landscape and transcript usage in spermatogonial cells during postnatal testis maturation**

Irina Lazar-Contes, Gretchen van Steenwyk, **Deepak K Tanwar**, Pierre-Luc Germain, Francesca Manuella, Martin Roszkowski, Niharika Gaur, Isabelle M Mansuy<sup>#</sup>

#Corresponding author

**DOI:** 10.1101/2020.08.20.259374 (Doctoral thesis, Chapter 3)

**Contributions:** *Analysis of RNA-seq and ATAC-seq data, and figure generation.*

# Appendix C

## shortRNA analysis steps in R (a short vignette)

### Package installation

```
BiocManager::install("mansuylab/shortRNA")
library(shortRNA)
```

### Quality check and trimming

```
qc_SE(file = fq_files, outdir = "output/", ad1 = adapter_sequence)
```

### FastQ files to sequence by counts matrix

```
m <- fastq2SeqCountMatrix(files = trimmed_fastq_files)
```

### Unique sequences for alignment

```
fa <- DNAStringSet(row.names(m))
names(fa) <- paste0("S", 1:length(fa))
writeXStringSet(fa, fasta_file)
```

### Obtaining databases for analysis

```
db <- getDB()
```

## Annotation preparation and genome index generation for alignment

```
a <- prepareAnnotation(
  ensdb = db$ensdb,
  output_dir = genomeDir,
  extra.gr = list(piRNA = db$piRNA_GR, miRNA = db$miRNA_GR),
  extra.seqs = list(rRNA = db$rRNA_fa, tRNA = db$tRNA_fa),
  resolveSplicing = NULL,
  rules = defaultAssignRules(),
  tRNAEnsembleRemove = FALSE,
  clusterMiRNA = TRUE
)
```

## Alignment

```
alignShortRNA(
  fastq = "unique.fasta",
  index = "genomeDir/customGenome",
  outDir = "align", GTF = exonsBy(db$ensdb),
  GTF.featureType = "exon", GTF.attrType = "gene_id"
)
```

## Overlapping aligned data with annotations

```
o <- overlapWithTx2(
  bamFile = align_file, annotation = a,
  ignoreStrand = TRUE, nbthreads = 16
)
```

## Assignment of overlapping reads to features with assignment rules

```
ar <- assignReads(sources = o, rules = defaultAssignRules())
```

## Converting features to FactorList

```
fl <- featuresAnnoToFL(a)
names(fl) <- lapply(fl, function(x) as.character(x[length(x)]))
```

## Assignment of reads to the features tree

```
mappedFeaturesDF <- ar
mappedFeaturesDF$seq <- rownames(mappedFeaturesDF)
ar_tree <- addReadsToTree(
  fL = fl,
  mappedFeaturesDF = mappedFeaturesDF,
  unassigned = FALSE,
  extraTreeBranch = NULL
)
```

## Creation of TreeSummarizedExperiment object

```
library(TreeSummarizedExperiment)

rt <- ar_tree
as <- list(counts = m)
cd <- DataFrame(samples = c(s1, s2), group = c("group1", "group2"))

tse <- TreeSummarizedExperiment(
  assays = as,
  rowTree = rt,
  colData = cd,
  rowData = ar[row.names(m), ],
  metadata = list()
```

```
    assignedReads = ar,
    counts = m,
    notAligned = getReadsFromBam(
      bam = align_file
    )
  )
)
```

## Differential analysis

```
library(treeClimbR)
dea <- runDA(TSE = tse, filter_min_count = 20)
out <- nodeResult(object = dea, n = Inf)

cand <- getCand(
  tree = dea$tree,
  score_data = out, node_column = "node",
  p_column = "PValue", sign_column = "logFC",
  message = FALSE, threshold = 0.05
)

candB <- evalCand(
  tree = dea$tree,
  levels = cand$candidate_list,
  score_data = out, node_column = "node",
  p_column = "PValue", sign_column = "logFC",
  method = "BH", limit_rej = 0.05,
  use_pseudo_leaf = FALSE,
  message = FALSE
)

result <- topNodes(object = candB, n = Inf, p_value = 0.05)
```

# Appendix D

## Simulated reads for testing shortRNA

### Libraries

```
library(Biostrings)
library(rtracklayer)
```

### miRNAs

```
fa <- readRNASTringSet("https://www.mirbase.org/ftp/CURRENT/mature.fa.gz")
fa <- DNAStringSet(fa)
names(fa) <- gsub(" .+", "", names(fa))
fa <- fa[grep(pattern = "mmu", x = names(fa))]
```

### cluster chr17:17830188-17830879

```
clusterMirs <- c(
  "mmu-miR-125a-5p", "mmu-miR-99b-5p", "mmu-let-7e-5p",
  "mmu-let-7e-3p", "mmu-miR-99b-3p", "mmu-miR-125a-3p"
)
clusterMirs <- fa[clusterMirs]
```

## Imputing differences for differential analysis

```
sizefacts <- c(
  SRR13129036 = 1.2, SRR13129037 = 0.99, SRR13129038 = 1.01,
  SRR13129039 = 1.01, SRR13129040 = 1.07, SRR13129041 = 0.56,
  SRR13129042 = 0.72, SRR13129043 = 0.51
)
```

## Read counts

```
set.seed(123)
clusterMirsCounts <- t(sapply(rgamma(length(clusterMirs),
  shape = 3
), function(x) {
  sizefacts *
  exp(1 + x) *
  rnorm(8, mean = rep(c(1, rnorm(1, 2, sd = 0.1)), each = 4), sd = 0.4)
}))
row.names(clusterMirsCounts) <- names(clusterMirs)
clusterMirsCounts <- matrix(rpois(length(clusterMirsCounts),
  lambda = clusterMirsCounts
),
nrow = nrow(clusterMirsCounts), dimnames = dimnames(clusterMirsCounts)
)
clusterMirsCounts
row.names(clusterMirsCounts) <- as.character(clusterMirs)
```

## miRNA precursor

```
mir144prec <- DNAStringSet(c(mir144precursor = substr(
  "GGCTGGGATATCATCATATACTGTAAGTTGTGATGAGACACTACAGTATAGATGATGTACTAGTC",
  1, 50
)))
mir144 <- c(
  mir144prec, fa["mmu-miR-144-3p"], fa["mmu-miR-144-5p"],
```

```
DNAStrongSet(c(
  mir144_invalid1 = "AAGTTTGTGATGAGACACTAC",
  mir144_invalid2 = "CTGTAAGTTGTGATGAGAC",
  mir144_invalid3 = "ATGTAAGTCTGGGTA"
))
)

set.seed(123)
mu <- rbind(
  abs(rnorm(8, 1)),
  abs(rnorm(8, rep(2:1, each = 4), 0.3)),
  abs(rnorm(8, rep(2:1, each = 4), 0.3)),
  abs(rnorm(8, 1)), abs(rnorm(8, 1)), abs(rnorm(8, 1))
)
mu <- 300 * t(t(mu) * sizefacts)
mir144Counts <- matrix(rpois(length(mu), lambda = mu),
  nrow = nrow(mu),
  dimnames = list(names(mir144), names(sizefacts)))
)
row.names(mir144Counts) <- as.character(mir144)
```

## Data to be simulated

```
e <- rbind(clusterMirsCounts, mir144Counts)
e
```



# **Appendix E**

Curriculum Vitae of the doctoral student.

# DEEPAK KUMAR TANWAR

Bioinformatics, multivariate analysis, methods development



## EDUCATION

- Mar. 2018 - ● **ETH Zurich**  
PhD Candidate  
**Supervisor:** Prof. Dr. Isabelle Mansuy  
**Thesis committee:** Prof. Mark Robinson and Prof. Tuncay Baubec  
📍 Zurich, Switzerland
- Aug. 2016 | Jan. 2018 ● **McGill University**  
Masters of Science (M.Sc.)  
**Supervisors:** Prof. Sarah Kimmins and Prof. Jianguo Xia  
**CGPA:** 3.57 / 4  
📍 Montréal, Canada
- Aug. 2009 | Feb. 2014 ● **Amity University Rajasthan**  
Bachelor of Technology (B.Tech.) in Bioinformatics  
**Supervisor:** Prof. Dr. Rainer König  
**Advisor:** Prof. Dr. A. N. Pathak  
**CGPA:** 7.11 / 10 (*First Class*)  
📍 Jaipur, India

PhD student specializing in multivariate data analysis, methods development, reproducible analyses, and epigenetics.

## RESEARCH EXPERIENCE

- Mar. 2018 | Dec. 2021 ● **Scientific Assistant**  
ETH Zurich  
• **Supervisor:** Prof. Dr. Isabelle Mansuy  
• Epigenetic inheritance research  
📍 Zurich, Switzerland
  - Methods and software development
  - Multi-omics data analysis
- Aug. 2016 | Jan. 2018 ● **Graduate Research Assistant**  
McGill University  
• **Supervisor:** Prof. Sarah Kimmins  
• **Co-supervisor:** Prof. Jianguo Xia  
📍 Montréal, Canada
  - Epigenetic inheritance research
  - Tools and pipelines development
- Oct. 2014 | Aug. 2016 ● **Visiting Research Scientist**  
University of Alabama at Birmingham  
• **Supervisor:** Prof. Malay Basu  
• Cancer research  
📍 Birmingham, USA
  - Multi-omics data analysis
  - Language of protein domain architecture
- Jun. 2013 | Jan. 2014 ● **Research Associate (Intern)**  
University of Jena  
• **Supervisors:** Prof. Dr. Rainer König  
• Sepsis data analysis  
📍 Jena, Germany
  - Network modeling
  - Mathematical modeling
- Jun.-Jul. 2012 ● **Internship**  
Rajiv Gandhi Centre for Biotechnology (RGCB)  
**Supervisors:** Dr. Sathish Mundayoor (Scientist G) and Mr. Siva Kumar  
**Project Title:** Molecular Docking of NCI Drug Ligands into HIV-1, using Schrödinger.  
📍 Thiruvananthapuram, India
- Jun.-Jul. 2011 ● **Industrial internship**  
IBI Biosolutions  
**Supervisor:** Dr. Rajnikant Singh  
**Project Title:** Designing of PERL Biological Module.  
📍 Chandigarh, India

## CONTACT INFO

✉ [tanward@ethz.ch](mailto:tanward@ethz.ch)  
📞 +41 44 635 33 49

## LINKS

- 👤 [0000-0001-8036-1989](#)
- 🗣 [dktanwar](#)
- 🐦 [d\\_k\\_tanwar](#)
- linkedin [dktanwar](#)
- globe [Deepak Tanwar](#)
- 戒 [Deepak\\_Tanwar2](#)
- 🌐 [Deepak Tanwar](#)

## TECHNICAL SKILLS

**Programming:** R, Perl, Python, UNIX, JavaScript, HTML and CSS  
**Documentation:** LaTeX, Markdown  
**Literate Programming:** Sweave, Knitr  
**Version control:** git  
**Cluster computing**

## TEACHING

2021	● <b>Bioinformatics and genomic data analysis</b> ETH Zurich Planned the computational part of the block course and delivered lectures in bioinformatics and literate programming	📍 Zurich, Switzerland	Study of Epigenetic Mechanisms in Mental Health (376-1346-00L)
2020	● <b>Introduction to Bioinformatics</b> ETH Zurich Introduction to bioinformatics and data analysis	📍 Zurich, Switzerland	Study of Epigenetic Mechanisms in Mental Health (376-1346-00L)
2019	● <b>Introduction to Biostatistics</b> ETH Zurich Introduction to variables, distributions and tests in statistics, applied towards biology	📍 Zurich, Switzerland	Study of Epigenetic Mechanisms in Mental Health (376-1346-00L)
2017	● <b>BTEC501: Bioinformatics</b> McGill University Taught R and, statistics and data visualization in R; organized weekly tutorials	📍 Montréal, Canada	Semester course
2016	● <b>GBSC 703-01E: Computational Biology and Bioinformatics</b> University of Alabama at Birmingham Taught R and data visualization in R and, assisted participants	📍 Birmingham, USA	Two weeks intensive course
2015	● <b>GBSC 703: Introduction to Scientific Computing</b> University of Alabama at Birmingham Assisted in teaching literate programming and helped participants	📍 Birmingham, USA	Two weeks intensive course

## MENTORING

2021	● <b>Julien Chabrey</b> M.Sc. in Biology, ETH Zurich <b>Title:</b> Investigating differential exon usage and differential 3' untranslated regions usage in spermatogonial cells across development	📍 Zurich, Switzerland	<b>Block course</b> Study of Epigenetic Mechanisms in Mental Health (376-1346-00L)
2021	● <b>David Bugliani</b> M.Sc. in Biology, ETH Zurich <b>Title:</b> Investigating differential exon usage and differential 3' untranslated regions usage in spermatogonial cells across development	📍 Zurich, Switzerland	<b>Block course</b> Study of Epigenetic Mechanisms in Mental Health (376-1346-00L)
2019	● <b>Andrew Acciardo</b> M.Sc. in Computational Biology and Bioinformatics, ETH Zurich <b>Title:</b> Computational study of the effects of early life trauma on gene expression and exon usage in various tissues and cells in <i>Mus musculus</i>	📍 Zurich, Switzerland	M.Sc. Thesis
2019	● <b>Hana Parizkova</b> M.Sc. in Computational Biology and Bioinformatics, ETH Zurich <b>Title:</b> Detecting and simulating inheritance of differential methylation	📍 Zurich, Switzerland	Semester project
2019	● <b>Daniela Schildknecht</b> M.Sc. in Computational Biology and Bioinformatics, ETH Zurich <b>Title:</b> An extension of IsoformSwitchAnalyzeR	📍 Zurich, Switzerland	Lab Rotation

## SCHOLARSHIP & AWARDS

- Sep. 2018 | Aug. 2021 ● **PhD Scholarship**  
**Swiss Government Excellence Scholarship:** Three years graduate scholarship for a PhD at ETH Zurich
- 2019 ● **Summer School**  
**Bioinformatics Summer School:** Travel award by UCLouvain
- 2017 ● **Travel and Workshop Awards**  
**Graduate Research Enhancement and Travel Award (GREAT):** Travel award by Animal Science Department, McGill University for the 4<sup>th</sup> Canadian Conference on Epigenetics  
**Galaxy Community Conference 2017:** Travel and registration award by GCC  
**Epigenomic Data Analysis Workshop:** Workshop Registration award by CRRD, McGill University

## VOLUNTEERING AND LEADERSHIP

- 2018 | 2021 ● **PhD student representative for SIB**  
Swiss Institute of Bioinformatics PhD Training Network co-representative for Zurich area
- 2021 ● **Abstract reviewing for BC2**  
Invited to review abstracts for workshop and tutorial session of the Basel Computational Biology Conference [BC]2 2021
- 2019 ● **Symposium organization**  
Organizing member of the ISCB Student Council Symposium (SCS) 2019
- 2019 ● **Abstract reviewing**  
Reviewed abstracts for GIW/ABACBS/COMBINE conference

## PROFESSIONAL SERVICE

- **Reviewer for PLOS Genetics**
- **Reviewed book proposals for CRC press**

## PRESENTATIONS AND POSTERS

- Sep. 2019 ● **shortRNA: A flexible framework for the analysis of short RNA sequencing data**  
Basel Life Conference

 Basel, Switzerland

Short presentation &  
Poster

- Aug. 2019
- **shortRNA: A flexible framework for the analysis of short RNA sequencing data applicable to studies on epigenetic inheritance**  
Epigenetics Inheritance Conference, ETH Zurich  
📍 Zurich, Switzerland
- Jun. 2019
- **Understanding the molecular mechanisms of germline- dependent epigenetic inheritance: Computational analysis of multi-omics data**  
HiFo-INI symposium, ETH Zurich  
📍 Zurich, Switzerland
- Jun. 2019
- **Computational analysis of multi-omics data from germ cells across development**  
PhD Training Network Retreat, Swiss Institute of Bioinformatics  
📍 Zurich, Switzerland
- May 2019
- **Computational analysis of multi-omics data across biological systems**  
ZNZ PhD Retreat, ETH Zurich  
HiFo PhD Day, ETH Zurich  
📍 Zurich, Switzerland
- Nov. 2018
- **Computational analysis of the genetic and epigenetic impact of environmental insults across generations**  
D-HEST 5<sup>th</sup> Research Day, ETH Zurich  
📍 Zurich, Switzerland
- May & Jun. 2018
- **The genome and epigenome from a bioinformatician's perspective**  
Inaugural Symposium of the Institute for Neuroscience (INS), ETH Zurich  
HiFo PhD Day, ETH Zurich  
📍 Zurich, Switzerland
- 2017
- **Pipeline for H3K4me3 data analysis from sperm**  
Presentation  
  
*Science share at McGill University*: A bioinformatics pipeline for sperm epigenome analysis (Montréal, Canada)  
📍 Canada and France
- YouTube
- Posters**
- The 4<sup>th</sup> Canadian Conference on Epigenetics* (Whistler, Canada)  
*Animal Science Research Day* (Montréal, Canada)  
*Galaxy Community Conference* (Montpellier, France)  
*CRRD Research Day* (Montréal, Canada)

## 💻 HACKATHONS PARTICIPATION AND PROJECT

- 2017
- **Hackathons**  
DeLEG: Deep Learning for EpiGenomics data to predict phenotype; Montréal, Canada  
Hack the Galaxy: ChIP-Seq flavored Galaxy image; Montpellier, France  
📍 Canada and France
- GitHub  
GitHub
- 2017
- **Project**  
CB2 McGill: co-founded a usergroup for *Computational Biology and Bioinformatics* at McGill University  
📍 Canada



## PUBLICATIONS

### ● Research papers and theses

#### Published papers

Anar Alshanbayeva, **Deepak K. Tanwar**, Martin Roszkowski, Francesca Manuella, Isabelle M. Mansuy. Early life stress affects the miRNA cargo of epididymal extracellular vesicles in mouse. *Biology of Reproduction*. doi: [10.1093/biolre/ioab156](https://doi.org/10.1093/biolre/ioab156)

Gretchen van Steenwyk, Katharina Gapp, Ali Jawaid, Pierre-Luc Germain, Francesca Manuella, **Deepak K. Tanwar**, Nicola Zamboni, Niharika Gaur, Anastasiia Efimova, Kristina M. Thumfart, Eric A. Miska, Isabelle M Mansuy. *The EMBO Journal*. doi: [10.1525/embj.2020104579](https://doi.org/10.1525/embj.2020104579)

Ejimedo Madogwe, **Deepak K. Tanwar**, Milena Taibi, Yasmin Schuermann, Audrey St-Yves and Raj Duggavathi. Global analysis of FSH-regulated gene expression and histone modification in mouse granulosa cells. *Molecular Reproduction and Development*. doi: [10.1002/mrd.23419](https://doi.org/10.1002/mrd.23419)

Irina Lazar-Contes, Martin Roszkowski, **Deepak K. Tanwar**, Isabelle M. Mansuy. Symposium summary: Epigenetic inheritance-impact for biology and society 26-28 August 2019, Zurich, Switzerland. *Environmental Epigenetics*. doi: [10.1093/EEP/DVAA004](https://doi.org/10.1093/EEP/DVAA004)

Yu, L., **Tanwar, D.**, Penha, E., Wolf, Y., Koonin, E., & Basu, M. (2019). Grammar of protein domain architectures. *Proceedings Of The National Academy Of Sciences*. doi: [10.1073/pnas.1814684116](https://doi.org/10.1073/pnas.1814684116)

**Tanwar, D.**, Parker, D., Gupta, P., Spurlock, B., Alvarez, R., Basu, M., & Mitra, K. (2016). Crosstalk between the mitochondrial fission protein, Drp1, and the cell cycle is identified across various cancer types and can impact survival of epithelial ovarian cancer patients. *Oncotarget*. doi: [10.18632/oncotarget.11047](https://doi.org/10.18632/oncotarget.11047)

#### Preprints

**Deepak K. Tanwar**<sup>†</sup>, Irina Lazar-Contes<sup>†</sup>, Pierre-Luc Germain, Niharika Gaur, Isabelle M. Mansuy. Transcriptome and epigenome characterization of mouse spermatogonial cells reveals distinct chromatin regulatory landscapes in postnatal and adult testis. doi: [10.1101/2020.08.20.259374](https://doi.org/10.1101/2020.08.20.259374)

#### In preparation

Kassandra Ma, **Deepak K. Tanwar**, Nicholas Petronella, Swapan Banerjee, Jennifer Ronholm. The Bivalve Microbiome Loses Diversity in the Retail Environment and is Distinct in Bivalves Colonized with *Vibrio vulnificus*

**Deepak K. Tanwar**, Jianguo Xia, Sarah Kimmins. EpiSpermHis: A Docker container to study H3K4me3 modifications in sperm using Galaxy

#### Theses

**Deepak Tanwar**, 2018. M.Sc. Thesis. EpiSpermHis: A Docker Container to Perform the Analysis of Sperm Histone ChIP-Seq Data in Galaxy [McGill University Libraries](#)

**Deepak Tanwar**, 2014. B.Tech. Thesis. Comprehensive Reanalysis of Genomic Storm (Transcriptomic) Data, Integrating Clinical Variables and Utilizing New and Old Approaches Munich, [GRIN Verlag](#), Available from [ResearchGate](#)

<sup>†</sup>: Equal contributions

# References

- Abels, E. R., & Breakefield, X. O. (2016). Introduction to extracellular vesicles: Biogenesis, RNA cargo selection, content, release, and uptake. *Cellular and Molecular Neurobiology*, 36(3), 301–312. <http://doi.org/10.1007/s10571-016-0366-z>
- Alshanbayeva, A., Tanwar, D. K., Roszkowski, M., Manuella, F., & Mansuy, I. M. (2021). Early life stress affects the miRNA cargo of epididymal extracellular vesicles in mouse†. *Biology of Reproduction*, 105(3), 593602. <http://doi.org/10.1093/biolre/ioab156>
- Altschul, S. F., Gish, W., Miller, W., Myers, E. W., & Lipman, D. J. (1990). Basic local alignment search tool. *Journal of Molecular Biology*, 215(3), 403–410. [http://doi.org/10.1016/s0022-2836\(05\)80360-2](http://doi.org/10.1016/s0022-2836(05)80360-2)
- Amezquita, R. A. (2018). Marge: An API for analysis of motifs using HOMER in r. <http://doi.org/10.1101/249268>
- Andersson, R., Gebhard, C., Miguel-Escalada, I., Hoof, I., Bornholdt, J., Boyd, M., ... Sandelin, A. (2014). An atlas of active enhancers across human cell types and tissues. *Nature*, 507(7493), 455–461. <http://doi.org/10.1038/nature12787>
- Andrews, S., Krueger, F., Segonds-Pichon, A., Biggins, L., Krueger, C., & Wingett, S. (2012). FastQC.
- Argelaguet, R., Arnol, D., Bredikhin, D., Deloro, Y., Velten, B., Marioni, J. C., & Stegle, O. (2020). MOFA+: A statistical framework for comprehensive integration of multi-modal single-cell data. *Genome Biology*, 21(1), 111. <http://doi.org/10.1186/s13059-020-02015-1>
- Argelaguet, R., Velten, B., Arnol, D., Dietrich, S., Zenz, T., Marioni, J. C., ... Stegle, O. (2018). Multi-omics factor analysis-a framework for unsupervised integration of multi-omics data sets. *Molecular Systems Biology*, 14(6), e8124. <http://doi.org/10.15252/msb.20178124>
- Barraud, P., & Tisné, C. (2019). To be or not to be modified: Miscellaneous aspects influencing nucleotide modifications in tRNAs. *IUBMB Life*, 71(8), 1126–1140. <http://doi.org/10.1002/iub.2041>
- Barrios, F., Filipponi, D., Pellegrini, M., Paronetto, M. P., Di Siena, S., Geremia, R., ... Dolci, S. (2010). Opposing effects of retinoic acid and FGF9 on Nanos2expression

- and meiotic entry of mouse germ cells. *Journal of Cell Science*, 123(6), 871–880. <http://doi.org/10.1242/jcs.057968>
- Barth, T. K., & Imhof, A. (2010). Fast signals and slow marks: The dynamics of histone modifications. *Trends in Biochemical Sciences*, 35(11), 618–626. <http://doi.org/10.1016/j.tibs.2010.05.006>
- Baumgart, M., Barth, E., Savino, A., Groth, M., Koch, P., Petzold, A., ... Cellerino, A. (2017). A miRNA catalogue and ncRNA annotation of the short-living fish Nothobranchius furzeri. *BMC Genomics*, 18(1). <http://doi.org/10.1186/s12864-017-3951-8>
- Beacon, T. H., Delcuve, G. P., López, C., Nardocci, G., Kovalchuk, I., van Wijnen, A. J., & Davie, J. R. (2021). The dynamic broad epigenetic (H3K4me3, H3K27ac) domain as a mark of essential genes. *Clinical Epigenetics*, 13(1), 138. <http://doi.org/10.1186/s13148-021-01126-1>
- Becker, P. B. (Ed.). (2011). A User's Guide to the Encyclopedia of DNA Elements (ENCODE). *PLoS Biology*, 9(4), e1001046. <http://doi.org/10.1371/journal.pbio.1001046>
- Benz, F., Roderburg, C., Vargas Cardenas, D., Vucur, M., Gautheron, J., Koch, A., ... Luedde, T. (2013). U6 is unsuitable for normalization of serum miRNA levels in patients with sepsis or liver fibrosis. *Experimental & Molecular Medicine*, 45, e42. <http://doi.org/10.1038/emm.2013.81>
- Berest, I., Arnold, C., Reyes-Palomares, A., Palla, G., Rasmussen, K. D., Giles, H., ... Zaugg, J. B. (2019). Quantification of differential transcription factor activity and multiomics-based classification into activators and repressors: diffTF. *Cell Reports*, 29(10), 3147–3159.e12. <http://doi.org/10.1016/j.celrep.2019.10.106>
- Bergmann, J. H., Li, J., Eckersley-Maslin, M. A., Rigo, F., Freier, S. M., & Spector, D. L. (2015). Regulation of the ESC transcriptome by nuclear long noncoding RNAs. *Genome Research*, 25(9), 1336–1346. <http://doi.org/10.1101/gr.189027.114>
- Bird, A. (2002). DNA methylation patterns and epigenetic memory. *Genes & Development*, 16(1), 6–21. <http://doi.org/10.1101/gad.947102>
- Bogenhagen, D. F. (2012). Mitochondrial DNA nucleoid structure. *Biochimica Et Biophysica Acta*, 1819(9-10), 914–920. <http://doi.org/10.1016/j.bbagr.2011.11.005>
- Bogliotti, Y. S., & Ross, P. J. (2012). Mechanisms of histone H3 lysine 27 trimethylation remodeling during early mammalian development. *Epigenetics*, 7(9), 976–981. <http://doi.org/10.4161/epi.21615>
- Bohacek, J., & Mansuy, I. M. (2015). Molecular insights into transgenerational non-genetic inheritance of acquired behaviours. *Nature Reviews. Genetics*, 16(11), 641–652. <http://doi.org/10.1038/nrg3964>

- Bonsergent, E., Grisard, E., Buchrieser, J., Schwartz, O., Théry, C., & Lavieu, G. (2021). Quantitative characterization of extracellular vesicle uptake and content delivery within mammalian cells. *Nature Communications*, 12(1), 1864. <http://doi.org/10.1038/s41467-021-22126-y>
- Bouckenheimer, J., Fauque, P., Lecellier, C.-H., Bruno, C., Commes, T., Lemaître, J.-M., ... Assou, S. (2018). Differential long non-coding RNA expression profiles in human oocytes and cumulus cells. *Scientific Reports*, 8(1). <http://doi.org/10.1038/s41598-018-20727-0>
- Bray, N. L., Pimentel, H., Melsted, P., & Pachter, L. (2016). Near-optimal probabilistic RNA-seq quantification. *Nature Biotechnology*, 34(5), 525–527. <http://doi.org/10.1038/nbt.3519>
- Brennecke, J., Aravin, A. A., Stark, A., Dus, M., Kellis, M., Sachidanandam, R., & Hannon, G. J. (2007). Discrete small RNA-generating loci as master regulators of transposon activity in drosophila. *Cell*, 128(6), 1089–1103. <http://doi.org/10.1016/j.cell.2007.01.043>
- Brown, J. (2018). Git-fat. Retrieved from <https://github.com/jedbrown/git-fat>
- Bruning, O., Rodenburg, W., Wackers, P. F. K., van Oostrom, C., Jonker, M. J., Dekker, R. J., ... Breit, T. M. (2016). Confounding factors in the transcriptome analysis of an in-vivo exposure experiment. *Plos One*, 11(1), e0145252. <http://doi.org/10.1371/journal.pone.0145252>
- Brunner, A. M., Nanni, P., & Mansuy, I. M. (2014). Epigenetic marking of sperm by post-translational modification of histones and protamines. *Epigenetics & Chromatin*, 7(1), 2. <http://doi.org/10.1186/1756-8935-7-2>
- Buenrostro, J. D., Giresi, P. G., Zaba, L. C., Chang, H. Y., & Greenleaf, W. J. (2013). Transposition of native chromatin for fast and sensitive epigenomic profiling of open chromatin, DNA-binding proteins and nucleosome position. *Nature Methods*, 10(12), 1213–1218. <http://doi.org/10.1038/nmeth.2688>
- Buenrostro, J. D., Wu, B., Chang, H. Y., & Greenleaf, W. J. (2015). ATAC-seq: A method for assaying chromatin accessibility genome-wide. *Current Protocols in Molecular Biology*, 109, 21.29.1–21.29.9. <http://doi.org/10.1002/0471142727.mb2129s109>
- Buffalo, V. (2020). Qrqc: Quick read quality control. Retrieved from <http://github.com/vsbuffalo/qrqc>
- Canovas, S., & Ross, P. J. (2016). Epigenetics in preimplantation mammalian development. *Theriogenology*, 86(1), 69–79. <http://doi.org/10.1016/j.theriogenology.2016.04.020>
- Casas, E., & Vavouri, T. (2014). Sperm epigenomics: Challenges and opportunities. *Frontiers in Genetics*, 5, 330. <http://doi.org/10.3389/fgene.2014.00330>
- Casas, E., & Vavouri, T. (2020). Mechanisms of epigenetic inheritance of variable traits through the germline. *Reproduction*, 159(6), R251–R263. <http://doi.org/10.1530/REP-19-0601>

- 19-0340
- Chacon, S., & Straub, B. (2021). *Pro git*. Retrieved from <https://git-scm.com/book/en/v2>
- Chan, F., Oatley, M. J., Kaucher, A. V., Yang, Q. E., Bieberich, C. J., Shashikant, C. S., & Oatley, J. M. (2014). Functional and molecular features of the Id4+ germline stem cell population in mouse testes. *Genes and Development*, 28(12), 1351–1362. <http://doi.org/10.1101/gad.240465.114>
- Chan, P. P., & Lowe, T. M. (2016). GtRNAdb 2.0: An expanded database of transfer RNA genes identified in complete and draft genomes. *Nucleic Acids Research*, 44(D1), D184–9. <http://doi.org/10.1093/nar/gkv1309>
- Chan, P., Lin, B., Mak, A., & Lowe, T. (2021). tRNAscan-SE 2.0: improved detection and functional classification of transfer RNA genes. *Nucleic Acids Research*, 49(16), 9077–9096. <http://doi.org/10.1093/nar/gkab688>
- Chen, C.-J., Servant, N., Toedling, J., Sarazin, A., Marchais, A., Duvernois-Berthet, E., ... Barillot, E. (2012). ncPRO-seq: A tool for annotation and profiling of ncRNAs in sRNA-seq data. *Bioinformatics*, 28(23), 3147–3149. <http://doi.org/10.1093/bioinformatics/bts587>
- Chen, W., Zhang, Z., Chang, C., Yang, Z., Wang, P., Fu, H., ... Wang, Y. (2020). A bioenergetic shift is required for spermatogonial differentiation. *Cell Discovery*, 6(1). <http://doi.org/10.1038/s41421-020-0183-x>
- Chen, Z., & Riggs, A. D. (2011). DNA methylation and demethylation in mammals. *The Journal of Biological Chemistry*, 286(21), 18347–18353. <http://doi.org/10.1074/jbc.R110.205286>
- Cheng, K., Chen, I.-C., Cheng, C.-H. E., Mutoji, K., Hale, B. J., Hermann, B. P., ... McCarrey, J. R. (2020). Unique epigenetic programming distinguishes regenerative spermatogonial stem cells in the developing mouse testis. *iScience*, 23(10), 101596. <http://doi.org/10.1016/j.isci.2020.101596>
- Consortium, G. O. (2021). The gene ontology resource: Enriching a GOld mine. *Nucleic Acids Research*, 49(D1), D325–D334. <http://doi.org/10.1093/nar/gkaa1113>
- Cooley, L., Appel, B., & Soll, D. (1982). Post-transcriptional nucleotide addition is responsible for the formation of the 5' terminus of histidine tRNA. *Proceedings of the National Academy of Sciences*, 79(21), 6475–6479. <http://doi.org/10.1073/pnas.79.21.6475>
- Corces, M. R., Trevino, A. E., Hamilton, E. G., Greenside, P. G., Sinnott-Armstrong, N. A., Vesuna, S., ... Chang, H. Y. (2017). An improved ATAC-seq protocol reduces background and enables interrogation of frozen tissues. *Nature Methods*, 14(10), 959–962. <http://doi.org/10.1038/nmeth.4396>
- Costoya, J. A., Hobbs, R. M., Barna, M., Cattoretti, G., Manova, K., Sukhwani, M., ... Pandolfi, P. P. (2004). Essential role of plzf in maintenance of spermatogonial stem cells.

- Nature Genetics*, 36(6), 653–659. <http://doi.org/10.1038/ng1367>
- Cozen, A. E., Quartley, E., Holmes, A. D., Hrabeta-Robinson, E., Phizicky, E. M., & Lowe, T. M. (2015). ARM-seq: AlkB-facilitated RNA methylation sequencing reveals a complex landscape of modified tRNA fragments. *Nature Methods*, 12(9), 879–884. <http://doi.org/10.1038/nmeth.3508>
- Dann, C. T., Alvarado, A. L., Molyneux, L. A., Denard, B. S., Garbers, D. L., & Porteus, M. H. (2008). Spermatogonial stem cell self-renewal requires OCT4, a factor down-regulated during retinoic acid-induced differentiation. *Stem Cells*, 26(11), 2928–2937. <http://doi.org/10.1634/stemcells.2008-0134>
- Darwin, C. (1871). Pangenesis. *Nature*, 3(78), 502–503. <http://doi.org/10.1038/003502a0>
- Davis, M. P., Carrieri, C., Saini, H. K., Dongen, S., Leonardi, T., Bussotti, G., ... Enright, A. J. (2017). Transposon-driven transcription is a conserved feature of vertebrate spermatogenesis and transcript evolution. *EMBO Reports*, 18(7), 1231–1247. <http://doi.org/10.15252/embr.201744059>
- Deaton, A. M., & Bird, A. (2011). CpG islands and the regulation of transcription. *Genes & Development*, 25(10), 1010–1022. <http://doi.org/10.1101/gad.2037511>
- DeFalco, T., Potter, Sarah J., Williams, Alyna V., Waller, B., Kan, Matthew J., & Capel, B. (2015). Macrophages Contribute to the Spermatogonial Niche in the Adult Testis. *Cell Reports*, 12(7), 1107–1119. <http://doi.org/10.1016/j.celrep.2015.07.015>
- Deniz, Ö., Frost, J. M., & Branco, M. R. (2019). Regulation of transposable elements by DNA modifications. *Nature Reviews. Genetics*, 20(7), 417–431. <http://doi.org/10.1038/s41576-019-0106-6>
- Desvignes, T., Batzel, P., Sydes, J., Eames, B. F., & Postlethwait, J. H. (2019). miRNA analysis with prost! Reveals evolutionary conservation of organ-enriched expression and post-transcriptional modifications in three-spined stickleback and zebrafish. *Scientific Reports*, 9(1), 3913. <http://doi.org/10.1038/s41598-019-40361-8>
- Donati, S., Ciuffi, S., & Brandi, M. L. (2019). Human circulating miRNAs real-time qRT-PCR-based analysis: An overview of endogenous reference genes used for data normalization. *International Journal of Molecular Sciences*, 20(18). <http://doi.org/10.3390/ijms20184353>
- Erkek, S., Hisano, M., Liang, C.-Y., Gill, M., Murr, R., Dieker, J., ... Peters, A. H. F. M. (2013). Molecular determinants of nucleosome retention at CpG-rich sequences in mouse spermatozoa. *Nature Structural & Molecular Biology*, 20(7), 868–875. <http://doi.org/10.1038/nsmb.2599>
- Ewels, P., Magnusson, M., Lundin, S., & Käller, M. (2016). MultiQC: Summarize analysis results for multiple tools and samples in a single report. *Bioinformatics*, 32(19), 3047–3048. <http://doi.org/10.1093/bioinformatics/btw354>

- Ewing, B., & Green, P. (1998). Base-calling of automated sequencer traces using phred. II. Error probabilities. *Genome Research*, 8(3), 186–194. Retrieved from <https://www.ncbi.nlm.nih.gov/pubmed/9521922>
- Faisal, I., Cisneros-Montalvo, S., Hamer, G., Tuominen, M. M., Laurila, P.-P., Tumiati, M., ... Kauppi, L. (2019). Transcription factor USF1 is required for maintenance of germline stem cells in male mice. *Endocrinology*, 160(5), 1119–1136. <http://doi.org/10.1210/en.2018-01088>
- Flickinger, C. J. (1967). The postnatal development of the Sertoli cells of the mouse. *Zeitschrift f?r Zellforschung Und Mikroskopische Anatomie*, 78(1), 92–113. <http://doi.org/10.1007/bf00344405>
- Fort, A., Hashimoto, K., Yamada, D., Salimullah, M., Keya, C. A., Saxena, A., ... Carninci, P. (2014). Deep transcriptome profiling of mammalian stem cells supports a regulatory role for retrotransposons in pluripotency maintenance. *Nature Genetics*, 46(6), 558–566. <http://doi.org/10.1038/ng.2965>
- Franklin, T. B., Russig, H., Weiss, I. C., Gräff, J., Linder, N., Michalon, A., ... Mansuy, I. M. (2010). Epigenetic transmission of the impact of early stress across generations. *Biological Psychiatry*, 68(5), 408415. <http://doi.org/10.1016/j.biopsych.2010.05.036>
- Freist, W., Verhey, J. F., Rühlmann, A., Gauss, D. H., & Arnez, J. G. (1999). Histidyl-tRNA synthetase. *Biological Chemistry*, 380(6), 623–646. <http://doi.org/10.1515/BC.1999.079>
- Fromant, M., Plateau, P., & Blanquet, S. (2000). Function of the Extra 5'-Phosphate Carried by Histidine tRNA. *Biochemistry*, 39(14), 4062–4067. <http://doi.org/10.1021/bi9923297>
- Frommer, M., McDonald, L. E., Millar, D. S., Collis, C. M., Watt, F., Grigg, G. W., ... Paul, C. L. (1992). A genomic sequencing protocol that yields a positive display of 5-methylcytosine residues in individual DNA strands. *Proceedings of the National Academy of Sciences of the United States of America*, 89(5), 1827–1831. <http://doi.org/10.1073/pnas.89.5.1827>
- Fu, L., & Zhang, L. (2019). Serotonylation: A novel histone H3 marker. *Signal Transduction and Targeted Therapy*, 4, 15. <http://doi.org/10.1038/s41392-019-0048-7>
- Fu, Y., Wu, P.-H., Beane, T., Zamore, P. D., & Weng, Z. (2018). Elimination of PCR duplicates in RNA-seq and small RNA-seq using unique molecular identifiers. *BMC Genomics*, 19(1), 531. <http://doi.org/10.1186/s12864-018-4933-1>
- Fukuda, N., & Touhara, K. (2005). Developmental expression patterns of testicular olfactory receptor genes during mouse spermatogenesis. *Genes to Cells*, 11(1), 71–81. <http://doi.org/10.1111/j.1365-2443.2005.00915.x>
- Fushan, A. A., Turanov, A. A., Lee, S.-G., Kim, E. B., Lobanov, A. V., Yim, S. H., ... Gladyshev, V. N. (2015). Gene expression defines natural changes in mammalian lifespan.

- Aging Cell*, 14(3), 352–365. <http://doi.org/10.1111/acel.12283>
- Gapp, K., & Bohacek, J. (2018). Epigenetic germline inheritance in mammals: Looking to the past to understand the future. *Genes, Brain, and Behavior*, 17(3), e12407. <http://doi.org/10.1111/gbb.12407>
- Gapp, Katharina, Parada, G. E., Gross, F., Corcoba, A., Kaur, J., Grau, E., ... Miska, E. A. (2021). Single paternal dexamethasone challenge programs offspring metabolism and reveals multiple candidates in RNA-mediated inheritance. *iScience*, 24(8), 102870. <http://doi.org/10.1016/j.isci.2021.102870>
- Gapp, K., van Steenwyk, G., Germain, P. L., Matsushima, W., Rudolph, K. L. M., Manuella, F., ... Miska, E. A. (2020). Alterations in sperm long RNA contribute to the epigenetic inheritance of the effects of postnatal trauma. *Molecular Psychiatry*, 25(9), 21622174. <http://doi.org/10.1038/s41380-018-0271-6>
- Garbuзов, A., Pech, M. F., Hasegawa, K., Sukhwani, M., Zhang, R. J., Orwig, K. E., & Artandi, S. E. (2018). Purification of GFR?1+ and GFR?1– Spermatogonial Stem Cells Reveals a Niche-Dependent Mechanism for Fate Determination. *Stem Cell Reports*, 10(2), 553–567. <http://doi.org/10.1016/j.stemcr.2017.12.009>
- Gerber, S., Schratt, G., & Germain, P.-L. (2021). Streamlining differential exon and 3' UTR usage with diffUTR. *BioRxiv*. <http://doi.org/10.1101/2021.02.12.430963>
- Germain, P.-L., Sonrel, A., & Robinson, M. D. (2020). pipeComp, a general framework for the evaluation of computational pipelines, reveals performant single cell RNA-seq preprocessing tools. *Genome Biology*, 21(1), 227. <http://doi.org/10.1186/s13059-020-02136-7>
- GM, F. (2018). tRNAdbImport. <http://doi.org/10.18129/B9.BIOC.TRNADBIMPORT>
- Goertz, M. J., Wu, Z., Gallardo, T. D., Hamra, F. K., & Castrillon, D. H. (2011). Foxo1 is required in mouse spermatogonial stem cells for their maintenance and the initiation of spermatogenesis. *Journal of Clinical Investigation*, 121(9), 3456–3466. <http://doi.org/10.1172/JCI57984>
- Gong, H., Liu, C.-M., Liu, D.-P., & Liang, C.-C. (2005). The role of small RNAs in human diseases: Potential troublemaker and therapeutic tools. *Medicinal Research Reviews*, 25(3), 361–381. <http://doi.org/10.1002/med.20023>
- Gontarz, P., Fu, S., Xing, X., Liu, S., Miao, B., Bazylianska, V., ... Zhang, B. (2020). Comparison of differential accessibility analysis strategies for ATAC-seq data. *Scientific Reports*, 10(1), 10150. <http://doi.org/10.1038/s41598-020-66998-4>
- Goodnight, A. V., Kremsky, I., Khampang, S., Jung, Y. H., Billingsley, J. M., Bosinger, S. E., ... Chan, A. W. S. (2019). Chromatin accessibility and transcription dynamics during in vitro astrocyte differentiation of huntington's disease monkey pluripotent stem cells.

- Epigenetics & Chromatin*, 12(1), 67. <http://doi.org/10.1186/s13072-019-0313-6>
- Green, C. D., Ma, Q., Manske, G. L., Shami, A. N., Zheng, X., Marini, S., ... Hammoud, S. S. (2018). A comprehensive roadmap of murine spermatogenesis defined by single-cell RNA-seq. *Developmental Cell*, 46(5), 651–667.e10. <http://doi.org/10.1016/j.devcel.2018.07.025>
- Green, R., & Noller, H. F. (1997). Ribosomes and translation. *Annual Review of Biochemistry*, 66, 679–716. <http://doi.org/10.1146/annurev.biochem.66.1.679>
- Griffiths-Jones, S., Saini, H. K., van Dongen, S., & Enright, A. J. (2008). miRBase: Tools for microRNA genomics. *Nucleic Acids Research*, 36(Database issue), D154–8. <http://doi.org/10.1093/nar/gkm952>
- Grive, K. J., Hu, Y., Shu, E., Grimson, A., Elemento, O., Grenier, J. K., & Cohen, P. E. (2019). Dynamic transcriptome profiles within spermatogonial and spermatocyte populations during postnatal testis maturation revealed by single-cell sequencing. *PLOS Genetics*, 15(3), e1007810. <http://doi.org/10.1371/journal.pgen.1007810>
- Gu, Z. (2021). *rGREAT: Client for GREAT analysis*.
- Gu, Z., Eils, R., & Schlesner, M. (2016). Complex heatmaps reveal patterns and correlations in multidimensional genomic data. *Bioinformatics*, 32(18), 28472849. <http://doi.org/10.1093/bioinformatics/btw313>
- Gu, Z., Eils, R., Schlesner, M., & Ishaque, N. (2018). EnrichedHeatmap: An r/bioconductor package for comprehensive visualization of genomic signal associations. *BMC Genomics*, 19(1), 234. <http://doi.org/10.1186/s12864-018-4625-x>
- Guo, J., Grow, E. J., Yi, C., Mlcochova, H., Maher, G. J., Lindskog, C., ... Cairns, B. R. (2017). Chromatin and single-cell RNA-seq profiling reveal dynamic signaling and metabolic transitions during human spermatogonial stem cell development. *Cell Stem Cell*, 21(4), 533–546.e6. <http://doi.org/10.1016/j.stem.2017.09.003>
- Hammoud, S. S., Low, D. H. P., Yi, C., Carrell, D. T., Guccione, E., & Cairns, B. R. (2014). Chromatin and transcription transitions of mammalian adult germline stem cells and spermatogenesis. *Cell Stem Cell*, 15(2), 239–253. <http://doi.org/10.1016/j.stem.2014.04.006>
- Hammoud, S. S., Low, D. H. P., Yi, C., Lee, C. L., Oatley, J. M., Payne, C. J., ... Cairns, B. R. (2015). Transcription and imprinting dynamics in developing postnatal male germline stem cells. <http://doi.org/10.1101/gad.261925>
- Handzlik, J. E., Tastsoglou, S., Vlachos, I. S., & Hatzigeorgiou, A. G. (2020). Manatee: Detection and quantification of small non-coding RNAs from next-generation sequencing data. *Scientific Reports*, 10(1), 705. <http://doi.org/10.1038/s41598-020-57495-9>
- Hanson, M. A., & Skinner, M. K. (2016). Developmental origins of epigenetic transgenerational inheritance. *Environmental Epigenetics*, 2(1). <http://doi.org/10.1093/eep/dvw002>

- Harrow, J., Frankish, A., Gonzalez, J. M., Tapanari, E., Diekhans, M., Kokocinski, F., ... Hubbard, T. J. (2012). GENCODE: The reference human genome annotation for the ENCODE project. *Genome Research*, 22(9), 1760–1774. <http://doi.org/10.1101/gr.135350.111>
- Hasegawa, K., & Saga, Y. (2014). FGF8-FGFR1 signaling acts as a niche factor for maintaining undifferentiated spermatogonia in the Mouse1. *Biology of Reproduction*, 91(6), 145–146. <http://doi.org/10.1095/biolreprod.114.121012>
- He, Z., Jiang, J., Kokkinaki, M., Golestaneh, N., Hofmann, M.-C., & Dym, M. (2008). Gdnf up-regulates c-fos transcription via the ras/Erk1/2 pathway to promote mouse spermatogonial stem cell proliferation. *Stem Cells*, 26(1), 266–278. <http://doi.org/10.1634/stemcells.2007-0436>
- Heard, E., & Martienssen, R. A. (2014). Transgenerational epigenetic inheritance: Myths and mechanisms. *Cell*, 157(1), 95–109. <http://doi.org/10.1016/j.cell.2014.02.045>
- Heinz, S., Benner, C., Spann, N., Bertolino, E., Lin, Y. C., Laslo, P., ... Glass, C. K. (2010). Simple combinations of lineage-determining transcription factors prime cis-regulatory elements required for macrophage and b cell identities. *Molecular Cell*, 38(4), 576–589. <http://doi.org/10.1016/j.molcel.2010.05.004>
- Hermann, B. P., Cheng, K., Singh, A., Cruz, L. R.-D. L., Mutoji, K. N., Chen, I. C., ... McCarrey, J. R. (2018). The mammalian spermatogenesis single-cell transcriptome, from spermatogonial stem cells to spermatids. *Cell Reports*, 25(6), 1650–1667.e8. <http://doi.org/10.1016/j.celrep.2018.10.026>
- Hou, Y.-M. (2010). CCA addition to tRNA: Implications for tRNA quality control. *IUBMB Life*, 62(4), 251–260. <http://doi.org/10.1002/iub.301>
- Howe, K. L., Achuthan, P., Allen, J., Allen, J., Alvarez-Jarreta, J., Amode, M. R., ... Flliceck, P. (2021). Ensembl 2021. *Nucleic Acids Research*, 49(D1), D884–D891. <http://doi.org/10.1093/nar/gkaa942>
- Huang, C., Xu, M., & Zhu, B. (2013). Epigenetic inheritance mediated by histone lysine methylation: Maintaining transcriptional states without the precise restoration of marks? *Philosophical Transactions of the Royal Society of London. Series B, Biological Sciences*, 368(1609), 20110332. <http://doi.org/10.1098/rstb.2011.0332>
- Huang, R., Soneson, C., Ernst, F. G. M., Rue-Albrecht, K. C., Yu, G., Hicks, S. C., & Robinson, M. D. (2020). TreeSummarizedExperiment: A S4 class for data with hierarchical structure. *F1000Research*, 9, 1246. <http://doi.org/10.12688/f1000research.26669.1>
- Huang, R., Soneson, C., Germain, P.-L., Schmidt, T. S. B., Mering, C. V., & Robinson, M. D. (2021). treeclimbR pinpoints the data-dependent resolution of hierarchical hypotheses. *Genome Biology*, 22(1). <http://doi.org/10.1186/s13059-021-02368-1>

- Huang, S., Chaudhary, K., & Garmire, L. X. (2017). More is better: Recent progress in multi-omics data integration methods. *Frontiers in Genetics*, 8, 84. <http://doi.org/10.3389/fgene.2017.00084>
- Huber, W., Carey, V. J., Gentleman, R., Anders, S., Carlson, M., Carvalho, B. S., ... Morgan, M. (2015). Orchestrating high-throughput genomic analysis with bioconductor. *Nature Methods*, 12(2), 115–121. <http://doi.org/10.1038/nmeth.3252>
- Ibba, M., & Soll, D. (2000). Aminoacyl-tRNA synthesis. *Annual Review of Biochemistry*, 69, 617–650. <http://doi.org/10.1146/annurev.biochem.69.1.617>
- Iwasaki, W., Miya, Y., Horikoshi, N., Osakabe, A., Taguchi, H., Tachiwana, H., ... Kurumizaka, H. (2013). Contribution of histone n-terminal tails to the structure and stability of nucleosomes. *FEBS Open Bio*, 3, 363–369. <http://doi.org/10.1016/j.fob.2013.08.007>
- Jassal, B., Matthews, L., Viteri, G., Gong, C., Lorente, P., Fabregat, A., ... D'Eustachio, P. (2020). The reactome pathway knowledgebase. *Nucleic Acids Research*, 48(D1), D498–D503. <http://doi.org/10.1093/nar/gkz1031>
- Jawaid, A., Jehle, K.-L., & Mansuy, I. M. (2021). Impact of parental exposure on offspring health in humans. *Trends in Genetics*, 37(4), 373–388. <http://doi.org/10.1016/j.tig.2020.10.006>
- Jawaid, A., & Mansuy, I. M. (2019). Inter- and transgenerational inheritance of behavioral phenotypes. *Current Opinion in Behavioral Sciences*, 25, 96–101. <http://doi.org/10.1016/j.cobeha.2018.12.004>
- Johnson, N. R., Yeoh, J. M., Coruh, C., & Axtell, M. J. (2016). Improved placement of multi-mapping small RNAs. *G3 (Bethesda, Md.)*, 6(7), 2103–2111. <http://doi.org/10.1534/g3.116.030452>
- Jones, P. A., & Takai, D. (2001). The role of DNA methylation in mammalian epigenetics. *Science*, 293(5532), 1068–1070. <http://doi.org/10.1126/science.1063852>
- Jühling, F., Mörl, M., Hartmann, R. K., Sprinzl, M., Stadler, P. F., & Pütz, J. (2009). tRNADB 2009: Compilation of tRNA sequences and tRNA genes. *Nucleic Acids Research*, 37(Database issue), D159–62. <http://doi.org/10.1093/nar/gkn772>
- Jung, Y. H., Bixler, B. J., Ruiz, D., Wang, H.-L. V., Linsenbaum, H., Xiang, J.-F., ... Corces, V. G. (2020). Transgenerational inheritance of BPA-induced obesity correlates with transmission of new CTCF sites in the fto gene. *BioRxiv*. <http://doi.org/10.1101/2020.11.20.391672>
- Jung, Y. H., Kremsky, I., Gold, H. B., Rowley, M. J., Punyawai, K., Buonanotte, A., ... Corces, V. G. (2019). Maintenance of CTCF- and transcription factor-mediated interactions from the gametes to the early mouse embryo. *Molecular Cell*, 75(1), 154–171.e5. <http://doi.org/10.1016/j.molcel.2019.04.014>

- Jung, Y. H., Sauria, M. E. G., Lyu, X., Cheema, M. S., Ausio, J., Taylor, J., & Corces, V. G. (2017). Chromatin states in mouse sperm correlate with embryonic and adult regulatory landscapes. *Cell Reports*, 18(6), 1366–1382. <http://doi.org/10.1016/j.celrep.2017.01.034>
- Kaisers, W. (2020). seqTools: Analysis of nucleotide, sequence and quality content on fastqfiles. Retrieved from <https://bioconductor.org/packages/release/bioc/html/seqTools.html>
- Kanatsu-Shinohara, M., Tanaka, T., Ogonuki, N., Ogura, A., Morimoto, H., Cheng, P. F., ... Shinohara, T. (2016). Myc/Mycn-mediated glycolysis enhances mouse spermatogonial stem cell self-renewal. *Genes & Development*, 30(23), 2637–2648. <http://doi.org/10.1101/gad.287045.116>
- Kanehisa, M., Furumichi, M., Sato, Y., Ishiguro-Watanabe, M., & Tanabe, M. (2021). KEGG: Integrating viruses and cellular organisms. *Nucleic Acids Research*, 49(D1), D545–D551. <http://doi.org/10.1093/nar/gkaa970>
- Kia, A., Gloeckner, C., Osothprarop, T., Gormley, N., Bomati, E., Stephenson, M., ... He, M. M. (2017). Improved genome sequencing using an engineered transposase. *BMC Biotechnology*, 17(1), 6. <http://doi.org/10.1186/s12896-016-0326-1>
- Kolasa, A., Misiakiewicz, K., Marchlewicz, M., & Wiszniewska, B. (2012). The generation of spermatogonial stem cells and spermatogonia in mammals. *Reproductive Biology*, 12(1), 5–23. [http://doi.org/10.1016/S1642-431X\(12\)60074-6](http://doi.org/10.1016/S1642-431X(12)60074-6)
- König, J., Zarnack, K., Rot, G., Curk, T., Kayikci, M., Zupan, B., ... Ule, J. (2010). iCLIP reveals the function of hnRNP particles in splicing at individual nucleotide resolution. *Nature Structural & Molecular Biology*, 17(7), 909–915. <http://doi.org/10.1038/nsmb.1838>
- Korotkevich, G., Sukhov, V., Budin, N., Shpak, B., Artyomov, M. N., & Sergushichev, A. (2016). Fast gene set enrichment analysis. *BioRxiv*. <http://doi.org/10.1101/060012>
- Kouzarides, T. (2007). Chromatin modifications and their function. *Cell*, 128(4), 693–705. <http://doi.org/10.1016/j.cell.2007.02.005>
- Kremsky, I., & Corces, V. G. (2020). Protection from DNA re-methylation by transcription factors in primordial germ cells and pre-implantation embryos can explain trans-generational epigenetic inheritance. *Genome Biology*, 21(1), 118. <http://doi.org/10.1186/s13059-020-02036-w>
- Krueger, F. (2015). Trim galore. A wrapper tool around cutadapt and FastQC to consistently apply quality and adapter trimming to FastQ files, [www.bioinformatics.babraham.ac.uk/projects/trim\\_galore/](http://www.bioinformatics.babraham.ac.uk/projects/trim_galore/)
- Krueger, F., & Andrews, S. R. (2011). Bismark: A flexible aligner and methylation caller for bisulfite-seq applications. *Bioinformatics*, 27(11), 1571–1572. <http://doi.org/10.1093/bioinformatics/btr167>

- Kubota, H., Avarbock, M. R., & Brinster, R. L. (2004a). Culture Conditions and Single Growth Factors Affect Fate Determination of Mouse Spermatogonial Stem Cells1. *Biology of Reproduction*, 71(3), 722–731. <http://doi.org/10.1095/biolreprod.104.029207>
- Kubota, H., Avarbock, M. R., & Brinster, R. L. (2004b). Growth factors essential for self-renewal and expansion of mouse spermatogonial stem cells. *Proceedings of the National Academy of Sciences of the United States of America*, 101(47), 16489–94. <http://doi.org/10.1073/pnas.0407063101>
- Kubota, H., & Brinster, R. L. (2018). Spermatogonial stem cells. *Biology of Reproduction*, 99(1), 52–74. <http://doi.org/10.1093/biolre/ioy077>
- Kuksa, P. P., Amlie-Wolf, A., Katanic, Ž., Valladares, O., Wang, L.-S., & Leung, Y. Y. (2018). SPAR: Small RNA-seq portal for analysis of sequencing experiments. *Nucleic Acids Research*, 46(W1), W36–W42. <http://doi.org/10.1093/nar/gky330>
- Lai, X., & Vera, J. (2013). MicroRNA clusters (pp. 1310–1314). Springer New York. [http://doi.org/10.1007/978-1-4419-9863-7\\_1121](http://doi.org/10.1007/978-1-4419-9863-7_1121)
- Langmead, B., & Salzberg, S. L. (2012). Fast gapped-read alignment with bowtie 2. *Nature Methods*, 9(4), 357–359. <http://doi.org/10.1038/nmeth.1923>
- Law, C. W., Chen, Y., Shi, W., & Smyth, G. K. (2014). Voom: Precision weights unlock linear model analysis tools for RNA-seq read counts. *Genome Biology*, 15(2), R29. <http://doi.org/10.1186/gb-2014-15-2-r29>
- Law, N. C., Oatley, M. J., & Oatley, J. M. (2019). Developmental kinetics and transcriptome dynamics of stem cell specification in the spermatogenic lineage. *Nature Communications*, 10(1), 2787. <http://doi.org/10.1038/s41467-019-10596-0>
- Lawrence, M., Daujat, S., & Schneider, R. (2016). Lateral thinking: How histone modifications regulate gene expression. *Trends in Genetics*, 32(1), 42–56. <http://doi.org/10.1016/j.tig.2015.10.007>
- Lazar-Contes, I., Tanwar, D. K., Germain, P.-L., Gaur, N., & Mansuy, I. M. (2020). Transcriptome and epigenome characterization of mouse spermatogonial cells reveals distinct chromatin regulatory landscapes in postnatal and adult testis. *BioRxiv*. <http://doi.org/10.1101/2020.08.20.259374>
- Lê Cao, K.-A., Boitard, S., & Besse, P. (2011). Sparse PLS discriminant analysis: biologically relevant feature selection and graphical displays for multiclass problems. *BMC Bioinformatics*, 12(1). <http://doi.org/10.1186/1471-2105-12-253>
- Li, H., Handsaker, B., Wysoker, A., Fennell, T., Ruan, J., Homer, N., ... Subgroup, 1000. G. P. D. P. (2009). The sequence alignment/map format and SAMtools. *Bioinformatics*, 25(16), 2078–2079. <http://doi.org/10.1093/bioinformatics/btp352>

- Li, J., Han, X., Wan, Y., Zhang, S., Zhao, Y., Fan, R., ... Zhou, Y. (2018). TAM 2.0: Tool for MicroRNA set analysis. *Nucleic Acids Research*, 46(W1), W180–W185. <http://doi.org/10.1093/nar/gky509>
- Li, X. Z., Roy, C. K., Dong, X., Bolcun-Filas, E., Wang, J., Han, B. W., ... Zamore, P. D. (2013). An ancient transcription factor initiates the burst of piRNA production during early meiosis in mouse testes. *Molecular Cell*, 50(1), 67–81. <http://doi.org/10.1016/j.molcel.2013.02.016>
- Li, Z., Ender, C., Meister, G., Moore, P. S., Chang, Y., & John, B. (2012). Extensive terminal and asymmetric processing of small RNAs from rRNAs, snoRNAs, snRNAs, and tRNAs. *Nucleic Acids Research*, 40(14), 6787–6799. <http://doi.org/10.1093/nar/gks307>
- Liao, Y., Smyth, G. K., & Shi, W. (2019). The r package rsubread is easier, faster, cheaper and better for alignment and quantification of RNA sequencing reads. *Nucleic Acids Research*, 47(8), e47e47. <http://doi.org/10.1093/nar/gkz114>
- Lo Cicero, A., Stahl, P. D., & Raposo, G. (2015). Extracellular vesicles shuffling intercellular messages: For good or for bad. *Current Opinion in Cell Biology*, 35, 69–77. <http://doi.org/10.1016/j.ceb.2015.04.013>
- Loher, P., Telonis, A. G., & Rigoutsos, I. (2017). MINTmap: Fast and exhaustive profiling of nuclear and mitochondrial tRNA fragments from short RNA-seq data. *Scientific Reports*, 7, 41184. <http://doi.org/10.1038/srep41184>
- Lord, T., Oatley, M. J., & Oatley, J. M. (2018). Testicular architecture is critical for mediation of retinoic acid responsiveness by undifferentiated spermatogonial subtypes in the mouse. *Stem Cell Reports*, 10(2), 538–552. <http://doi.org/10.1016/j.stemcr.2018.01.003>
- Lorena Pantano [Aut, Cre], Georgia Escaramis [Aut], ChristosArgyropoulos [Aut]. (2017). isomiRs. <http://doi.org/10.18129/B9.BIOC.ISOMIRs>
- Lu, J. Y., Shao, W., Chang, L., Yin, Y., Li, T., Zhang, H., ... Shen, X. (2020). Genomic repeats categorize genes with distinct functions for orchestrated regulation. *Cell Reports*, 30(10), 3296–3311.e5. <http://doi.org/10.1016/j.celrep.2020.02.048>
- Lun, A. T. L., & Smyth, G. K. (2015). CsaW: A bioconductor package for differential binding analysis of ChIP-seq data using sliding windows. *Nucleic Acids Research*, 44(5), e45. <http://doi.org/10.1093/nar/gkv1191>
- Luo, C., Hajkova, P., & Ecker, J. R. (2018). Dynamic DNA methylation: In the right place at the right time. *Science*, 361(6409), 1336–1340. <http://doi.org/10.1126/science.aat6806>
- Magee, R., Loher, P., Londin, E., & Rigoutsos, I. (2017). Threshold-seq: A tool for determining the threshold in short RNA-seq datasets. *Bioinformatics*, 33(13), 2034–2036. <http://doi.org/10.1093/bioinformatics/btx073>

- Mao, S., Li, Y., Liu, B., & Chi, T. (2017). Mouse models of epigenetic inheritance: Classification, mechanisms, and experimental strategies (pp. 231–243). Elsevier. <http://doi.org/10.1016/B978-0-12-805388-1.00015-8>
- Marmorstein, R., & Trievel, R. C. (2009). Histone modifying enzymes: Structures, mechanisms, and specificities. *Biochimica Et Biophysica Acta*, 1789(1), 58–68. <http://doi.org/10.1016/j.bbagr.2008.07.009>
- Martínez-Zamudio, R. I., Roux, P. F., Freitas, J. A. N. L. F. de, Robinson, L., Doré, G., Sun, B., ... Bischof, O. (2020). AP-1 imprints a reversible transcriptional programme of senescent cells. *Nature Cell Biology*, 22(7), 842–855. <http://doi.org/10.1038/s41556-020-0529-5>
- Mayr, C. (2019). What are 3' utrs doing? *Cold Spring Harbor Perspectives in Biology*, 11(10). <http://doi.org/10.1101/cshperspect.a034728>
- McCarthy, D. J., & Smyth, G. K. (2009). Testing significance relative to a fold-change threshold is a TREAT. *Bioinformatics*, 25(6), 765–771. <http://doi.org/10.1093/bioinformatics/btp053>
- McLean, C. Y., Bristor, D., Hiller, M., Clarke, S. L., Schaar, B. T., Lowe, C. B., ... Bejerano, G. (2010). GREAT improves functional interpretation of cis-regulatory regions. *Nature Biotechnology*, 28(5), 495–501. <http://doi.org/10.1038/nbt.1630>
- Meissner, A., Gnirke, A., Bell, G. W., Ramsahoye, B., Lander, E. S., & Jaenisch, R. (2005). Reduced representation bisulfite sequencing for comparative high-resolution DNA methylation analysis. *Nucleic Acids Research*, 33(18), 5868–5877. <http://doi.org/10.1093/nar/gki901>
- Morgan, M., Anders, S., Lawrence, M., Aboyoun, P., Pagès, H., & Gentleman, R. (2009). ShortRead: A bioconductor package for input, quality assessment and exploration of high-throughput sequence data. *Bioinformatics*, 25(19), 2607–2608. <http://doi.org/10.1093/bioinformatics/btp450>
- Morgan, M., Obenchain, V., Hester, J., & Pagès, H. (2020). SummarizedExperiment: SummarizedExperiment container. Retrieved from <https://bioconductor.org/packages/SummarizedExperiment>
- Mutoji, K., Singh, A., Nguyen, T., Gildersleeve, H., Kaucher, A. V., Oatley, M. J., ... Hermann, B. P. (2016). TSPAN8 expression distinguishes spermatogonial stem cells in the prepubertal mouse testis. *Biology of Reproduction*, 95(6), 117. <http://doi.org/10.1095/biolreprod.116.144220>
- Nagy, C., & Turecki, G. (2015). Transgenerational epigenetic inheritance: An open discussion. *Epigenomics*, 7(5), 781–790. <http://doi.org/10.2217/epi.15.46>
- Niu, Z., Goodyear, S. M., Rao, S., Wu, X., Tobias, J. W., Avarbock, M. R., & Brinster, R. L. (2011). MicroRNA-21 regulates the self-renewal of mouse spermatogonial stem cells. *Proceedings of the National Academy of Sciences*. <http://doi.org/10.1073/pnas.1109987108>

- O'Brien, K., Breyne, K., Ughetto, S., Laurent, L. C., & Breakefield, X. O. (2020). RNA delivery by extracellular vesicles in mammalian cells and its applications. *Nature Reviews Molecular Cell Biology*, 21(10), 585–606. <http://doi.org/10.1038/s41580-020-0251-y>
- Oatley, J. M., & Griswold, M. D. (Eds.). (2017). *The biology of mammalian spermatogonia*. Springer New York. <http://doi.org/10.1007/978-1-4939-7505-1>
- Oldfield, A. J., Yang, P., Conway, A. E., Cinghu, S., Freudenberg, J. M., Yellaboina, S., & Jothi, R. (2014). Histone-fold domain protein NF-y promotes chromatin accessibility for cell type-specific master transcription factors. *Molecular Cell*, 55(5), 708–722. <http://doi.org/10.1016/j.molcel.2014.07.005>
- Pagès, H., Aboyoun, P., Gentleman, R., & DebRoy, S. (2020). Biostrings: Efficient manipulation of biological strings. Retrieved from <https://bioconductor.org/packages/Biostrings>
- Park, P. J. (2009). ChIP-seq: Advantages and challenges of a maturing technology. *Nature Reviews Genetics*, 10(10), 669–680. <http://doi.org/10.1038/nrg2641>
- Patro, R., Duggal, G., Love, M. I., Irizarry, R. A., & Kingsford, C. (2017). Salmon provides fast and bias-aware quantification of transcript expression. *Nature Methods*, 14(4), 417–419. <http://doi.org/10.1038/nmeth.4197>
- Pisco, A. O., Fouquier d'Herouel, A., & Huang, S. (2016). Conceptual confusion: The case of epigenetics. *BioRxiv*. <http://doi.org/10.1101/053009>
- Pratt, A. J., & MacRae, I. J. (2009). The RNA-induced silencing complex: A versatile gene-silencing machine. *The Journal of Biological Chemistry*, 284(27), 17897–17901. <http://doi.org/10.1074/jbc.R900012200>
- Quast, C., Pruesse, E., Yilmaz, P., Gerken, J., Schweer, T., Yarza, P., ... Glöckner, F. O. (2013). The SILVA ribosomal RNA gene database project: Improved data processing and web-based tools. *Nucleic Acids Research*, 41(Database issue), D590–6. <http://doi.org/10.1093/nar/gks1219>
- R Core Team. (2019). *R: A language and environment for statistical computing*. Vienna, Austria: R Foundation for Statistical Computing. Retrieved from <https://www.R-project.org>
- Rahman, R.-U., Gautam, A., Bethune, J., Sattar, A., Fiosins, M., Magruder, D. S., ... Bonn, S. (2018). Oasis 2: Improved online analysis of small RNA-seq data. *BMC Bioinformatics*, 19(1), 54. <http://doi.org/10.1186/s12859-018-2047-z>
- Ramirez, F., Ryan, D. P., Grüning, B., Bhardwaj, V., Kilpert, F., Richter, A. S., ... Manke, T. (2016). deepTools2: A next generation web server for deep-sequencing data analysis. *Nucleic Acids Research*, 44(W1), W160W165. <http://doi.org/10.1093/nar/gkw257>

- Rando, O. J. (2016). Intergenerational transfer of epigenetic information in sperm. *Cold Spring Harbor Perspectives in Medicine*, 6(5). <http://doi.org/10.1101/cshperspect.a022988>
- Reik, W., Dean, W., & Walter, J. (2001). Epigenetic Reprogramming in Mammalian Development. *Science*, 293(5532), 1089–1093. <http://doi.org/10.1126/science.1063443>
- Ritchie, M. E., Phipson, B., Wu, D., Hu, Y., Law, C. W., Shi, W., & Smyth, G. K. (2015). Limma powers differential expression analyses for RNA-sequencing and microarray studies. *Nucleic Acids Research*, 43(7), e47. <http://doi.org/10.1093/nar/gkv007>
- Robinson, M. D., McCarthy, D. J., & Smyth, G. K. (2010). edgeR: A bioconductor package for differential expression analysis of digital gene expression data. *Bioinformatics*, 26(1), 139140. <http://doi.org/10.1093/bioinformatics/btp616>
- Robinson, M. D., & Oshlack, A. (2010). A scaling normalization method for differential expression analysis of RNA-seq data. *Genome Biology*, 11(3), R25. <http://doi.org/10.1186/gb-2010-11-3-r25>
- Robles, V., Valcarce, D. G., & Riesco, M. F. (2019). Non-coding RNA regulation in reproduction: Their potential use as biomarkers. *Non-Coding RNA Research*, 4(2), 54–62. <http://doi.org/10.1016/j.ncrna.2019.04.001>
- Rohart, F., Gautier, B., Singh, A., & Lê Cao, K.-A. (2017). mixOmics: An r package for 'omics feature selection and multiple data integration. *PLoS Computational Biology*, 13(11), e1005752. <http://doi.org/10.1371/journal.pcbi.1005752>
- Rooij, D. G. de. (2017). The nature and dynamics of spermatogonial stem cells. *Development*, 144(17), 3022–3030. <http://doi.org/10.1242/DEV.146571>
- Royo, H., Stadler, M. B., & Peters, A. H. F. M. (2016). Alternative computational analysis shows no evidence for nucleosome enrichment at repetitive sequences in mammalian spermatozoa. *Developmental Cell*, 37(1), 98–104. <http://doi.org/10.1016/j.devcel.2016.03.010>
- Rozowsky, J., Kitchen, R. R., Park, J. J., Galeev, T. R., Diao, J., Warrell, J., ... Gerstein, M. (2019). exceRpt: A comprehensive analytic platform for extracellular RNA profiling. *Cell Systems*, 8(4), 352357.e3. <http://doi.org/10.1016/j.cels.2019.03.004>
- Rueda, A., Barturen, G., Lebrón, R., Gómez-Martín, C., Alganza, Á., Oliver, J. L., & Hackenberg, M. (2015). sRNAToolbox: An integrated collection of small RNA research tools. *Nucleic Acids Research*, 43(W1), W467–73. <http://doi.org/10.1093/nar/gkv555>
- Sada, A., Suzuki, A., Suzuki, H., & Saga, Y. (2009). The RNA-Binding Protein NANOS2 Is Required to Maintain Murine Spermatogonial Stem Cells. *Science*, 325(5946), 1394–1398. <http://doi.org/10.1126/science.1172645>
- Sakashita, A., Maezawa, S., Takahashi, K., Alavattam, K. G., Yukawa, M., Hu, Y.-C., ... Namekawa, S. H. (2020). Endogenous retroviruses drive species-specific germline transcriptomes in mammals. *Nature Structural & Molecular Biology*, 27(10), 967–977.

- http://doi.org/10.1038/s41594-020-0487-4
- Saxton, D. S., & Rine, J. (2019). Epigenetic memory independent of symmetric histone inheritance. *eLife*, 8. http://doi.org/10.7554/eLife.51421
- Sayols, S., Scherzinger, D., & Klein, H. (2016). dupRadar: A bioconductor package for the assessment of PCR artifacts in RNA-seq data. *BMC Bioinformatics*, 17(1), 428. http://doi.org/10.1186/s12859-016-1276-2
- Schaefer, S., & Nadeau, J. H. (2015). The genetics of epigenetic inheritance: Modes, molecules, and mechanisms. *The Quarterly Review of Biology*, 90(4), 381–415. http://doi.org/10.1086/683699
- Shaulian, E., & Karin, M. (2002). AP-1 as a regulator of cell life and death. *Nature Cell Biology*, 4(5), E131–E136. http://doi.org/10.1038/ncb0502-e131
- Shavlakadze, T., Morris, M., Fang, J., Wang, S. X., Zhu, J., Zhou, W., ... Glass, D. J. (2019). Age-Related Gene Expression Signature in Rats Demonstrate Early, Late, and Linear Transcriptional Changes from Multiple Tissues. *Cell Reports*, 28(12), 3263–3273.e3. http://doi.org/10.1016/j.celrep.2019.08.043
- Shi, J., Ko, E.-A., Sanders, K. M., Chen, Q., & Zhou, T. (2018). SPORTS1.0: A tool for annotating and profiling non-coding RNAs optimized for rRNA- and tRNA-derived small RNAs. *Genomics, Proteomics & Bioinformatics / Beijing Genomics Institute*, 16(2), 144–151. http://doi.org/10.1016/j.gpb.2018.04.004
- Shinohara, T., Orwig, K. E., Avarbock, M. R., & Brinster, R. L. (2001). Remodeling of the postnatal mouse testis is accompanied by dramatic changes in stem cell number and niche accessibility. *Proceedings of the National Academy of Sciences*, 98(11), 6186–6191. http://doi.org/10.1073/pnas.111158198
- Siklenka, K., Erkek, S., Godmann, M., Lambrot, R., McGraw, S., Lafleur, C., ... Kimmins, S. (2015). Disruption of histone methylation in developing sperm impairs offspring health transgenerationally. *Science*, 350(6261), aab2006. http://doi.org/10.1126/science.aab2006
- Sims, J. K., Houston, S. I., Magazinnik, T., & Rice, J. C. (2006). A trans-tail histone code defined by monomethylated H4 lys-20 and H3 lys-9 demarcates distinct regions of silent chromatin. *The Journal of Biological Chemistry*, 281(18), 12760–12766. http://doi.org/10.1074/jbc.M513462200
- Skog, S., Örkenby, L., Kugelberg, U., Tariq, K., Farrants, A.-K. Ö., Öst, A., & Nätt, D. (2021). Seqpac: A new framework for small RNA analysis in r using sequence-based counts. *BioRxiv*. http://doi.org/10.1101/2021.03.19.436151
- Smallwood, S. A., & Kelsey, G. (2012). De novo DNA methylation: a germ cell perspective. *Trends in Genetics*, 28(1), 33–42. http://doi.org/10.1016/j.tig.2011.09.004

- Smith, Z. D., & Meissner, A. (2013). DNA methylation: Roles in mammalian development. *Nature Reviews. Genetics*, 14(3), 204–220. <http://doi.org/10.1038/nrg3354>
- Sprinzl, M., & Cramer, F. (1979). The -c-c-a end of tRNA and its role in protein biosynthesis (pp. 1–69). Elsevier. [http://doi.org/10.1016/s0079-6603\(08\)60798-9](http://doi.org/10.1016/s0079-6603(08)60798-9)
- Starks, R. R., Biswas, A., Jain, A., & Tuteja, G. (2019). Combined analysis of dissimilar promoter accessibility and gene expression profiles identifies tissue-specific genes and actively repressed networks. *Epigenetics and Chromatin*, 12(1). <http://doi.org/10.1186/s13072-019-0260-2>
- Stocks, M. B., Moxon, S., Mapleson, D., Woolfenden, H. C., Mohorianu, I., Folkes, L., ... Moulton, V. (2012). The UEA sRNA workbench: A suite of tools for analysing and visualizing next generation sequencing microRNA and small RNA datasets. *Bioinformatics*, 28(15), 2059–2061. <http://doi.org/10.1093/bioinformatics/bts311>
- Subramanian, A., Tamayo, P., Mootha, V. K., Mukherjee, S., Ebert, B. L., Gillette, M. A., ... Mesirov, J. P. (2005). Gene set enrichment analysis: A knowledge-based approach for interpreting genome-wide expression profiles. *Proceedings of the National Academy of Sciences of the United States of America*, 102(43), 15545–15550. <http://doi.org/10.1073/pnas.0506580102>
- Sullivan, R. (2016). Epididymosomes Role of extracellular microvesicles in sperm maturation. *Frontiers in Bioscience*, 8(1), 106–114. <http://doi.org/10.2741/s450>
- Sun, Z., Zhu, M., Lv, P., Cheng, L., Wang, Q., Tian, P., ... Wen, B. (2018). The long noncoding RNA Lncenc1 maintains naive states of mouse ESCs by promoting the glycolysis pathway. *Stem Cell Reports*, 11(3), 741–755. <http://doi.org/10.1016/j.stemcr.2018.08.001>
- Sundaram, V., Cheng, Y., Ma, Z., Li, D., Xing, X., Edge, P., ... Wang, T. (2014). Widespread contribution of transposable elements to the innovation of gene regulatory networks. *Genome Research*, 24(12), 1963–1976. <http://doi.org/10.1101/gr.168872.113>
- Sundaram, V., & Wysocka, J. (2020). Transposable elements as a potent source of diverse cis-regulatory sequences in mammalian genomes. *Philosophical Transactions of the Royal Society of London. Series B, Biological Sciences*, 375(1795), 20190347. <http://doi.org/10.1098/rstb.2019.0347>
- Supek, F., Bošnjak, M., Škunca, N., & Šmuc, T. (2011). REVIGO Summarizes and Visualizes Long Lists of Gene Ontology Terms. *PLoS ONE*, 6(7), e21800. <http://doi.org/10.1371/journal.pone.0021800>
- Surani, M. A., Hayashi, K., & Hajkova, P. (2007). Genetic and epigenetic regulators of pluripotency. *Cell*, 128(4), 747–762. <http://doi.org/10.1016/j.cell.2007.02.010>
- Susiarjo, M. (2016). Introduction to epigenetic mechanisms (pp. 49–62). Elsevier. <http://doi.org/10.1016/B978-0-12-801383-0.00004-9>

- Talevich, E., Shain, A. H., Botton, T., & Bastian, B. C. (2016). CNVkit: Genome-wide copy number detection and visualization from targeted DNA sequencing. *PLoS Computational Biology*, 12(4), e1004873. <http://doi.org/10.1371/journal.pcbi.1004873>
- Tarasov, A., Vilella, A. J., Cuppen, E., Nijman, I. J., & Prins, P. (2015). Sambamba: Fast processing of NGS alignment formats. *Bioinformatics*, 31(12), 2032–2034. <http://doi.org/10.1093/bioinformatics/btv098>
- Tenenhaus, A., Philippe, C., Guillemot, V., Le Cao, K.-A., Grill, J., & Frouin, V. (2014). Variable selection for generalized canonical correlation analysis. *Biostatistics*, 15(3), 569–583. <http://doi.org/10.1093/biostatistics/kxu001>
- Thompson, Peter J., Macfarlan, Todd S., & Lorincz, Matthew C. (2016). Long Terminal Repeats: From Parasitic Elements to Building Blocks of the Transcriptional Regulatory Repertoire. *Molecular Cell*, 62(5), 766–776. <http://doi.org/10.1016/j.molcel.2016.03.029>
- Thurman, R. E., Rynes, E., Humbert, R., Vierstra, J., Maurano, M. T., Haugen, E., ... Stamatoyannopoulos, J. A. (2012). The accessible chromatin landscape of the human genome. *Nature*, 489(7414), 75–82. <http://doi.org/10.1038/nature11232>
- Tsagiopoulou, M., Maniou, M. C., Pechlivanis, N., Togkousidis, A., Kotrová, M., Hutzenlaub, T., ... Psomopoulos, F. (2021). UMIc: A preprocessing method for UMI deduplication and reads correction. *Frontiers in Genetics*, 12. <http://doi.org/10.3389/fgene.2021.660366>
- Vakoc, C. R., Sachdeva, M. M., Wang, H., & Blobel, G. A. (2006). Profile of histone lysine methylation across transcribed mammalian chromatin. *Molecular and Cellular Biology*, 26(24), 9185–9195. <http://doi.org/10.1128/MCB.01529-06>
- van Steenwyk, G., Gapp, K., Jawaid, A., Germain, P.-L., Manuella, F., Tanwar, D. K., ... Mansuy, I. M. (2020). Involvement of circulating factors in the transmission of paternal experiences through the germline. *The EMBO Journal*, 39(23), e104579. <http://doi.org/10.15252/embj.2020104579>
- van Steenwyk, G., Roszkowski, M., Manuella, F., Franklin, T. B., & Mansuy, I. M. (2018). Transgenerational inheritance of behavioral and metabolic effects of paternal exposure to traumatic stress in early postnatal life: Evidence in the 4th generation. *Environmental Epigenetics*, 4(2), dvy023. <http://doi.org/10.1093/EEP/DVY023>
- Vanderhaeghen, P., Schurmans, S., Vassart, G., & Parmentier, M. (1997). Specific Repertoire of Olfactory Receptor Genes in the Male Germ Cells of Several Mammalian Species. *Genomics*, 39(3), 239–246. <http://doi.org/10.1006/geno.1996.4490>
- Veselovska, L., Smallwood, S. A., Saadeh, H., Stewart, K. R., Krueger, F., Maupetit-Méhouas, S., ... Kelsey, G. (2015). Deep sequencing and de novo assembly of the mouse oocyte transcriptome define the contribution of transcription to the DNA methylation landscape. *Genome Biology*, 16, 209. <http://doi.org/10.1186/s13059-015-0769-z>

- Vitsios, D. M., & Enright, A. J. (2015). Chimira: Analysis of small RNA sequencing data and microRNA modifications. *Bioinformatics*, 31(20), 3365–3367. <http://doi.org/10.1093/bioinformatics/btv380>
- Vitting-Seerup, K., & Sandelin, A. (2017). The landscape of isoform switches in human cancers. *Molecular Cancer Research*, 15(9), 1206–1220. <http://doi.org/10.1158/1541-7786.MCR-16-0459>
- Vitting-Seerup, K., & Sandelin, A. (2019). IsoformSwitchAnalyzeR: Analysis of changes in genome-wide patterns of alternative splicing and its functional consequences. *Bioinformatics*, 35(21), 4469–4471. <http://doi.org/10.1093/bioinformatics/btz247>
- Waddington, C. H. (1942). The epigenotype. *Endeavour*, 1(18).
- Wang, M., Liu, X., Chang, G., Chen, Y., An, G., Yan, L., ... Qiao, J. (2018). Single-cell RNA sequencing analysis reveals sequential cell fate transition during human spermatogenesis. *Cell Stem Cell*, 23(4), 599–614.e4. <http://doi.org/10.1016/j.stem.2018.08.007>
- Wang, W., & Carroll, T. (2020). Rfastp: An ultra-fast and all-in-one fastq preprocessor (QualityControl, adapter, low quality and polyX trimming) and UMISequencing parsing). Retrieved from <http://www.bioconductor.org/packages/release/bioc/html/Rfastp.html>
- Weismann, A. (1893). *The germ-plasm: A theory of heredity. Translated by w. Newton parker and harriet rönnfeldt*. New York: Scribner. <http://doi.org/10.5962/bhl.title.25196>
- Wickham, H. (2016). *ggplot2: Elegant graphics for data analysis*. Springer-Verlag New York. Retrieved from <https://ggplot2.tidyverse.org>
- Wu, D. C., Yao, J., Ho, K. S., Lambowitz, A. M., & Wilke, C. O. (2018). Limitations of alignment-free tools in total RNA-seq quantification. *BMC Genomics*, 19(1), 510. <http://doi.org/10.1186/s12864-018-4869-5>
- Wu, D., Lim, E., Vaillant, F., Asselin-Labat, M.-L., Visvader, J. E., & Smyth, G. K. (2010). ROAST: Rotation gene set tests for complex microarray experiments. *Bioinformatics*, 26(17), 2176–2182. <http://doi.org/10.1093/bioinformatics/btq401>
- Wu, D., & Smyth, G. K. (2012). Camera: A competitive gene set test accounting for inter-gene correlation. *Nucleic Acids Research*, 40(17), e133. <http://doi.org/10.1093/nar/gks461>
- Wu, J., Liu, Q., Wang, X., Zheng, J., Wang, T., You, M., ... Shi, Q. (2013). mirTools 2.0 for non-coding RNA discovery, profiling, and functional annotation based on high-throughput sequencing. *RNA Biology*, 10(7), 1087–1092. <http://doi.org/10.4161/rna.25193>
- Wu, Xiaogang, Kim, T.-K., Baxter, D., Scherler, K., Gordon, A., Fong, O., ... Wang, K. (2017). sRNAnalyzer-a flexible and customizable small RNA sequencing data analysis pipeline. *Nucleic Acids Research*, 45(21), 12140–12151. <http://doi.org/10.1093/nar/gkx999>

- Wu, Xin, Oatley, J. M., Oatley, M. J., Kaucher, A. V., Avarbock, M. R., & Brinster, R. L. (2010). The POU Domain Transcription Factor POU3F1 Is an Important Intrinsic Regulator of GDNF-Induced Survival and Self-Renewal of Mouse Spermatogonial Stem Cells. *Biology of Reproduction*, 82(6), 1103–1111. <http://doi.org/10.1095/biolreprod.109.083097>
- Yang, Q.-E., Racicot, K. E., Kaucher, A. V., Oatley, M. J., & Oatley, J. M. (2013). MicroRNAs 221 and 222 regulate the undifferentiated state in mammalian male germ cells. *Development*, 140(2), 280–290. <http://doi.org/10.1242/dev.087403>
- Yi, L., Liu, L., Melsted, P., & Pachter, L. (2018). A direct comparison of genome alignment and transcriptome pseudoalignment. *BioRxiv*. <http://doi.org/10.1101/444620>
- Young, M. D., Wakefield, M. J., Smyth, G. K., & Oshlack, A. (2010). Gene ontology analysis for RNA-seq: Accounting for selection bias. *Genome Biology*, 11(2), R14. <http://doi.org/10.1186/gb-2010-11-2-r14>
- Yuan, X., Liu, C., Yang, P., He, S., Liao, Q., Kang, S., & Zhao, Y. (2009). Clustered microRNAs' coordination in regulating protein-protein interaction network. *BMC Systems Biology*, 3, 65. <http://doi.org/10.1186/1752-0509-3-65>
- Zhang, T., Zhang, Z., Dong, Q., Xiong, J., & Zhu, B. (2020). Histone H3K27 acetylation is dispensable for enhancer activity in mouse embryonic stem cells. *Genome Biology*, 21(1), 45. <http://doi.org/10.1186/s13059-020-01957-w>
- Zhang, Y., Liu, T., Meyer, C. A., Eeckhoute, J., Johnson, D. S., Bernstein, B. E., ... Liu, X. S. (2008). Model-based analysis of ChIP-seq (MACS). *Genome Biology*, 9(9), R137. <http://doi.org/10.1186/gb-2008-9-9-r137>
- Zhao, S., Zhang, Y., Gamini, R., Zhang, B., & Schack, D. von. (2018). Evaluation of two main RNA-seq approaches for gene quantification in clinical RNA sequencing: polyA+ selection versus rRNA depletion. *Scientific Reports*, 8(1), 4781. <http://doi.org/10.1038/s41598-018-23226-4>
- Zhu, H., Wang, G., & Qian, J. (2016). Transcription factors as readers and effectors of DNA methylation. *Nature Reviews Genetics*, 17(9), 551–565. <http://doi.org/10.1038/nrg.2016.83>
- Zhu, J., Chen, G., Zhu, S., Li, S., Wen, Z., Bin Li, ... Shi, L. (2016). Identification of tissue-specific protein-coding and noncoding transcripts across 14 human tissues using RNA-seq. *Scientific Reports*, 6, 28400. <http://doi.org/10.1038/srep28400>
- Zuo, L., Wang, Z., Tan, Y., Chen, X., & Luo, X. (2016). piRNAs and Their Functions in the Brain. *International Journal of Human Genetics*, 16(1-2), 53–60. <http://doi.org/10.1080/09723757.2016.11886278>